A comparative study investigating the effects of different methodologies on the maturation of human induced pluripotent stem cell derived cardiomyocytes

A thesis submitted to The University of Manchester for the degree of Doctor of Philosophy
in the Faculty of Biology Medicine and Health

2022

KATIE E RYDING

School of Medical Sciences

Contents

Word count: 45,280

List of Figures

List of Tables

List of Abbreviations

β-AR	β-adrenergic receptor
ATP	Adenosine triphosphate
AU	Arbitrary units
BMP	Bone morphogenetic protein
BrS	Brugada syndrome
BSA	Bovine serum albumin
CaMKII	Calmodulin-dependent protein kinase II
cAMP	Cyclic adenosine monophosphate
CASQ2	Calsequestrin 2
cGMP	Cyclic guanosine monophosphate
CICR	Calcium induced calcium release
CPVT	Catecholaminergic polymorphic ventricular tachycardia
cTnI	Cardiac troponin I
cTnT	Cardiac troponin T
DAD	Delayed afterdepolarisation
Dex	Dexamethasone
DMEM	Dulbecco's Modified Eagle's Medium
EAD	Early afterdepolarisation
EC	Excitation-contraction
ECG	Electrocardiogram
ECM	Extracellular matrix
EHT	Engineered heart tissue
GPCR	G protein coupled receptor
GSK3β	Glycogen synthase kinase 3β
hiPSC	Human induced pluripotent stem cells
hiPSC-CM	Human induced pluripotent stem cell derived cardiomyocytes
ICD	Implantable cardioverter defibrillator
JCN	Junctin
jSR	Junctional SR
LCSD	Left cardiac sympathetic denervation
LQTS	Long QT syndrome

LTCC	L-type calcium channel
MACS	Magnetic-activated cell sorting
MFs	Maturation factors
MHC	Myosin heavy chain
MMM	Metabolic maturation medium
NCX	Sodium-calcium exchanger
PAK1	P21-activated kinase 1
PBS	Phosphate buffered saline
PDE5	Phosphodiesterase 5
PKA	Protein kinase A
PLN	Phospholamban
RT-qPCR	Real-time quantitative PCR
RYR2	Cardiac ryanodine receptor 2
SADS	Sudden arrhythmic death syndrome
SCD	Sudden cardiac death
SERCA2a	SR calcium ATPase
SOICR	Store overload induced calcium release
SR	Sarcoplasmic reticulum
ssTnI	Slow skeletal troponin I
T-tubules	Transverse tubules
T3	Triiodothyronine
TBS	Tris-buffered saline
TRDN	Triadin
VUS	Variant of unknown significance
WGA	Wheat germ agglutinin
Wnt	Wingless/INT

Abstract

Introduction: Despite important contributions to our understanding, animal models do not reliably recapitulate human cardiac physiology or the disease complexity of cardiac channelopathies. The development of human induced pluripotent stem cells (hiPSCs) has provided an unprecedented opportunity to generate a cell-based model for human diseases such as catecholaminergic polymorphic ventricular tachycardia (CPVT); an inherited cardiac channelopathy, predominantly caused by mutations in the *RYR2* gene, that can predispose the heart to life-threatening, adrenergically mediated arrhythmic activity. However, hiPSC-derived cardiomyocytes (hiPSC-CMs) harbour an immature phenotype, limiting their implementation as physiologically relevant *in vitro* disease models.

Aim: To generate hiPSC-CMs with a greater degree of maturity, thus physiological relevance, for assessing the CPVT disease phenotype and pharmacological treatments by incorporating reported hiPSC-CM maturation approaches into the cardiomyocyte differentiation protocol.

Methods and results: The small-molecule based directed differentiation of hiPSC-CMs was optimised for the RYR2 patient cell line. Four hiPSC-CM maturation approaches were then evaluated. Prolonged culture, and thyroid (T3) and glucocorticoid (Dex) hormone supplementation significantly upregulated β_1-adrenergic receptor expression ($p<0.0001$), as shown by RT-qPCR and western blot. Subsequent incorporation of a nanopatterned culture surface topography resulted in a significant increase of hiPSC-CM aspect ratio ($p<0.001$) and the development of rod-shaped cells. Live fluorescent calcium imaging was also performed. Despite a slower rate of rise ($p<0.05$) and reduced amplitude ($p<0.05$), the calcium transient rate of decay accelerated ($p<0.001$). The implementation of a more physiologically relevant culture medium improved the efficiency of SERCA2a activity.

Conclusions: The incorporation of hiPSC-CM maturation approaches into the well-established small-molecule based differentiation protocol resulted in some structural and functional development of the RYR2 hiPSC-CMs. The lack of development of a T-tubular network is believed to be a major limiting factor with regards to hiPSC-CM calcium handling properties. Further maturation is required to fully recapitulate CPVT, and for hiPSC-CMs to become a reliable mainstream model for drug screening.

Declaration

I declare that no portion of the work referred to in the thesis has been submitted in support of an application for another degree or qualification of this or any other university or other institute of learning.

Copyright Statement

i. The author of this thesis (including any appendices and/or schedules to this thesis) owns certain copyright or related rights in it (the "Copyright") and s/he has given The University of Manchester certain rights to use such Copyright, including for administrative purposes.

ii. Copies of this thesis, either in full or in extracts and whether in hard or electronic copy, may be made only in accordance with the Copyright, Designs and Patents Act 1988 (as amended) and regulations issued under it or, where appropriate, in accordance with licensing agreements which the University has from time to time. This page must form part of any such copies made.

iii. The ownership of certain Copyright, patents, designs, trademarks and other intellectual property (the "Intellectual Property") and any reproductions of copyright works in the thesis, for example graphs and tables ("Reproductions"), which may be described in this thesis, may not be owned by the author and may be owned by third parties. Such Intellectual Property and Reproductions cannot and must not be made available for use without the prior written permission of the owner(s) of the relevant Intellectual Property and/or Reproductions.

iv. Further information on the conditions under which disclosure, publication and commercialisation of this thesis, the Copyright and any Intellectual Property and/or Reproductions described in it may take place is available in the University IP Policy (see http://documents.manchester.ac.uk/DocuInfo.aspx?DocID=2442 0), in any relevant Thesis restriction declarations deposited in the University Library, The University Library's regulations (see http://www.library.manchester.ac.uk/about/regulations/) and in The University's policy on Presentation of Theses

Acknowledgements

This research was funded by the British Heart Foundation.

I would like to acknowledge my supervisors, Dr Luigi Venetucci and Professor Andrew Trafford, for their guidance and support during this PhD.

I would like to extend my thanks to Dr Nigel Hodson for his help and enthusiasm with the atomic force microscopy undertaken during this project.

I would also like to thank the Division of Cardiovascular Sciences, in particular Professor Elizabeth Cartwright (PhD programme director and Head of Division), for the opportunity and pastoral guidance.

A special thanks to Dr Miriam Lettieri for her support, encouragement and friendship over the years.

Last but not least, I would like to thank my family and friends. To my parents, for their continued love and support. To Cali and Lottie, without whom the past five years would not have been the same. Thank you for being there during the highs, the lows and everything in between. Finally, to Dave who endured the PhD process with me. Thank you for your encouragement, patience and love. I hope this thesis makes you all proud.

Chapter 1

Introduction

1 Introduction

1.1 Sudden cardiac death

Sudden cardiac death (SCD) is defined as the unexpected natural death due to the occurrence of a cardiac event, within one hour of symptom onset in a person without any known pre-existing conditions[1]. The assumed mechanism for such deaths is ventricular arrhythmia caused by electrical instability[2]. In the general population across Europe and the USA, SCD is estimated to have an annual incidence of 50-100 per 100,000[3]. The majority of SCDs occur within the adult population - coronary heart disease being the most common underlying cardiac pathology responsible. In young adults and children SCD is a much rarer event but accounts for a greater proportion of deaths[2]. In these younger victims the underlying pathophysiology can be much more varied - inherited cardiomyopathies and primary electrical disorders prevailing[2,4]. Identifying the underlying pathology through post-mortem examination and toxicology assessments can potentially prevent further events occurring within family members. However structurally normal hearts and a negative toxicology are observed in up to 60% of SCDs in young people. These cases are termed sudden arrhythmic death syndrome (SADS)[5]. Inherited primary electrical disorders, also known as cardiac channelopathies, have been identified as the probable cause of death in up to 40% of SADS cases following genetic examination of surviving relatives[5,6].

1.1.1 Cardiac channelopathies

Cardiac channelopathies are a heterogeneous group of disorders that result from a mutation(s) in a gene(s) encoding a cardiac ion channel, its' receptor or regulatory protein. The consequent impaired ion channel expression and/or function can alter intrinsic electrical activity and calcium handling in the heart. Ultimately, the resultant dysfunction predisposes the heart to life-threatening arrhythmic activity[4].

In order to further understand how these cardiac channelopathy causing mutations can lead to cardiac arrhythmias, the sequence of electrical excitation and physiology of the ventricular action potential will first be reviewed.

1.2 Cardiac excitation and arrhythmia

The function of the heart is to pump oxygenated blood to, and deoxygenated blood from, the peripheral tissues of the body. The mechanical force required to pump blood depends on the systematic electrical excitation and recovery of the myocardium. The intrinsic electrical activity of the heart originates in the cardiac conduction system sinoatrial node - a specialised structure consisting of pacemaker cells that undergo periodical electrical oscillations of their membrane potential. These periodical oscillations regulate the rhythm of the heart. Upon the membrane potential reaching a threshold level an action potential is triggered. The action potential impulse spreads from the sinoatrial node throughout the cardiac conduction system during systole. The impulse is rapidly propagated from the sinoatrial node through the atrial walls to the atrioventricular node. Here the impulse is stalled allowing for the atria to contract and ventricles to fill with blood. The atrioventricular (His) bundle passes the electrical impulse from the atria to the ventricular conduction system for activation of ventricular contraction[7]. Following the onset of an action potential, cardiac cells enter a state of recovery known as the refractory period in which external stimuli are unable to produce a new action potential in order to prevent premature re-excitation[8].

1.2.1 The ventricular action potential

The established and renowned shape of the ventricular action potential is underpinned by changes in the membrane potential, caused by the movement of ions across the surface membrane. The action potential can be broken down into five distinct phases (0-4) as illustrated in Figure 1.1. Each phase is characterised by the opening and closing of specific ion channels, the direction of ion flow, and the amplitude of each current. Briefly, phase 0 represents a rapid depolarisation from the resting membrane potential (phase 4) - the result of a large inward current as cardiac voltage-gated sodium channels (I_{Na}) are activated. The following 'notch' of phase 1 is caused by the inactivation of these sodium channels and brief activation of the transient outward potassium current (I_{to}) initiating a rapid repolarisation. Phase 2 is known as the 'plateau' phase. During phase 2 the depolarising L-type calcium channel (LTCC) current (I_{Ca}) and remaining non-inactivated sodium channels balance the repolarising currents of the delayed rectifier potassium channels (slow, I_{Ks} and rapid, I_{Kr}). This current balance is crucial to the control

of action potential duration. As the positive inward currents reduce due to channel inactivation at the end of phase 2, the outward potassium currents dominate. Thus the action potential undergoes repolarisation (phase 3). As the membrane potential returns to diastolic levels the delayed rectifier potassium channels inactivate. The resting membrane potential (phase 4) is maintained by the inwardly rectifying potassium current (I_{K1}) until the next action potential is initiated.

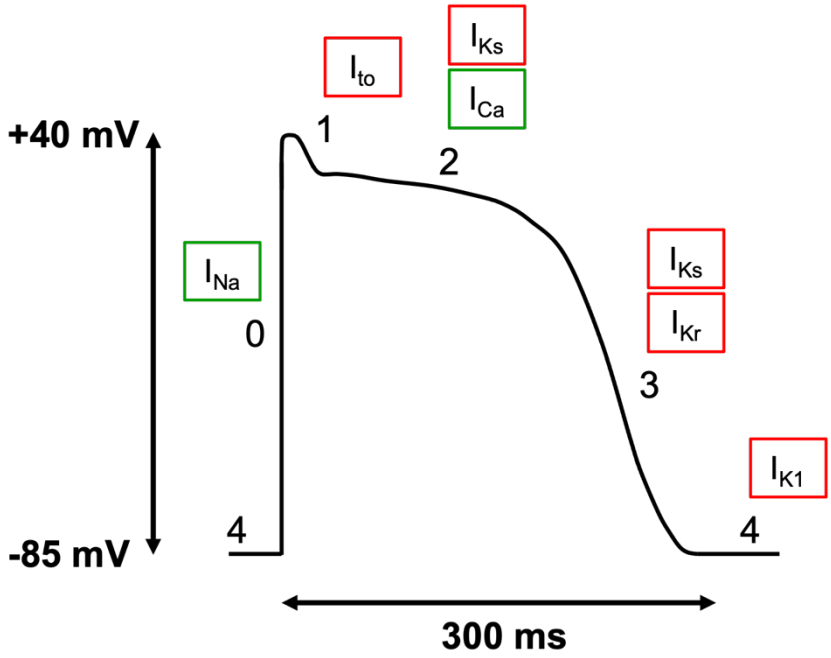

Figure 1.1: The ventricular action potential

Phase 0, rapid depolarisation; phase 1 'notch', rapid repolarisation; phase 2 'plateau', balance of depolarising and repolarising currents; phase 3, repolarisation; and phase 4, resting membrane potential. The predominant ionic currents active in each phase are labelled - green, inward current; red, outward current.

A genetic abnormality that alters the expression or function of a cardiac ion channel can impact the magnitude and/or timing of the ionic currents that constitute the ventricular action potential[9]. Disruption to just one of the currents (sodium[10], potassium[11] or calcium[12]) can alter the specialised conduction sequence of the electrical impulse, the rhythm of the heart, and ultimately the ability of the heart to pump blood. An abnormal heart rhythm is known as an arrhythmia. Arrhythmic activity can be caused by the heart beating too fast (tachycardia), too slow (bradycardia) or irregularly.

1.2.2 Mechanisms of arrhythmia

Different electrophysiological properties within adjacent regions of the myocardium can induce arrhythmic activity that is often observed in patients with a cardiac channelopathy. Transmural heterogeneity of action potential conduction that originates in the ventricles can be caused by either triggered activity or re-entry.

Triggered activity

Aberrant membrane depolarising activity during, or immediately following an action potential is known as an afterdepolarisation[13,14]. Afterdepolarisations are classified as either early, interrupting phase 2 or phase 3 of an action potential or delayed, occurring after full repolarisation. If the amplitude of an early afterdepolarisation (EAD) or delayed afterdepolarisation (DAD) reaches the threshold potential of the membrane, a spontaneous action potential is triggered and induces extrasystoles/ectopic activity (heartbeats outside the physiological heart rhythm) (Figure 1.2A). Extrasystoles can degenerate into tachyarrhythmias.

Re-entry

Circus movement re-entry occurs when an action potential impulse propagates around an anatomic or functional obstacle, following a distinct pathway in which it returns to its point of origin[13,14]. The cells in the path recover from excitation prior to the impulse returning hence can be re-excited (Figure 1.2B). In phase 2 re-entry transmural heterogeneity of recovery from refractoriness, often a result of dispersion of repolarisation, exists between two sites. Consequently, the site with delayed recovery is able to re-excite the recovered neighbouring site.

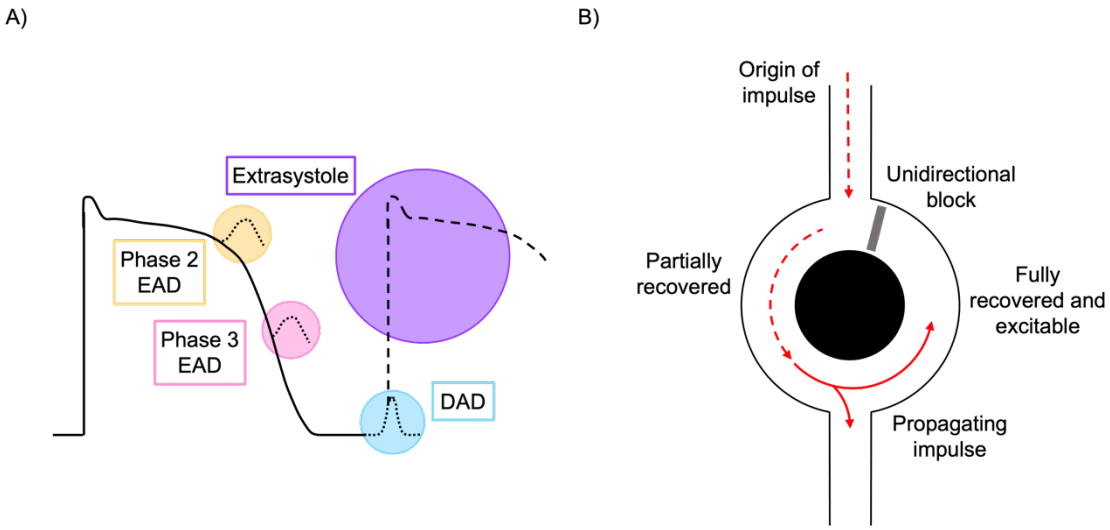

Figure 1.2: Schematic diagrams illustrating mechanisms of arrhythmia

(A) Triggered activity including examples of phase 2 (yellow) and phase 3 (pink) early afterdepolarisations (EADs), delayed afterdepolarisation (DAD, blue) and DAD-induced extrasystole (purple). (B) Re-entry: An unexcitable obstacle (black circle) determines the presence of two pathways. A propagating electrical impulse encounters a unidirectional conduction block (grey) and travels down the other pathway. The area of block recovers and is excited from the opposite side initiating a re-entrant circuit, this concept is known as the excitable gap.

1.2.3 The role of ion channels in inherited arrhythmogenic diseases

Sustained arrhythmic activity and SADS are often discovered to be caused by inherited cardiac channelopathies. The prevailing inherited cardiac channelopathies associated with cardiac arrhythmias are long QT syndrome (LQTS), Brugada syndrome (BrS) and catecholaminergic polymorphic ventricular tachycardia (CPVT). LQTS and BrS are most commonly caused by genetic variations in genes encoding for sodium and potassium channel subunits expressed in the heart, whereas CPVT is coupled with abnormal calcium handling.

Sodium channels

To date ten subtypes of voltage-gated sodium channels, each encoded for by different genes, have been discovered[15]. The predominant α subunit isoform expressed in cardiac tissue is $Na_v1.5$ which is encoded for by the *SCN5A* gene. The α subunit of voltage-gated sodium channels is the pore-forming subunit that consists of the channel pore, gates and voltage sensors[16]. $Na_v1.5$ sodium channels are mainly localised to the intercalated

discs of cardiomyocytes[17] which corresponds to their function: propagation of the action potential between adjacent cardiomyocytes; the initial rapid depolarisation of phase 0; and the conduction of a small proportion of current during the plateau phase.

Potassium channels

As alluded to in section 1.2.1, many different voltage-gated potassium channel subtypes exist within the cardiac membrane. The subtypes are characterised by the subunit composition that forms their structure: α-subunits form the conductance pore and β-subunits are accessory proteins that modulate the voltage- and time- dependent properties of each channel[18]. The expression of each channel varies throughout regions of the myocardium: atria and ventricles; epicardium, mid-myocardium and endocardium; and apex and base[11]. Each channel has a specific role, contributing to a particular phase(s) of the action potential whereby they control action potential repolarisation and duration, and the resting membrane potential. Alterations to the systematically regulated ventricular repolarisation and heterogeneous distribution of channels can affect action potential duration within regions. Regional changes to action potential duration increase the risk of afterdepolarisations developing.

Long QT syndrome

Congenital LQTS is the most commonly inherited arrhythmia syndrome, affecting approximately 1:2000 individuals[19]. It is characterised by delayed ventricular repolarisation (leading to prolongation of the action potential), often denoted clinically by a prolonged QTc interval reflected in the 12-lead electrocardiogram (ECG), and an increased risk of the life-threatening polymorphic ventricular tachycardia known as torsade de pointes[9,20]. LQTS has a list of reported causative genes that has grown to 17 (LQT1-17)[9] - loss of function mutations in potassium channel subunit genes or gain-of-function mutations in *SCN5A* are often accountable. However in a recent international, multi-centred, evidence-based reappraisal of genes reported to cause congenital LQTS only three genes (*KCNQ1*, LQT1; *KCNH2*, LQT2; and *SCN5A*, LQT3) were identified as definitive genes for typical LQTS[21].

KCNQ1 and *KCNH2* genes encode $K_v7.1$ and $K_v11.1$ pore-forming α subunits that pass I_{Ks} and I_{Kr} respectively. Loss-of-function mutations in these genes reduce the major

repolarisation currents of phases 2 and 3, and cause LQT1 and LQT2 - the most common potassium channel cardiac channelopathies. Distinctive patterns for cardiac events in LQT1 and LQT2 have been shown. In LQT1 patients arrhythmic events are associated with sustained high sympathetic tone such as during exercise or emotional stress, whereas LQT2 patients are sensitive to sympathetic surges that occur during periods of rest (e.g. startling noise, alarm clock)[22]. Mutations in *KCNE1* and *KCNE2,* which encode accessory β-subunits of the slow and rapid delayed rectifier channels, have also been associated with LQTS.

Prolonged repolarisation occurs as the amplitude of the counterbalancing inward depolarising currents (phase 2) are greater relative to the reduced potassium currents. Furthermore, the delayed repolarisation provides a larger window of activation for the depolarising currents enabling them to inactivate and reactivate prior to voltage-dependent inactivation. Reactivation of depolarising currents causes oscillations in the membrane potential promoting EADs. Moreover the threshold for an atypical action potential may be triggered. Ectopic activity can degenerate when occurring repeatedly and at a rapid rate to 'fibrillatory' conduction and sustained tachyarrhythmia[11].

Of the delayed rectifier potassium currents, I_{Kr} is considered the dominant repolarising current. β-adrenergic receptor (β-AR) stimulation significantly augments I_{Ks} in a time-dependent manner[23–25]. However differences in the time course of the response relative to I_{Ca} have been demonstrated and are unmasked in the presence of an I_{Kr} deficit[23]. In LQT1 the lower I_{Ks} impairs the ability of adrenergic modulation to shorten the QT interval and antagonise I_{Ca} as the heart rate increases. A delayed response of I_{Ks} to adrenergic stimulation compared to I_{Ca} creates a high-risk window for EADs in LQT2 patients with a prolonged repolarisation due to dysfunctional I_{Kr}[23].

Changes to the final repolarisation and/or resting membrane potential caused by loss-of-function mutations in *KCNJ2* are linked to LQT7. Reduced I_{K1} prolongs the terminal repolarisation phase enabling late phase 3 EADs to trigger ventricular ectopy[26]. Additionally, reduced I_{K1} can destabilise the resting membrane potential causing abnormal automaticity and DADs that have the potential to initiate an aberrant action potential as the threshold for activating $Na_v1.5$ channels is more readily achieved[11].

In contrast LQT3 is typically caused by gain-of-function mutations in *SCN5A*. The mutations cause sustained/delayed inactivation, or accelerated recovery from inactivation of $Na_v1.5$, promoting an enhanced late I_{Na} during phase 2 of the action potential[16,27]. The resultant prolongation of phase 2 induces dispersion of refractoriness as LTCCs are able to reactivate prior to or during early phase 3 repolarisation. Reactivation of LTCCs causes membrane potential oscillations (EADs). If these reach the action potential threshold they can re-excite a region of the myocardium. Consequently heterogeneous repolarisation is observed transmurally. If adjacent regions of the myocardium have different electrophysiological properties and multiple regions develop EADs synchronously, triggered activity and ventricular arrhythmias can initiate[27–29].

Brugada syndrome

Like LQTS, BrS is characterised clinically by an abnormal ECG reading - ST segment elevation. ST segment elevation is associated with an increased risk of ventricular fibrillation and SCD. The prevalence of BrS varies across populations. In Southeast Asia it is estimated to be more than 1:1000 compared to less than 1:2000 in Western countries[30]. Mutations in ~20 genes are associated with BrS causality[31] but the contribution of these genes to disease prevalence is unclear. Only *SCN5A* accounts for a significant proportion of BrS cases according to a study investigating the burden of rare genetic variants among BrS arrhythmia-susceptibility genes[32]. These findings were supported by the more recent evidence-based reappraisal of gene validity for BrS[33].

SCN5A mutations cause a loss-of-function that reduces I_{Na}. The loss of current has been associated with decreased protein expression, expression of non-functional proteins, impaired channel trafficking, and changes to channel gating (delayed activation, premature inactivation, enhanced slow inactivation, slower recovery from inactivation)[34]. The pathophysiology responsible for BrS however is not yet fully understood and remains debated[35]. There are two main theories: the 'depolarisation hypothesis' and the 'repolarisation hypothesis'. The former proposes delayed depolarisation/slower conduction velocity in the right ventricle only, due to conduction disturbances and mild structural abnormalities, whilst the latter postulates dispersion

of repolarisation between the right ventricular epicardium and endocardium, as the relative amplitude of I_{to} is increased to a much greater extent in the epicardium[10,34,35]. Regardless of the underlying pathophysiology, cell membrane voltage heterogeneity causes the characteristic ST-segment elevation, phase 2 re-entry and ventricular fibrillation[10].

The ryanodine receptor 2 channel

Identified mutations in *RYR2* are also associated with a number of different cardiac phenotypes however the majority (~50%) give rise to the inherited arrhythmogenic channelopathy called CPVT, type 1[36,37]. Ryanodine receptor 2 channels (RYR2) are calcium release channels localised in cardiac muscle; specifically, the membrane of a specialised organelle responsible for intracellular calcium storage and release, known as the sarcoplasmic reticulum (SR)[38]. Under 'normal' healthy circumstances RYR2 channels are a crucial component of cardiomyocyte function – playing a pivotal role in cardiac calcium handling during the excitation-contraction (EC) coupling process required for initiation of contraction. In the following section this phenomenon will be described prior to reviewing RYR2 channels and the pathophysiology associated with their dysfunction.

1.3 Excitation-contraction coupling in healthy cardiomyocytes

The EC coupling process is the conversion of an electrical impulse (action potential) to mechanical contraction of the cardiac muscle. On reaching individual ventricular myocytes the electrical signal is converted into mechanical energy through calcium signalling activating the contractile machinery[39].

1.3.1 Calcium handling

Changes in the intracellular calcium concentration of cardiomyocytes regulates cardiac contractility. At the level of individual ventricular cardiomyocytes, diastolic depolarisation of the sarcolemma induces a rapid and synchronous rise in intracellular calcium. This rise in intracellular calcium is facilitated by the ultrastructure possessed by cardiomyocytes. Deep invaginations of the sarcolemma known as transverse (T) tubules harbour voltage sensitive LTCCs that open in response to membrane depolarisation. The

subsequent influx of extracellular calcium into a micro-domain of the cardiomyocyte, known as a dyad, triggers a more substantial release of calcium from the SR through activation and opening of RYR2 channels that are located in close proximity to the LTCCs. This phenomenon is termed calcium induced calcium release (CICR). The combination of calcium influx and SR release activates neighbouring RYR2 channels leading to an intracellular calcium transient that promotes activation of myofilaments[39,40]. Synchronously individual cardiomyocytes contract generating a large, uniform production of force. The contractile force generated is modulated by the amplitude and duration of the calcium transient, in addition to the responsiveness of myofilaments to calcium[39], thus RYR2 plays a critical role in modulating contraction.

Equally as important, the intracellular calcium concentration must reduce in order for muscle relaxation and in preparation for the next excitation. RYR2 channels close inhibiting further release of calcium from the SR. The existing cytosolic calcium concentration is predominantly reduced via the SR calcium ATPase (SERCA2a) returning calcium back into the SR (75%) but also via sodium-calcium exchanger extrusion (NCX, ~25%, three sodium ions for each calcium ion - net inward depolarising current of +1), and uptake into mitochondria. The lowered 'free' intracellular calcium concentration promotes dissociation of calcium from the contractile machinery. Crucially, the SR becomes refractory preventing spontaneous reactivation of CICR during the diastolic period[39–41]. Figure 1.3 summarises these events.

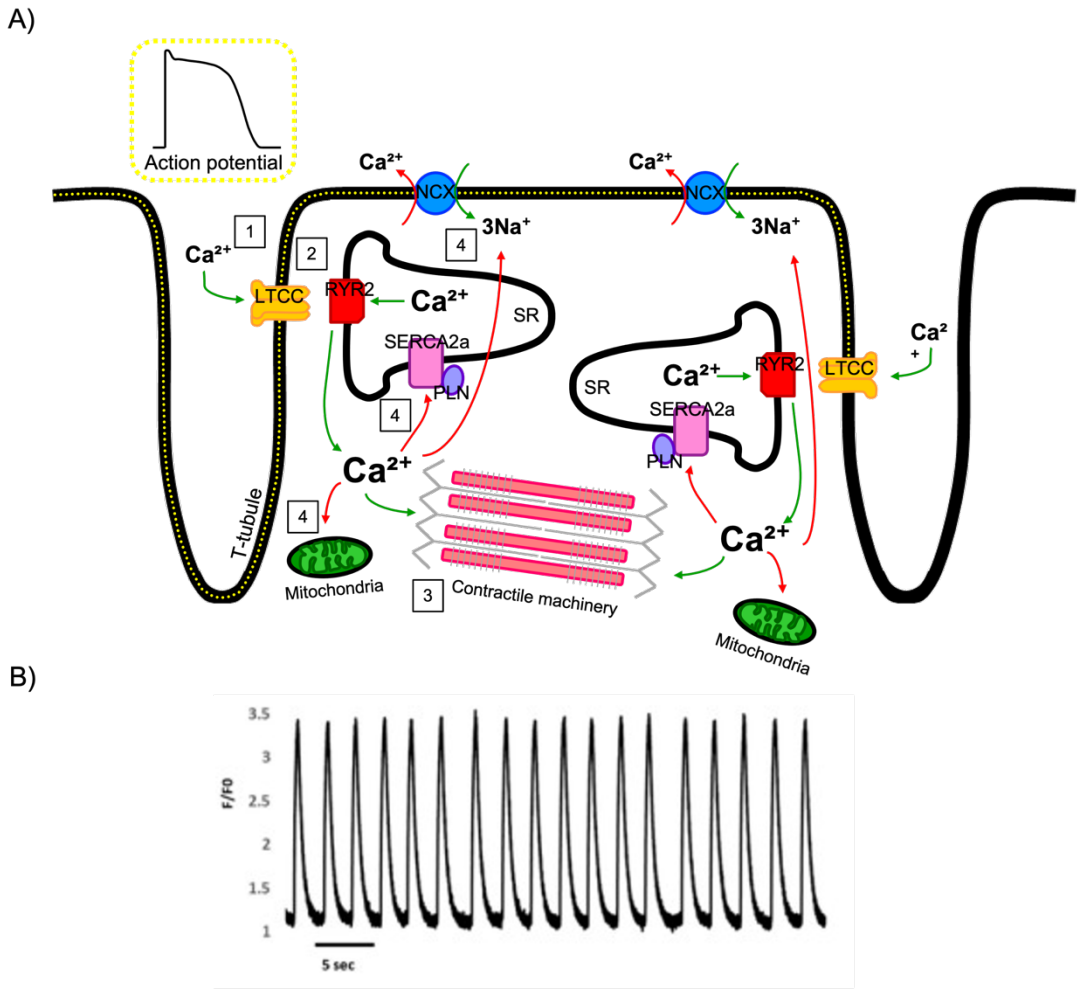

Figure 1.3: Calcium handling in cardiomyocytes

(A) [1] An action potential depolarises the cell membrane causing an influx of calcium via the L-type calcium channels (LTCC). [2] The calcium influx stimulates opening of ryanodine receptor 2 (RYR2) channels promoting a greater release of calcium from the sarcoplasmic reticulum (SR). This is known as calcium induced calcium release. [3] Calcium binds to and activates the myofilaments of the contractile machinery. [4] Calcium is removed from the cytosol via SR calcium ATPase (SERCA2a), sodium-calcium exchanger (NCX) and mitochondria. PLN, phospholamban. (B) Representative line scan trace showing changes in intracellular calcium in human induced pluripotent stem cell derived cardiomyocytes generated from a healthy individual. Trace taken from Hopton *et al*. 2022[42].

1.4 The cardiac ryanodine receptor channel

There are three different isoforms of ryanodine receptors, encoded for by different genes, that have been identified and characterised: *RYR1*, predominantly expressed in skeletal muscle; *RYR2,* primarily expressed in cardiac muscle; and *RYR3,* expressed

throughout many tissues including the brain[38]. The gene encoding the cardiac isoform, *RYR2,* is located at chromosome 1q43, spanning over 790 kilobases and consisting of 105 exons[37]. RYR2 channels are homotetrameric proteins with each monomer consisting of a large N-terminal cytoplasmic domain that contains binding sites for regulatory proteins, a transmembrane calcium pore-forming domain and a short channel domain at the carboxyl terminal[43]. Located in the SR membrane of cardiomyocytes, RYR2 proteins act as large-conductance calcium release channels. Calcium release from the SR via RYR2 channels plays an essential role in the EC coupling process (refer to section 1.3.1).

Mutations within the *RYR2* gene can alter calcium handling during EC coupling and ultimately lead to the arrhythmic activity observed prior to SCD. Over 150 *RYR2* mutations have been associated with cardiac arrhythmias to date[44]. The majority of the mutations are clustered in four highly conserved 'hotspot' regions that correspond to three functionally important domains[43,45]. They are most commonly missense ('point') mutations in which a single nucleotide is replaced altering the coded amino acid[45], however in-frame deletions have also been reported[46]. Dysfunctional release of calcium from the SR can also be caused by altered activity of factors that modulate RYR2.

1.4.1 Endogenous modulation of RYR2

Calcium

The activity of RYR2 is modulated by the cytosolic and SR (luminal) calcium concentrations within a cardiomyocyte. As previously described the level of cytosolic calcium increases during the early phases of an action potential - extracellular calcium enters the cardiomyocytes through opened LTCCs and activates RYR2 channels. However intracellular calcium regulates RYR2 in a bimodal/local negative feedback manner - concentrations between 10 μM and 100 μM activate CICR, resulting in a gradual prolongation of the RYR2 channel average open time; whereas concentrations above 100 μM inhibit CICR by increasing the duration of channel closure time[39,47].

The concentration of calcium held within the SR also modulates RYR2. It was first identified back in 1975 by Fabiato and Fabiato that the level of SR calcium correlates with the magnitude of SR calcium release during CICR[48]. More recently, it has been

suggested that in addition to the cytoplasmic RYR2 calcium sensor there may be a structurally different luminal calcium sensor that also regulates RYR2 channel open probability. At high, inhibitory concentrations (1 mM) of cytosolic calcium, elevation of luminal calcium increased the activity of RYR2 channels[47]. Furthermore, overloading of the SR causes spontaneous calcium releases from RYR2 channels independent of an action potential. This phenomenon has been termed store overload induced calcium release (SOICR). SOICR occurs when the SR reaches a critical threshold level of calcium[49]. The calcium level within the SR is determining RYR2 activity and thus supporting the hypothesis for a calcium sensing site on the luminal side. However the mechanism by which SR luminal calcium regulates RYR2 channel activity has not yet been established and remains controversial. Studies to identify the potential luminal calcium sensor have been extensive. One suggested protein is calsequestrin (CASQ2). CASQ2 is one of several accessory proteins known to modulate RYR2 activity.

Calsequestrin

CASQ2 is the predominant calcium binding buffer within the SR. Each CASQ2 molecule is reported to be able to bind between 20-40 calcium ions[50,51]. CASQ2 is located at the SR luminal membrane and forms a junctional complex (jSR) with intramembrane proteins: triadin (TRDN), junctin (JCN) and RYR2. TRDN and JCN act as anchoring proteins, binding directly to RYR2 and CASQ2 to ensure their close proximity[52].

In addition to its' role as a storage reservoir for calcium, CASQ2 is actively involved in the release of calcium from the SR. It is thought CASQ2 co-ordinates the rate of calcium release whilst conserving calcium within the store. At low luminal calcium CASQ2 binds to TRDN and JCN, inhibiting RYR2 activity. At elevated luminal calcium CASQ2 binds to the calcium, weakening the electrostatic interaction between TRDN/JCN and itself; thus relieving RYR2 inhibition. When CASQ2 dissociates from the RYR2 complex, RYR2 channel activity is maximally activated[53–55].

SR luminal calcium content is regulated by RYR2 (extrusion) and SERCA2a (uptake). Both of these proteins are mediated by their (or their regulatory proteins') potential to be in a phosphorylated or unphosphorylated state. Phosphorylation occurs in response to β-AR stimulation.

β-adrenergic receptor stimulation

Three subtypes of cardiac β-ARs have been identified: β_1-AR, β_2-AR, and β_3-AR. In a healthy human heart β_1-ARs are the predominant subtype to be expressed; β_2-ARs and β_3-ARs are expressed to a lesser extent[56,57]. β-ARs are G protein coupled receptors (GPCRs) mediated by the catecholamines, adrenaline and noradrenaline. The receptors undergo a conformational change on binding of these catecholamines. The induced exchange of guanosine diphosphate for guanosine triphosphate activates G_α and $G_{\beta\gamma}$ protein subunits as they dissociate. The G_α subunit is then able to regulate downstream effector molecules. Activation of the stimulatory G_α protein subunit in turn activates adenylyl cyclase which catalyses the conversion of adenosine triphosphate (ATP) into cyclic adenosine monophosphate (cAMP). The subsequent rise in cAMP triggers the protein kinase A (PKA) pathway. Several effector molecules are consequently phosphorylated leading to increased chronotropy, inotropy, and lusitropy[58]. The calmodulin dependent protein kinase II (CaMKII) signalling pathway is also activated following β-AR stimulation although the mechanism of activation and subsequent roles of CaMKII are poorly understood. It is generally accepted however that CaMKII and PKA pathways share many intracellular target proteins[59].

Regarding the modulation of RYR2, β-AR stimulation can have direct and indirect effects. Phosphorylation of RYR2 increases the sensitivity of the receptor to changes in cytosolic calcium levels. Indirectly, phosphorylation of phospholamban (PLN, regulatory protein of SERCA2a) disinhibits SERCA2a calcium reuptake hence elevates SR calcium content. Phosphorylation of LTCCs increases permeability and therefore calcium influx into cardiomyocytes, promoting CICR[60,61].

1.4.2 RYR2 channel dysfunction and cardiac arrhythmias

Dysfunction of RYR2 is caused by mutations within the *RYR2* gene and genes encoding for proteins which regulate or modulate the RYR2 channel. As a result calcium handling within cardiomyocytes can be altered (impaired SR storage and release) and lead to arrhythmic activity. Mutations cause calcium leak from the SR during diastole, particularly following β-AR stimulation. How the mutations and β-AR stimulation lead to arrhythmias is not fully established. One of the first explanations suggested that

mutations increase the open probability of RYR2 channels and decrease the critical threshold level for calcium waves[62]. Although leaky RYR2 channels would decrease the calcium release threshold, calcium extrusion would diminish SR calcium content and terminate the spontaneous releases. A further two explanations are that following stimulation of β-ARs SR calcium content is increased due to activated SERCA2a and LTCCs, or that phosphorylation of RYR2 decreases the threshold level for calcium waves[63]. Additionally, impaired refractory behaviour of RYR2 channels must be induced[64].

Irrespective of the explanation, the SR becomes overloaded with calcium triggering spontaneous calcium releases during diastole (SOICR). This begins as a localised event (calcium spark) but as the calcium spreads it can trigger further calcium releases from neighbouring calcium release units (CICR). This is a calcium wave (Figure 1.4A). The increased diastolic intracellular calcium concentration causes oscillations in the membrane potential activating calcium sensitive currents. Forward direction NCX (extrusion of one calcium ion, influx of three sodium ions) is triggered and hence an influx of net positive charge. Consequently, the cell depolarises as the membrane potential becomes less negative and triggers a DAD (Figure 1.4B). If the depolarisation activates additional sodium currents, the amplitude can reach the threshold required to initiate a propagating action potential[29]. The cycle length (time between action potentials) reduces, raising the heart rate and promotes the degeneration of DADs into sustained arrhythmic activity: ventricular tachycardia and ventricular fibrillation.

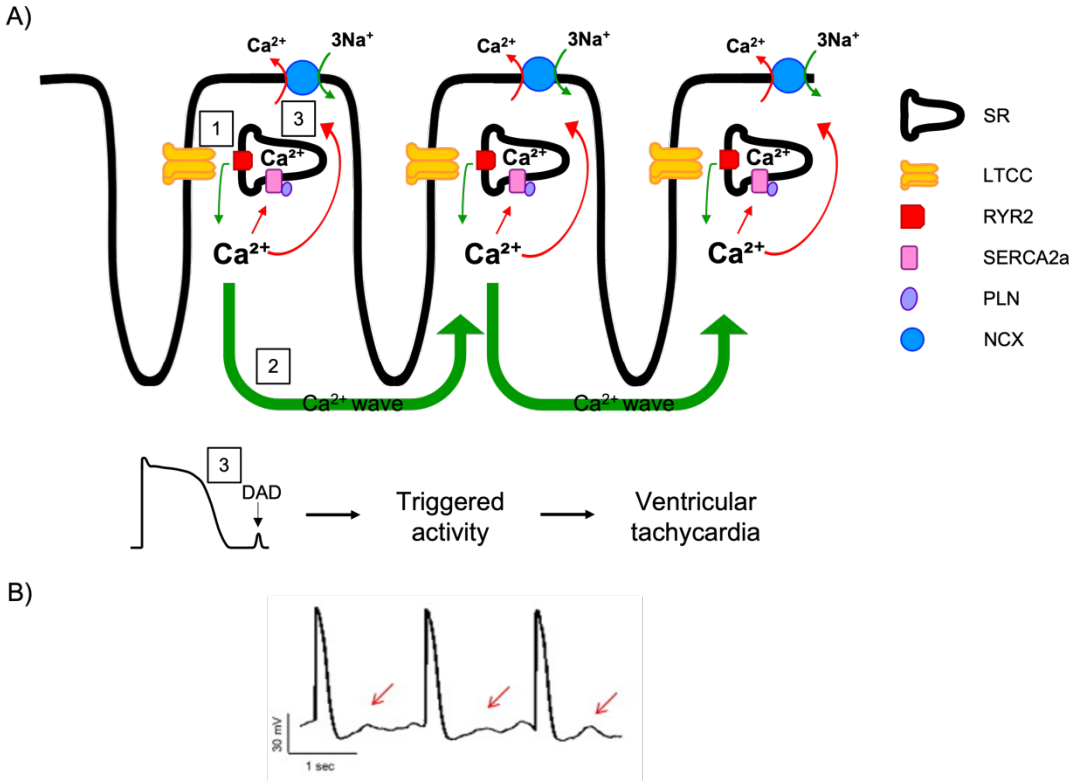

Figure 1.4: Development of arrhythmias due to RYR2 dysfunction

(A) [1] Sarcoplasmic reticulum (SR) is overloaded with calcium. A threshold level is reached triggering spontaneous calcium releases through open ryanodine receptor 2 (RYR2) channels. [2] This calcium spark moves across the cell and opens neighbouring RYR2 channels. Further calcium is released into the cytosol leading to a calcium wave. [3] Calcium is removed by SR calcium ATPase (SERCA2a) and sodium-calcium exchanger (NCX). Forward direction NCX results in a net inward current resulting in delayed afterdepolarisations (DADs) which can degenerate into ventricular arrhythmias. LTCC, L-type calcium channel; PLN, phospholamban. (B) Example action potential trace from human induced pluripotent stem cell derived cardiomyocytes harbouring an RYR2 mutation, note the development of phase 4 afterdepolarisations (red arrows). Trace taken from Itzhaki *et al.* 2012[65].

1.5 Catecholaminergic polymorphic ventricular tachycardia

CPVT was first described by Reid *et al*. in 1975[66]. It is a rare (estimated prevalence of 1:10,000) inherited disorder characterised by adrenergically mediated arrhythmias. It is usually inherited in an autosomal dominant manner meaning the affected individual requires only one mutant gene for disorder manifestation[67]. Due to its hereditary nature CPVT usually presents in early life. The median age for symptom onset is 9 years for probands and 12 years for carriers[68]. A family history of unexplained SCD under the age

of 40 years is reported in a third of individuals diagnosed with CPVT[36], and often this is the first indication of CPVT existing within a family. During times of emotion, exertion or stress some individuals harbouring a CPVT-causing mutation experience syncopal events (dizziness, fainting, loss of consciousness) and seizures, but many individuals are asymptomatic. This is because mutations demonstrate incomplete penetrance. Incomplete penetrance is a phenomenon in which only a proportion of all individuals harbouring a pathogenic mutation display a clinical phenotype - complicating diagnosis[36,68].

Diagnosing CPVT remains challenging as patients display a structurally normal heart and present with a normal resting ECG. In order to confirm a CPVT diagnosis bidirectional or polymorphic ventricular tachycardia must be induced upon an exercise-induced stress test[36,68]. This reproduces the catecholaminergic response typical of the cardiac phenotype. In suspected CPVT cases genetic testing for mutations in *RYR2 and CASQ2* is also recommended by experts to help with diagnosis[69]. However genetic testing can create further challenges as false positive variants or variants of unknown significance (VUS) may be reported[70]. In these cases a genetic variant (an alteration from the most common DNA nucleotide sequence) is identified but it may be benign or its' effect may be unknown respectively.

Mutations observed in *RYR2* cause CPVT1, and these account for approximately 50% of CPVT cases[36]. Mutations in genes that encode for other proteins involved in calcium handling and that mediate the activity of RYR2 can also cause subtypes of CPVT. To date five subtypes have been reported[12] (Table 1). Throughout this thesis CPVT will refer to CPVT1 only.

Subtype	Gene	Protein	Inheritance pattern
CPVT1	*RYR2*[36,71]	RYR2	Autosomal dominant
CPVT2	*CASQ2*[72,73]	Calsequestrin 2	Autosomal recessive
CPVT3	*TECRL*[74]	Trans-2,3-Enoyl-CoA Reductase Like	Autosomal recessive
CPVT4	*CALM1*[75,76]	Calmodulin 1	Autosomal dominant
CPVT5	*TRDN*[77]	Triadin	Autosomal recessive

Table 1: Summary of CPVT subtypes

1.5.1 Interventions for the prevention and treatment of arrhythmias in CPVT

Without treatment the outlook for CPVT patients is poor - mortality by the age of 30 years is approximately 30%[78]. Currently no specific RYR2-targeting or completely effective treatment exists. An expert consensus of recommendations has been published regarding the specific treatment of CPVT, including pharmacological and non-pharmacological treatments (Table 2)[79,80]. The strength of recommendation is classified according to a review of the published evidence for CPVT management.

Class	Recommendation
I	Lifestyle changes; treatment with β-blockers for symptomatic patients; and implantable cardioverter defibrillator (ICD) implantation in patients who suffer cardiac arrest or symptom manifestation despite optimal medical management
IIa	Addition of flecainide to β-blockers and/or ICD in patients who suffer symptom manifestation despite β-blocker treatment or experience appropriate ICD shocks
IIb	Left cardiac sympathetic denervation (LCSD) in patients who experience syncope, ventricular tachycardia or several appropriate ICD shocks whilst taking β-blockers (±flecainide) and in patients with an intolerance/contraindication to β-blockers
III	ICD is not indicated as a standalone therapy in asymptomatic, diagnosed CPVT patients. Also programmed electrical stimulation is not indicated in any CPVT patients

Table 2: Expert consensus recommendations for CPVT therapeutic intervention

Lifestyle changes

Due to the catecholaminergic-adrenergic nature of CPVT, situations which may provoke a catecholamine surge are recommended to be limited or avoided. Such situations include taking part in strenuous exercise and competitive sports, and exposure to stressful environments[79].

Drug therapy

Treatment with β-blockers is the mainstay for CPVT. They provide protection from arrhythmias by competing with catecholamines for β-ARs. Binding of β-blockers to β-ARs inhibits stimulation and downstream signalling that can directly and indirectly impact RYR2 activity and SR calcium content. Currently, nadolol is the clinically preferred drug therapy - a long lasting, non-selective β-blocker. Reports indicate nadolol is more effective than other β-blockers[81], and more specifically β_1-selective β-blockers (metoprolol and bisoprolol)[82], at preventing cardiac events such as ventricular

arrhythmias in patients with CPVT. Omitted from these studies, the effective non-selective β-blocker carvedilol has been shown to also have direct effects on RYR2. Novel carvedilol analogues (e.g. VK-II-86)[83] and the *R*-carvedilol enantiomer[84] alter RYR2 gating and decrease RYR2 channel opening duration respectively; preventing spontaneous calcium waves whilst exhibiting minimal β-blockade.

Despite being the frontline agents for CPVT, β-blockers provide incomplete protection from the recurrence of arrhythmic events in a proportion of patients. Follow-up studies have reported over 25% of patients experience treatment failure[81,85] – highlighting the requirement for more effective treatments.

Suboptimal adherence is also a common problem, leaving patients vulnerable to symptoms and SCD. β-blocker non-compliance accounts for approximately 5% of SCDs in CPVT[86]. Factors associated with low compliance include adverse side effects caused by the high doses of β-blockers required[86]; young age; poor understanding of their condition; and low confidence in ability to take medication each day[87].

Often when β-blockers fail to fully control arrhythmic events dual therapy with flecainide is directed. Flecainide is predominantly considered as a sodium channel inhibitor; acting upon the activated state of $Na_v1.5$ channels, where it blocks the pore and inhibits sodium current. With respect to arrhythmic events observed in CPVT flecainide increases the threshold required to trigger an action potential, and reduces intracellular sodium influx thus promoting NCX calcium efflux. Consequently, the decreased intracellular calcium concentration/SR calcium content reduces the incidence of spontaneous SR calcium release[88]. However there is also suggestion flecainide can act directly on RYR2, reducing channel open time[89].

At present only small studies have reported on the efficacy and safety of flecainide. In a study of 29 genotype-positive CPVT patients, 76% displayed an improved exercise-induced ventricular arrhythmia score following addition of flecainide to their standard therapy. Furthermore in 48% of patient's addition of flecainide completely suppressed ventricular arrhythmias[90]. A second study assessed eight CPVT patients harbouring pathogenic *RYR2* mutations as they were transitioned from β-blocker therapy to

flecainide. The study concluded flecainide monotherapy was at least as effective as standalone β-blockers at reducing exercise-induced arrhythmia however combination therapy was likely to be most effective at suppressing arrhythmias[91]. More recently a randomised placebo controlled clinical trial was conducted. Patients recruited had a clinical CPVT diagnosis, a functioning implantable cardioverter defibrillator (ICD) in place and a stable dosage of β-blocker therapy. A significant reduction in ventricular ectopy during exercise was observed during combined therapy compared with placebo and with β-blocker monotherapy. No change was reported between baseline and placebo[92]. These studies indicate flecainide is better tolerated than β-blockers and also suggest a proportion of the cardiac events observed during flecainide treatment were a result of a suboptimal β-blocker agent/dosage. Nevertheless to establish flecainide monotherapy for CPVT larger trials are required to determine its efficacy.

Also as a combination therapy, β-blockers and calcium channel antagonists, such as verapamil, can be prescribed to patients with a CPVT diagnosis. Calcium channel blockers inhibit the LTCC, reducing calcium influx and CICR. Additionally, cAMP-mediated effects on LTCC will be lessened[93]. Similarly to flecainide, verapamil has been suggested to directly interact with RYR2[94]. The combined therapy of a β-blocker and verapamil has been indicated to decrease exercise-induced arrhythmic activity and increase the threshold heart rate at which arrhythmias initiate compared to β-blocker treatment alone[93,95].

Implantable cardioverter defibrillator

The implantation of ICDs for the management of CPVT is considered controversial. ICD implantation is used for the prevention of sudden death; particularly in CPVT patients who have suffered an aborted cardiac arrest, or recurrent syncope despite optimal drug therapy[79]. Despite offering appropriate and a potentially life-saving shock upon detection of ventricular fibrillation, the use of ICDs is complicated by the unique characteristics of CPVT. In a retrospective study of CPVT patients who had undergone ICD implantation, 68% of appropriate shocks were ineffective at terminating sustained arrhythmia and restoring sinus rhythm. Accounting for 91% of the ineffective shocks, the complex characterised triggered activity (bidirectional and polymorphic ventricular tachycardia) of CPVT did not respond to the ICD shocks[96].

A further issue with ICD therapy is the occurrence of inappropriate shocks. Inappropriate shocks are usually the result of lead failure or non-ventricular tachycardias. The pain, and thus psychological and emotional stress associated with the experience can trigger a catecholamine surge, and hence be pro-arrhythmic. In a second retrospective review of ICD efficacy in CPVT patients, 46% of patients suffered inappropriate shocks. Of these patients 29% experienced electrical storm events secondary to ICD firing[97].

Re-intervention during follow-up due to surgical or device complications is also a frequent problem. Additionally, the explantation of old devices and subsequent implantation of a new device is required at regular time points as a result of battery depletion and device upgrades[98]. This is accentuated by the younger nature of CPVT patients, and in combination with the psychological effects of ICD shocks has been associated with a reduced quality of life[99].

Left cardiac sympathetic denervation

Left cardiac sympathetic denervation (LCSD) has become an established therapy for CPVT patients who experience syncope or cardiac events despite optimal drug therapy and ICD implantation. The surgery results in reduced cardiac sympathetic activity by interrupting neural pathways and inhibiting the release of catecholamines[100]. Furthermore it has been shown that LCSD does not reduce heart rate or ventricular performance[101] as the right-sided sympathetic nerves are known to predominantly control the sinus node[102] and contribute to left ventricular innervation[103].

LCSD has been demonstrated to be anti-arrhythmic in CPVT. An initial case series of three symptomatic patients were asymptomatic following LCSD[104]. More recently an international study was conducted. Despite optimal medical therapy 70% experienced major cardiac events (defined as syncope, aborted cardiac arrest or ICD appropriate discharges) prior to LCSD. Following LCSD only 22% of patients suffered a major cardiac event. Moreover the mean annual rate of event per patient decreased by 92%[105].

CPVT remains difficult to manage. The mainstay therapy, β-blockers, do not fully protect many patients from arrhythmic activity and due to the high dose requirement the majority of patients suffer side effects which leads to a lack of adherence[81,85]. Additional available therapies aid in the protection from CPVT, often when in combination with a β-blocker, but insufficient evidence exists for their use as monotherapies. Consequently, the development of novel therapeutics for the treatment of CPVT is required.

1.6 Modelling cardiac channelopathies in animals

Studying human heart (patho)physiology is consistently challenged by the lack of a reliable model system. The inaccessibility of human cardiac tissue, and limited ability to perform in-depth cardiac electrophysiology and arrhythmogenesis investigations in human patients means animal models, particularly rodents, have been heavily relied up on. Transgenic or genetically modified animal models have been generated to recapitulate and understand the underlying mechanisms of cardiac channelopathies and arrhythmogenesis. Furthermore, novel anti-arrhythmic treatments and their mechanisms have been identified. Yet despite many positive and important contributions to cardiovascular research, animal models differ in their genetics; physiology; and pharmacokinetics. Inevitably this means they often do not fully reflect human disease complexity and frequently experimental results do not translate to humans[106].

1.6.1 Small animal models

Mouse models

In addition to the considerably different dimensions of mouse and human hearts, at rest the mouse has a heart rate of ~600 beats per minute – 10 times faster than humans. To function at such high heart rates, mouse cardiomyocytes have a short ventricular action potential (50 ms vs 250 ms in humans), with pronounced differences in the expression and functional relevance of contributing ion channel proteins and currents, calcium handling, and contractile machinery. In the mouse waveform, the phase 2 plateau is absent and displays a rapid repolarisation as the LTCC current contributes to a lesser extent. The repolarisation phase is primarily driven by potassium I_{to} currents in mice, as opposed to the potassium I_{Kr} and I_{Ks} currents of humans[107,108]. There are also differences

in the intracellular calcium removal process during diastole. In humans SR calcium reuptake and NCX extrusion account for 70% and 30% of calcium removal respectively, while in mice SR calcium reuptake accounts for 90%[108]. Furthermore, humans predominantly express the slow β-myosin heavy chain (MHC) contractile proteins, whilst fast α-MHC proteins are found in mice[106]. As a result of these differences, mouse models have been generated targeting native mouse proteins and by introduction of mutated human proteins[109]. Despite the low incidence of ventricular arrhythmias in mice, they have been used to model LQTS, BrS and CPVT.

LQTS has been the most widely modelled[109,110]. Mouse models with altered potassium channel expression have only partially mimicked the human LQTS phenotype. On the whole they have demonstrated the characteristic prolongation of the action potential and/or QT interval[111–115]; however few models also exhibited spontaneous or inducible ventricular arrhythmia[113,116,117]. It is suggested mice are protected from arrhythmic activity due to a physiological compensatory mechanism as multiple models demonstrated upregulation of an unaffected repolarising current[111,118,119]. This means no viable model of LQT1 or LQT2 exists. In contrast, mice modelling sodium channel-associated LQTS have exhibited a prolonged action potential duration and QT interval, and also displayed the arrhythmic phenotype with the occurrence of spontaneous or inducible ventricular arrhythmia[120–125]. Furthermore the underlying mechanism observed in humans was indicated in these models, although an additional pro-arrhythmic mechanism not reported in humans has also been indicated[120,121].

As with CPVT, β-blockers are the mainstay treatment for LQTS. Nevertheless extensive assessment of β-blockers has presented conflicting data regarding their anti-arrhythmic effect in mouse models[122,124,125]. Sodium channel blockers have also been evaluated in mouse models harbouring sodium mutations[121,122,124]. Their suppression of arrhythmias in mice, and subsequent clinical data, has led to them being indicated with caution (due to non-selective inhibition) as a recommended add-on therapy in the European Society of Cardiology guidelines for the prevention of SCD (2015)[80].

Patients with BrS display an elevated ST segment and often experience conduction abnormalities including prolonged PR and QRS intervals[126]. Most pathogenic variants are

located in the *SCN5A* gene, which encodes for the alpha subunit of the cardiac sodium channel[127]. BrS features: reduced sodium channel expression and current, and conduction abnormalities, have been reported in mouse models[128–130]. However, only the heterozygous knockout mouse model exhibited monomorphic ventricular tachycardia[128]. This is of note as no mouse model of BrS has recapitulated the ECG pattern (polymorphic ventricular tachycardia) observed in BrS patients without additional pharmacological induction[131,132].

Several CPVT mouse models have also been successfully generated - harbouring genetic modifications to RYR2[133–139] and CASQ2[140–142]. Abnormal calcium handling was observed in all models at the minimum following adrenergic stimulation/caffeine challenge but many also displayed the bidirectional/polymorphic ventricular tachycardia characteristic of CPVT. Anti-arrhythmic pharmacological challenges however have shown mixed success in mice. Suppression of arrhythmic activity with β-blockers has exhibited unreliable efficacy[133,142]; although this is consistent with clinical studies in patients[36,81,85]. Of class I anti-arrhythmic drugs only those that directly inhibit RYR2 (flecainide and propafenone) effectively suppressed exercise-induced ventricular arrhythmia[89,143]. Consequently the addition of flecainide to standard therapy was evaluated in CPVT patients[89,90]. Due to its' effectiveness, it is now recommended as an additional therapy to β-blockers in patients who experience recurrent syncope or ventricular tachycardia[80]. However, notably flecainide failed to prevent CPVT in mice with a severe phenotype[142,144]. The calcium channel blocker verapamil has also been shown to significantly lower the prevalence of arrhythmic activity in mice. Furthermore, when combined with the β-blocker propranolol, at doses ineffective as monotherapies, arrhythmias were completely abolished[142]. Yet in CPVT patients the results of combined therapy have been mixed[95,142].

Rabbit models

Many aspects of the rabbit myocardium have greater similarity to humans than rodents. Rabbit heart rates for example range from 200-300 beats per minute[106] – still higher than humans but much lower than mice. The cardiac electrophysiological, calcium handling and mechanical characteristics of rabbits are also more representative of humans: the prominent plateau phase that conveys action potential shape and is absent

in rodents is present; both predominantly rely on I_{Kr} and I_{Ks} repolarising currents; the respective contributions of SERCA2a and NCX for intracellular calcium removal are comparable, and the β-MHC contractile protein isoform predominates[106,109,145–147].

Rabbit models of LQTS are cardiac-specific overexpression of dominant-negative mutated human genes encoding for voltage-gated potassium channels. Similarly to mouse models, prolongation of the action potential duration is observed in rabbit models, however only models of LQT2 have developed spontaneous ventricular tachycardia and resulted in SCD[148]. The incidence of arrhythmia in LQT1 rabbits was not significantly different to littermate controls at baseline[148,149]. However sympathetic stimulation by exposure to isoprenaline induced persistent early afterdepolarisations at the cellular and organ level in LQT1 rabbit hearts[23]. Continuous tachypacing of LQT1 rabbit models also significantly increased arrhythmogenesis[150]. In contrast, LQT2 rabbit hearts demonstrated early afterdepolarisations prior to and immediately after initial isoprenaline exposure before being abolished[23]. These observations are in line with genotype-specific arrhythmia triggers in LQTS patients; persistent elevation of adrenergic tone (e.g. during exercise) in LQT1 and sudden sympathetic surges (e.g. auditory startle) in LQT2[22,151].

To date, rabbit models of BrS and CPVT do not exist. Classic approaches for the generation of transgenic rabbit models have low efficiency and limitations regarding the sizes of the genes that can be targeted[147]. Consequently, attempts to generate rabbit models of cardiac arrhythmia diseases associated with larger genes, such as *RYR2,* have failed[152]. The recent advances and continued improvement of new genome-editing techniques has led to the successful creation of knock-out rabbit models of different diseases associated with lipid metabolism and atherosclerosis[153,154]. With modifications to the technique, the ability to produce novel rabbit models of monogenic cardiac diseases and channelopathies like BrS and CPVT, with point mutations in large genes such as *SCN5A* and *RYR2*, might soon be feasible[147].

1.6.2 Large animal models

Large animal models (canine, porcine, ovine) share many cardiac characteristics with humans. Electrophysiological aspects: heart rate, action potential waveform and

currents, and the respective SERCA2a and NCX contributions to intracellular calcium removal are all comparable to humans[106]. Nevertheless some differences are reported. Despite the main ionic currents in canine cardiac cells appearing very similar to humans, differences exist in the quantitative contribution of some repolarising currents, and as a result their sensitivity to pharmacological agents[155,156]. The ionic currents and calcium handling properties of the porcine action potential are less well-studied however a species-dependent current difference responsible for phase 1 repolarisation is reported. In humans $I_{to,\ 1}$ ($I_{to,\ f}$ and $I_{to,\ s}$) is responsible but in pigs these currents have been shown to be absent and $I_{to,\ 2}$ active[157]. Dogs and sheep (and rabbits) express both $I_{to,\ 1}$ and $I_{to,\ 2}$[157]. Sheep are considered to be more resilient to ventricular arrhythmias and SCD than humans[158]. The contraction mechanics of large animals also correspond to those of humans. Each expresses the slow β-MHC isoform of cardiac myosin, demonstrates similar contraction kinetics, and exhibit positive force-frequency responses[106].

A porcine model of BrS was developed harbouring a mutation in the *SCN5A* gene[159]. The reduced expression level of the $Na_v1.5$ protein resulted in a lower current density and a slower conduction velocity. Furthermore, the experimental hearts demonstrated an increased susceptibility to spontaneous and inducible ventricular arrhythmia not seen in wild-type controls. The characteristic BrS-type ECG pattern was not observed however. Pharmacological modulation of arterially perfused canine ventricular wedges have also been utilised to model LQT2 and LQT3[160], and BrS[161,162]. The models have been used to mimic and understand the contribution of transmural differences in action potential morphology in these arrhythmic diseases.

1.6.3 The *perfect* model

The perfect animal model to study cardiac electrophysiology does not exist. No animal heart fully represents the cardiac physiology of humans, and therefore the clinical relevance of animal-based research studies is continually challenged. Given their similarity, thus increased relevance to humans, large animal models are often preferred. Nevertheless, the expense of housing and maintaining the animals, in addition to ethical restrictions and current difficulties producing genetically modified models, means mouse models are often utilised instead. In spite of their limitations (significant species-

specific differences and ability to electrically remodel) mice are easy to breed, relatively cheap to house and can be genetically modified.

The discovery and development of human induced pluripotent stem cells (hiPSCs)[163,164] has provided a new and exciting model with the potential to study the human heart and related diseases. Compared to established animal models, hiPSCs have advantageous properties[165]: 1) hiPSCs are reprogrammed somatic cells with the ability to self-renew, this means they provide an unlimited pluripotent cell source; 2) unlike with human embryonic stem cells the ethical issues and restrictions are much less due to their *in vitro* derivation; 3) hiPSCs harbour the same genetic and epigenetic background of the individual they are isolated from; and 4) hiPSCs can be differentiated into derivatives of the three germ layers and thus into any cell type.

Within the field of cardiovascular sciences, hiPSC-derived cardiomyocytes (hiPSC-CMs) are already being utilised for multiple applications due to these outlined benefits. Firstly, they are routinely being used for a diverse range of basic science studies, from RNA and protein biochemistry to cellular electrophysiology. Moreover, as hiPSCs maintain the same genetic background as the donor, they provide the opportunity to model inherited cardiac diseases and develop patient-specific therapies, including in regenerative medicine. In the pharmaceutical industry, hiPSC-CMs are being applied for use in drug development and as a tool for screening compounds for cardiotoxicity.

1.7 Human induced pluripotent stem cell derived cardiomyocytes

Human iPSCs are generated through the reprogramming of adult human somatic cells; the major sources of which are dermal fibroblasts[164] and peripheral blood[166]. The cultured cells are dedifferentiated by the transduction of transcription factors known to induce pluripotency (OCT4, SOX2, c-Myc and Klf4)[164,166]. Pluripotent stem cells are characterised by their ability to self-renew indefinitely and give rise to cells from all three embryonic germ layers: ectoderm, endoderm and mesoderm[167]. Specialisation, or differentiation, occurs in response to intracellular and extracellular factors.

The cardiac cells of the mammalian heart derive from the mesoderm lineage, with signals beginning during embryogenesis and continuing through foetal development. Mesoderm formation and cardiogenesis are controlled by three families of growth factors: transforming growth factor β proteins, and Wingless/INT (Wnt) proteins and fibroblast growth factors[168]. Through mimicking the activity of signalling pathways from developmental biology, successful *in vitro* differentiation of hiPSCs to cardiomyocytes has been demonstrated.

1.7.1 Generation of hiPSC-CMs

The first 2D monolayer hiPSC directed cardiac differentiation protocols involved the sequential application of activin A and bone morphogenetic protein (BMP) 4 growth factors (transforming growth factor β cytokines), in serum-free medium, to induce mesoderm derivatives and cardiac lineage specification; initially demonstrated in human embryonic stem cells[169] prior to hiPSCs[164]. Sequential treatment with activin A and BMP4 induces key endogenous canonical Wnt ligands as shown by addition of Wnt3a (a canonical Wnt ligand) or Dkk1 (a canonical Wnt inhibitor) during directed differentation[170].

Wnt proteins are signalling molecules that initiate an array of intracellular signalling pathways. The canonical Wnt/β-catenin pathway plays a critical role in cardiogenesis[171]. In the absence of Wnt ligands, cytoplasmic β-catenin levels are maintained low through phosphorylation by glycogen synthase kinase 3β (GSK3β), a component of the β-catenin destruction complex. β-catenin is subsequently ubiquitylated and degraded by the proteosome[172]. On binding of Wnt ligands to a receptor complex (Frizzled receptor and low-density lipoprotein receptor-related protein), phosphorylation of β-catenin by GSK3β is inhibited. As a result β-catenin accumulates in the cytoplasm and is translocated to the nucleus where it regulates transcription of Wnt target genes[172]. Studies have identified a required biphasic role of Wnt/β-catenin signalling for cardiogenesis: potentiation prior to specification of germ layer, and attenuation during cardiac mesoderm induction (Figure 1.5). Activation of the pathway during mesoderm specification inhibits cardiomyocyte formation[170,173].

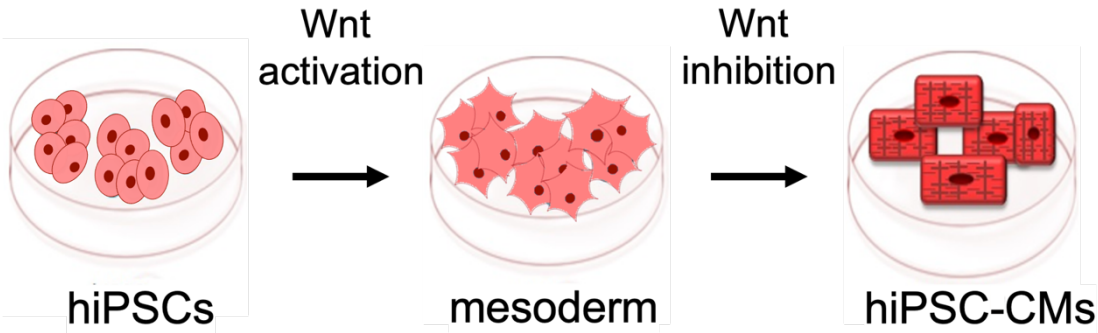

Figure 1.5: Schematic diagram of hiPSC-CM generation

Biphasic role of Wnt signalling for hiPSC differentiation to cardiomyocytes – induction followed by inhibition.

In line with this knowledge a second protocol for directed cardiac differentiation, based on temporal Wnt signalling modulation using small molecules (agonist followed by antagonist), was developed by Lian *et al*.[174]. It should be noted however that the application of these directed differentiation protocols to multiple cell lines has highlighted variability in cardiomyocyte yield – particularly the growth factor-based method. The requirement for stage-specific optimisation for each individual cell line is indicated due to pattern differences in endogenous signalling and cell culture confluency[170,175–177].

Spontaneously contracting cardiomyocytes can usually be visually observed by day 10 of differentiation[178,179]. Early characterisation analysis indicated the development of heterogenous cardiomyocyte populations (atrial, nodal and ventricular-like cells)[179–181], and further characterisation revealed the hiPSC-CMs exhibit an immature phenotype when compared to native adult cardiomyocytes[182–185].

1.7.2 Comparison of hiPSC-CMs to native adult human cardiomyocytes

The characteristics of hiPSC-CMs have been described as being more comparable to foetal human cardiomyocytes than adult human cardiomyocytes with regards to their morphology, intracellular structure (schematically illustrated in Figure 1.6), and functional properties. The low degree of hiPSC-CM maturity is a major limiting factor in

achieving their full potential and is ultimately hindering their implementation as a biological research tool.

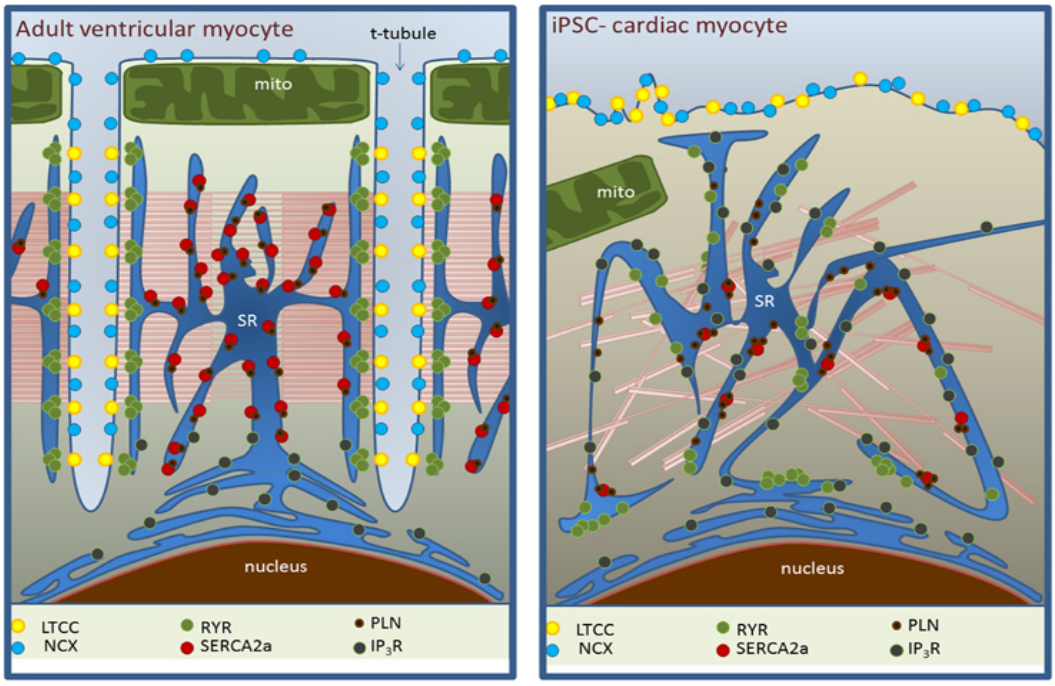

Figure 1.6: Ultrastructural differences between native adult cardiomyocytes and hiPSC-CMs

The absence of a T-tubular network is associated with a lack of regular organisation and localisation of L-type calcium channels (LTCCs) with ryanodine receptor 2 (RYR2) channels in the dyads. Reduced SR calcium ATPase (SERCA2a) and sodium-calcium exchanger (NCX) expression slows calcium extrusion during diastole. IP_3R, inositol-triphosphate receptor. Mito, mitochondria. PLN, phospholamban. SR, sarcoplasmic reticulum. Image taken from Kane *et al*. 2015[186].

Morphology and structure

Adult human ventricular myocytes are characteristically rod-shaped and have a length to width aspect ratio mean of approximately 7[187,188], with typical length and width measurements of 100-150 μm and 20-35 μm respectively[189,190]. They are often binucleated with a well-aligned and highly organised surrounding intracellular structure. Sarcomeres become increasingly organised with development, exhibiting a longitudinal pattern oriented perpendicular to the long axis[191,192]. An extensive SR and T-tubular network localises key calcium handling proteins, forming dyads throughout the cells. These structures are critical for rapid, uniform SR calcium release and synchronous contraction[193,194]. Furthermore mitochondria are regularly distributed, occupying approximately 25% of cell volume[195].

Human iPSC-CMs are much smaller and form in a variety of shapes including round, triangular, elongated and irregular[196,197]. Additionally, limited binucleation of hiPSC-CMs has been observed and internal structures are disorganised/immature: sarcomeres are shorter and generate radial or irregular patterns[191,198]; the SR is underdeveloped; they lack the presence of T-tubules[199]; and have long, slender mitochondria which cluster around the nucleus and in the cell periphery[196].

Electrophysiology and calcium handling

Adult ventricular cardiomyocytes require electrical stimulation to initiate the process of EC coupling. Key ionic currents including I_{Na}, I_{Ca}, I_{to}, I_{Kr}, I_{Ks}, and I_{K1} underlie the ventricular action potential phases[8]. During the plateau phase, the influx of extracellular calcium triggers a further release of calcium from the SR. A co-ordinated rise of intracellular calcium throughout the cell is important for the synchronised contraction of the sarcomeres. In the relaxation phase, calcium is removed from the cytosol back into the SR by SERCA2a and extruded from the cell via NCX[39,40] (refer to see section 1.3).

Cultures of hiPSC-CMs display mixed action potential morphologies (atrial, nodal and ventricular-like) and often beat spontaneously. The funny (I_f) current, usually expressed in pacemaker cells only, has been shown to be present and is suggested to contribute to the spontaneous activity[181,200,201]. Moreover the I_{K1} current, responsible for stabilising the resting membrane potential, is minimal or absent[181,200,202]. Consequently, the maximum diastolic potential is less negative and the threshold for an action potential is reached more readily. The characteristics of the cardiac I_{Na} and I_{Ca} currents, responsible for the action potential upstroke and plateau phases respectively, appear to be relatively comparable with adult cardiomyocytes. The slower recovery from inactivation indicated of the I_{to} current and the relatively depolarised resting membrane potential could explain the less pronounced action potential notch (phase 1)[203]. The presence of the delayed rectifier potassium current I_{Ks} has been detected in multiple studies but only in a fraction of assessed cells and at low densities[181,204–206]. In contrast I_{Kr} has been shown to play a prominent role in the repolarisation phase[203]. These similarities and differences are summarised in Figure 1.7. Furthermore, the underdeveloped SR and absent T-tubular network mean hiPSC-CMs do not have rapid, uniform SR calcium releases or

optimal calcium transient dynamics[196,199,207]. It has been reported that the SR calcium contribution to calcium transients is less than 30%[199].

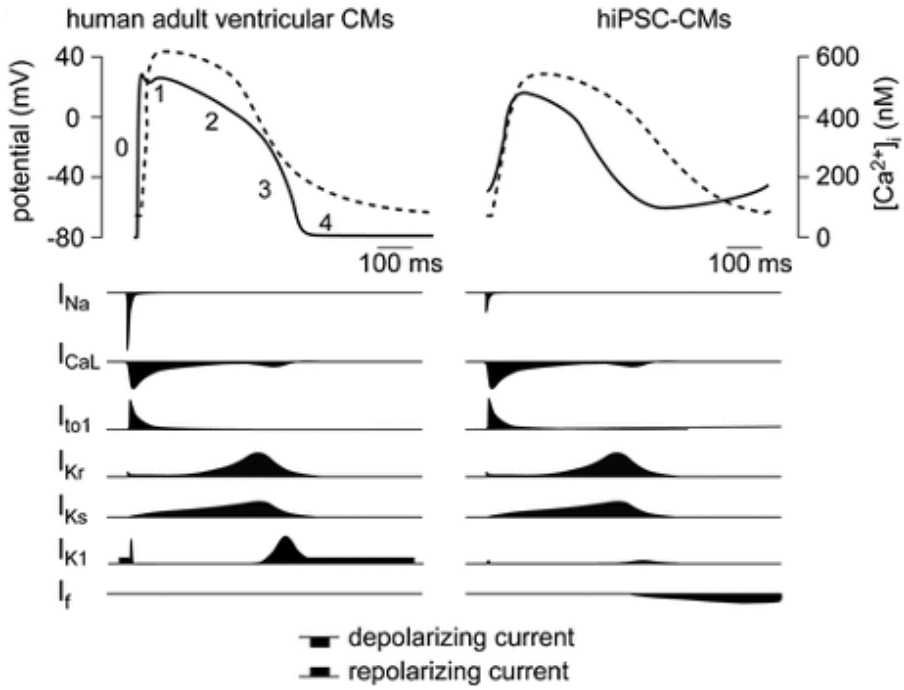

Figure 1.7: Electrophysiological phenotype differences between human adult ventricular cardiomyocytes and hiPSC-CMs

Examples of action potential (solid line) and calcium transient (dashed line) profiles, with schematic representation of the time course and magnitude of ionic currents in human adult ventricular myocytes (left) and hiPSC-CMs (right). Figure taken from Casini *et al.* 2017[203].

β-adrenergic receptor signalling

The intrinsic signalling pathway initiated following catecholamine stimulation of β-ARs was previously described in section 1.4.1. The pathway is a key modulator of cardiac calcium handling and contractility. In native adult cardiomyocytes β_1-AR are the predominant subtype, distributed across the entire cell surface. In contrast β_2-ARs and their respective cAMP signalling are compartmentalised by structural restriction to caveolae and T-tubules[208,209].

Evaluation of hiPSC-CM β-ARs expression indicated β_2-ARs to be the dominant subtype. Low production of isoprenaline-mediated cAMP was exhibited and attributed to relatively low expression of β-ARs and adenylyl cyclases. Correspondingly low levels of PKA-mediated phosphorylation of target proteins were reported. Furthermore a lack of

β_2-AR compartmentalisation was observed in the absence of a T-tubular network and reduced expression of functional caveolae[210].

Metabolism

The foetal heart is predominantly reliant on glucose as its metabolic substrate[211]. This is due to a hypoxic, high lactate, low fatty acid environment where there is an abundance of glycolytic enzymes and low mitochondrial content[212]. Following birth there is an increased workload, thus energy demanded of the heart that can only be met by mitochondrial fatty acid oxidation and ATP production. Accordingly mitochondrial biogenesis increases, improving the oxidative capacity and becoming the major source for energy production in adult cardiomyocytes[211,212].

Consistent with the accepted understanding that hiPSC-CMs are immature, it has been demonstrated that they utilise glycolytic metabolism for their energy production, instead of fatty acid metabolism[213,214].

Cardiac gene expression

During foetal to adult cardiomyocyte maturation, some genes undergo a complete transition or a switch in the predominantly expressed isoform. Sarcomeric genes are examples. Three isoforms of troponin I have been discovered: slow skeletal (ssTnI, *TNNI1*), fast skeletal (*TNNI2*), and cardiac (cTnI, *TNNI3*). During cardiac development, both ssTnI and cTnI isoforms are expressed. Yet after birth, ssTnI is completely substituted as cTnI levels increase[215,216]. There are two cardiac MHC isoforms: the α-isoform (*MYH6*) and the β-isoform (*MYH7*). Differential isoform expression is observed following cardiac maturation. At all stages ventricular expression of β-MHC is greater than α-MHC, however more α-MHC is observed in foetal than adult cardiomyocytes[217]. Titin, a protein involved in the maintenance of sarcomere integrity and elasticity, also undergoes an isoform switch with cardiomyocyte maturation from the compliant N2BA isoform, to the shorter and stiffer N2B isoform[218].

These genes are useful for assessing the maturation status of hiPSC-CMs. Gene expression analyses have shown that hiPSC-CMs predominantly express N2BA, α-MHC

and ssTnI isoforms[184,219,220]. It should be noted that the relative hiPSC-CM expression level of most cardiac genes is low when compared to adult human heart tissue.

1.7.3 Modelling cardiac channelopathies in hiPSC-CMs

Human iPSC lines have been generated from patients with inherited cardiac arrhythmias including LQTS, BrS and CPVT, for use as a disease model. Despite their immaturity, the hiPSC-CM models appear to recapitulate the key pathological phenotypes associated with each condition.

LQT1 and LQT2 are caused by loss-of-function mutations affecting I_{Ks} (*KCNQ1*) and I_{Kr} (*KCNH2*) respectively. Accordingly, *in vitro,* marked reductions in the magnitude of the respective currents have been observed when compared to hiPSC-CMs from healthy donors or to isogenic controls. LQT1[204,221–226] and LQT2[20,227–234] hiPSC-CM models have also demonstrated prolongation of both field potential and action potential duration; altered ion channel localisation/distribution and gating kinetics; abnormal calcium transients; and spontaneous and/or pharmacologically evoked arrhythmic events. LQT3 is caused by a gain-of-function to I_{Na} (*SCN5A*). Similarly to LQT1 and LQT2, LQT3 hiPSC-CMs have exhibited differences in current density (increased I_{Na}) compared to control lines. In addition further phenotype characteristics such as prolonged field potential and action potential duration; altered gating kinetics; and EADs have been reported[235–240]. Furthermore, LQTS hiPSC-CMs have responded in an expected manner to pharmacological and genetic therapies (partially) rescuing the respective disease phenotype[20,204,222,223,226,227,230,231,236,238–240].

The majority of BrS cases are associated with a loss-of-function of I_{Na} (*SCN5A*) – a reduced current density due to a lower expression of functional protein. Human iPSC-CM models of BrS with identified pathogenic mutations have recapitulated the characteristic phenotype: reduced and irregular $Na_v1.5$ expression; reduced I_{Na} current density and a slower action potential upstroke/conduction velocity; abnormal activation/inactivation kinetics; and arrhythmic activity[241–246]. However in a study using cell lines derived from BrS patients without *SCN5A* mutations, electrophysiological differences were not observed when compared to control cell lines[247]. Correction of BrS genetic mutations using CRISPR/Cas9 has been shown to improve upstroke velocity and

reduce arrhythmic activity as current density was partially rescued by increased channel expression[241]. Moreover, hiPSC-CM models have enabled observations of interplay between different currents that could be responsible for BrS in a co-ordinated manner[243,246].

As discussed in section 1.5, mutations in the *RYR2* gene are responsible for CPVT1. Dysfunctional RYR2, in association with β-AR stimulation, alters the calcium handling of cardiomyocytes promoting arrhythmic activity. CPVT hiPSC-CMs have been generated and appear to recapitulate the pathophysiological characteristics of the disease. In the presence of a β-AR agonist (or increased pacing frequency), studies have shown CPVT hiPSC-CMs to exhibit abnormal calcium handling including spontaneous calcium sparks, increased fractional calcium release and elevated diastolic calcium levels. Furthermore, arrhythmic events such as EADs and DADs have been reported[65,248–257]. The anti-arrhythmic effects of pharmacological therapeutic options have also been assessed. Many have demonstrated a positive effect by reducing, if not abolishing, arrhythmic events however due to mutation-specific differences underlying the disease mechanism the most effective drug varied[65,249,251,252,254,256,257]. More recently, CRISPR/Cas9 gene editing has successfully been used to identify a molecular pathway that explains how a catecholamine surge can provoke arrhythmias in CPVT patients[249].

1.7.4 Promoting hiPSC-CM maturation

The need to generate hiPSC-CMs with specificity and improved maturity remains in spite of the apparent reproduction of inherited cardiac channelopathy disease phenotypes in the patient and gene-edited models. The generation of a mixed cardiomyocyte subtype population in differentiated cultures means additional isolation procedures are necessary to achieve enriched cultures of a specific subtype. Additionally, high variability in hiPSC-CM characteristics within and between differentiated cell lines is also often reported, for example action potential duration. The differences in current contribution compared to native adult cardiomyocytes means the hiPSC-CM cardiac action potential is not wholly physiologically relevant. Therefore the severity of a disease phenotype could be masked or exacerbated by an unrelated difference in ion channel gating activity and the resultant contribution of ionic current. This is particularly important as altered gating kinetics have been indicated as key mechanisms of pathophysiology[34,62,258]. The

structural and signalling pathway shortcomings could also compromise the observations of disease mechanism and drug efficacy studies. With specific regards to CPVT, the β-AR signalling pathway that mediates arrhythmic activity is not fully functional. Potential CPVT treatments such as neuronal sodium channel inhibitors and phosphodiesterase 5 (PDE5) inhibitors would require a T-tubular network and compartmentalisation of fully functioning cAMP/cGMP (cyclic guanosine monophosphate) signalling pathways respectively.

Currently there is an evident lack of, yet desire for, established quality standards for defining cell maturity within the field to minimise the variability and improve reproducibility. There is also a requirement for experimental development and optimisation with regards to differentiation platforms as current methodologies do not offer reproducible, cost-effective or scalable manufacturing platforms for the high-throughput research necessary for clinical translation and success of treatments.

In order to take advantage of hiPSC-CMs full potential for research and clinical purposes, much focus within the field is on acquiring an adult-like maturation status. Intrinsic maturation is regulated by systemic and local cues, mechanical forces and cell-cell interactions. To date, a variety of approaches have been assessed and enhanced hiPSC-CMs (Figure 1.8). However the mature hiPSC-CM still alludes researchers.

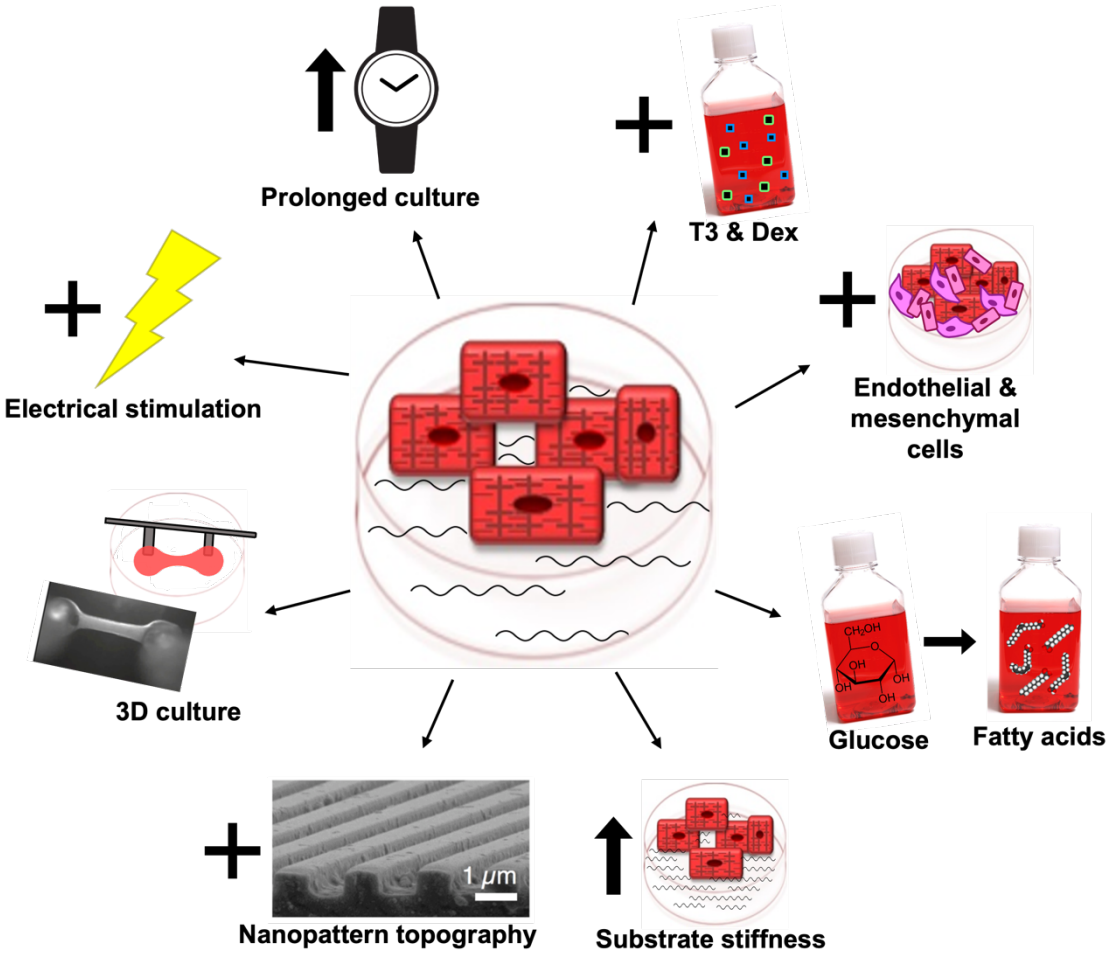

Figure 1.8: Schematic diagram of in vitro maturation approaches for hiPSC-CMs

Methods include (clockwise from top left): prolongation of culture; hormone supplementation of culture medium; coculture; transition of energy substrate; physiological substrate stiffness; nanopatterned culture surface (scanning electron micrograph image taken from NanoSurface Cultureware Manual of NanoSurface Biomedical Inc.); 3D culture (live photo taken from Mannhardt *et al*. 2016[259]), and electrical stimulation. T3, triiodothyronine; Dex, dexamethasone.

Prolonged culture period

Maturation, the third stage of cardiac development occurs over an approximate 10-year period[260–262]. Thus the immature nature of hiPSC-CMs is unsurprising considering cultures are often analysed after only 20-35 days of differentiation[204,225,227,235,248,256,257]. In studies assessing the effect of culture duration on maturation hiPSC-CMs have been cultured for up to 360 days[210,220,263–266]. With an extended culture period hiPSC-CMs have displayed an increased cell size, elongation and binucleation. The contractile machinery also appears to mature as the structure of myofibrils and sarcomeres improved - increasing in density, alignment and organisation. Correspondingly, modest

improvements in contractile and calcium transient parameters have been reported. Key cardiac-specific genes are upregulated although expression levels remain significantly lower than in native adult cardiomyocytes. Similarly, the expression and function of the β-AR signalling pathway demonstrates maturation but remains relatively immature. The effect of prolonging culture on hiPSC-CM beating rate however is mixed and appears to be dependent on culture length. Studies culturing cells for less than 60 days reported no change in beat rate[220,264]. By contrast, culture for 90 days or longer significantly reduced the beat rate[210,263]. Overall, prolonging the period of culture develops the hiPSC-CM phenotype morphologically, structurally and functionally. Nevertheless for hiPSC-CMs to become the mainstay disease model, development of physiologically-relevant cells will need to be achieved in a much shorter time frame.

Biochemical cues

Hormonal cues are known to have crucial roles during development of cardiac physiology. Triiodothyronine (thyroid hormone, T3) is among the most characterised. The level of T3 rises sharply after birth[267]. Responsive genes encode for both structural and regulatory proteins of the heart[268]. An initial study demonstrated incubating hiPSC-CMs with T3 caused differential gene transcription associated with an enhanced phenotype[269]. A more comprehensive study showed that T3-treated hiPSC-CMs exhibited an increased cell size and decreased circularity index. Furthermore sarcomere length, contractile force and kinetics, calcium handling kinetics, and mitochondrial activity improved[270]. T3 has also been shown to increase the resting membrane potential[271].

Glucocorticoid hormones are key regulators of cardiac maturation, with their levels rising in late gestation[272]. Via glucocorticoid receptors, glucocorticoid hormones also act to regulate gene expression in the heart. With regards to cardiomyocyte maturation the expression of genes encoding calcium handling, contractile proteins and mitochondrial activity are of note[273,274]. Although treatment of hPSC-CMs with the synthetic glucocorticoid hormone, dexamethasone (Dex) had a positive effect on calcium handling properties[275], it had more notable effects in combination with T3 and insulin-like growth factor-1[271] and with T3 and Matrigel mattress culture surface[199].

Energy substrate

The energy substrate(s) available to cardiomyocytes directly impacts the energy pathways utilised for ATP production. Native cardiomyocytes undergo an important switch in their predominant energy substrate from glucose to fatty acids (glycolysis to oxidative metabolism) soon after birth, in order to meet the energy demands of the heart. In response metabolic and mitochondrial maturation occurs. However, most culture media designed for maintenance of hiPSC-CMs have a glucose-rich, lipid-poor composition. Transitioning of the hiPSC-CM culture medium to one adapted to the metabolic requirements of adult cardiomyocytes led to maturation of mitochondria and metabolism. Furthermore morphological, structural, electrophysiological and mechanical maturation was also observed[214,276].

Cell-cell interaction

In the native adult heart, cardiomyocytes account for only ~18% of cells. The remaining proportion is mainly comprised of cardiac endothelial and mesenchymal (predominantly cardiac fibroblasts) cells[277,278]. Despite substantial differences in their primary roles (generation of contractile force; maintenance of the cardiac microvascular system; and production of connective tissue such as the extracellular matrix [ECM] respectively), the different cell types can communicate through direct physical contact (intercalated discs, gap junctions) and paracrine signalling in order to induce structural and functional adaptations in response to internal and external stimuli. Endothelial cells and cardiac fibroblasts can influence cardiomyocyte morphology/structure, contractility and hypertrophy, in addition to apoptosis, oxidative stress, cell activity and the release of proinflammatory factors[279]. In efforts to mature hiPSC-CMs, mimicking the cellular interactions of the cardiac microenvironment has been assessed *in vitro* through coculture of hiPSC-CMs with endothelial and/or mesenchymal cells[280–282]. Coculture mediated structural, electrical, contractile, and metabolic maturation of hiPSC-CMs.

Substrate stiffness and topographical cues

Cardiomyocytes are embedded in the ECM network secreted by mesenchymal cells. This network regulates the elastic modulus (or stiffness) of the tissue balancing the intracellular tension required for retainment of myofibril organisation and the contractility of the heart in order to pump blood[283]. Typical coated cell culture dishes

have a much higher elastic modulus compared to hearts. Thus seeding hiPSC-CMs on a substrate of more relevant physiological stiffness was hypothesised and subsequently shown to improve the cell aspect ratio, myofibril alignment, and contractility[283,284]. In combination with T3 and Dex culture medium supplementation, an increased substrate stiffness (Matrigel mattress method) has facilitated T-tubule formation, enhanced calcium handling and EC coupling kinetics[199,202].

The ECM of the heart also creates an interface with nanoscale, microscale, and macroscale topographic patterns. Cardiomyocytes are sensitive to these local, nanoscale cues which impact both structure and function[285]. However the majority of cell culture dishes do not offer a biomimetic surface which recapitulates the topographical cues provided by the ECM. The capacity of hiPSC-CMs to respond to structural cues was demonstrated by Carson *et al*.[286]. Furthermore the results indicated optimal development on grooves with dimensions in the upper nanometre range. Analysis of the hiPSC-CMs reported an increase in size (area and perimeter), alignment and sarcomere length whilst the circularity index was reduced.

3D culture and biophysical stimulation

Traditional 2D monolayer cultures are limited by their single cell sheet complexion and the consequent apical-basal polarity they induce. The 3D tissue architecture of the native adult heart means cardiomyocytes exist in a more complex microenvironment with stimuli emanating from neighbouring cells in all directions. To reproduce the *in vivo* complexity, 3D culture systems incorporating hiPSC-CMs have been investigated. One of the most reported 3D approaches is the engineered heart tissue (EHT) model. Cells are trapped between silicone posts in ECM derived hydrogels. The cardiomyocytes elongate along the force lines and form cell-cell contacts. The developing tissue starts to beat and perform auxotonic contractile work against the elastic resistance of the silicone posts[287]. Compared to the conventional monolayer, 3D cardiac tissues have demonstrated increased maturity with regards to morphology and structure; electrophysiology and contraction kinetics, including response to physiological and pharmacological regulators/modulators; and metabolism[259,288–292].

The maturation level of 3D tissue cultures can be further promoted by combination with the approaches already described. One method not considered so far is biophysical stimulation. Electrical stimulation[293,294] and progressive stretching[295] have both been shown to increase the maturity of 3D EHTs compared to control EHT conditions (no stimulation/stretch). Under these conditions cardiomyocytes developed adult-like gene expression and ultrastructure, although there are mixed reports of T-tubule development. EC coupling characteristics matured as reduced excitation thresholds, more negative resting membrane potentials, and improved calcium handling (CICR, systolic calcium amplitude) were observed. Furthermore increased contractility (force generation, response to β-AR stimulation) was demonstrated in parallel with enhanced bioenergetics (oxidative metabolism) and respiratory capacity.

In vitro hiPSC-CM technology and models offer a unique opportunity for studying human heart physiology, pathophysiology and drug screening/cardiotoxicity. They have the potential to harbour a physiological relevance no current disease model could match. Nevertheless, generated hiPSC-CMs do not yet fully correspond to the native adult cardiomyocyte phenotype. Their immature properties mean *in vitro* observations may not accurately recapitulate clinical investigations hence their implementation is limited. Further research into hiPSC-CM maturation is required in order to establish a model with the desired degree of maturity.

1.8 The present study

This study utilises an hiPSC cell line derived from a young woman identified to harbour a novel, heterozygous nonsense variant in the *RYR2* gene, c.14368C>T p.R4790*, following genetic testing. The proband suffered a cardiac arrest during sexual intercourse and had previously suffered episodes of syncope associated with emotional stress during childhood. No structural abnormalities were reported following a cardiac magnetic resonance imaging scan and a resting ECG showed no evidence of arrhythmic activity. Due to the development of hypoxic brain injury as a result of the cardiac arrest, an exercise-induced stress ECG could not be performed. An ICD has since been

implanted and she is currently treated with the β-blocker bisoprolol. No further arrhythmic episodes have been documented.

To our knowledge R4790* is the first reported nonsense mutation of RYR2 associated with a cardiac phenotype and thus was classified as a VUS. This nonsense point VUS causes deletion of the last 177 amino acids (3.5%), resulting in a truncated protein. Residing in the pore domain of the protein, expression of the variant would affect RYR2 channel gating. Previous work by Dr Claire Hopton in the Venetucci laboratory investigated the cardiac phenotype by generating hiPSCs from dermal fibroblasts of the proband, and differentiating these into cardiomyocytes (herein referred to as RYR2 hiPSC-CMs)[42]. RYR2 hiPSC-CMs displayed significantly more calcium handling abnormalities than control hiPSC-CMs at baseline (Figure 1.9A). Of those that demonstrated normal calcium transients at baseline, significantly more RYR2 hiPSC-CMs developed abnormalities following incubation with isoprenaline (Figure 1.9B). The propensity to develop spontaneous calcium releases increased with elevated external calcium concentrations. Treatment with RYR2 channel inhibitors (carvedilol and nebivolol) significantly reduced the proportion of cells displaying calcium transient abnormalities. Together these observations suggest a gain-of-function phenotype of the cardiac RYR2 channel.

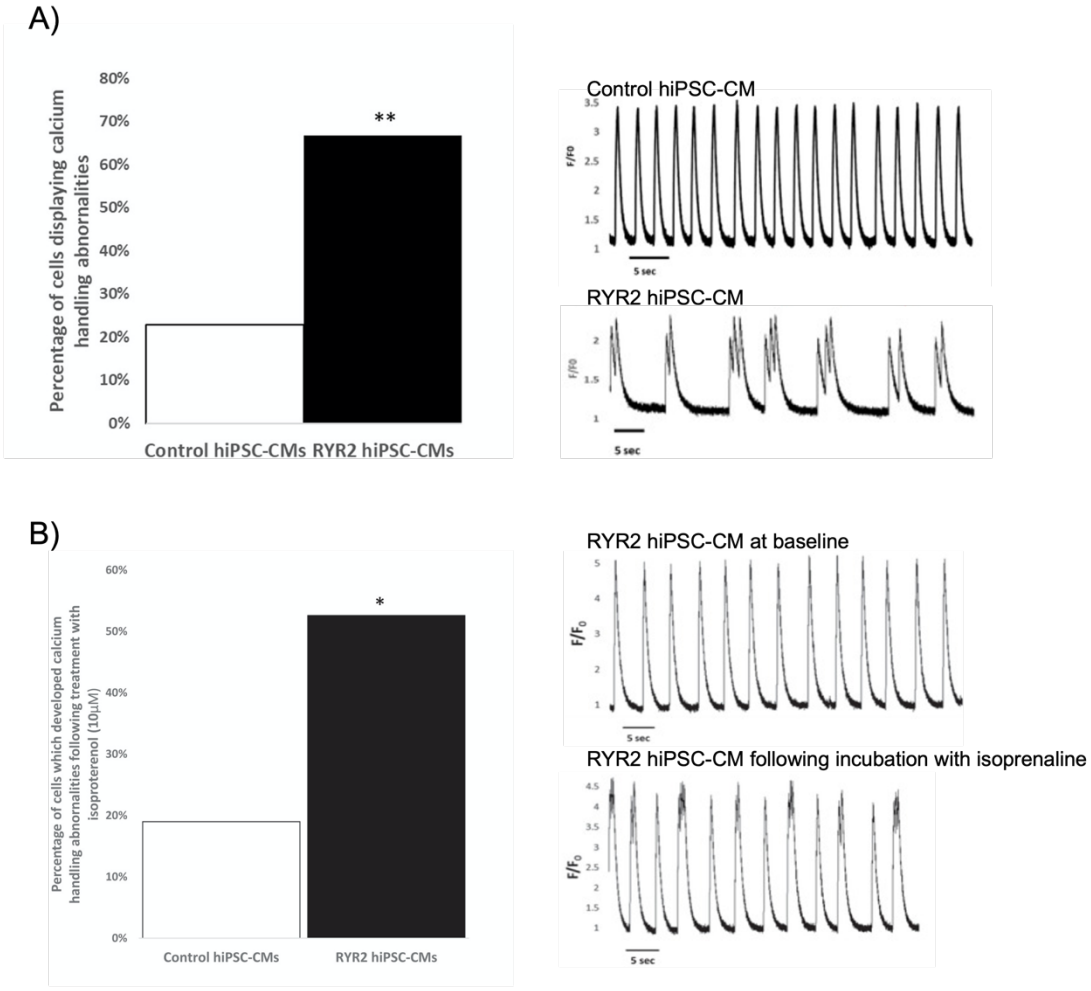

Figure 1.9: Calcium handling abnormalities in RYR2 hiPSC-CMs

(A) Left: RYR2 hiPSC-CMs developed significantly more calcium handling abnormalities at baseline compared to control hiPSC-CMs. Right: Representative line scan traces, note the multiple peaked transients in RYR2 hiPSC-CMs. (B) Left: Significantly more RYR2 hiPSC-CMs demonstrating normal calcium transients at baseline developed calcium handling abnormalities following incubation with 10 μM isoprenaline compared to control hiPSC-CMs. Right: Representative paired line scan traces of RYR2 hiPSC-CMs before and after isoprenaline treatment, note the development of multiple peaked transients. Figures and traces taken from Hopton *et al.* 2022[42].

These studies were undertaken using hiPSC-CMs with a low degree of maturity. The differentiation protocol developed by Burridge *et al*.[179] was followed with no cell line specific optimisation completed. None of the approaches previously described that promote maturity (section 1.7.4) were incorporated into the protocol. CPVT is a complex inherited cardiac pathology that involves the detailed ultrastructure of cardiomyocytes. As discussed, the CPVT disease phenotype appears to be successfully recapitulated in immature hiPSC-CMs however genetic, ultrastructural and signalling pathway

inconsistencies could alter the disease phenotype potency and the effects of pharmacological agents.

1.8.1 PhD hypotheses and aims

In order to address the issues outlined the overall aims of the present study were to improve the efficiency of the differentiation protocol for, and improve the degree of maturity of, the RYR2 hiPSC-CM disease model.

Hypothesis 1: RYR2 hiPSC line specific optimisation of the cardiac differentiation protocol will improve differentiation efficiency.

Aim 1: To improve the cardiomyocyte yield of the RYR2 hiPSC specific cardiac differentiation protocol by assessing differentiation with:

a) Two different differentiation culture media
b) Varying concentrations of Wnt pathway agonist (CHIR99021)

Hypothesis 2: Incorporating reported hiPSC-CM maturation approaches into the protocol will generate RYR2 hiPSC-CMs more similar to native adult-like cardiomyocyte, and with greater physiological relevance for assessing the CPVT disease phenotype and pharmacological treatments.

Aim 2: To generate RYR2 hiPSC-CMs with a greater level of maturity with regards to gene expression, morphology and intracellular structure, calcium handling properties and protein expression. Cardiomyocyte maturation will be promoted by:

a) Prolonged culture
b) Hormone supplementation of culture medium
c) A nanopatterned culture surface topography
d) Transition to a metabolic maturation medium

Chapter 2

Materials and methods

2 Materials and methods

2.1 Ethics and funding

This study was funded by the British Heart Foundation. Ethical approval was obtained from the Central Manchester Research Ethics Committee.

2.2 Human induced pluripotent stem cells

2.2.1 Cell lines

The patient *RYR2*$^{(wt/R4790*)}$ iPSC line was generated in Professor L Gepstein's laboratory at the Technion in Haifa, Israel. Primary dermal fibroblasts were isolated from a skin biopsy obtained from the patient. The primary dermal fibroblasts were subsequently reprogrammed following treatment with valproic acid and transfection by retroviral delivery of human transcription factors: *OCT4, SOX2* and *KLF4*[65,164].

Throughout this study two commercially available control hiPSC lines were used:

1. UKBi005. Dermis fibroblasts collected from a healthy female individual, aged 20-24 (at collection). Purchased from EBiSC, #66540008.
2. Human Episomal iPSC Line. Available from Gibco, #A18945. Cryogenically stored vial kindly donated by Professor E Cartwright's laboratory (University of Manchester, UK).

2.2.2 Coating of cell culture plates

All cell culture plates and dishes used in this study for culturing hiPSCs and hiPSC-CMs were pre-coated with diluted growth factor-reduced Matrigel (Corning, #356231). The Matrigel was diluted 1:200 with Dulbecco's Modified Eagle's Medium – high glucose (DMEM, Sigma Aldrich, D6429). Coated plates were stored in an incubator (37°C, 5% CO_2) for a minimum of 1 hour and maximum of 2 weeks prior to cell seeding.

2.2.3 Thawing of hiPSCs

Cryopreserved hiPSCs were removed from liquid nitrogen storage and thawed at 37°C. Dropwise, mTeSR Plus medium (StemCell Technologies, #100-276) was added and the cell suspension centrifuged at 1100 rpm for 5 minutes. The resultant cell pellet was

resuspended in mTeSR Plus medium supplemented with 2 μM thiazovivin (Sigma Aldrich, #SML1045) and seeded into pre-coated tissue culture treated 6-well plates (CytoOne, #CC7682-7506). The plates were placed in an incubator maintained at 37°C, 5% CO_2.

The mTeSR Plus medium was replaced daily and the hiPSCs were regularly screened for mycoplasma contamination using the MycoAlert Kit (Lonza, #LT07) in the Media Facility (Faculty of Biology, Medicine and Health, University of Manchester).

The volume of cell culture medium added to vessels was maintained at 0.637 ml per cm^2 throughout all experiments.

2.2.4 Passaging of hiPSCs

Human iPSCs were passaged on reaching 70-80% confluency (typically every 3-4 days) using a ratio of 1:12. Cells were washed with Dulbecco's Phosphate-Buffered Saline without Ca^{2+} and Mg^{2+} (PBS, Sigma Aldrich, #D8537) prior to incubation with the enzyme-free dissociation reagent ReLeSR (StemCell Technologies, #05872) at 37°C for 3 minutes. The plate was gently tapped to aid cell detachment and an equal volume of pre-prepared mTeSR Plus medium supplemented with 2 μM thiazovivin was added to the cells. The cell suspension was triturated with a P1000 pipette tip and added to the remaining pre-prepared supplemented medium before being seeded in Matrigel coated tissue culture treated 6-well plates. The passaged hiPSCs were returned to the incubator and mTeSR plus medium replaced daily.

2.3 Human induced pluripotent stem cell derived cardiomyocytes

2.3.1 The basic differentiation protocol

On reaching 80% confluency, hiPSCs were differentiated to cardiomyocytes. The small molecule-based protocols published by Burridge *et al*.[176,179] and Lian *et al*. [178] provided the basis for the method used in this study. Briefly, on day 0 mTeSR Plus medium was replaced with differentiation medium supplemented with 6-10 μM CHIR99021 (Selleck Chemicals, #S1263). On day 2, fresh differentiation medium supplemented with 2 μM Wnt-C59 (Selleck Chemicals, #S7037) was applied. From day 4 cells were maintained in

differentiation medium alone. The medium was replaced every 48 hours (Figure 2.1). Initiation of contraction was typically observed between days 8 and 10.

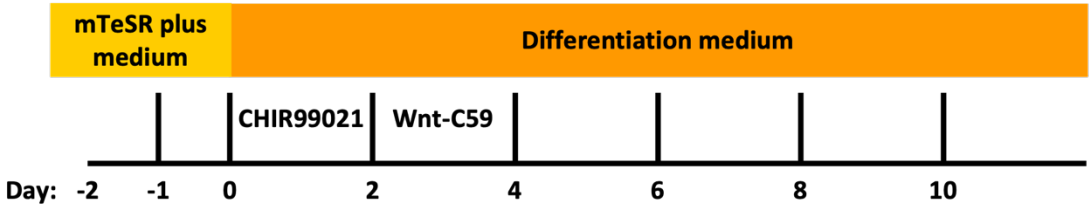

Figure 2.1: Schematic overview of the basic protocol for differentiating hiPSCs into hiPSC-CMs

Based on a differentiation protocol published by Burridge *et al*.[179] using small molecules. Cardiac differentiation was initiated at day 0 (~80% confluency) by supplementation of differentiation medium with CHIR99021. After 48 hours this was replaced with fresh medium supplemented with Wnt-C59. From day 4 the differentiation medium was replaced every 48 hours. Contracting cardiomyocytes were typically observed between days 8 and 10.

2.3.2 Optimisation of the differentiation protocol

To optimise the differentiation protocols' effectiveness at generating cardiomyocytes two factors were considered: the differentiation medium and the concentration of CHIR99021. Firstly, the small molecules CHIR99021 (6 μM) and Wnt-C59 were supplemented to two different cardiac differentiation media: CDM3 medium (Table 3) and RPMI B27 (-insulin) medium (Table 4). The number of cell culture plate wells with contracting hiPSC-CMs at day 10 of differentiation was counted.

Using the RPMI B27 (-insulin) differentiation medium, the following concentrations of CHIR99021 were assessed: 4 μM, 6 μM, 8 μM, 10 μM and 12 μM. Qualitative analyses were conducted.

Component	Final concentration	Source
RPMI 1640	-	Gibco, #21875-091
O.satvia-derived recombinant human albumin	500 μg/ml	Sigma Aldrich, #A0237
L-ascorbic acid 2-phosphate	213 μg/ml	Sigma Aldrich, #A8960
Penicillin-Streptomycin	1x	Sigma Aldrich, #P4333

Table 3: Composition of CDM3 medium

Component	Final concentration	Source
RPMI 1640	-	Gibco, #21875-091
B27 minus insulin supplement	2%	Gibco, #A1895601
Penicillin-Streptomycin	1x	Sigma Aldrich, #P4333

Table 4: Composition of RPMI B27 (-insulin) medium

2.3.3 Dissociation of hiPSC-CMs

The hiPSC-CM monolayers were dissociated from the plate and into single cells for culture purification and for downstream analysis, such as protein assays. TrypLE Select 10X (Gibco, #A1217701), an enzyme-based dissociation reagent was used.

Cultures were washed with PBS prior to incubation with TrypLE Select 10X at 37°C for 10 minutes. Fetal bovine serum (5% in DMEM, Biowest, #S1810) was added to the cells. The cell suspension was then triturated with a P1000 tip and centrifuged at 1100 rpm for 5-10 minutes.

2.3.4 Purification of hiPSC-CM cultures

Following hiPSC-CM differentiation, the cultures often contain a mixture of cell populations. To enrich the cell cultures with cardiomyocytes, they were purified by the removal of other cell types. Two established purification methods were considered: metabolic selection and magnetic-activated cell sorting (MACS).

Cardiomyocytes harbour a unique metabolic characteristic - they can use lactate as an alternative energy substrate to glucose. Hence culturing in glucose-depleted, lactate-supplemented conditions promotes cardiomyocyte survival, and cell death of all other cell types[296]. This is known as metabolic selection. Following the initial differentiation phase, the cell cultures were incubated with RPMI B27 (-insulin) medium without glucose (Table 5) through days 10 to 16. The medium was replaced every 48 hours. From day 16 the purified cardiomyocytes were incubated in RPMI B27 medium (Table 6).

MACS involves the depletion of unwanted cell populations from a culture through magnetic separation. This was performed using Miltenyi Biotec's PSC-Derived Cardiomyocyte Isolation Kit, human (#130-110-188) according to the manufacturer's protocol. Briefly, on day 14 of differentiation hiPSC-CMs were dissociated as described previously (section 2.3.3). The cell pellet was resuspended in MACS Buffer 1 (Table 7), filtered through a 70 μM strainer (Falcon, #352350/pluriSelect, #43-10070) and centrifuged at 3000 rpm for 3 minutes. The cells were incubated with MACS Buffer 1 and the non-cardiomyocyte depletion cocktail at 4°C for 5 minutes. After centrifuging, the cells were incubated with fresh MACS Buffer 1 and the Anti-biotin MicroBeads at 4°C for 10 minutes. The cell suspension was applied to an LS column (Miltenyi Biotec, #130-042-401), located in a QuadroMACS Separator (Miltenyi Biotec, #130-090-976). The flow-through containing the unlabelled cells (enriched hiPSC-CMs) was collected in RPMI B27 medium supplemented with 2 μM thiazovivin. The LS column was washed three times with MACS Buffer 2 (Table 8) - the flow-through was added to the cardiomyocyte-enriched suspension. The cardiomyocytes were centrifuged at 1100 rpm for 10 minutes and resuspended in RPMI B27 supplemented with 2 μM thiazovivin. Viable cardiomyocytes were counted and seeded in appropriate Matrigel-coated dishes. RPMI B27 was replaced every 48 hours.

Component	Final concentration	Source
RPMI 1640, no glucose	-	Gibco, #11879-020
B27 minus insulin supplement	2%	ThermoFisher Scientific, #A1895601
Sodium L-lactate	5 mM	Sigma Aldrich, #L7022
Penicillin-Streptomycin	1x	Sigma Aldrich, #P4333

Table 5: Composition of RPMI B27 (-insulin) medium without glucose

Component	Final concentration	Source
RPMI 1640	-	Gibco, #21875-091
B27 supplement	2%	Gibco, #17504044
Penicillin-Streptomycin	1x	Sigma Aldrich, #P4333

Table 6: Composition of RPMI B27 medium

Component	Final concentration	Source
Dulbecco's Phosphate Buffered Saline	-	Sigma Aldrich, #D8537
Bovine Serum Albumin	10%	Sigma Aldrich, #A9418
EDTA	1 mM	Invitrogen, #15575-038

Table 7: Composition of MACS buffer 1

Component	Final concentration	Source
Dulbecco's Phosphate Buffered Saline	-	Sigma Aldrich, #D8537
Bovine Serum Albumin	10%	Sigma Aldrich, #A9418
EDTA	0.1 mM	Invitrogen, #15575-038

Table 8: Composition of MACS buffer 2

2.4 Maturation of hiPSC-CMs

The hiPSC-CMs generated using protocols similar to the one described here (section 2.3.1) are accepted to be structurally and functionally immature. To develop the maturity of the cardiomyocytes - to produce cardiomyocytes more similar in phenotype, and consequently more behaviourally representative of native adult cardiomyocytes - four independent approaches were considered: prolonged culture length, hormone supplementation, culture surface topography, and the metabolic substrate composition of the maintenance medium. These approaches have the potential to be supportive and mutually inclusive of each other.

2.4.1 Prolonged culture length

It has been demonstrated that experimental protocols with prolonged culture periods generate hiPSC-CMs with a more mature phenotype[210,220,263,265]. Following cardiomyocyte differentiation and purification, hiPSC-CMs were maintained in culture to either day 30 or day 45 before harvesting for downstream analysis (Figure 2.2).

2.4.2 Hormone supplementation: triiodothyronine and dexamethasone

Triiodothyronine (T3) is produced and released from the thyroid gland. It has roles fundamental to cardiac development and cardiovascular physiology[268]. Dexamethasone (Dex) is a synthetic glucocorticoid hormone. Glucocorticoids are known to promote maturation of the foetal heart structure and function[273,274]. From day 16 of differentiation, the RPMI B27 medium was supplemented with 0.1 μM T3 (Sigma Aldrich, #T2877) and 1 μM Dex (Cayman Chemical Company, #11015) until the cardiomyocytes were harvested (Figure 2.2).

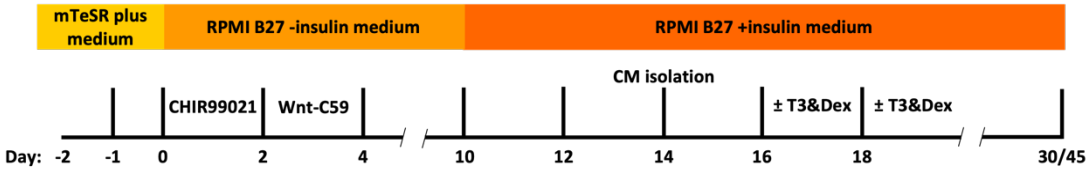

Figure 2.2: Schematic overview of the developed differentiation protocol to improve hiPSC-CM maturity

Extension of the basic differentiation protocol to assess factors with the potential to develop hiPSC-CM maturity. Hormone supplementation from day 16: triiodothyronine (T3, 0.1 μM) and dexamethasone (Dex, 1μM). Culture length: maintenance for 30 days or 45 days. CM, cardiomyocyte.

2.4.3 Culture dish topography: smooth vs nanopattern

Culturing cardiomyocytes on a topography more representative of the ECM environment they exist on within the native heart is suggested to aid their structural maturity[199,285,286]. Following MACS culture purification, hiPSC-CMs were seeded at a density of 160,000 cells/cm^2 in 35 mm dishes with either a smooth (MatTek Corporation, #P35G-0-20-C) or nanopatterned (Curi Bio, #ANFS-0001-10) topography (Figure 2.3).

To confirm the nanopattern groove depths (600 nm), and ridge and groove widths (800 nm) were maintained following Matrigel coating, atomic force microscopy was used. This was performed by Dr Nigel Hodson (University of Manchester) using a JPK NanoWizard IV (JPK Instruments) mounted on a Zeiss AX10 inverted light microscope under JPK NanoWizard Control software. Images were captured in fluid using QI Advanced Imaging mode and ScanAsyst Air cantilevers (Bruker) with nominal spring constant, frequency and tip radius of 0.4 N/m, 70 kHz and <10 nm respectively. Data was processed using JPK Data Processing software and was 1st order flattened prior to analysis.

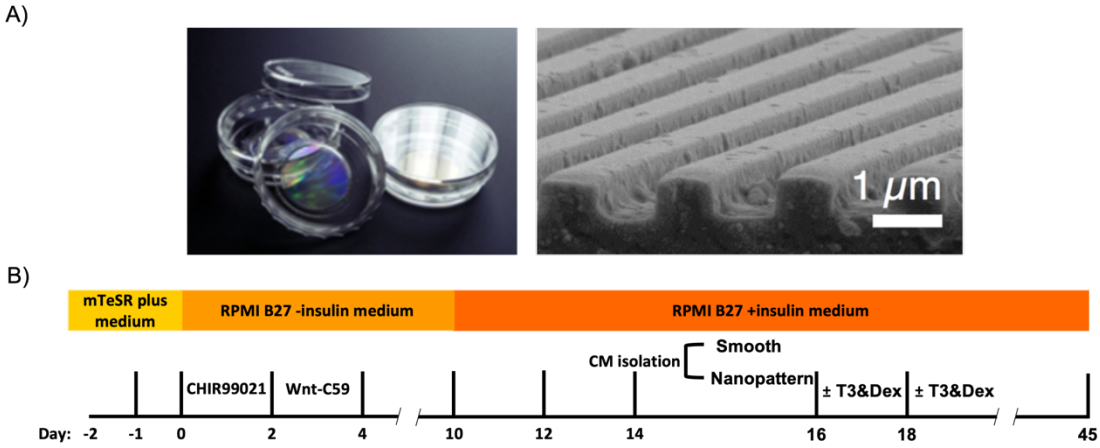

Figure 2.3: Schematic overview of the developed differentiation protocol incorporating nanopatterned culture dishes

(A) Photograph of nanopatterned culture dishes (left) and scanning electron micrograph of the surface topography (right). Images taken from NanoSurface Cultureware Manual of NanoSurface Biomedical Inc. (B) Further extension of the basic differentiation protocol to improve hiPSC-CM maturity by reseeding purified hiPSC-CM cultures on nanopatterned culture dishes - with a groove depth of ~600 nm, and ridge and groove widths of ~800 nm. CM, cardiomyocyte; T3, triiodothyronine; Dex, dexamethasone.

2.4.4 Metabolic maturation medium

Many cardiac differentiation protocols rely on RPMI B27 - a glucose-rich, lipid-poor medium. However, during foetal development cardiomyocytes switch from glycolytic to oxidative metabolism to support the energy demands of the heart[211]. Suppressing or restricting fatty acid oxidation potentially limits the metabolic maturation of hiPSC-CMs. Feyen *et al*.[214] developed a medium adapted to the metabolic needs of cardiomyocytes. To support cardiomyocyte energetics the medium was composed of glucose and calcium (at physiologically appropriate levels), supplemented with a complex mixture of fatty acids and other components (Table 9).

On day 20 of differentiation, RPMI B27 medium was replaced with the metabolic maturation medium (MMM) (Figure 2.4). The maturation medium was replaced twice a week (Tuesday and Friday). Cardiomyocytes had previously been purified using MACS and seeded on nanopatterned dishes.

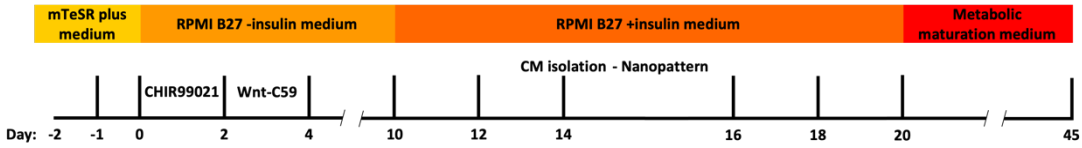

Figure 2.4: Schematic overview of the differentiation protocol used for assessing the metabolic maturation medium

On day 20 of differentiation, following cardiomyocyte (CM) isolation, the maintenance medium was switched from RPMI B27 +insulin to Feyen *et al*.'s[214] metabolic maturation medium. The medium was refreshed twice a week.

Component	**Final concentration**	**Source**
Dulbecco's Modified Eagle's Medium, no glucose	-	Gibco, #11966025
AlbuMAX| Lipid-Rich Bovine Serum Albumin	0.5% (w/v)	Gibco, #11020021
B27 supplement	2%	Gibco, #17504044
Biotin	0.82 μM	Sigma Aldrich, #B4639
Creatine monohydrate	5 mM	Sigma Aldrich, #C3630
D-(+)-Glucose	3 mM	Sigma Aldrich, #G7021
KnockOut Serum Replacement	1%	Gibco, #10828028
L-Ascorbic acid 2-phosphate sesuimagnesium salt hydrate	0.5 mM	Sigma Aldrich, #A8960
L-Carnitine hydrochloride	2 mM	Sigma Aldrich, #C0283
MEM Non-Essesntial Amino Acids Solution	1x	Gibco, #11140050
Penicillin-Streptomycin	1x	Sigma Aldrich, #P4333
Sodium L-lactate	10 mM	Sigma Aldrich, #71718
Taurine	2 mM	Sigma Aldrich, #T0625
Vitamin B_{12}	5 μg/ml	Sigma Aldrich, #V6629

Table 9: Composition of Metabolic maturation medium

2.5 Immunocytochemistry

Immunocytochemistry was first used to demonstrate the pluripotent nature of hiPSCs. The technique was also applied to differentiated hiPSCs for measurement of cardiomyocyte morphology parameters, and to assess the expression and spatial arrangement of target proteins.

2.5.1 Immunofluorescence labelling for pluripotency

To confirm the pluripotent status of the *RyR*$^{(wt/R4790*)}$ hiPSC line the expression of four key transcription factors was investigated. This was performed using the Pluripotent Stem Cell 4-Marker Immunocytochemistry Kit (Invitrogen, #A24881), according to the manufacturer's instructions. Briefly, cells were fixed in 4% formaldehyde (in PBS) for 15 minutes. The fixative solution was then replaced with permeabilisation solution (1% saponin in PBS) for 15 minutes, after which cells were blocked using 3% bovine serum albumin (BSA, in PBS) for 30 minutes. Primary antibody was subsequently added directly to the blocking solution. Cells were dual-stained for either: SSEA4 (1:100) and OCT4 (1:200), or SOX2 (1:100) and TRA-1-60 (1:100) by incubation at 4°C overnight. Appropriate secondary antibodies, diluted 1:250 in blocking solution, were added and cells incubated in the dark for 1 hour. NucBlue Fixed Cell Stain (nuclear DNA stain) was added for 5 minutes during the final of 3x PBS wash steps. Stained hiPSCs were imaged using a Nikon Eclipse Ti inverted microscope with A1R confocal module and viewed in Nikon's NIS-Elements software. All steps were performed at room temperature unless stated otherwise.

2.5.2 Immunofluorescence labelling of hiPSC-CMs

Human iPSC-CMs were labelled for the plasma membrane for measurement of cell morphology parameters, and alpha actinin-2 (a ubiquitously expressed sarcomere protein) for qualitative assessment of cardiac cytoskeleton organisation.

Labelling of the plasma membrane using wheat germ agglutinin (WGA) was performed on live hiPSC-CMs. First, cardiomyocytes were washed with PBS and then incubated with 5 μg/ml WGA, Alexa Fluor 488 conjugate (Invitrogen, #W11261) for 10 minutes. Cells

underwent 2x PBS washes, prior to fixing and permeabilisation, to remove any unbound WGA that could bind to internal structures.

The WGA-labelled cardiomyocytes were fixed through incubation in 4% formaldehyde solution (Thermo Scientific, #28906) for 10 minutes. Following 2x 5 minute PBS washes, cells were permeabilised with 0.25% Triton X-100 (Sigma Aldrich, #T8787) for 15 minutes. After a further 2x washes, Image-iT FX Signal Enhancer (Invitrogen, #I36933) was applied for 30 minutes to reduce charge-based, non-specific binding of Alexa Fluor dyes. To further limit non-specific binding of primary and secondary antibodies, the cardiomyocytes were blocked with 10% goat serum (Sigma Aldrich, #G9023), 1% BSA in PBS for 90 minutes. The blocking solution was replaced with mouse monoclonal Anti-alpha-actinin primary antibody solution (1:150, Sigma Aldrich, #A7811) and incubated on a plate rocker at 4°C overnight. The cells were washed prior to incubation with the secondary antibody: Goat anti-Mouse IgG (H+L), Alexa Fluor 594 (1:500, Invitrogen, #A11032) in the dark for 1 hour. Both the primary and secondary antibodies were diluted in 5% goat serum, 1% BSA, PBS. After incubation with the secondary antibody, cells were washed twice and incubated with the classic nuclear counterstain, DAPI (5 μg/ml, Invitrogen, #D1306) for 5 minutes. After the final 2x washes, immunofluorescence-labelled hiPSC-CMs were imaged using a Nikon Eclipse Ti inverted microscope with A1R confocal module and viewed in Nikon's NIS-Elements software. All steps were performed at room temperature, unless stated otherwise.

2.5.3 Measurement of hiPSC-CMs morphology parameters

The length and width of WGA-labelled hiPSC-CMs were measured. Using ImageJ software (National Institutes of Health), lines were drawn down the length, and across the width of cardiomyocytes at the midpoint. The measurements were recorded and the length to width ratio calculated.

2.6 RNA analysis

RNA was extracted from hiPSCs and hiPSC-CMs to investigate target gene expression by real-time quantitative PCR (RT-qPCR). For hiPSCs, RT-qPCR was used to assess pluripotency. For hiPSC-CMs, the technique was first used to identify the most stable

reference (housekeeping) gene, prior to quantifying and comparing the expression of genes critical for cardiac calcium handling and cardiomyocyte structure.

2.6.1 RNA extraction and cDNA conversion

RNA was extracted from cultured hiPSCs and hiPSC-CMs using the *mir*Vana miRNA Isolation Kit, without phenol (Invitrogen, #AM1561), according to the manufacturer's instructions. To remove any contaminating DNA, RNA preparations were treated with the DNA-*free* DNA Removal Kit (Invitrogen, #AM1906). RNA sample concentrations were quantified using a NanoDrop 1000 Spectrophotometer. The samples were stored at -80°C.

RNA was then converted to cDNA using the High-Capacity RNA-to-cDNA Kit (Applied Biosystems, #4387406), according to the manufacturer's instructions. A negative control reaction where the RNA was substituted for nuclease-free water was also performed. The resultant cDNA was diluted 1:5 with nuclease-free water, and used for PCR and RT-qPCR analysis. The cDNA samples were stored at -20°C.

2.6.2 Reference gene selection

RT-qPCR data is usually normalised to a constitutively expressed reference gene for accurate target gene expression measurements. Using the Primerdesign geNorm Reference Gene Selection kit (according to the manufacturer's instructions) and analysis in the qBase^{+} software, the candidate genes were ranked according to their stability in the RYR2 hiPSC-CMs. The candidate reference genes assessed were: *18S*, *ACTB*, *B2M*, *GAPDH*, *RPL13A*, *UBC* and *YWHAZ*.

2.6.3 Primer design for RT-qPCR analysis

Primers were designed for genes that encode for cardiac structural proteins and those involved in cardiac calcium handling. Nucleotide sequences for each gene were downloaded from NCBI to SnapGene software. A region of interest was chosen and using Primer3 Input, forward and reverse primer sequences (Table 10) were selected according to stated conditions: length, 18-25 base pairs; primer melting temperature,

57-62°C; base composition, 40-60% GC. Primers were purchased from Integrated DNA Technologies.

In order to confirm the designed primer sequences annealed to and amplified the desired region only, cDNA was amplified using a PCR reaction and the product size was verified. The REDExtract-N-Amp PCR ReadyMix (Sigma Aldrich, #R4775) and a BioRad thermocycler were used (PCR conditions are outlined in Table 11). Two negative controls were also run: the first where the RNA was substituted for nuclease-free water during the cDNA conversion, and second where the cDNA was substituted for nuclease-free water. The PCR products were then analysed by high-resolution capillary electrophoresis using a QIAGEN QIAxcel Advanced System.

	Gene	Forward primer (5' → 3')	Reverse primer (5' → 3')	Product size (bp)
SR proteins	Ryanodine receptor 2 (RYR2)*	ACAGAGTTTGGCACACAGCAG	ACAGCAACATGACCACCATATCC	155
	Calsequestrin (CASQ2)	ATTGCCATCCCCAACAAACC	CTCAGATCGGGGTTGTCAGT	233
	Sarco-endoplasmic reticulum calcium-ATPase (ATP2A2)	ACGAGTTACCGGCTGAAGAA	TCCTGCCATACACCCACAAT	211
	Phospholamban (PLN)	AAACTCCCCAGCTAAACACC	GAACTTCAGAGAAGCATCACGATGATA	335
	Triadin (TRDN)	AGCCATTCCACCTCCCTTAC	TTTCAGAAGCTTTTCCCGGC	209
	Junctin (ASPH)	CTCAGAGTCCACGAGCAAGA	AATTGTTGCCTGTCTGAGCG	181
Contractile proteins	Troponin I (TNNI3)*	AGTCACCAAGAACATCACGGAGAT	GCAGCGCCTGCATCATG	125
	Troponin T (TNNT2)	CAAAGGAGGCTGAAGATGGC	CAAAGTGAGCCTCGATCAGC	177
	Myosin heavy chain 6 (MYH6)*	TACAGGACCTGGTGGACAAGC	TTGCGGAACTTGGACAGGTGG	103
	Myosin light chain 2 (MYL2)	AGGCTGATTACGTTCGGGAA	TCTCTTCTCCGTGGGTGATG	150
T-tubule proteins	Dysferlin (DYSF)	TGCGATGGACAAGGACTCTT	TCGTACAGCTCCACCACAAT	195
	Bridging integrator 1 (BIN1)	GCAGTGCGTCCAGAATTTCA	CAGCAGGTCGTTGTTCTCTG	196
	Junctophilin 2 (JPH2)	CACAACGTGCTGGTCAAGG	CGAGCAATGTTGGACTCCTG	221
Post-translational modulators	Phosphodiesterase 5 (PDE5)	CCTCGGTTCAATGCAGAAGT	TCTCTTGTTCTCCAGCAGTGA	243
	P21-activated kinase 1 (PAK1)	TAACCCCAGAGCAGAGCAAA	TTCTGAAGTTCTGGGGTCCC	217
	Adenylyl cyclase 5 (ADCY5)	TCCAAGATGAACAGCACCCT	TACTCGGGGAAGTTGCAGTT	239
	Adenylyl cyclase 6 (ADCY6)	AAAGAGGAGAAGGCCATGCT	CTCATCCTCAGGGTTCAGGG	192
Membrane-bound ion channels	Sodium-calcium exchanger (SLC8A1)	TCCTTGAGATTGGAGAGCCC	CGCCTCTCCTCTTCCTCTTT	223
	Sodium voltage-gated channel alpha subunit 1 (SCN1A)	TCTCCGAGCATTGAAGACGA	ATTCCTCAGGTTGCCCATGA	166
	Sodium voltage-gated channel alpha subunit 3 (SCN3A)	CACTACCCCATGACTGAGCA	TCGCAGTACAGACAATCCCT	213
	Sodium voltage-gated channel alpha subunit 5 (SCN5A)	CCTTTGGCCCCAGTAAACAG	TGCTTCAGAACCCAGGTCTC	231

	Sodium voltage-gated channel alpha subunit 8 (SCN8A)	CACGCCTGCCTTGTACATTT	TCCCTGTGAACGTGTACTCC	179
	Sodium voltage-gated channel alpha subunit 10 (SCN10A)	ACTTGGAGGATGATGGTGGG	GCCAGGTCCTCAGAAGATGT	151

*not designed during this project

Table 10: Primer sequences

Stage	**Temperature (°C)**	**Duration**	**Cycles**
Denaturation	94	3 minutes	x1
	94	30 seconds	x35
Annealing	60	30 seconds	
Extension	72	1 minute	
	72	5 minutes	x1
Hold	4	∞	x1

Table 11: PCR reaction conditions

Stage	**Temperature (°C)**	**Duration**	**Cycles**
Holding	95	5 minutes	x1
Cycling	95	10 seconds	x40
	60	20 seconds	
	72	20 seconds	
Melt curve	95	15 seconds	x1
	60	60 seconds	
	95	15 seconds	
Holding	4	∞	

Table 12: RT-qPCR reaction conditions

2.6.4 RT-qPCR

RT-qPCR was undertaken using SYBR Green PCR Master Mix (Applied Biosystems, #4309155). Forward and reverse primers (1 μM) were added to the master mix and loaded into MicroAmp Fast Optical 96-well Reaction plates (Applied Biosystems, #4346906) prior to the addition of 20 ng cDNA. Each reaction was performed in triplicate. Two negative controls were also run: the first where the RNA was substituted for nuclease-free water during the cDNA conversion, and second where the cDNA was substituted for nuclease-free water. The RT-qPCRs were performed using an Applied Biosystems Viia7 Real-time PCR system and software. RT-qPCR conditions are outlined in Table 12.

2.6.5 RT-qPCR analysis

RT-qPCR data was first analysed using the LinRegPCR programme[297]. This was used to perform a baseline correction on each sample and calculate the PCR efficiency. Using the calculated amplification efficiency and Ct values, the target gene expression data was normalised to the reference gene *UBC* and expressed relative to the baseline culture condition: 30 days without hormone supplementation.

2.7 Protein analysis by western blot

In order to quantify and compare the abundance of proteins critical for cardiomyocyte structure and cardiac calcium handling, western blot analyses were performed.

2.7.1 Protein extraction and quantification

Human iPSC-CMs were washed with PBS and dissociated using TrypLE Select 10X. After incubation, RPMI B27 medium was added and the cells scraped (Greiner Bio-One, #541070) off the plate. The cell suspension was centrifuged at 3000 rpm for 5 minutes, washed via resuspension in PBS and re-centrifuged. The supernatant was discarded, and the pellet snap frozen using liquid nitrogen. Samples were stored at -80°C.

To extract protein, the samples were thawed on ice and vortexed to disrupt the cell pellet. RIPA buffer (for cell lysis, Sigma Aldrich, #R0278) supplemented with

phosphatase (sodium orthovanadate, 1 mM) and protease (aprotinin, 1 μg/ml; leupeptin, 1 μg/ml; and phenylmethylsulfonyl fluoride, 0.1 mg/ml) inhibitors was added to the cell suspension. The samples were rotated at 40 rpm, 4°C for 30 minutes before being centrifuged at 12,000 rpm, 4°C for 10 minutes. The supernatant was aspirated to a fresh tube and the remaining cell pellet discarded. The protein samples were stored at -80°C.

The protein concentration of each sample was quantified using the colorimetric *RC DC* protein assay (Bio-Rad, #5000122) and Quick Start BSA Standards (Bio-Rad, #500-0206), according to the manufacturer's instructions. Protein samples were diluted 1:10 with RIPA buffer before addition. The 'blank' (RIPA buffer), BSA standards and experimental samples were performed in triplicate in a 96-well TC-Treated Microplate (Corning, #CLS3596). A BioTek Synergy HTX Multi-Mode Reader and the BioTek Gen5 software were used to measure the protein concentration using the absorbance reading obtained at wavelength 750 nm. A standard curve was created using the assay standards' readings and subsequently used to ascertain the concentration of protein present in the diluted samples. These concentrations were then multiplied by 10 to correct for the dilution.

2.7.2 Gel electrophoresis and protein transfer

To separate proteins by molecular weight, protein samples were prepared for denaturing gel electrophoresis. Protein (30 μg) was combined with 1x NuPAGE LDS Sample Buffer (4x stock, Invitrogen, #NP0007), NuPAGE Sample Reducing Agent (10x stock, Invitrogen, #NP0009) and RIPA buffer (final volume of 20 μl). The preparation was incubated at 70°C for 10 minutes prior to loading in NuPAGE 4-12% Bis-Tris protein gels (Invitrogen, #NP0321). The molecular weight marker, Precision Plus Protein All Blue Standards (Bio-Rad, #161-0373), was also loaded into a well of each protein gel. The inner and outer chambers of the XCell *SureLock* Mini-Cell electrophoresis system (Invitrogen) were filled with 1x NuPAGE MES SDS Running Buffer (20x stock, Invitrogen, #NP0002) in distilled H_2O. NuPAGE Antioxidant (0.25%, Invitrogen, #NP0005) was added to the inner chamber. Using a PowerPac 300 (Bio-Rad), gel electrophoresis was run at 200 V for 45-50 minutes.

Following gel electrophoresis, the wet transfer method was used to transfer the proteins to Amersham Protran Supported 0.45 μM nitrocellulose membrane (GE Healthcare Life Sciences, #10600018). Foam pads - soaked in 1x NuPAGE Transfer Buffer (20x stock, Invitrogen, #NP00061) in 20% methanol, distilled H_2O - were placed in an XCell II Blot Module (Invitrogen, #EI0002). The protein gel was removed from the cast on soaked Whatman Grade 1 Qualitative Filter Paper (Whatman, #1001-240), and placed on top of the foam pads. Soaked nitrocellulose membrane was added next, prior to a second piece of soaked filter paper. Trapped air bubbles were removed using a western blot roller (Thermo Scientific, #84747). A soaked foam pad was added, and the process was repeated for a second protein gel. The XCell II Blot Module was placed in the XCell *SureLock* Mini-Cell electrophoresis system and filled with transfer buffer supplemented with 0.1% NuPAGE Antioxidant. The outer chamber was filled with distilled H_2O. The system was placed on ice and proteins transferred at 30 V for 90 minutes.

2.7.3 Total protein staining

For accurate target protein expression measurements, data was normalised to the total protein loaded and transferred for each sample run. To quantify the total protein, protein-bound nitrocellulose membranes were removed from the XCell II Blot Module and washed with distilled H_2O. The membranes were incubated in Revert 700 Total Protein Stain (LI-COR, #926-11015) at room temperature for 5 minutes. After incubation, the membranes were returned to distilled H_2O and imaged using the LI-COR Biosciences Odyssey CLx Imager, in the 700 nm channel.

2.7.4 Membrane blocking and protein detection

To prevent non-specific antibody binding and reduce background fluorescence, protein-bound nitrocellulose membranes were blocked with 5% or 10% non-fat dried milk (Table 13) in 1x Tris-buffered saline, 0.1% Tween20, distilled H_2O (TBS-T). Blocking occurred at room temperature, on a rocker for 1 hour. After blocking, the membrane was briefly washed with distilled H_2O.

Next, blocked protein-bound nitrocellulose membranes were incubated with target protein primary antibodies (Table 13) at 4°C overnight. Primary antibodies were diluted in TBS-T. The membranes underwent 3x 5 minute TBS-T washes prior to incubation with

the secondary antibodies at room temperature for 1 hour. The secondary antibodies (Table 13) were also diluted in TBS-T. Following the final 3x 5 minute TBS-T washes, the membranes were imaged in both the 700 nm (molecular weight marker) and 800 nm (target protein bands) channels, using the LI-COR Biosciences Odyssey CLx Imager.

2.7.5 Analysis

Western blot analysis was performed using Image Studio Lite software. Target protein expression was normalised to total protein signal (loading and transfer control). To measure the total protein signal, a rectangle was drawn around the first protein-containing lane. The rectangle was copied, pasted over the second lane, and aligned with the rectangle over the first lane. This was repeated for all lanes containing protein sample. To measure the background signal, a rectangle was drawn over an area of the membrane without protein sample. The background signal intensity was subtracted from the total protein signal intensity to give the background-corrected total protein signal. To measure the target protein signal, the process was repeated - ensuring the rectangle drawn was around the target protein band only. The background-corrected values were exported to Microsoft Excel for normalisation and averaging.

Target protein and molecular weight	Membrane blocking	Primary antibody: source and dilution	Secondary antibody: source and dilution
β1- adrenergic receptor (ADRβ1) 50 kDa	10% milk	Rabbit polyclonal Santa Cruz Biotechnology, #sc-568 1:1000	IRDye 800CW Goat anti-Rabbit IgG (H+L) LI-COR Biosciences, #926-32211 1:20,000
Phospholamban (PLN) 6 kDa	5% milk	Mouse monoclonal Invitrogen, #MA3-922 1:5000	IRDye 800CW Goat anti-Mouse IgG (H+L) LI-COR Biosciences, #926-32210 1:20,000
Phosphorylated phospholamban Thr17 (phosPLN) 6 kDa	5% milk	Rabbit polyclonal Badrilla, #A010-13 1:2500	IRDye 800CW Goat anti-Rabbit IgG (H+L) LI-COR Biosciences, #926-32211 1:20,000
SR calcium ATPase (SERCA2a) 100 kDa	5% milk	Mouse monoclonal Santa Cruz Biotechnology, #sc-73022 1:2500	IRDye 800CW Goat anti-Mouse IgG (H+L) LI-COR Biosciences, #926-32210 1:20,000
Sodium-calcium exchanger (NCX) 116 kDa	5% milk	Mouse monoclonal Swant, #R3F1 1:1000	IRDye 800CW Goat anti-Mouse IgG (H+L) LI-COR Biosciences, #926-32210 1:20,000

Table 13: Western blot conditions for protein targets

2.8 Functional analysis: calcium imaging

2.8.1 Loading hiPSC-CMs

Human iPSC-CMs were loaded with 4 μM Fluo-4, AM (Invitrogen, #F14201), in either RPMI B27 medium or metabolic maturation medium, in an incubator (37°C, 5% CO_2) for 25 minutes. To allow for de-esterification of the dye, loaded cardiomyocytes were incubated in fresh medium supplemented with 250 μM probenecid (Invitrogen, #P36400) for a further 25 minutes. Following de-esterification, fresh medium supplemented with 125 μM probenecid was applied. De-esterification is required for complete hydrolysis of the AM esters to avoid fluorescence variation artefacts. Probenecid inhibits organic anion transporters hence improving intracellular retention of the dye. Note the hiPSC-CMs were maintained in culture medium throughout experiments.

2.8.2 Recording calcium transients

Calcium transients were recorded from hiPSC-CM monolayers using a custom-made calcium and voltage dual channel optical mapping system (Cairn Research). The setup included an openFrame inverted microscope with Piezo-Z stage, Prime BSI Express Scientific CMOS, 89 North laser diode illuminator, and a photomultiplier tube detection system.

To measure calcium transients, cardiomyocytes were excited at 488 nm and the emitted light was collected through a 10X Olympus UPlanXApo objective. Data acquisition was facilitated by Micro-Manager and ImageJ software. The recording area was maintained at 1048x1048 pixels, and acquisition settings of 600x frames, 20 ms exposure, 0 ms interval used. All recordings were 12 seconds. Recordings were taken at room temperature, or 37°C using a Quick Exchange Platform (Warner Instruments). In some experiments, hiPSC-CMs were electrically stimulated at 50 V with a 10 ms pulse duration, at 0.5 Hz using a SD9 stimulator (Grass Technologies) through silver/silver chloride electrodes (World Precision Instruments, #EP1).

Baseline recordings were taken at three different, randomly selected regions of interest (ROI) in each cell culture dish prior to pharmacological studies. Recordings taken

throughout pharmacological studies were taken in the same area as the third baseline recording – generating paired data. Three recordings were also taken at different, randomly selected areas following the pharmacological study.

2.8.3 Pharmacological studies

Isoprenaline

Isoprenaline (Abcam, #ab146724) was dissolved in sterile H_2O supplemented with 10 mM L-Ascorbic acid (Sigma Aldrich, #PHR1008) to a concentration of 1 mM. L-ascorbic acid is a water soluble anti-oxidant capable of protecting cell cultures from toxic doses of isoprenaline[298]. Freshly prepared stock solutions (in RPMI B27 medium) were added to cell culture dishes to make up final concentrations of 100 nM, 500 nM, 1 μM, 5 μM and 10 μM. Cardiomyocytes were incubated with each dose for 2 minutes prior to a recording being taken.

Thapsigargin and ryanodine

Thapsigargin (1 mM, Millipore, #586005) was dissolved in sterile H_2O. Ryanodine (20 mM, Tocris, #1329) was dissolved in dimethyl sulphoxide. Following baseline recordings, hiPSC-CMs were incubated with 10 μM thapsigargin for 15 minutes prior to recording. Ryanodine was then applied (10 μM) for 2 minutes before another recording was taken.

2.8.4 Calcium transient analysis

Recordings were analysed by measuring the rate of rise, amplitude and rate of decay of the calcium transients. Data was extracted from five different, randomly selected areas (100x100 pixels) within an ROI (conserved for paired recordings). Using the ImageJ plugin: Time series analyser V3, the average fluorescence intensity at each frame was calculated. Three to five transients per trace were measured and averaged for an ROI value. The three ROI values were then averaged for a culture dish value. For analysis of calcium transient kinetics, the data was normalised to the lowest fluorescence intensity recorded. Transient amplitude was derived by subtracting the lowest fluorescence signal (diastolic calcium level) from the peak signal (F/F0). Rate of rise was calculated from the change in fluorescence signal divided by time (F/F0 s^{-1}). The rate constant of decay was

measured using the Greensmith's method - a custom-made Microsoft Excel programme[299].

2.9 Statistical analysis

Unless stated otherwise, data is presented as a mean value (±SEM). The number (n) of technical and biological replicates are stated in each figure. For expression and functional analyses, biological replicates are defined as the number of samples or dishes assessed (across a minimum of three independent differentiations unless stated otherwise). Expression analyses were performed in triplicate. For functional analyses, technical replicates are total ROIs (typically three ROIs/dish). Biological replicates were used for statistical analysis. Unpaired students t-test was used to test for changes between two groups. One-way ANOVA with multiple comparisons was used to test for changes between more than two culture conditions or following pharmacological challenges; the mixed effects model was used when values were missing. Two-way ANOVA with multiple comparisons was used to test for changes between culture conditions where two factors were assessed. Three-way ANOVA with multiple comparisons was used when two factors were assessed, and the data was expressed dependent on calcium transient frequency. Statistical significance was expressed when $p<0.05$.

Chapter 3

Characterisation of RYR2 hiPSCs and optimisation of their differentiation to cardiomyocytes

3 Characterisation of RYR2 hiPSCs and optimisation of their differentiation to cardiomyocytes

3.1 Introduction

In this study, our focus concentrates on a hiPSC line derived from a patient who suffered a cardiac arrest, and following investigation was identified to harbour a heterozygous nonsense point variant R4790* in the *RYR2* gene. Nonsense mutations result in a premature stop codon. To our knowledge this is the first reported nonsense mutation of *RYR2* associated with a cardiac phenotype[42,300]. On reprogramming of the patients' primary dermal fibroblasts to hiPSCs, cells exist in a pluripotent state regulated by the expression of transcription factors[164]. This means they have the ability to give rise to cells from all three of the major embryonic germ layers: the endoderm, the ectoderm, and the mesoderm[301]. These three lineages have the capability to differentiate into any of the body's specialised cell types.

To generate hiPSC-CMs *in vitro*, hiPSCs must exit their pluripotent state and undergo directed differentiation. Cardiomyocytes are derived from the mesoderm germ layer[302] hence production of mesodermal cells is promoted first before being directed into the cardiac lineage. Monolayer-based differentiation methods often rely on the addition and removal of growth factors or small molecules to/from the culture medium at specific times. For efficient differentiation the specific kinetics should be optimised for each hiPSC line[174,175,177,178,182] – this is due to heterogeneity of endogenous signalling between cell lines.

The approach to cardiac differentiation mimics the stages of embryonic cardiac development. Developmental research has identified three families of protein growth factors which can control cardiac development: transforming growth factor β (including BMPs and activins), Wnt proteins and fibroblast growth factors[182].

Direct sequential application of activin A and BMP4 can influence the Activin/Nodal/BMP4 signalling pathways towards the induction of the mesoderm and cardiac progenitors, respectively[164,169,174]. An alternative method, shown to be more

robust[174], involves biphasic modulation of the Wnt signalling pathway. The canonical Wnt signalling pathway is a key regulator of cardiac development[303]. GSK3β activity leads to the phosphorylation and degradation of β-catenin. By inhibiting GSK3β activity with the small molecule CHIR99021, degradation of β-catenin is prevented. Cytosol accumulation of β-catenin results in its' translocation to the nucleus. In the nucleus, β-catenin forms a complex with transcription factor proteins and consequently activates expression of Wnt pathway gene targets. Long-term (days, opposed to hours) Wnt pathway activation, induces differentiation to mesoderm derivatives[304]. To direct the mesodermal cells into the cardiac lineage the Wnt pathway is inhibited (with small molecule Wnt-C59) – causing suppression of cardiac deregulators MSX1 and CDX2[305] and inducing expression of cardiovascular markers, GATA4 and NKX-2.5[177].

When considering *in vitro* cardiogenesis the culture medium hiPSCs are maintained in, and to which the small molecules are added, is a critical parameter. The undefined make-up of culture media components, such as serum, impacts reproducibility[182]. Additionally, it was identified that the hormone insulin inhibits cardiogenesis[178,306]. Subsequently the field has moved towards chemically defined culture conditions.

Two established cardiac differentiation culture media dominate the literature. The chemically defined basal medium RPMI 1640 served as the basis for both media. The widely utilised RPMI B27 (-insulin) adds the B27 (-insulin) supplement - a serum-free complex mix of 21 components, many of animal origin. RPMI B27 was originally designed for the culture of hippocampal neurons[307]. It remains undetermined if the supplement negatively influences reproducibility of differentiation. It was for this reason that Burridge *et al.* developed a fully defined medium – CDM3. Consisting of only the necessary macromolecules required for the production of hiPSC-CMs, CDM3 is also free of animal-derived products[179]. By systematically eliminating one component found in the B27 (-insulin) supplement at a time, they identified three that were essential to hiPSC cardiac differentiation: RPMI 1640 basal medium, L-ascorbic acid 2-phosphate and BSA. To ensure the medium was free of animal-derived products they replaced BSA for recombinant human albumin.

The aims of this chapter were two-fold:

- To demonstrate the pluripotent state of the patient RYR2 hiPSC line and the subsequent loss of pluripotent marker expression following differentiation to cardiomyocytes
- To identify the culture medium and small molecule kinetics that provide the most efficient differentiation to cardiomyocytes

3.2 Results

3.2.1 RYR2 hiPSCs are pluripotent

To confirm the pluripotency of the RYR2 patient line, hiPSCs were immunostained for four pluripotent markers: nuclear transcription factors, OCT4 and SOX2; and cell surface antigens, SSEA4 and TRA-1-60 (Figure 3.1). Nuclear localisation of OCT4 and SOX2, and cell surface expression of SSEA4 and TRA-1-60 were observed.

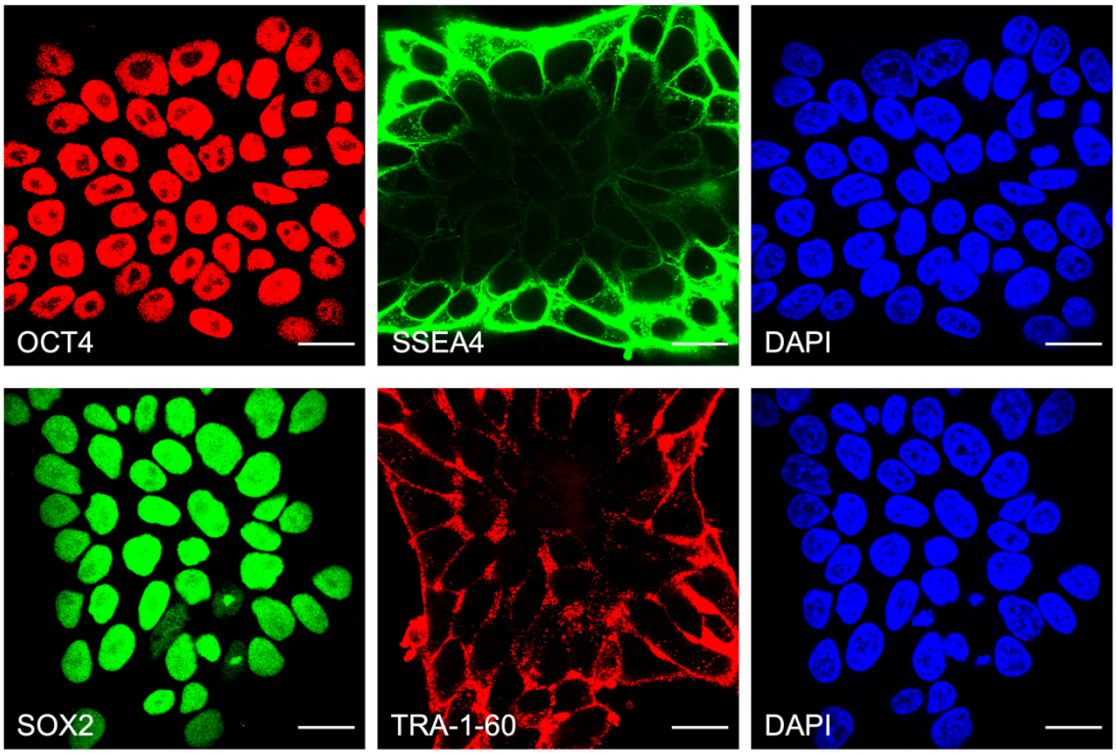

Figure 3.1: Immunostaining of pluripotency markers in hiPSCs

Immunostaining of RYR2 hiPSCs for pluripotency markers OCT4, SSEA4, SOX2 and TRA-1-60. Nuclei stained with DAPI. Scale bar = 20 μm. n=2 biological samples.

To further confirm the RYR2 hiPSCs were pluripotent, RT-qPCR was performed. The expression stability of candidate housekeeping genes were first validated in order to

select a reference gene for data normalisation (Figure 3.2). The geNorm software available in qBase+ by Biogazelle was used; a low M value indicates greater expression stability. The analysis identified *UBC* to be the most stable housekeeping gene in the RYR2 hiPSCs thus was selected as the reference gene for normalisation.

Subsequently, the expression of pluripotency markers NANOG and OCT4 were assessed (Figure 3.3). Both NANOG and OCT4 displayed significantly greater expression in hiPSCs than hiPSC-CMs.

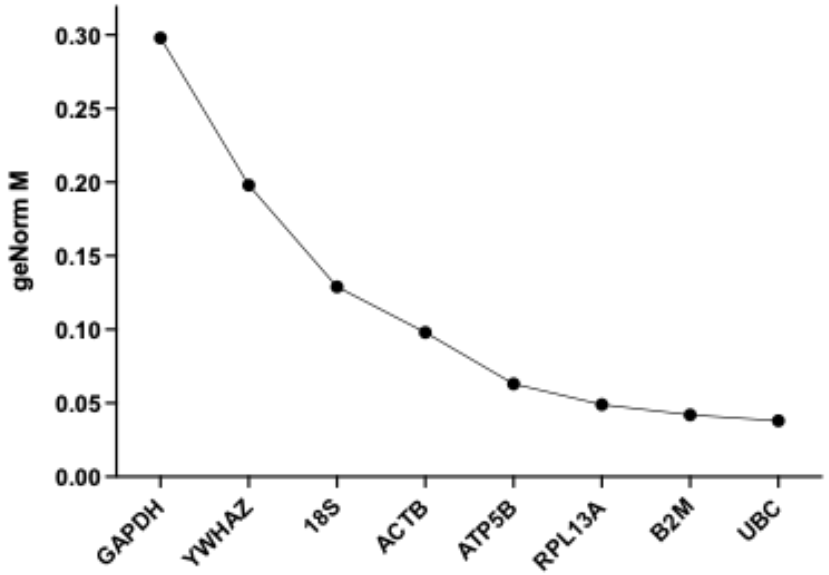

Figure 3.2: Ranked gene expression stability of housekeeping genes in RYR2 hiPSCs

M values were calculated by geNorm and genes ranked in order of stability. A lower M value indicates a high expression stability. M values below 0.5 are typically observed in homogenous samples[308].

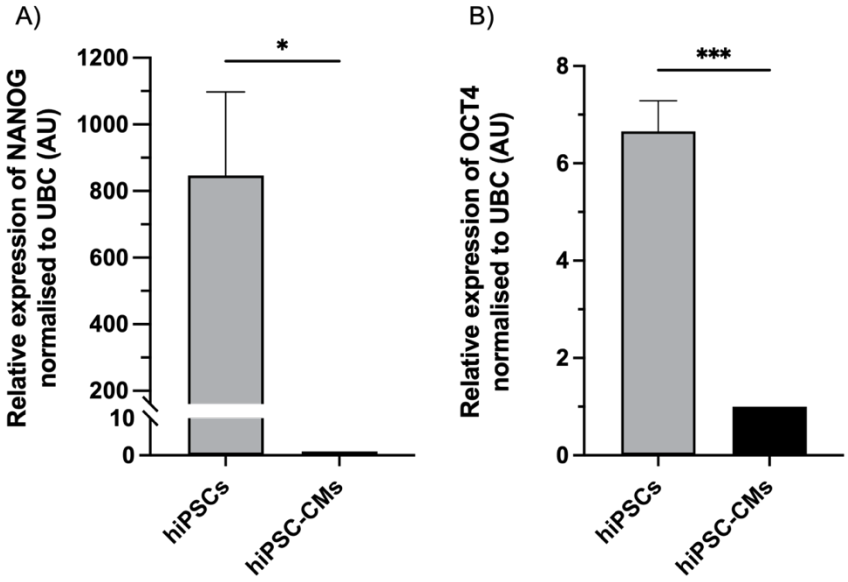

Figure 3.3: Pluripotency marker expression in hiPSCs

RT-qPCR performed on cDNA from RYR2 hiPSCs and hiPSC-CMs to assess the expression of the pluripotency markers *NANOG* (A) and *OCT4* (B). Data was normalised to *UBC* and hiPSC expression is shown relative to hiPSC-CM in arbitrary units (AU). Values are mean ±SEM, n=3 biological samples performed in triplicate. Two-tailed, unpaired t-test was performed. *p<0.05 ***p<0.001

3.2.2 Differentiation optimisation of hiPSCs to hiPSC-CMs

The hiPSCs were differentiated to hiPSC-CMs using a 2D monolayer-based small molecule differentiation protocol. To optimise the differentiation conditions for generation of RYR2 hiPSC-CMs, the culture medium and concentration of CHIR99021 used for induction of the mesoderm were considered.

Two established cardiac differentiation media were compared. The first was a chemically defined platform termed CDM3. The second medium was the more widely utilised RPMI B27 (-insulin). To ascertain which of the media aided more effective cardiomyocyte generation, the percentage of cell culture plate wells inhabited by beating areas at day 10 of differentiation was calculated (Figure 3.4). Only 13% of wells where differentiation took place in CDM3 medium had beating areas compared to 83% of wells in RPMI B27 (-insulin). Thus RPMI B27 (-insulin) was selected as the culture medium of choice.

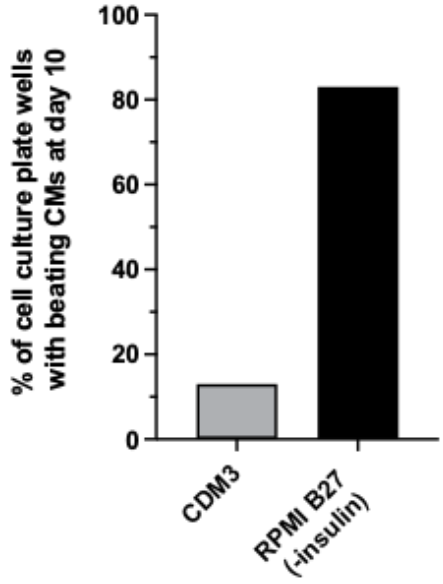

Figure 3.4: RPMI B27 (-insulin) is more effective at generating hiPSC-CMs vs CDM3

Percentage of cell culture plate wells with beating cardiomyocytes (CMs) at day 10 of differentiation. CDM3 medium vs RPMI B27 (-insulin) medium, n=6/44 and n=70/84 culture plate wells, from 4 and 8 independent differentiations respectively.

The optimal concentration of the GSK3β inhibitor (Wnt pathway activator) CHIR99021 used to induce hiPSC differentiation to the mesoderm varies between cell lines. To determine the optimal concentration required for the RYR2 hiPSC line, a range of concentrations were qualitatively assessed (Figure 3.5). Both 6 μM and 8 μM were successful at generating beating areas of cardiomyocytes. Concentrations below 6 μM or above 8 μM resulted in cell death.

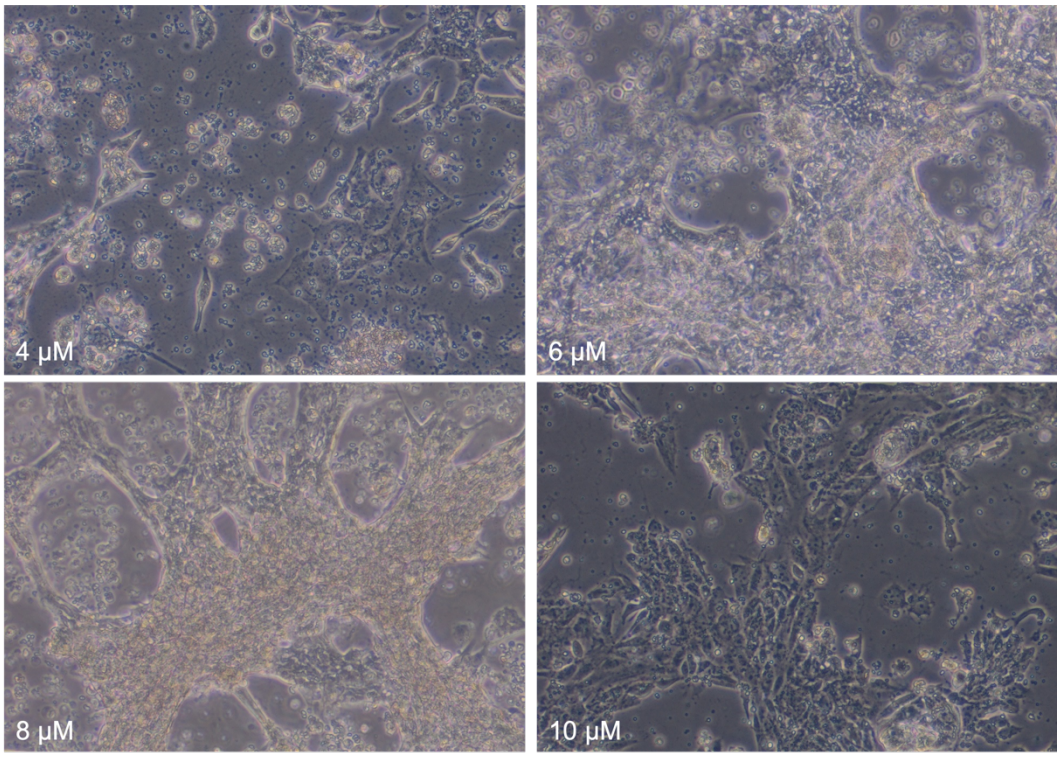

Figure 3.5: Optimal CHIR99021 concentration for generating RYR2 hiPSC-CMs

Representative images following hiPSC differentiation to cardiomyocytes using 4 µM, 6 µM, 8 µM and 10 µM CHIR99021. Note the hiPSC-CM (beating) monolayers at 6 µM and 8 µM CHIR99021.

3.3 Discussion

In this chapter it was confirmed that the RYR2 hiPSC line was pluripotent. Furthermore RPMI B27 (-insulin) culture medium was identified as the most appropriate culture medium, and 6 - 8 µM as the optimal concentrations of CHIR99021, for differentiation of the RYR2 hiPSC line to cardiomyocytes.

Since the successful development of hiPSCs from adult dermal fibroblasts in 2007[163] there has been much scientific interest in the opportunities these cells have the potential to fulfil. Human iPSCs can differentiate into any of the three primary germ layers and hence they have the capability to become any cell type of the human body. Across many specialities within medical science, protocols have been described for the generation of respective cell lineages, often following the stages that occur in embryological development[309–313]. The focus of this study is on hiPSC differentiation to cardiomyocytes for studying of inherited cardiac arrhythmia.

3.3.1 Characterisation of the RYR2 hiPSC line

A detailed characterisation of the generated RYR2 hiPSC line was performed by Dr. Claire Hopton[300]. This included staining for key pluripotency markers; directed differentiation into the three germ lineages; karyotyping to assess genetic integrity; and sequencing to confirm the presence of the nonsense variant. As the hiPSC line had been expanded and undergone multiple passages, it was important to reaffirm the pluripotent nature of the hiPSCs.

The pluripotency of the RYR2 hiPSC line was confirmed through immunostaining and RT-qPCR expression of key pluripotency markers. Maintaining pluripotency in hiPSC lines is critical as once a cell loses pluripotency through differentiation, spontaneously or directed, it cannot differentiate into any other cell type without reprogramming. The confluency of iPSC cultures at the time of harvesting can account for variability in pluripotency marker expression. Cell culture density positively correlates with metabolic activity, resulting in acidification of culture media. It has been demonstrated in mouse iPSCs that alterations to media pH lead to a reduction of pluripotency[314]. This effect can be regulated by more frequent media changes as cell density increases or by use of a cell culture perfusion bioreactor.

For accurate pluripotent gene expression profiles, data was normalised to *UBC* - one of four genes encoding for a polyubiquitin precursor protein. Data must be normalised to a reference gene with stable expression as this removes sample differences such as RNA quantity and quality so real expression profile variations can be identified. The expression of commonly used housekeeping genes varies between cell types; in hPSCs this is poorly understood[315]. Together with cell line variability, this makes systematically identifying the best reference gene important. Application of geNorm software analysis provides a gene stability measure (M) for a candidate reference gene based on the expression variation for that gene. Step-wise exclusion of the gene with the highest M value (lowest stability) allows ranking of the candidate genes[316]. In the RYR2 hiPSCs *UBC* displayed the most stable expression.

3.3.2 Differentiation of hiPSC-CMs – optimised kinetics

The second aim of this chapter was to optimise the initial stages of the differentiation protocol. The differentiation culture medium was considered first, followed by the concentration of the small molecule CHIR99021 required to induce differentiation into the cardiac lineage. Over the past 10+ years, hiPSC differentiation protocols have progressed however they continue to undergo refinement in order to improve their efficiency and reproducibility. Due to variability between cell lines, published protocols are not always reproducible thus the requirement for optimisation for each hiPSC line has been highlighted[175,177]. Here 2D monolayer-based differentiation using small molecules to induce the cardiac lineage was used.

Qualitative analysis of hiPSC-CM beating was used to select for optimal conditions. An alternative more accurate, quantitative method to assess the cultures for cardiac differentiation and yield is flow cytometry for a cardiac-specific protein. This method was attempted but challenges were incurred regarding cell death during preparation of the hiPSC-CMs.

3.3.3 The importance of the differentiation medium

Initial cardiac differentiation protocols included both serum and insulin in the medium. It has since been demonstrated that the presence of serum in the differentiation culture medium negatively affects the morphology and number of beating areas in cultures. Furthermore, mRNA and protein expression of cardiac structural proteins was reduced[317]. Similarly, the presence of insulin in differentiation medium inhibits early differentiation towards mesodermal lineages, and therefore cardiomyocytes. The addition of insulin from day 5 does not appear to be inhibitory[306]. Together these highlight the importance of defining differentiation media components and understanding their role.

Two established differentiation culture media were compared. The widely utilised RPMI B27 (-insulin) and the fully defined CDM3. Differentiating the RYR2 hiPSC line with both media in parallel demonstrated that RPMI B27 (-insulin) supported hiPSC differentiation to cardiomyocytes to a much greater extent than CDM3. This was surprising as the use of CDM3 had been successfully reproduced and efficiently differentiated in 11 hiPSC

lines when developed[179]. Although interestingly in more recent years the laboratory in which CDM3 was developed have moved towards the use of RPMI B27 (-insulin) for cardiac differentiation[318–321]. This suggests that despite CDM3 comprising of only the necessary components for cardiac specification, the additional components of the B27 (-insulin) provide some beneficial aspect.

3.3.4 CHIR99021 concentration alters cardiac differentiation efficiency

Application of CHIR99021 to hPSCs affects both the cell cycle and differentiation - the conditions under which CHIR99021 is added influences the affects it has. For high efficiency cardiac differentiation, pluripotency (>85%) and a high S/G2/M cell-cycle profile (>20%) are recommended. Moreover it has been demonstrated that cell culture confluency impacts the cell-cycle profile: high density cultures (>90%) reduced the S/G2/M cell-cycle phase profile and resulted in a loss of cardiac differentiation efficiency. However 5-7% S/G2/M cell cycle reductions could be restored by lowering the CHIR99021 dose by 2 μM in monolayer cultures[177]. The optimal concentration of CHIR99021 for cardiogenesis is therefore dependent on these three factors.

Successful differentiation to beating cardiomyocytes was observed at both 6 and 8 μM in the RYR2 hiPSC line. As the hiPSCs were not seeded at a specific density during passaging (typically a split ratio of 1:12, every 3-4 days) this is perhaps unsurprising because the culture density will have varied between cultures and passages. It has also been suggested that as culture densities increase, proliferation slows due to contact inhibition and restricted cell expansion[322]. Hence fewer cells would be in the S/G2/M cell-cycle phase so would require the lower CHIR99021 concentration for optimal differentiation efficiency. By using both concentrations of CHIR99021 the variability in culture confluency was accounted for and improved the consistency in cardiomyocyte yield per culture batch.

3.3.5 Control hiPSC line differentiation

The optimised differentiation protocol outlined in this chapter was tested in the two control hiPSC lines. Cardiomyocytes were successfully generated in RPMI B27 (-insulin) medium. The UKBi005 line required 8-10 μM CHIR99021 and the human Episomal iPSC line required 6-8 μM CHIR99021.

3.3.6 Purification of hiPSC-CM cultures

In parallel, metabolic selection and MACS were evaluated as methods for purifying the differentiated cultures - enriching them with cardiomyocytes. Neither method was identified as being superior; for practicality reasons MACS was selected as the method of choice.

3.3.7 Limitations of hiPSC-CMs as a model

An important note to consider when using hiPSC-CMs as a model is that current, well-established protocols such as the ones used as a basis for the method here[178,179], generate all subtypes of cardiomyocytes: atrial, nodal and ventricular[180]. This should be taken into consideration, particularly when considering electrophysiological analysis. Subtype specific protocols have been developed[323–325] but an alternative method would be to separate the subtypes by fluorescence activated cell sorting.

Furthermore, despite optimisation of the differentiation culture medium and kinetics, the hiPSC-CMs generated are phenotypically immature. Morphologically, hiPSC-CMs are smaller and do not conform to the characteristic rod-shaped cardiomyocyte[197]. Structurally, vital components of the calcium release unit are under-developed and are not co-localised with absent T-tubules, and sarcomeres present in a disorganised manner[196]. As a result calcium handling properties and EC coupling are affected.

Human iPSC-CMs also possess an altered gene expression profile, often accounting for further functional short-comings. Many genes encoding for ion channel subunits critical to the cardiac action potential and EC coupling are expressed at lower levels, including sodium, calcium and potassium channels[183]. Consequently, hiPSC-CM action potential and calcium transients display a slower rate of rise and decay. Addition of β-AR agonists such as isoprenaline require higher concentrations to provoke the expected chronotropic response[180,300]. A minimal or lack of response to β-AR pathway stimulation suggests reduced β_1-AR expression.

Mitochondria account for roughly 25% of an adult cardiomyocytes' volume and are regularly distributed, however in hiPSC-CMs mitochondria are smaller and cluster

together. Furthermore, native cardiomyocytes undergo a switch from glycolytic metabolism to fatty acid metabolism as they mature[326]. Current culture media compositions mean hiPSC-CMs rely on glycolysis for production of energy thus metabolic maturation is prohibited.

3.3.8 Maturation of the hiPSC-CM phenotype

Developing strategies to mature hiPSC-CMs so they are more representative of native adult cardiomyocytes remains an important challenge facing scientists in the field. Over the past few years multiple techniques have been demonstrated to enhance hiPSC-CM structure, function and metabolism: 1) a prolonged culture period[220,263]; 2) biochemical cues such as hormones[199] and changes to culture medium components (glucose/lactate to fatty acids)[214]; 3) cocultures[280,281]; 4) biophysical stimulation[294]; and 5) 3D culture[259].

3.4 Conclusion and future work

This chapter has confirmed the pluripotent nature of our RYR2 hiPSC line. Additionally, it has demonstrated the preferential cardiac differentiation culture medium to be RPMI B27 (-insulin) and the optimal CHIR99021 concentration to be 6-8 μM. However further work is required to develop the structural, functional and metabolic phenotypes of generated hiPSC-CMs to enhance their ability to recapitulate and model human cardiac diseases, and aid in the discovery of new potential therapeutics and preclinical toxicology assessments. In the following chapters the differentiation protocol will be developed in order to produce RYR2 hiPSC-CMs with matured morphology and improved calcium handling properties.

Chapter 4

The effect of prolonged culture and hormone supplementation on RYR2 hiPSC-CM maturation

4 The effect of prolonged culture and hormone supplementation on RYR2 hiPSC-CM maturation

4.1 Introduction

Cardiomyocytes derived from patient-specific hiPSCs theoretically offer an infinite source for studying both basic science and applied science - from investigating cardiac disease mechanisms to drug discovery, cardiotoxicity, and efficacy assessments. However, hiPSC-CMs have an immature phenotype relative to native adult cardiomyocytes. Hence their current suitability as a model for such applications is not clear.

Inherited cardiac arrhythmia disorders were among the first to be modelled in hiPSC-CMs[20,65,204,248]. CPVT is an inherited cardiac channelopathy characterised by ventricular tachycardia following stress or exercise induced catecholamine stimulation of β-ARs. Cardiac arrhythmias, such as CPVT, are caused by calcium handling abnormalities. To date mutations in genes including *RYR2*, *CASQ2, TECRL, CALM1*, and *TRDN* have been identified as the genetic cause of CPVT. Each of the genes encode proteins that are directly involved in cardiac calcium homeostasis and/or handling[12]. The mechanisms underlying each genes' role in CPVT are still debated. Nonetheless it is widely accepted that the mutations impair SR calcium storage and release, leading to pathological calcium release during diastole[12,327]. In order to recapitulate cardiac arrhythmia diseases such as CPVT accurately, it is fundamental that *in vitro* hiPSC-CM models recreate the electrophysiological properties, intracellular processes (e.g. EC coupling and calcium handling), and signalling pathways (e.g. β-AR) of adult cardiomyocytes reliably.

Following basic hiPSC differentiation, hiPSC-CMs have been reported to demonstrate action potential characteristics similar to human ventricular myocytes. Expression of major cardiac ion channels responsible for the ionic currents of the ventricular action potential have been detected including the cardiac sodium channel, *SCN5A*; calcium channel, *CACNA1C*; and potassium channels *KCNH2* and *KCNQ1*[328–330]. However a comparable gene expression does not always translate to a comparable current density[331]. Conversely, substantial differences in the expression level of *KCNJ2* (reduced

or absent) and *HCN4* (increased) have been reported[330]. Together these lead to a less negative resting membrane potential and promote spontaneous automaticity.

Regarding key components of calcium handling (RYR2, CASQ2, SERCA2a, PLN, NCX) and the contractile machinery (alpha actinin, cTnI, cardiac troponin T [cTnT], β-MHC) gene and protein expressions have been confirmed in hiPSC-CMs, albeit at low levels relative to the adult human heart[210,216,220,330,332,333]. As a result the kinetics of the calcium transient, particularly the decay rate, are much slower. Furthermore, low level expression of β-ARs (β_1 and β_2) has been reported relative to human ventricular myocytes[210,266,329] suggesting functionally the signalling pathway is relatively immature.

The implementation of hiPSC-CMs as models for cardiac channelopathies has been increasingly reported. Despite sharing molecular, structural and functional properties, and displaying phenotypes consistent with a variety of diseases, the observed differences between native adult cardiomyocytes and hiPSC-CMs show that hiPSC-CM technology still requires refinement. In recent years, strategies have emerged for improving the maturation of hiPSC-CMs.

In the previous chapter the initial stages of differentiation to hiPSC-CMs were optimised. Now, two approaches to enhance the maturation of the differentiated RYR2 hiPSC-CMs are evaluated. The first was a prolonged culture period. Full maturation of the native adult heart is known to take years thus it seems reasonable that with an extended culture period RYR2 hiPSC-CMs would develop in maturity. This hypothesis is supported by work in other cell lines where changes in morphology have been observed including increased cell size, and organisation of myofibrils and sarcomeres. Moreover the expression of ion channels and cardiac-specific genes increased, and functional improvements have been demonstrated[210,220,263,265].

The second approach involved application of additional hormones to the culture medium. Thyroid hormone is known to circulate in the blood[334] and acts on most cells and organs in the body[335]. During postnatal cardiac development, thyroid hormone exerts its effects through both genomic and nongenomic mechanisms. Genomically thyroid hormone binds to nuclear receptors and in turn these bind to thyroid hormone

response elements in gene targets, activating or repressing gene expression. Thyroid hormone-regulated gene expression effects synthesis of structural and regulatory cardiac proteins altering their activity during EC coupling[334,336]. Nongenomic thyroid hormone mediates changes to the functional properties of plasma membrane ion channels and pumps by modifying current densities and the inactivation of channels thus altering action potential duration; protein trafficking, leading to small changes in cell surface and SR protein densities e.g. adrenoceptors and SERCA2a; the force of myocardial contractility; and myocardial glucose metabolism[337]. Glucocorticoids are also vital for cardiac development, although primarily during late foetal maturation[273,274]. Like thyroid hormone they exert genomic and nongenomic effects by regulating gene transcription and interacting with other cytoplasmic signalling proteins respectively. Conditional disruption of the glucocorticoid receptor in cardiomyocytes and vascular smooth muscle cells impairs foetal heart function – the expression of genes encoding calcium handling and contractile proteins is disrupted, and structural immaturity is observed[273]. Accordingly, addition of exogenous glucocorticoids to primary-mouse-foetal cardiomyocytes improved EC coupling properties and promoted structural organisation[274].

The principal aim of this chapter was:

- To evaluate the effects of prolonged culture, and the supplementation of thyroid and glucocorticoid hormones to the culture medium, on RYR2 hiPSC-CM maturity

As such, RYR2 hiPSC-CMs were cultured for either 30 days or 45 days, with or without hormone supplementation (0.1 μM T3 and 1 μM Dex) from day 16 (Figure 4.1). This was predominantly assessed through changes in gene expression including those encoding for SR proteins (calcium handling), contractile proteins, T-tubule related proteins, membrane-bound ion channels, and β-ARs and their signalling apparatus. Prior to the gene expression studies primer pairs were designed and confirmed for specificity, and a reference gene with expression stability in the RYR2 hiPSC-CMs was elucidated for data normalisation.

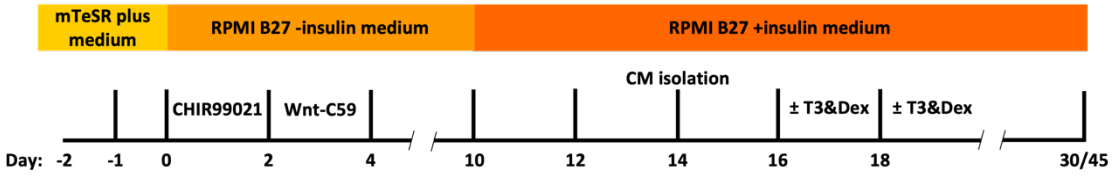

Figure 4.1: Cardiac differentiation protocol with prolonged culture and hormone supplementation

Extension of basic differentiation protocol used to assess the effects of prolonged culture and hormone supplementation on hiPSC-CM maturity. Hormone supplementation from day 16: triiodothyronine (T3, 0.1 μM) and dexamethasone (Dex, 1μM). Culture length: maintenance for 30 days or 45 days. CM, cardiomyocyte. Identical to Figure 2.2.

4.2 Results

4.2.1 PCR products confirm primer specificity

Primers were designed for each of the cardiac-related genes selected to determine RYR2 hiPSC-CM maturity. To confirm the designed primer pairs annealed to and amplified the desired fragment only, PCR products were analysed by high-resolution capillary electrophoresis to ensure they matched the expected size (Figure 4.2). Each primer pair amplified only one DNA fragment which equated to the expected product size (refer to Table 10); therefore primers were suitable for gene expression studies.

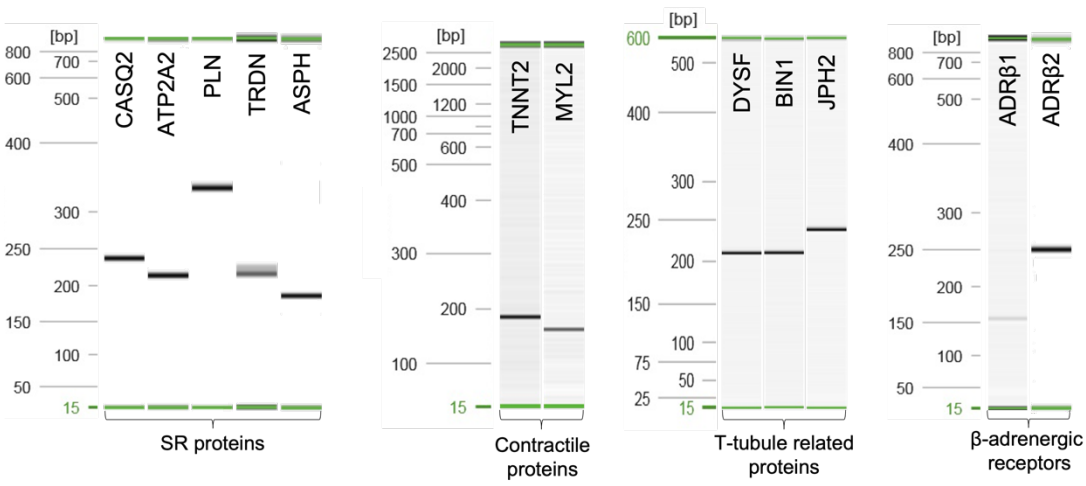

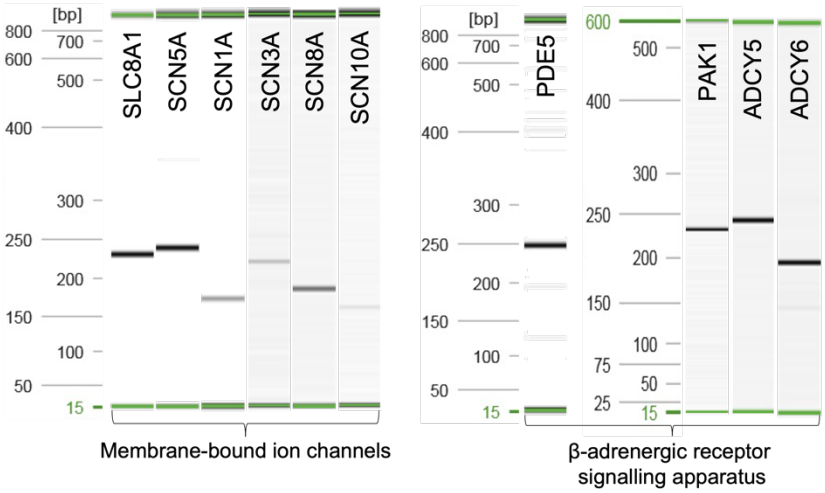

Figure 4.2: Confirmation of primer specificity

High-resolution capillary electrophoresis of PCR products to confirm specificity of designed primer pairs. Genes encode for cardiac proteins important for EC coupling and related activity. SR, sarcoplasmic reticulum.

4.2.2 Identification of a reference gene for RYR2 hiPSC-CM RT-qPCR data normalisation

To determine a suitable reference gene for gene expression data normalisation, the stability of a selection of candidate housekeeping genes in the RYR2 hiPSC-CMs was calculated (M value). The genes were ranked in order of stability (Figure 4.3). This was performed using the software tool qBase^{+}. A low M value corresponds to more stable gene expression. The housekeeping gene (from the candidate list assessed) with the most stable expression was *UBC*. Consequently *UBC* was implemented for RYR2 hiPSC-CM RT-qPCR data normalisation.

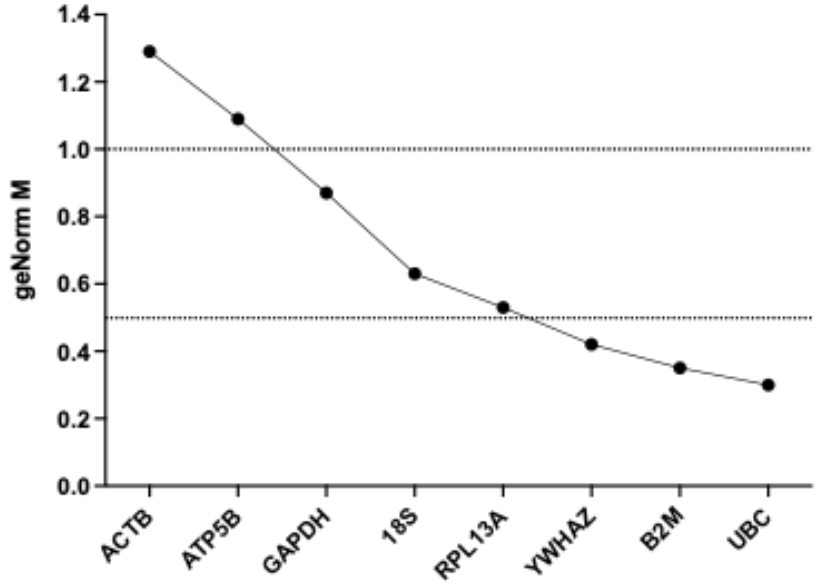

Figure 4.3: Ranked gene expression stability of housekeeping genes in RYR2 hiPSC-CMs

Housekeeping gene stability in RYR2 hiPSC-CMs represented by M values calculated by geNorm. Genes are ranked in order of stability. A lower M value indicates a high expression stability. M values below 1 and 0.5 are typically observed for stably expressed reference genes in heterogenous and homogenous samples respectively[308].

4.2.3 Gene expression of cardiac SR proteins

To characterise the calcium handling properties of RYR2 hiPSC-CMs following 30 days or 45 days of culture, with and without culture medium hormone supplementation, the gene expression of cardiac SR proteins were validated by RT-qPCR (Figure 4.4): *RYR2* (RYR2), main calcium release channel; *CASQ2* (CASQ2), binds and stores calcium in the SR lumen; *ATP2A2* (SERCA2a), pump responsible for majority of calcium reuptake from cytosol during diastole; *PLN* (PLN), modulates activity of SERCA2a; *TRDN* (TRDN) and *ASPH* (JCN), involved in the regulation of calcium release. The expression of target genes was normalised to *UBC* and are displayed relative to the baseline culture condition: 30 days without hormone supplementation.

In the absence of supplementary hormones, the expression of *CASQ2* increased with prolonged culture (Figure 4.4B). However, with the addition of hormones the reverse is observed – a significant decrease in *CASQ2* expression. This suggests prolonged culture and hormone supplementation have opposing effects on *CASQ2* expression; the influence of the supplementary hormones nullifies those of prolonged culture.

Surprisingly, the changes in *CASQ2* expression were isolated with regards to the other SR proteins evaluated, as no changes in the expression of *RYR2*, *ATP2A2*, *PLN*, *TRDN*, or *ASPH* were observed.

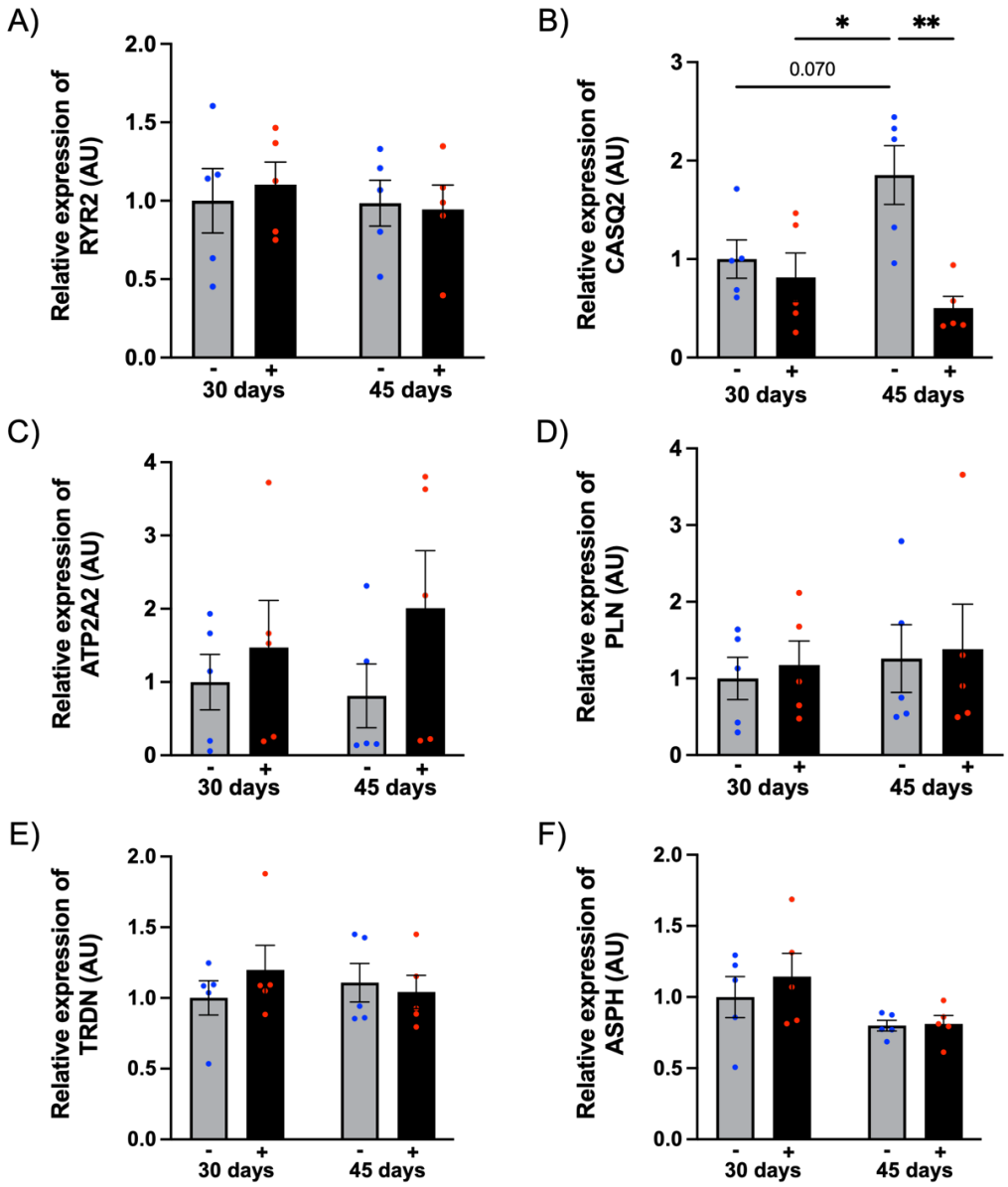

Figure 4.4: Expression of cardiac SR proteins

RT-qPCR performed on RYR2 hiPSC-CMs to assess the expression of cardiac SR proteins at 30 days and 45 days of culture, ±hormone supplementation (T3 and Dex). (A) *RYR2*, (B) *CASQ2,* (C) *ATP2A2*, (D) *PLN*, (E) *TRDN*, (F) *ASPH*. Data was normalised to *UBC* and expression is shown relative to 30 days without hormone supplementation in arbitrary units (AU). Values are mean ±SEM, n=5 biological samples performed in triplicate. Two-way ANOVA was performed followed by Tukey's multiple comparisons test. *p<0.05 **p<0.01

4.2.4 Gene expression of cardiac T-tubule related proteins

The expression of genes encoding for proteins associated with cardiac T-tubule formation and maintenance: *DYSF* (dysferlin)[338,339], *BIN1* (bridging integrator 1)[340,341] and *JPH2* (junctophilin 2)[342–344] were also assessed (Figure 4.5). Hormone supplementation caused a decrease in the expression of each gene, irrespective of culture length. Notably the effect was only significant for *BIN1*. Although the combined effect of the maturation factors (MFs) significantly reduced *DYSF* expression compared to baseline culture conditions.

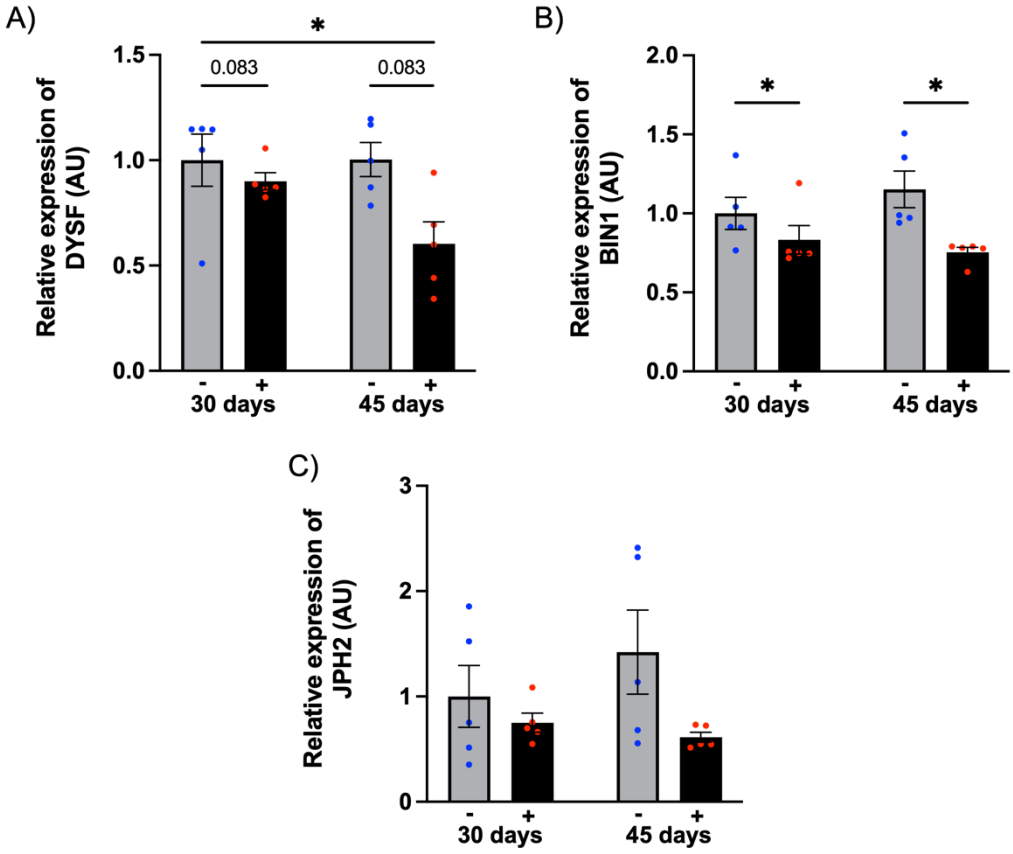

Figure 4.5: Expression of cardiac T-tubule related proteins

RT-qPCR performed on RYR2 hiPSC-CMs to assess the expression of proteins associated with cardiac T-tubule formation and maintenance, at 30 days and 45 days of culture ±hormone supplementation (T3 and Dex). (A) *DYSF*, (B) *BIN1*, (C) *JPH2*. Data was normalised to *UBC* and expression is shown relative to 30 days without hormone supplementation in arbitrary units (AU). Values are mean ±SEM, n=5 biological samples performed in triplicate. Two-way ANOVA was performed followed by Tukey's multiple comparisons test. *p<0.05

4.2.5 Gene expression of cardiac contractile proteins

The gene expression of myofilament proteins: *TNNI3* (cTnI), *TNNT2* (cTnT), *MYH6* (α-MHC) and *MYL2* (myosin light chain 2) were evaluated as markers of cardiac muscle contraction (Figure 4.6). No expression differences were detected among culture conditions.

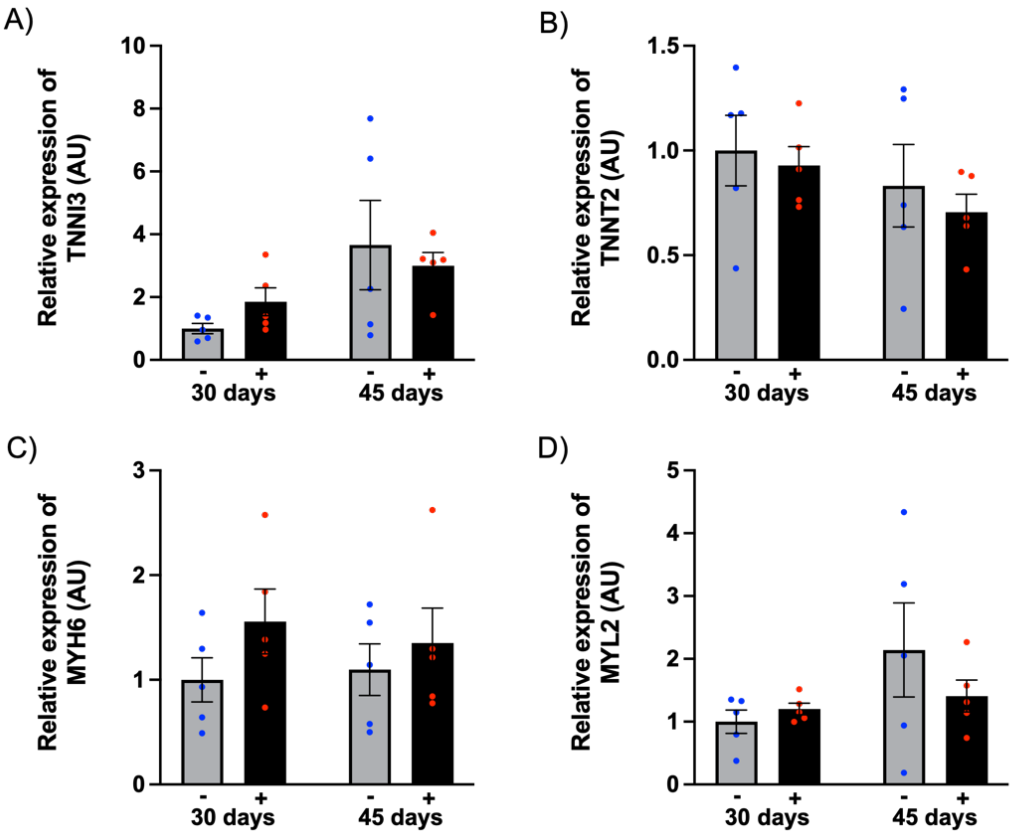

Figure 4.6: Expression of cardiac contractile proteins

RT-qPCR performed on RYR2 hiPSC-CMs to assess the expression of cardiac contractile proteins at 30 days and 45 days of culture, ±hormone supplementation (T3 and Dex). (A) *TNNI3*, (B) *TNNT2*, (C) *MYH6*, (D) *MYL2*. Data was normalised to *UBC* and expression is shown relative to 30 days without hormone supplementation in arbitrary units (AU). Values are mean ±SEM, n=5 biological samples performed in triplicate. Two-way ANOVA was performed followed by Tukey's multiple comparisons test.

4.2.6 Sodium channel subunit expression (and NCX)

To understand the effect of prolonged culture and hormone supplementation on some of the electrophysiological properties of RYR2 hiPSC-CMs, the gene expression of sodium membrane-bound ion channels, including NCX, was validated. With respect to calcium handling sodium channel activity is firmly linked with intracellular calcium concentrations[39,40].

The addition of supplementary hormones caused a significant downregulation in the expression of *SCN1A*, irrespective of culture length (Figure 4.7A). A similar trend was observed in *SCN3A* expression but statistical significance was not reached (Figure 4.7B). The combined effects of prolonged culture and hormone treatment also appeared to reduce *SCN8A* expression (Figure 4.7D). No changes in the expression of the cardiac isoform *SCN5A* (Figure 4.7C), or *SCN10A* (Figure 4.7E) were observed. Furthermore the gene expression of *SLC8A1* which encodes NCX did not demonstrate differential expression following prolonged culture and/or hormone supplementation either (Figure 4.7F).

When considering the ratio of sodium channel subunits within each culture condition, *SCN1A* was the predominant subunit across all conditions, followed by *SCN5A* (Figure 4.8). However with extended culture and additional culture medium hormones, the expression ratios of *SCN1A* and *SCN5A* altered. *SCN1A* expression decreased (20%) and *SCN5A* increased (20%) – potentially indicating a switch in the predominant subunit was emanating (Figure 4.8E).

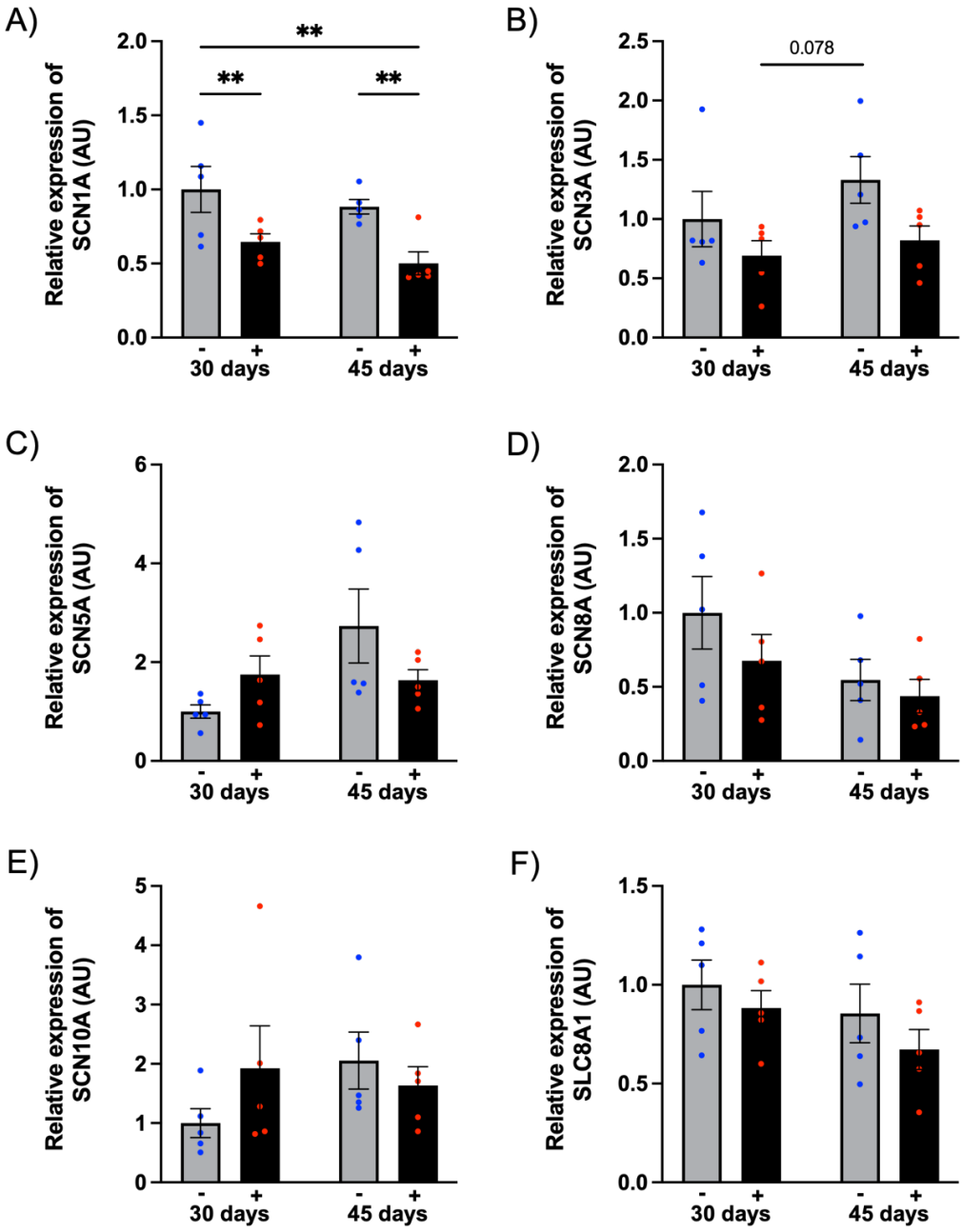

Figure 4.7: Expression of sodium channel subunits and NCX

RT-qPCR performed on RYR2 hiPSC-CMs to assess the expression of sodium channel subunits and NCX at 30 days and 45 days of culture, ±hormone supplementation (T3 and Dex). (A) *SCN1A* (B) *SCN3A*, (C) *SCN5A*, (D) *SCN8A*, (E) *SCN10A*, (F) *SLC8A1*. Data was normalised to *UBC* and expression is shown relative to 30 days without hormone supplementation in arbitrary units (AU). Values are mean ±SEM, n=5 biological samples performed in triplicate. Two-way ANOVA was performed followed by Tukey's multiple comparisons test. *p<0.05 **p<0.01

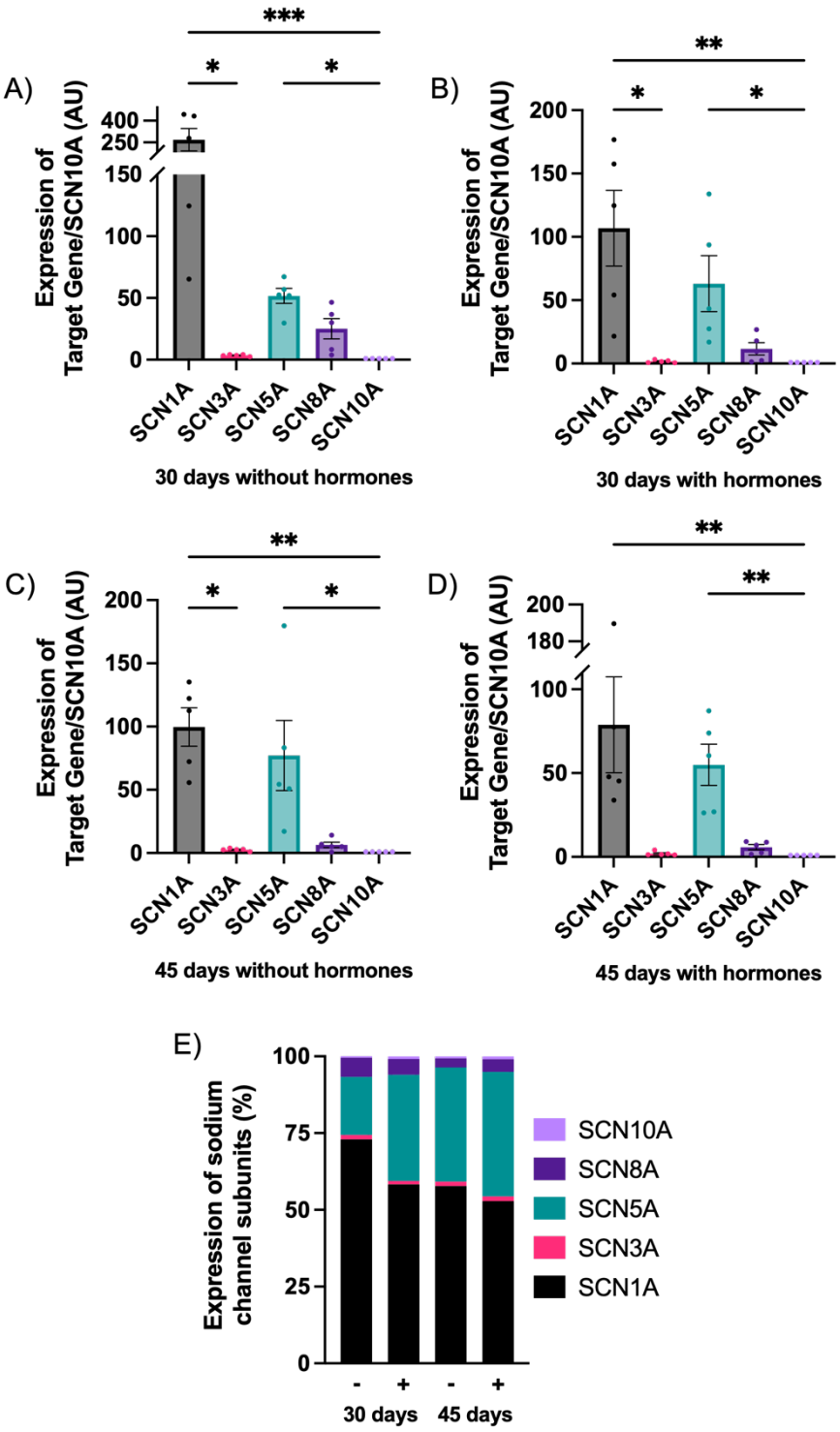

Figure 4.8: Ratio of sodium channel subunits

RT-qPCR performed on RYR2 hiPSC-CMs to compare the expression of sodium channel subunits at 30 days and 45 days of culture, ±hormone supplementation (T3 and Dex). (A) 30 days without hormones, (B) 30 days with hormones, (C) 45 days without hormones, (D) 45 days with hormones. Expression is shown relative to *SCN10A* in arbitrary units (AU). (E) Sodium channel subunit expression as a % of total subunits measured in same sample. All data was normalised to *UBC* and values are mean ±SEM, n=5 biological samples performed in triplicate. One-way ANOVA was performed followed by Dunn's multiple comparisons test. *p<0.05 **p<0.01 ***p<0.001

4.2.7 Expression of β-adrenergic receptors

As previously explained catecholamine stimulation of β-ARs, particularly the β_1 subtype, is a major part of the mechanism underlying the arrhythmias characterising CPVT. Hence the final expression properties of the RYR2 hiPSC-CMs used to evaluate maturity following prolonged culture and hormone supplementation were those of β_1- and β_2-ARs (*ADRβ1* and *ADRβ2*) and their signalling apparatus.

ADRβ1 expression significantly increased in hormone-treated hiPSC-CMs, irrespective of culture length. Prolonged culture also significantly increased expression, although only in hormone-treated hiPSC-CMs (Figure 4.9A). Conversely, there were no statistically significant *ADRβ2* expression changes observed between the culture conditions; despite prolonged culture exhibiting an overall trend of decreased expression (Figure 4.9B).

Figure 4.9C-D illustrate the ratio of *ADRβ1* and *ADRβ2* expression within each culture condition. At 30 days without hormones, the expression of *ADRβ1* and *ADRβ2* is almost equal. However the MFs significantly altered this ratio. At 30 days, hormones increased the ratio of *ADRβ1*:*ADRβ2* by 4.7 times. In the absence of hormones, 45 days of culture led to *ADRβ1* expression double that of *ADRβ2*. Neither were reported as significant. At 45 days with hormones, the ratio of *ADRβ1* to *ADRβ2* was 17:1. This was significantly higher than any of the other culture conditions: prolonged culture increased the ratio by 3.6 times; hormone supplementation by almost 9 times; and the combination of both variables by more than 16.5 times. When calculated as a percentage of combined receptor expression, at 30 days without hormones *ADRB1* accounted for 42%. This increased to 93% at 45 days with hormones.

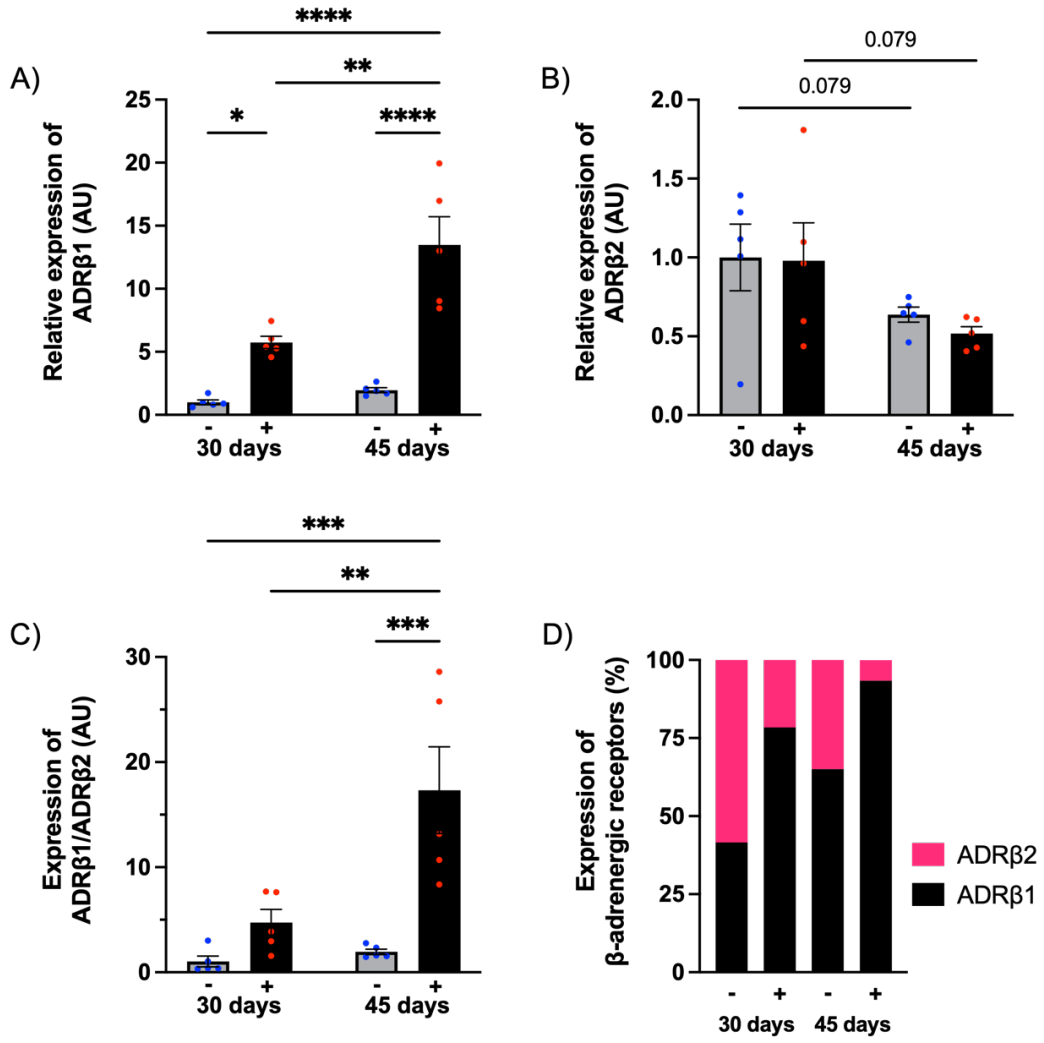

Figure 4.9: Gene expression of β-adrenergic receptors

RT-qPCR performed on RYR2 hiPSC-CMs to assess the expression and ratio of cardiac β-adrenergic receptors at 30 days and 45 days of culture, ±hormone supplementation (T3 and Dex). (A) *ADRβ1*, (B) *ADRβ2*. Expression is shown relative to 30 days without hormone supplementation in arbitrary units (AU). (C) Ratio of β-adrenergic receptors. (D) β-adrenergic receptor expression as a % of total receptors measured in same sample. All data was normalised to *UBC* and values are mean ±SEM, n=5 biological samples performed in triplicate. Two-way ANOVA was performed followed by Tukey's multiple comparisons test. *p<0.05 **p<0.01 ***p<0.001 ****p<0.0001

To substantiate the increased *ADRβ1* gene expression observed with prolonged culture and hormone supplementation, western blots were performed to investigate changes in ADRβ1 protein expression between the culture conditions (Figure 4.10). As observed following analysis of *ADRβ1* gene expression, hormone supplementation and culture length were responsible for significant changes to the protein expression of ADRβ1. A

synergistic effect of the MFs was observed: ADRβ1 expression was significantly increased at 45 days with hormones compared to 45 days without hormones, and both 30 days with and without hormones. See Appendix for a representative full western blot image.

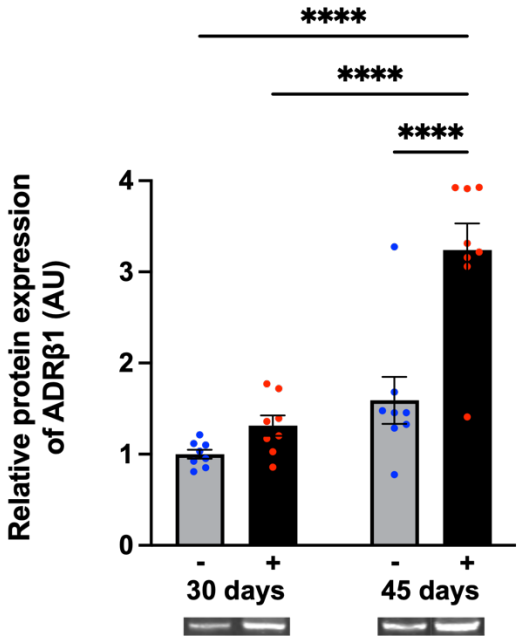

Figure 4.10: Protein expression of β-adrenergic receptors

Western blots performed on RYR2 hiPSC-CMs to assess the expression of ADRβ1 at 30 days and 45 days of culture, ±hormone supplementation (T3 and Dex). Expression is shown relative to 30 days without hormone supplementation in arbitrary units (AU). Values are mean ±SEM, n=8 biological samples performed in triplicate. Two-way ANOVA was performed followed by Tukey's multiple comparisons test. ****p<0. 0001

4.2.8 Gene expression of cardiac β-adrenergic receptor signalling apparatus

Figure 4.11 displays the gene expression of cardiac β-AR signalling effectors (*PDE5*, PDE5; *PAK1*, p21-activated kinase 1 [PAK1]; *ADCY5*, adenylyl cyclase 5; and *ADCY6*, adenylyl cyclase 6) involved in the regulation of protein phosphorylation and in turn the dynamics of contraction. The addition of hormones, irrespective of culture length, caused a significant reduction in *PAK1* expression. No statistically significant changes in expression were observed for *PDE5*, *ADCY5* or *ADCY6*. Nevertheless there was an overall trend of increased *PDE5* expression with prolonged culture and hormone treatment, and the combination of MFs appeared to cause a reduction in both *ADCY5* and *ADCY6* expression.

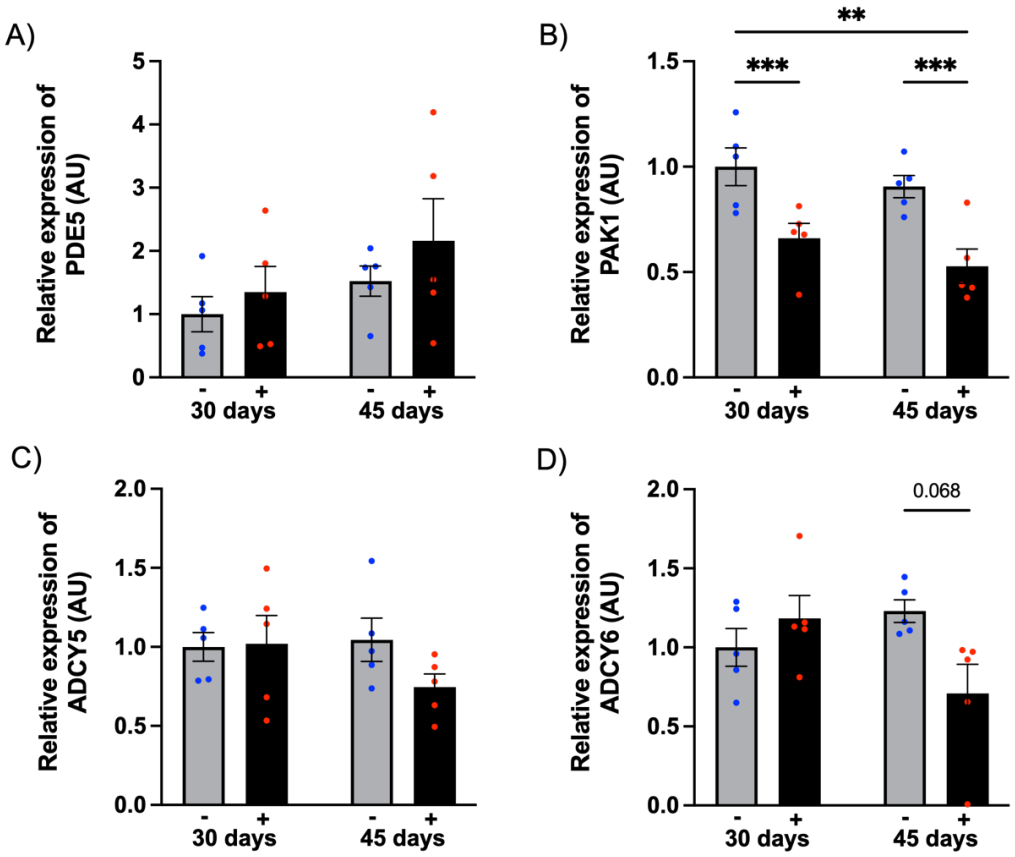

Figure 4.11: Expression of β-adrenergic signalling apparatus

RT-qPCR performed on RYR2 hiPSC-CMs to assess the expression of cardiac β-adrenergic signalling effectors at 30 days and 45 days of culture, ±hormone supplementation (T3 and Dex). (A) *PDE5*, (B) *PAK1*, (C) *ADCY5*, (D) *ADCY6*. Data was normalised to *UBC* and expression is shown relative to 30 days without hormone supplementation in arbitrary units (AU). Values are mean ±SEM, n=5 biological samples performed in triplicate. Two-way ANOVA was performed followed by Tukey's multiple comparisons test. *p<0.05 **p<0.01

4.3 Discussion

In recent years hiPSC-CMs have been used to model inherited cardiac arrhythmia diseases. The properties of patient-specific hiPSCs: the ability to be cultured indefinitely and them harbouring the same genetic background as the donor, makes them an attractive model despite their shortcomings. Nevertheless, it is important to know and acknowledge the differences between hiPSC-CMs and the native adult cardiomyocytes they are representing. As highlighted in Chapter 3, a variety of methods for differentiating hiPSCs to cardiomyocytes exists (e.g. culture media composition, induction via growth factors or small molecules) and these continue to be developed to

improve hiPSC-CM maturity. Accordingly, it is also pertinent to recognise that individual cell lines differentiated using different protocols, and maintained under different conditions may show different properties and therefore should always be characterised.

In this chapter, the differentiation protocol was evolved with the aim of developing RYR2 hiPSC-CMs with increased maturity. The effects of prolonged culture (30 days vs 45 days) and hormone supplementation (with vs without T3 and Dex) were assessed by a systematic characterisation of gene expression. Designed primer pairs for each gene were confirmed for specificity – also demonstrating the expression of each gene in the RYR2 hiPSC-CMs. Relative mRNA levels of each gene, which encode for proteins critical to normal cardiac function, were presented. The relative protein expression of ADRβ1 was also evaluated. Surprisingly, few changes were observed with application of the MFs.

The main findings were:

- An increase in *ADRβ1* expression (at the genomic and protein level)
- A reduction in *CASQ2* expression
- A reduction in *PAK1* expression

4.3.1 β-adrenergic receptors

In cardiomyocytes β-AR signalling is a fundamental process for regulating cardiac function. It relies on distinct microdomains for coupling catecholamine stimulation to PKA activation in order to bring about changes in cardiac contractility. Following basic differentiation methods, β-AR expression is much lower than that of human left ventricular cardiomyocytes[210,264]. Independently and in combination, prolonged culture and hormone supplementation resulted in significantly increased *ADRβ1* gene expression in RYR2 hiPSC-CMs. These data were validated by protein expression analyses. Interestingly, neither variable led to a change in *ADRβ2* expression. Consequently, the ratio of *ADRβ1* to *ADRβ2* expression altered – increasing the proportion of *ADRβ1*. In terms of modelling CPVT, in which individuals develop adrenergically mediated arrhythmias, the observed increase in ADRβ1 expression was essential and compelling.

The increase in ADRβ1 expression appeared to be primarily a result of thyroid and glucocorticoid hormone supplementation - enhanced by prolonged culture. To date, reports regarding the effect of thyroid or glucocorticoid hormones on hiPSC-CM maturity focus on structural and functional changes[199,270,271]. In depth gene expression characterisations are limited in hiPSC-CMs. The independent effects of thyroid hormone on β-ARs in other mammalian models however have long been described. Under conditions of excess thyroid hormone a significant increase in the number of β-ARs has been consistently reported in the rat ventricle[345]. In baboons with induced clinical thyrotoxicosis, left ventricular β_1 and β_2 -AR subtype densities significantly increased compared to control baboons[346]. Furthermore, in healthy human subjects oral administration of thyroid hormone led to a ~30% increase in β-AR density in skeletal muscle[347]. Concurrently, in hypothyroid rat hearts β-AR number has been consistently reported to decrease[345,348].

Studies investigating the effects of glucocorticoids on β-AR expression report mixed results. Similar to the observations in the present study, Kawano *et al.*[349] demonstrated a significant increase in Sprague-Dawley rat left ventricular β_1 subtype mRNA following Dex administration. No difference in β_2 subtype mRNA was observed. Contrastingly, hydrocortisone treatment of Wistar rats caused significant increases in the density of both β_1 and β_2 subtypes in the atria, but only β_2 in ventricles[350]. Dangel *et al.*[351] reported upregulation of β_2 subtype mRNA and protein in a rat heart cell line, with no changes in the expression of β_1 subtype. However, this could potentially be explained by the receptor subtype ratio being reversed compared to human heart[352,353], and adult rat heart[348].

Prolonging the culture length of RYR2 hiPSC-CMs enhanced the ADRβ1 expression increase caused by the hormone supplementation. This is perhaps unsurprising if you consider the human heart takes years to reach full maturation[260,262]. The time-dependent effect on the expression pattern of β-ARs in hiPSC-CMs is more widely reported than hormone supplementation. At 30 days post-initiation of differentiation to cardiomyocytes, β_2-ARs are the dominant subtype[210,264,266], corroborating the results observed in this study. ADRβ2 expression significantly increases, but not exclusively, in early stages of differentiation (0-30 days)[210,264,266]. ADRβ1 displays later-onset

expression development in comparison; to our knowledge no significant expression changes have been observed prior to 30 days of differentiation. Significant increases in ADRβ1 expression are observed at varying time points between 30 days and 90 days after differentiation[210,264,266]. Accordingly, a switch in dominant β-AR subtype from β_2 to β_1[210,264] further supports the data presented in this study, and represents the native healthy adult cardiomyocyte phenotype more closely - where a ventricular β_1**:** β_2 subtype ratio of 80:20 distribution is reported[352,354].

4.3.2 β-adrenergic signalling apparatus

Following catecholamine stimulation of β-ARs, the stimulatory G_α subunit dissociates from the GPCR complex rendering activity. In turn the adenylyl cyclase's are activated and catalyse the production of cAMP from ATP. The primary function of cAMP is to provoke PKA phosphorylation of regulatory proteins to initiate positive inotropic, chronotropic and lusitropic responses[355,356]. On the other hand, soluble guanyl cyclase produced cGMP (through stimulation of β_3-ARs) promotes protein kinase G phosphorylation of regulatory proteins to induce a negative functional response. PDE5 serves to inhibit cGMP produced in this manner[356,357].

Despite significant gene and protein increases in ADRβ1 expression, no changes were observed in the expression of either of the dominant cardiac adenylyl cyclase isoforms or PDE5 between 30 days and 45 days. Accordingly, Wu *et al.*[264] observed the greatest increases in *ADCY5* and *ADCY6* in the first couple of weeks after initiation of differentiation, and reached comparable levels to adult human left ventricle by 30 days. Expression was maintained at similar levels to 30 days after 60 days of culture. In contrast Jung *et al.*[210] observed the greatest increase in both subtypes between 30 days and 60 days of culture, with further increases by 90 days. This suggests there is variability between cell lines in the onset of *ADCY5* and *ADCY6* expression. It would be advantageous to compare *ADCY5* and *ADCY6* levels with earlier time points as well as further extending culture length to identify when expression upregulation occurs in the RYR2 hiPSC-CMs. Hormone supplementation had no effect on adenylyl cyclase expression. These observations are consistent with studies in which rats were rendered hyperthyroid[358] and transgenic mice with cardiac-specific thyrotoxicosis[359].

PAK1 is also part of a signalling pathway with regulatory effects on cardiac calcium handling. Upon activation PAK1 and protein phosphatase 2A form a complex which dephosphorylates: LTCCs, reducing the calcium current during systole[360]; RYR2 channels, decreasing their opening probability hence calcium release[360]; cTnI, increasing myofilament calcium sensitivity, slowing its' dissociation and thus the rate of relaxation[361,362]; and PLN, promoting its' inhibitory effects on SERCA2a thereby reducing calcium reuptake during diastole[362]. Consequently, PAK1 is believed to have a protective role against adrenergically mediated arrhythmic activity.

In this study hormone supplementation had the inverse effect on *PAK1* expression compared to *ADRβ1*: addition of hormones at both 30 days and 45 days led to significantly reduced *PAK1*. This result is very interesting considering inhibitory GPCR induced PAK1 activity, via protein phosphatase 2A, opposes many effects of β_1-AR stimulation on cardiac calcium handling. Combined reduced *PAK1* and increased *ADRβ1* expression would augment the effects of β_1-AR stimulation in cardiomyocytes and lead to arrhythmic activity[363], particularly in cardiomyocytes with CPVT-related mutations like the RYR2 hiPSC-CM cell line used here. It would be interesting to understand the expression pattern of *PAK1* during human cardiac development; in support of the observations here PAK1 protein expression has been detected to downregulate in rat ventricle during postnatal development[364]. With regards to using hiPSC-CMs to model CPVT the observed expression pattern of *PAK1* could be beneficial.

4.3.3 SR proteins

EC coupling links the electrical excitation of cardiomyocyte cell membranes with the mechanics of cardiac contraction. The kinetics of intracellular calcium are critical in modulating the synchronous contraction of the heart. The SR is the main intracellular calcium store thus, along with proteins that regulate calcium SR release and sequestration from the cytosol, it plays a key role in the calcium handling phenomenon of EC coupling[39]. RYR2, CASQ2, TRDN and JCN form a complex known as the jSR. The jSR regulates calcium storage and release. SERCA2a is the main SR calcium reuptake pump, and its' activity is regulated by the phosphorylation status of PLN. The calcium handling properties of hPSC-CMs cultured under basic conditions for a limited period are immature. In early hPSC-CM days, prior to the development of hiPSC-CMs, the

expression of RYR2 and SERCA2a were confirmed however CASQ2, PLN, TRDN and ASPH were absent[365,366]. Although the expression of RYR2, *ATP2A2*, *CASQ2* and *PLN* were demonstrated soon after the successful generation of hiPSC-CMs[332,367], the lack of structural organisation and absence of T-tubules resulted in poor localisation and functionality.

In the data presented here prolonged culture and hormone supplementation of RYR2 hiPSC-CMs induced one isolated change in the gene expression of assessed SR proteins. *CASQ2* expression significantly increased with prolonged culture but the addition of hormones significantly reversed this effect - with greater potency. Under healthy conditions CASQ2 binds to RYR2 and reduces its' open probability (at low luminal calcium concentrations)[55]. One hypothesis for the underlying mechanism of CPVT, in the presence of *RYR2* mutations, suggests the threshold for SOICR is reduced[368]. If hiPSC-CMs exhibit decreased *CASQ2* expression, as indicated here, the SR calcium buffering capacity would be lowered. Consequently, the free SR calcium concentration would be raised and lie closer to the RYR2 mutation-induced reduced threshold for SOICR, increasing the RYR2 open probability and thus promoting arrhythmic activity through increased propensity of abnormal calcium release.

The overall lack of changes to gene expression patterns was unexpected. However studies that have investigated the effect of prolonged culture on the expression of SR proteins in hiPSC-CMs report similar results to those in this study. Lewandowski *et al*.[220] observed a significant increase in *ATP2A2* expression up to 40 days of culture (vs hiPSCs). This was supported by other studies in which increases in gene or protein levels were seen immediately after differentiation only[210] – no further changes were seen between 30 days and 90 days[210,333]. Another study reported no changes in *ATP2A2* mRNA expression during human heart development (from gestation to adult) despite significant increases in SERCA2a protein levels[369]. No changes in *RYR2* were reported from 30 days[333] but PLN protein levels significantly increased to 60 days[210].

Here, a significant increase in the expression of *CASQ2* with prolonged culture (30 days vs 45 days) was shown. Interestingly, Sasaki *et al*.[333] also saw a significant increase in *CASQ2* expression with prolonged culture (30 days to 90 days) in their CPVT hiPSC-CM

line, yet in their control hiPSC-CM line the increase did not reach significance. In a separate study, control hiPSC-CMs changes in *CASQ2* expression mainly occurred between 30 days and 80 days. This was further exhibited by late-onset protein expression - significant increases were only observed from 60 days[210].

The addition of hormones opposed the effects of prolonged culture, decreasing *CASQ2* expression. As already mentioned, current literature regarding the effect of thyroid and glucocorticoid hormones on hiPSC-CM gene expression is limited. The effect of hyper- and hypothyroidism on some SR components have been investigated in rabbits[370] and rats[371] however (gene and protein levels respectively). Following administration of thyroid hormone, significant increases in *RYR2* and *ATP2A2*/SERCA2a were reported. Correspondingly in hypothyroid animals expression significantly decreased. In contrast, the gene and protein expression of PLN in hyperthyroid animals significantly reduced, and no changes in CASQ2 expression were indicated.

Endogenous glucocorticoids are produced by the adrenal glands. In rats which had undergone a bilateral adrenalectomy, no significant changes in the expression of cardiac SR proteins (RYR2, SERCA2a, PLN, and CASQ2) were evidenced. Furthermore treatment with Dex, following sham operation or bilateral adrenalectomy, did not lead to any changes either. Notably, there was a significant increase in the protein level of CaMKII[372]. CaMKII mediates phosphorylation of SR proteins to modulate their activity. Thus glucocorticoid treatment may indirectly effect the activity of SR proteins and lead to positive functional responses. In isolated rat left ventricular myocytes, combined treatment of Dex and insulin led to a significant decrease in PLN, and a significant increase in phosphorylated PLN (phosPLN) – with no changes in SERCA2a[373].

Despite expecting more changes in the expression of SR proteins with prolonged culture and hormone supplementation, overall the data presented here compares with other published reports. In order to see more significant changes, extending the culture period further to at least 60 days, but ideally over 90 days, would be preferential as it appears maturation of some key components have later onsets. Additionally, the period in which these changes occur can vary between cell lines. In terms of hormone supplementation, it would seem thyroid hormone is more important regarding the gene expression of SR

proteins. The effects of thyroid hormone reported in animal models are not reflected here in the RYR2 hiPSC-CMs however with further extended culture length it would be interesting to review gene expression.

4.3.4 T-tubule related proteins

T-tubules are invaginations of the cell surface membrane. Described as a "mesh-like" network they are interconnected by longitudinal tubules, wrap around the myofilaments and are anchored at the sarcomeric z-discs[374]. T-tubules are organelles consisting of microdomains compartmentalising membrane-bound ion channels and signalling molecules, in order to modulate cardiac electrophysiology during EC coupling. An important example is the localisation of LTCCs close to jSR RYR2 channels – forming calcium release units (dyads) which are critical for CICR and synchronous whole-cell calcium transients[374]. Human iPSC-CMs do not possess a T-tubular network, thus the coupling of functional dyads is limited. Consequently, hiPSC-CMs have an increased reliance on the influx of calcium through LTCCs. This results in non-uniform calcium transients with an increased time to peak[199]. The processes of T-tubular biogenesis, maintenance and dyadic coupling have not yet been established however several proteins have been implicated including bridging integrator 1[340,341], dysferlin[338,339] and junctophilin 2[342–344].

The gene expression patterns outlined in this study suggest prolonged culture to 45 days had no effect on the expression of *BIN1*, *DYSF* or *JPH2;* and the addition of hormones appeared to negatively influence gene expression. T-tubules are known to develop postnatally[343,375]. Merely extending culture to 45 days of differentiation is probably too early in hiPSC-CM maturation to expect any indications of T-tubule development. In contrast to the data presented here, Parikh *et al*.[199] observed some T-tubule formation following T3 and Dex treatment. Yet for robust T-tubule development seeding of hiPSC-CMs on a Matrigel mattress of physiological stiffness was necessary. Under these conditions significant increases in the expression of bridging integrator 1 and junctophilin 2 were reported.

4.3.5 Contractile proteins

Components of the contractile machinery are often used as cardiac markers and for determining the level of sarcomeric organisation in hiPSC-CMs[179,280,332]. Cardiac TnI binds to actin inhibiting myosin cross-bridge cyclin and dissociates on binding of calcium-bound troponin C. Cardiac TnT anchors the troponin complex to tropomyosin, linking it to the actin thin filament[376]. Myosin is the major component of the thick filament and is able to generate the force required for contraction. Myosin molecules are made up of heavy chain (MHC) and light chain subunits[377].

Between the culture conditions (30 vs 45 days, ±hormones) no expression differences were noted of any of the myofilament genes. This observation is consistent with other published studies. Bedada *et al.*[216] reported limited but detectable cTnI expression after two months of culture but the level of expression did not alter when compared to 9.5 months, and there was no evidence of ssTnI (*TNNI1,* the dominant isoform during development) diminution. Furthermore, media supplementation with T3 did not affect the hiPSC-CM TnI isoform profile. Another study showed *TNNI3* to display a trend towards increased expression (insignificantly) in the first 40 days of differentiation[220]. Accordingly, they also demonstrated *TNNI1* to be significantly upregulated at 20 days (vs hiPSCs) before its' expression significantly decreased by 40 days. This indicated a switch in isoform to *TNNI3*. The same study also identified a significant increase in *TNNT2* expression however this occurred prior to 20 days and did not increase further with prolonged culture to 40 days. Additionally, no difference in *TNNT2* expression was reported when 30 days was compared to 90, 180 and 360 days culture[263].

In foetal and adult myocardium *MYH6* is mainly expressed in atria, with low level *MYH7*. The opposite pattern exists in ventricles, *MYH7* predominates[217,377]. Our findings were consistent with Kamakura *et al.*[263]: no significant change in *MYH6* expression with prolonged culture. They also reported no change in *MYH7* expression. These results are inconsistent with Lewandowski's study[220]. At 20 days *MYH6* and *MYH7* expression were similar. However, between 20 days and 40 days *MYH6* expression significantly reduced, whilst MYH7 significantly increased. Although compared to adult ventricular heart muscle *MYH6* expression remained significantly higher and *MYH7* significantly lower the changes indicated a transition towards ventricular specialisation. The variability

between hiPSC-CMs generated from different cell lines, under different differentiation conditions is particularly highlighted here as Lundy *et al*.[265] observed significantly increased expression of both *MYH6* and *MYH7* between early (<40 days) and late (>80 days) stage hiPSC-CMs. There appears to be no consistent change in *MYH6* or *MYH7* expression with prolonged culture. This could be linked with differences in nodal, atrial and ventricular subtype ratios in the different cardiomyocyte cultures.

It has been demonstrated that thyroid hormone has a pronounced effect on MHC expression. A hyperthyroid state enhances *MYH6* expression and represses *MYH7* whereas as a hypothyroid state has the inverse effect[378,379]. These effects are species-specific and inversely proportional to the level of activity (in euthyroid state) so it is unclear if we should expect the same ratio alterations[380,381]. Despite a trend, significant upregulation of *MYH6* was not displayed in the hormone-treated RYR2 hiPSC-CMs. It is possible prolonged culture and ventricular specialisation were influencing contradictory effects to hormone treatment. Furthermore, it is difficult to make a full conclusion without assessing *MYH7* expression and calculating the ratio within each culture condition.

4.3.6 Membrane-bound ion channels

Depolarisation of the cell surface membrane during an action potential results in a large influx of sodium ions. This change in membrane potential leads to opening of LTCCs and the calcium influx ultimately required for contraction. Sodium and calcium currents are further linked by the NCX: influx of three sodium ions, efflux of one calcium ion in forward mode. NCX is critical to the regulation of intracellular calcium[39,382]. In this study, no significant changes in *SLC8A1* expression were observed. Assessment of human myocardium development identified increases in NCX mRNA and protein during foetal development followed by decreases at neonatal and adult stages. The authors suggest NCX plays a greater role in calcium handling during cardiac development when SR function is immature[383].

Each of the voltage-gated sodium channel subunits also assessed here have been shown to be expressed in the heart however *SCN1A*, *SCN3A* and *SCN8A* are primarily expressed in the nervous system, and *SCN10A* in dorsal root ganglia[384] (with further debated roles

in the heart[385]). *SCN5A* is the main cardiac isoform. Few changes in the expression of voltage-gated sodium channels were observed in RYR2 hiPSC-CMs. The lack of a significant increase in *SCN5A* expression was perhaps surprising. It is however supported by other hiPSC-CM studies in which prolonged culture led to gradual, insignificant increases in *SCN5A*[265,329,386], and T3 and Dex treatment did not increase *SCN5A* despite an enhanced sodium current[202]. In developing rat hearts, the mRNA level of *SCN1A* increases dramatically after birth before significantly decreasing during postnatal development. Conversely, *SCN5A* significantly increases after birth and remains high[387]. The change in the proportions of *SCN1A* and *SCN5A* seen in the RYR2 hiPSC-CMs with extended culture length and hormone supplementation are consistent with maturation from a foetal to adult phenotype. Additionally, it is proposed that the high *SCN1A* expression could be compensating for low *SCN5A* levels in hiPSC-CMs. This could also provide a potential explanation as to why hiPSC-CM models of BrS, derived from patients without putative *SCN5A* mutations, have not displayed expected abnormalities in sodium current properties (vs control hiPSC-CMs)[247,388,389].

4.4 Study limitations and further work

The major limitation of this study is that the expression data was not compared to that of human adult cardiomyocytes. Studies of the human heart are limited by ethical concerns and the highly invasive nature of the procedure (with significant risks) that would be involved in obtaining a cardiac biopsy. In order to sidestep this limitation many published studies compare hiPSC-CM data from patient lines to healthy control lines; yet control hiPSC-CMs display similar structural and functional immaturities to patient lines, thus are not able to fully represent native adult cardiomyocytes. Expression data of the target genes assessed was not collected from RYR2 hiPSCs or hiPSC-CMs immediately following differentiation. This would have aided our understanding of the initial expression changes in the first 30 days – in this study only changes between 30 days and 45 days have been considered. Additionally, only one clone from a single (patient) cell line was investigated. Gene expression analyses in multiple cell lines, including control lines derived from healthy individuals, are necessary to substantiate the findings presented in this study.

As discussed in Chapter 3, it is necessary to normalise gene expression data to a reference gene with stable expression within the cell type of interest. In the RYR2 hiPSC-CMs, *UBC* was determined to be the most stably expressed of the candidate genes. However, using only one reference gene has limitations. Despite identifying the most stable gene, expression variation can remain within cell type samples, particularly those cultured under different conditions[390]. It is therefore suggested that candidate reference genes are validated for each experimental condition individually and a subset of stably expressed genes are used to facilitate accurate data normalisation.

The expression of 27 cardiac-related genes was evaluated in four different culture conditions. Nevertheless, some genes were omitted that could have facilitated the understanding of RYR2 hiPSC-CM maturation with prolonged culture and hormone supplementation. In particular, genes encoding for proteins which undergo a switch from a foetal to adult isoform during development such as cTnI (*TNNI1* to *TNNI3*) or those which undergo a switch in ratio with maturity e.g. *MYH6* and *MYH7*. Moreover the genes evaluated were primarily selected due to their involvement in cardiac calcium handling and mechanical contraction. Consequently, potential changes to the expression levels of genes encoding for the delayed and inwardly rectifying potassium channel subunits were not assessed. Published reports demonstrate low or absent potassium currents, which are critical for repolarisation and maintenance of the resting membrane potential[181,200]. Crucially, data for genes encoding cardiac LTCC subunits CACNA1C and CACNA1D are absent due to an experimental error. With additional time and resources, a more comprehensive assessment of the influence of prolonged culture and hormone supplementation on RYR2 hiPSC-CM gene expression could have been performed through the application of RNA sequencing technologies.

The study was further limited by the practicalities of independent culturing and maintenance of hiPSC-CMs. The maturation of hiPSC-CMs is demonstrated to be time-dependent hence extending culture length further than 45 days would potentially have allowed for further gene expression maturation.

4.5 Conclusion

This chapter has demonstrated that even with a short period of prolonged culture and hormone treatment, particularly T3, hiPSC-CMs are gradually directed towards a more mature phenotype. Crucially, a significant increase in the expression of ADRβ1 at the mRNA and protein level was observed in the RYR2 hiPSC-CMs. Furthermore the reduction in *PAK1* could enhance β-AR signalling and the decreased *CASQ2* expression could be representative of the RYR2 hiPSC-CM CPVT phenotype. It is important to note that changes in gene expression do not always translate to the protein or functional level. On the other hand, the lack of widespread changes may indicate proportional gene expression maturity, and instead be limited by structural and functional development. To promote structural maturity, and in turn the process of calcium handling, reports suggest seeding hiPSC-CMs on a nanopatterned surface in order to replicate the native physiological microenvironment[199,286]. Thus, the effect of a nanopatterned culture surface on RYR2 hiPSC-CM structure and function will be assessed in the next chapter.

Chapter 5

The effect of a nanopatterned culture surface with hormone supplementation on hiPSC-CM structure and function

5 The effect of a nanopatterned culture surface with hormone supplementation on hiPSC-CM structure and function

5.1 Introduction

The native myocardium displays complex architecture and organisation at the macro-, micro- and nanoscale. Cardiomyocytes account for approximately 75% of adult human heart volume, despite representing only 18% of the total number of cells – endothelial and mesenchymal cells (fibroblasts) constituting the majority of the remaining proportion[277,278]. The cells of the myocardium are embedded in an extensive ECM network[391]. At the macroscale the sheets of parallel cardiomyocytes composing the left ventricular wall are guided into their anisotropic alignment by the ECM; mechanically connected to adjacent cardiomyocytes; provide an axis for action potential propagation; and contribute to the direction of contractile force exertion[392] for the expulsion of blood from the ventricles. At the microscale cardiomyocytes are rod-shaped and contain a highly organised internal structure (T-tubule network, jSR, sarcomeres) for efficient coupling of electrical signals to mechanical contraction. At the nanoscale localisation of calcium handling proteins, and the precise arrangement and interaction of sarcomeric proteins enable the co-ordinated electromechanical function of contractions[393].

Standard *in vitro* culturing methods for cardiomyocytes result in the loss, or lack of development of the native tissue organisation, and the consequent random distribution of intracellular structures leading to suboptimal electromechanical coupling and contraction physiology. Typical cell culture vessels have an unpatterned smooth surface[394] for cardiomyocytes to adhere to, thus are not representative of the native micro-environment of cardiomyocytes. Cardiomyocytes are receptive to variation of topographical and molecular patterns of macro-, micro- and nanoscales[285]. To establish an appropriate structure-function relationship in 2D cultured cardiomyocytes it is essential the *in vitro* cell-substratum association mimics the *in vivo* cell-ECM interaction.

A variety of methods have been implemented to create a patterned surface and promote topographical alignment of cardiomyocytes in 2D cultures[392]. As a result elongated rod-shaped cardiomyocytes with improved sarcomere organisation,

developed anisotropic action potential propagation and faster conduction velocities have formed[284,395–399]. To promote structural and functional hiPSC-CM maturity, Parikh *et al*.[199] coupled a microscale topography of physiological stiffness with addition of T3 and Dex hormones. Most notable of their observations was the developing T-tubular network. Requiring the combination of both hormones and the physiological substrate stiffness, hiPSC-CM T-tubule density was reported to exceed healthy human atrial cardiomyocytes but remained lower, and less well-organised than the network displayed in ventricular cardiomyocytes. Almost certainly, the presence of a T-tubular network will have facilitated the enhanced calcium handling and EC coupling observed.

The patterns designed by the majority of studies have microscale ridges and grooves - yet it has been demonstrated that cardiomyocytes are influenced by ECM fibres with nanoscale features. Furthermore, differences in the specifics of cardiomyocyte morphology and electrophysiological characteristics have been observed to be dependent on the nanotopographic pattern parameters (ridge-groove widths and depths) on which they were cultured[285]. The optimal dimensions of the nanopattern for promoting hiPSC-CM maturity towards adult human cardiomyocytes was investigated by Carson *et al.*[286]. They identified the upper nanometre range to be most advantageous, with peak structural maturation being observed on patterns with ridges and groove widths of 800 nm.

In Chapter 4, 45 days of culture (vs 30 days) and hormone supplementation were demonstrated to generate RYR2 hiPSC-CMs with a more mature phenotype at the genomic and protein level. In this chapter hiPSC-CM maturity is further challenged by a period of culture on dishes with a nanopatterned surface (commercially available) to improve cardiomyocyte structure, and both the electrophysiology and mechanical forces of contraction. Following differentiation and column purification, hiPSC-CMs were seeded on either smooth or nanopatterned dishes. Each group was divided into two subgroups and cultured with or without additional hormones. Cardiomyocytes were analysed at 45 days of culture (Figure 5.1).

The aims of this chapter were as follows:

- To assess the effect of a nanopatterned culture surface and hormone supplementation on RYR2 hiPSC-CM morphology and sarcomeric structure
- To investigate if improved hiPSC-CM structure translates to efficient calcium handling
- To evaluate if improved hiPSC-CM structure influences protein expression

To address the first aim immunocytochemistry techniques were carried out on RYR2 hiPSC-CMs for the measurement of morphology parameters, and to assess the spatial arrangement of the target sarcomeric protein: alpha actinin. Baseline and pharmacologically challenged calcium transients, of RYR2 and control hiPSC-CMs, were analysed following live calcium imaging to investigate the functional status of cardiac calcium handling. Western blots were performed to identify changes in the expression of proteins involved in cardiac calcium handling.

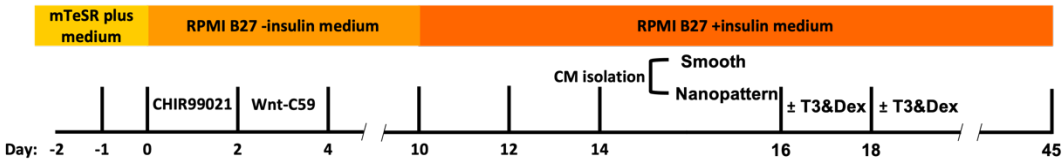

Figure 5.1: Cardiac differentiation protocol with hormone supplementation and a nanopatterned culture surface

Further extension of the basic differentiation protocol to improve hiPSC-CM maturity by reseeding purified hiPSC-CM cultures on nanopatterned culture dishes - with a groove depth of ~600 nm, and ridge and groove widths of ~800 nm. CM, cardiomyocyte; T3, triiodothyronine; Dex, dexamethasone. Identical to Figure 2.3B.

5.2 Results

5.2.1 Atomic force microscopy confirms nanopattern dimensions

As demonstrated by Carson *et al*.[286] topography-induced structural maturation of hiPSC-CMs appears optimal on 800 nm features. Cultureware utilising biomimetic surface topography with ridge and groove widths of 800 nm, and groove depths of 600 nm were purchased (Figure 5.2A). To ensure the nanopattern dimensions were maintained after coating with Matrigel basement membrane matrix, atomic force microscopy was performed. The surface topography was imaged (Figure 5.2B) and the cross-sectional profile measured confirming retainment of the groove depth and ridge width

dimensions. However, the groove width appeared to be smaller – likely due to residual excess Matrigel (Figure 5.2C). The dishes were used for subsequent culture of hiPSC-CMs.

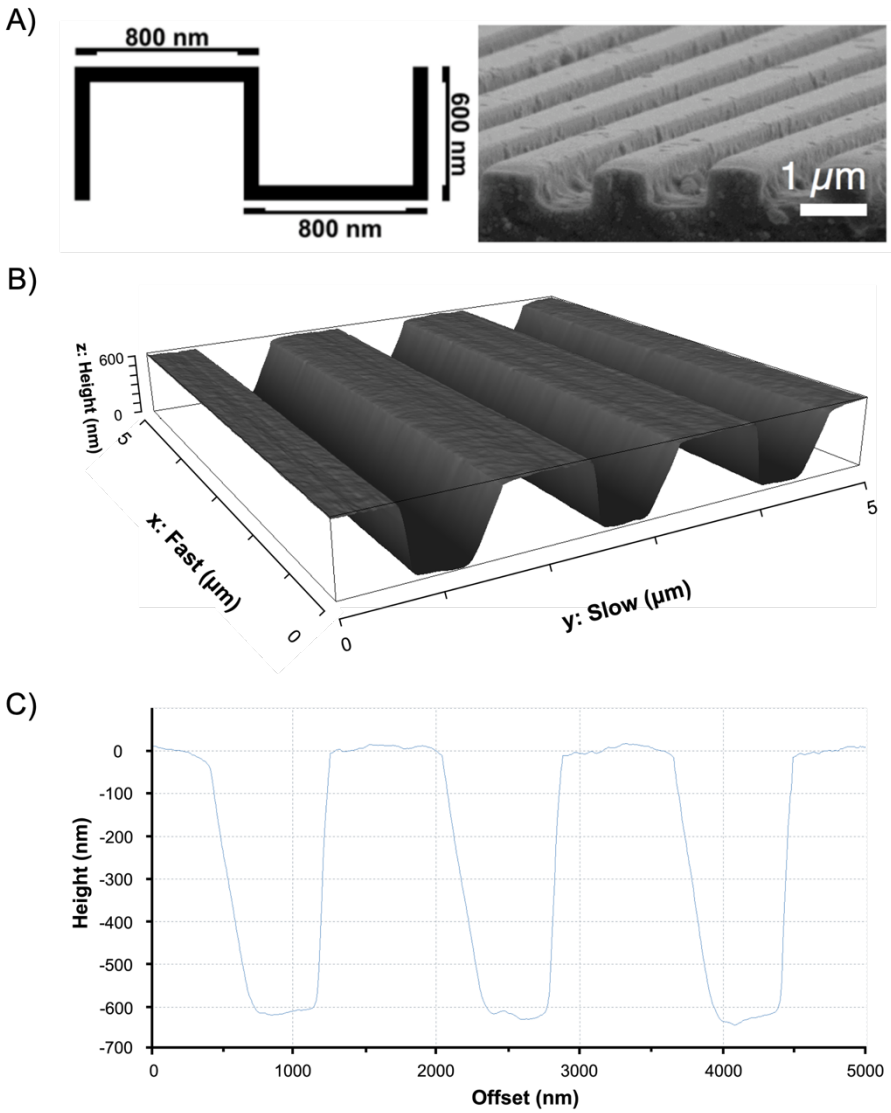

Figure 5.2: Topography of nanopatterned cultureware

Atomic force microscopy performed on culture dishes with a nanopatterned surface to confirm topography dimensions. (A) Schematic illustration of approximate nanopattern cross-section dimensions (left) and scanning electron micrograph of the nanopattern surface (right). Image taken from NanoSurface Cultureware Manual of NanoSurface Biomedical Inc. (B) 3D atomic force microscopy image of the nanopattern surface after coating with Matrigel basement membrane matrix. (C) Cross-sectional profile indicating ridge and groove dimensions.

5.2.2 RYR2 hiPSC-CM morphology

To evaluate the organisation and structural development of RYR2 hiPSC-CMs cultured on the nanopatterned topography with hormones for four weeks, cardiomyocytes were immunostained for glycoproteins of the cell membrane (using WGA) and the sarcomeric protein alpha actinin. The representative confocal images displayed in Figure 5.3 highlight the differences in cardiomyocyte morphology and organisation of structural components. On the smooth surface cardiomyocytes showed multiaxial orientation and frequently overlapped each other. The cells were often round, triangular or of irregular shape, and their sarcomeres appeared disorganised. In contrast the cardiomyocytes seeded on the nanopattern topography orientated into a parallel array along the grooves and presented as a single monolayer. Furthermore the cells appeared greater in size, rod-shaped and alpha actinin molecules aligned indicating sarcomeric organisation. Each of these observations induced by the nanopatterned topography was further enhanced by the presence of additional hormones in the culture medium.

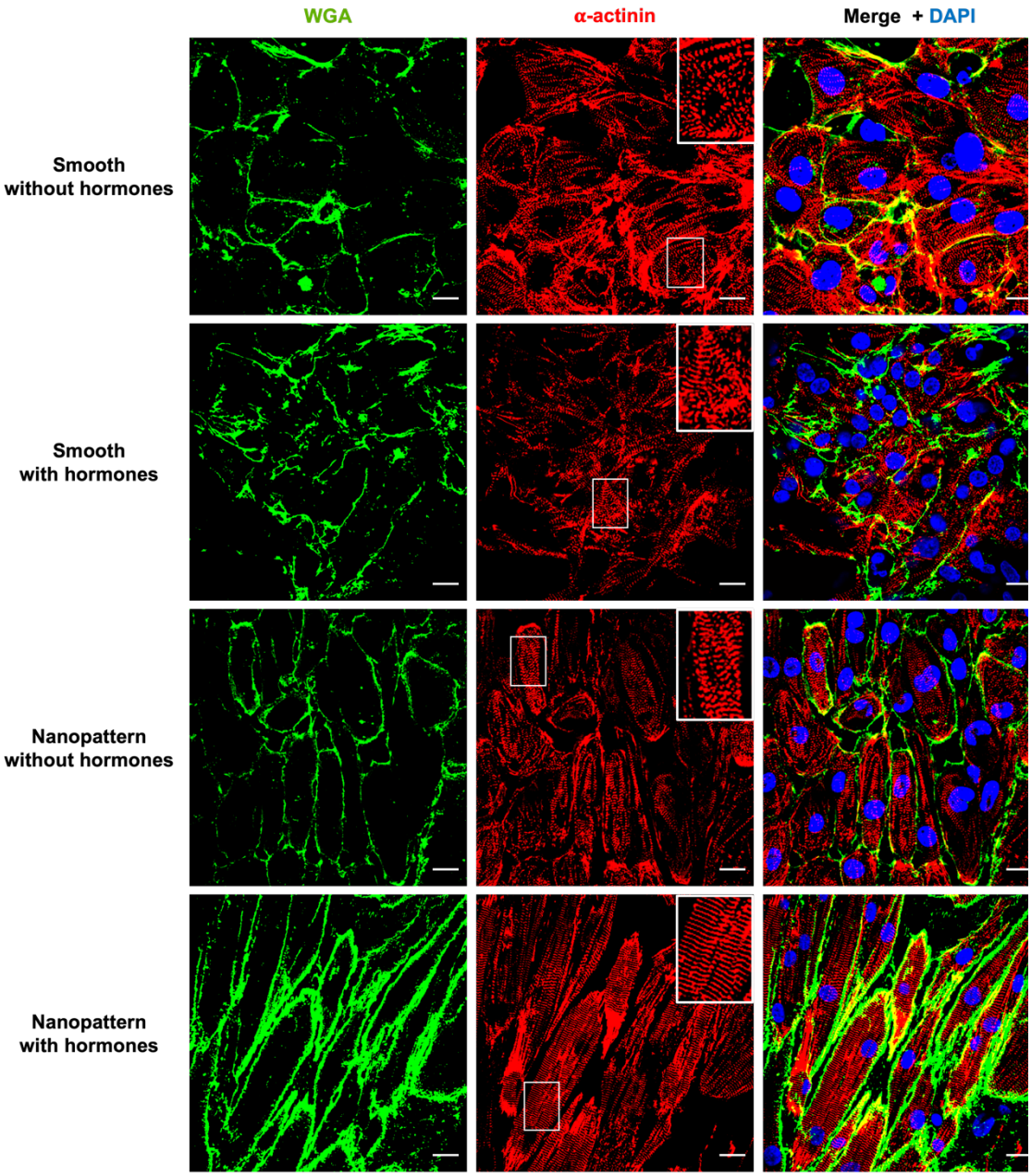

Figure 5.3: Immunostaining of RYR2 hiPSC-CMs cultured on different topographic surfaces

Confocal images of RYR2 hiPSC-CMs fixed and immunolabelled four weeks post replating on smooth or nanopatterned cultureware ±hormone supplementation (T3 and Dex). Green, WGA; red, α-actinin; blue, DAPI nuclear stain. Inset image shows a zoom-in of the α-actinin staining. Scale bar = 20 μm.

The changes in cardiomyocyte morphology were assessed in greater depth by quantitatively measuring cell length and width. Analysis identified significant differences in cardiomyocyte length only. Irrespective of hormone supplementation, cell length was significantly increased on the nanopatterned topography (Figure 5.4A). The aspect ratio was calculated. Combining the nanopatterned surface with supplementary hormones

significantly increased the aspect ratio of RYR2 hiPSC-CMs when compared to each of the other culture conditions (Figure 5.4C).

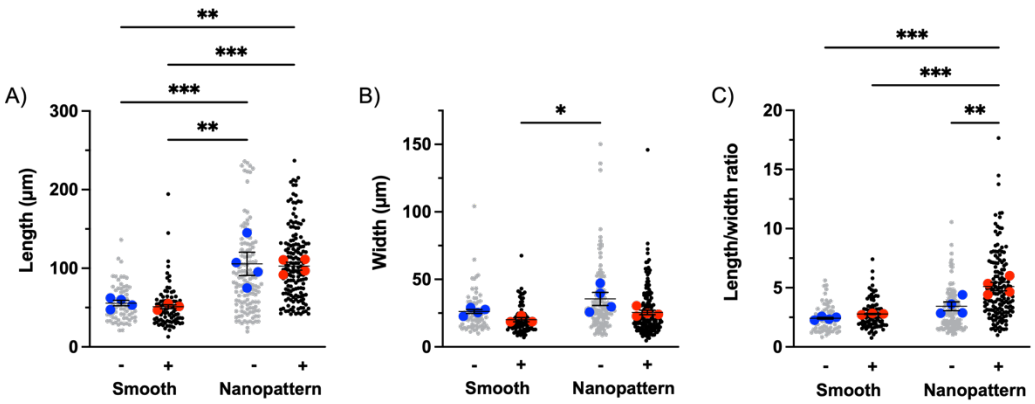

Figure 5.4: Morphological parameters of RYR2 hiPSC-CMs cultured on different topographic surfaces

Quantitative analysis of RYR2 hiPSC-CM morphology in response to culture on a nanopatterned surface ±hormone supplementation (T3 and Dex). (A) Length, (B) width, (C) aspect ratio. Values are mean ±SEM, n=14-61 cells per dish (grey/black), 3-4 dishes (blue/red) from 1 differentiation. Two-way ANOVA was performed followed by Tukey's multiple comparisons test. *p<0.05 **p<0.01 ***p<0.001

Based on these findings it was hypothesised that calcium handling in hiPSC-CMs, with corresponding morphology and sarcomeric organisation to native adult cardiomyocytes, would be improved compared to those cultured without MFs.

5.2.3 Experimental conditions for hiPSC-CM functional data collection

In the following sections calcium transient characteristics are reported. It is important to note that recordings were taken under different experimental conditions. RYR2 hiPSC-CM recordings were taken from a mixture of spontaneously firing and electrically stimulated (0.5Hz) cells. It was noted that a greater proportion of RYR2 hiPSC-CMs cultured with hormone supplementation spontaneously contracted. All experiments were conducted at 37°C. All control hiPSC-CMs spontaneously fired. Initial experiments conducted at 37°C demonstrated a greater frequency of calcium transients in the control hiPSC-CMs (Figure 5.5B). Hence subsequent experiments were conducted at room temperature to enable analysis of the traces generated from the recordings.

It is recognised that spontaneously firing hiPSC-CMs have variable firing rates and consequently calcium transient frequencies, as demonstrated by Figure 5.5A.

Furthermore, firing rates are temperature sensitive (Figure 5.5C). These differences can interfere with data interpretation. To check for potential differences caused by different firing rates, calcium transient properties are expressed dependent on transient frequency (< 1Hz ≤). However, due to low n numbers limited statistical analysis could be performed in the control hiPSC-CMs; consequently, data interpretation was restricted.

To determine if hormone supplementation and a nanopatterned surface topography promote hiPSC-CM functional maturity calcium transient frequency, rate of rise, amplitude, and rate of decay properties were analysed at baseline. Figure 5.6 shows representative traces of intracellular calcium transients recorded from fluo-4 loaded hiPSC-CMs for each culture condition. Calcium transient frequency and rate of decay were also evaluated following: 1) sequential block of SERCA2a and RYR2 channels to examine SR function; and 2) stimulation of β-ARs to assess the maturity of adrenergic signalling pathways. Presented data is from experiments conducted at 37°C for RYR2 hiPSC-CMs, and room temperature for control hiPSC-CMs.

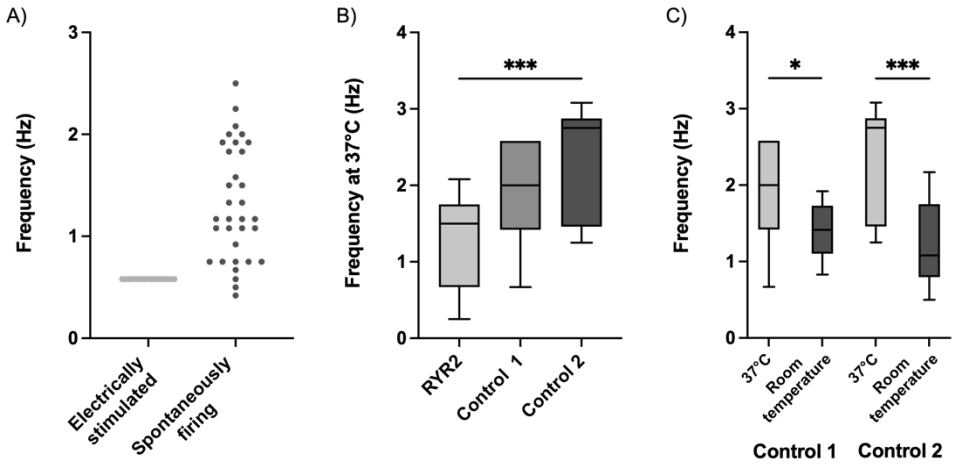

Figure 5.5: hiPSC-CM calcium transient frequency is sensitive to experimental conditions

Representative data highlighting differences caused by experimental conditions. (A) The variability of calcium transient frequency in spontaneously firing RYR2 hiPSC-CMs. Paced hiPSC-CMs were electrically stimulated at 0.5Hz. Smooth surface +hormones; n=15-33 ROIs, 6-11 dishes. (B) Control hiPSC-CMs displayed an increased frequency of calcium transients at 37°C (vs spontaneously firing RYR2 hiPSC-CMs). Nanopattern surface +hormones; n=6-27 ROIs, 2-9 dishes, 1-5 independent differentiations. One-way ANOVA was performed followed by Tukey's multiple comparisons test. (C) Conducting experiments at room temperature reduced the frequency of calcium transients in control hiPSC-CMs (vs 37°C). Nanopattern surface +hormones; n=6-20 ROIs, 2-6 dishes, 1-3 independent differentiations. Two-tailed, unpaired t-test was performed. Box, 25th-75th percentiles; central line, median; whiskers, min to max. *p<0.05 p<0.001***

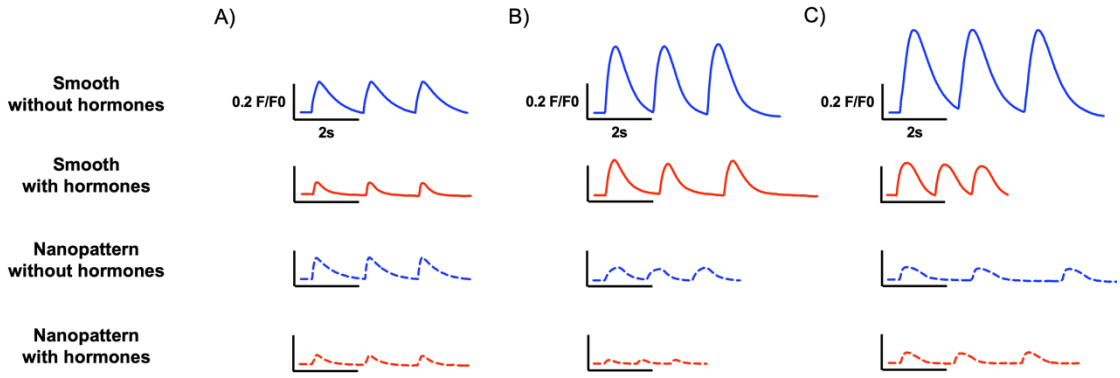

Figure 5.6: Representative calcium transient traces from hiPSC-CMs

Intracellular calcium transient traces recorded from fluo-4 loaded hiPSC-CMs cultured on smooth and nanopatterned surfaces ±hormone supplementation. (A) RYR2 hiPSC-CMs (B) control 1 hiPSC-CMs, (C) control 2 hiPSC-CMs.

5.2.4 Frequency of hiPSC-CM calcium transients

Calcium transient frequency can be used as a marker of hiPSC-CM maturity. The frequency of calcium transients in RYR2 and control hiPSC-CMS, cultured on smooth and nanopatterned surfaces ±hormone supplementation, was determined from 12s live calcium imaging recordings. In RYR2 hiPSC-CMs, the addition of supplementary hormones significantly increased transient frequency, independent of culture surface topography (Figure 5.7A). Similar effects of hormone supplementation were observed in control 1 and control 2 hiPSC-CMs (Figure 5.7B-C). In control 1 hiPSC-CMs, culture on the nanopatterned surface also significantly increased transient frequency (Figure 5.7B).

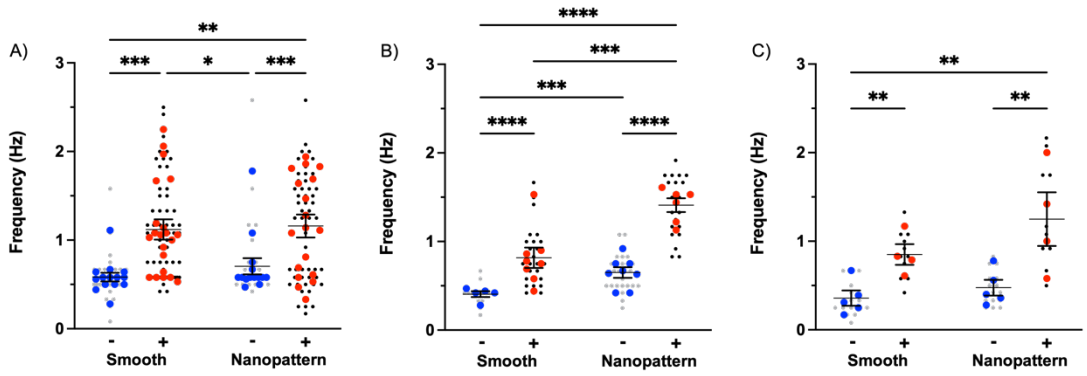

Figure 5.7: Calcium transient frequency in hiPSC-CMs

Comparison of calcium transient activity in hiPSC-CMs cultured on smooth and nanopatterned surfaces ±hormone supplementation (T3 and Dex). (A) RYR2 hiPSC-CMs, (B) control 1 hiPSC-CMs, (C) control 2 hiPSC-CMs. The frequency was determined from 12s live calcium imaging recordings. Values are mean ±SEM, n=11-63 ROIs (grey/black), 4-21 dishes (blue/red), 2-8 independent differentiations. Two-way ANOVA was performed followed by Tukey's multiple comparisons test. *p<0.05 **p<0.01 ***p<0.001 ****p<0.0001

5.2.5 Rate of intracellular calcium rise in hiPSC-CMs

The effect of calcium transient frequency on the rate of calcium rise is displayed first (Figure 5.8A-C left). Due to the low numbers of biological replicates limited statistical analysis could be performed. Transient frequency had no effect on the rate of calcium rise within culture conditions.

Next, the effect of hormone treatment and a nanopatterned culture surface on the rate of rise of intracellular calcium was considered in hiPSC-CMs with a transient frequency <1Hz. Although neither hormone treatment nor a nanopatterned surface significantly

changed the rate of intracellular calcium rise independently in RYR2 hiPSC-CMs, their combined effect significantly decelerated the rate of rise (Figure 5.8A). In contrast the nanopatterned surface significantly decelerated calcium rise in both control hiPSC-CM lines (Figure 5.8B-C).

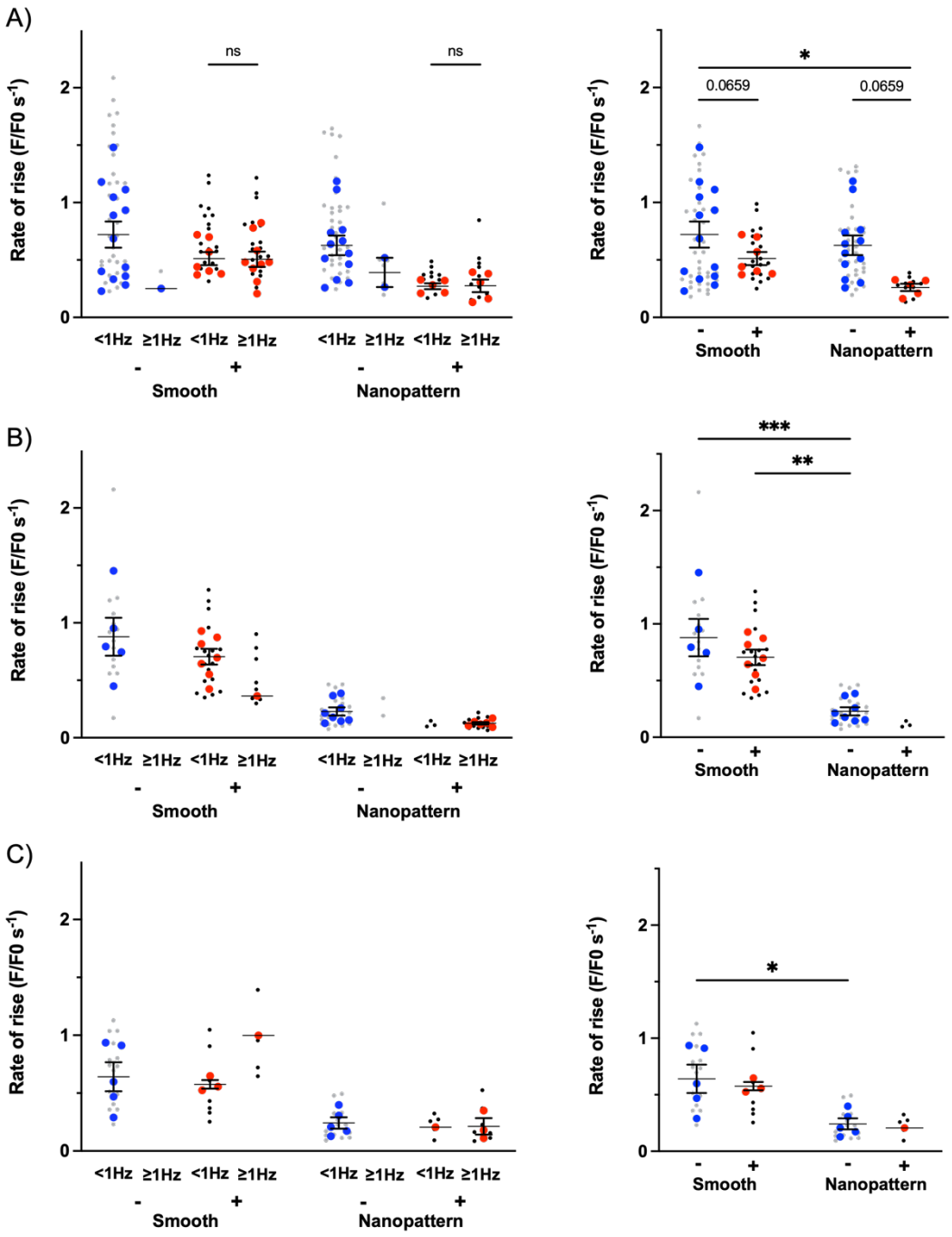

Figure 5.8: Hormone-treated hiPSC-CMs cultured on a nanopatterned surface demonstrate decelerated intracellular calcium rise

Rate of intracellular calcium rise measured from fluo-4 loaded hiPSC-CMs cultured on smooth and nanopatterned surfaces ±hormone supplementation (T3 and Dex). (A) RYR2 hiPSC-CMs at 37°C, (B) control 1 hiPSC-CMs at room temperature, (C) control 2 hiPSC-CMs at room temperature. Left: Data is expressed dependent on calcium transient frequency (< 1Hz ≤). Values are mean ±SEM, n=11-41 ROIs (grey/black), 4-16 dishes (blue/red), 2-8 independent differentiations. Two-tailed, unpaired t-test was performed. Right: hiPSC-CMs with a transient frequency <1Hz only. Two-way ANOVA was performed followed by Tukey's multiple comparisons test. *p<0.05 **p<0.01 ***p<0.001 ns indicates non-significant

5.2.6 Calcium transient amplitude of hiPSC-CMs

No effect of calcium transient frequency on the intracellular calcium amplitude, within culture conditions, was established in RYR2 or control hiPSC-CMs (Figure 5.9A-C left).

In contrast, the conditions in which the cells (with a transient frequency <1Hz) were cultured did lead to significant changes in calcium transient amplitude. Hormone-treated RYR2 hiPSC-CMs displayed a significantly decreased peak calcium amplitude, independent of culture surface (Figure 5.9A). Hormone treatment also led to a significantly reduced peak amplitude in control 1 hiPSC-CMs. However, the most significant reduction in peak amplitude for control hiPSC-CM cell lines was seen on the nanopatterned culture surface (Figure 5.9B-C).

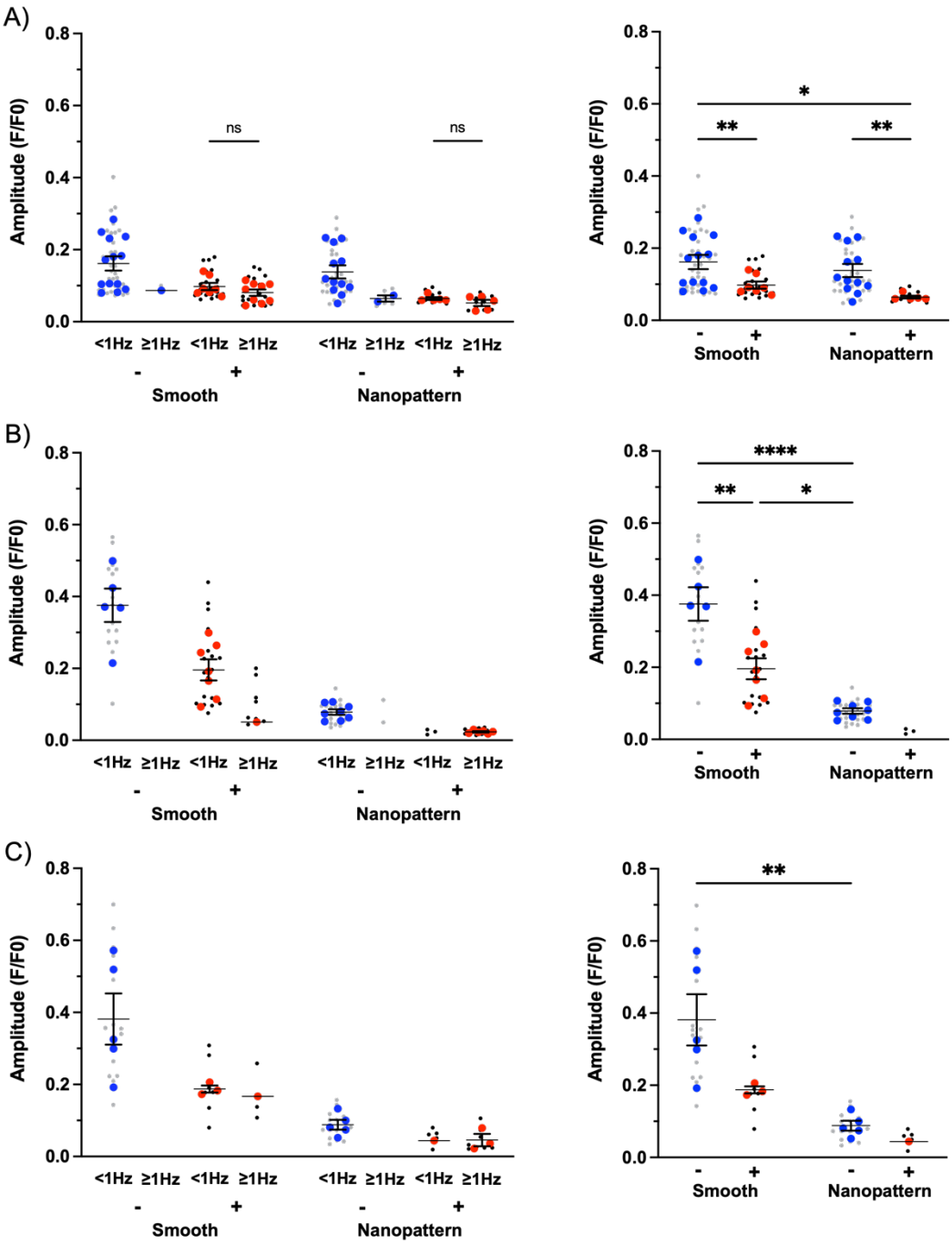

Figure 5.9: Reduced calcium transient amplitude in hormone-treated hiPSC-CMs cultured on a nanopatterned surface

Intracellular calcium amplitude measured from fluo-4 loaded hiPSC-CMs cultured on smooth and nanopatterned surfaces ±hormone supplementation (T3 and Dex). (A) RYR2 hiPSC-CMs at 37°C, (B) control 1 hiPSC-CMs at room temperature, (C) control 2 hiPSC-CMs at room temperature. Left: Data is expressed dependent on calcium transient frequency (< 1Hz ≤). Values are mean ±SEM, n=11-41 ROIs (grey/black), 4-16 dishes (blue/red), 2-8 independent differentiations. Two-tailed, unpaired t-test was performed. Right: hiPSC-CMs with a transient frequency <1Hz only. Two-way ANOVA was performed followed by Tukey's multiple comparisons test. *p<0.05 **p<0.01 ****p<0.0001 ns indicates non-significant

5.2.7 Rate of intracellular calcium decay in hiPSC-CMs

As with rate of calcium rise and calcium amplitude, rate of decay was expressed dependent on transient frequency (< 1Hz ≤) to check for potential differences caused by variable firing rates (Figure 5.10A-C left). No significant differences in calcium transient rate of decay were reported within the experimental culture conditions of RYR2 and control 1 hiPSC-CMs.

To determine any effects of hormone supplementation and/or a nanopatterned culture surface on hiPSC-CM function, the calcium transient rate of decay at baseline was further analysed. The addition of supplementary hormones to the culture medium significantly increased the rate of decay on both smooth and nanopatterned surfaces in RYR2 hiPSC-CMs (Figure 5.10A). Contrarily in control 2 hiPSC-CMs, the nanopatterned surface was accountable for accelerated calcium decay (Figure 5.10C). No changes were observed in the rate of calcium decay in control 1 hiPSC-CMs (Figure 5.10B).

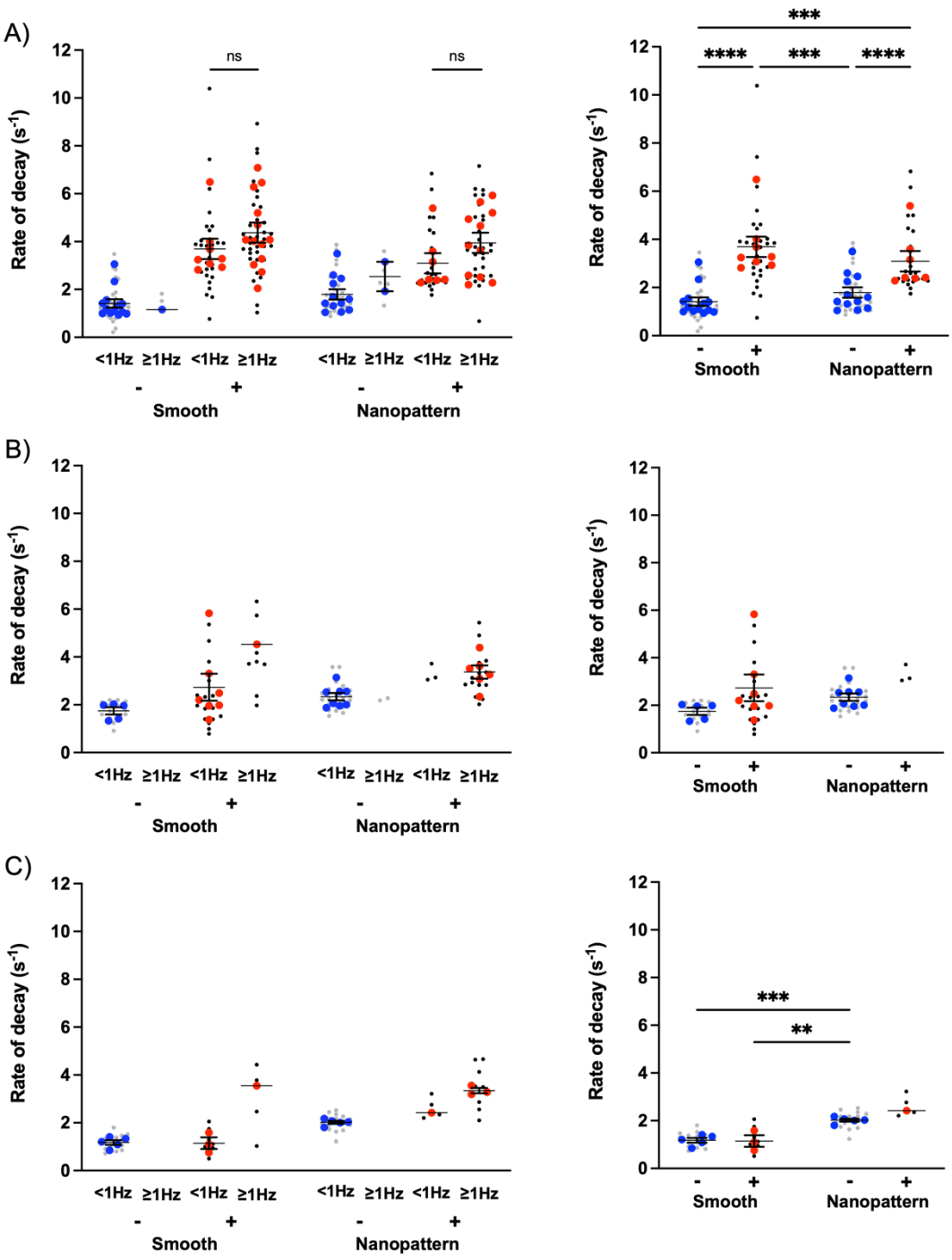

Figure 5.10: Hormone-treated hiPSC-CMs cultured on a nanopatterned surface demonstrate accelerated intracellular calcium decay

Rate of calcium decay measured from fluo-4 loaded hiPSC-CMs cultured on smooth and nanopatterned surfaces ±hormone supplementation (T3 and Dex). (A) RYR2 hiPSC-CMs at 37°C, (B) control 1 hiPSC-CMs at room temperature, (C) control 2 hiPSC-CMs at room temperature. Left: Data is expressed dependent on calcium transient frequency (< 1Hz ≤). Values are mean ±SEM, n=11-63 ROIs (grey/black), 4-21 dishes (blue/red), 2-8 independent differentiations. Two-tailed, unpaired t-test was performed. Right: hiPSC-CMs with a transient frequency <1Hz only. Two-way ANOVA was performed followed by Tukey's multiple comparisons test. **p<0.01 ***p<0.001 ****p<0.0001 ns indicates non-significant

5.2.8 SR block of hiPSC-CMs

To assess hiPSC-CM SR function and its contribution to calcium handling, SERCA2a and RYR2 activity were sequentially inhibited by thapsigargin (10 μM) and ryanodine (10 μM) respectively. Thapsigargin treatment appeared to increase transient frequency in RYR2 hiPSC-CMs cultured on a smooth surface with hormone treatment (Figure 5.11A). However no other differences were observed under other culture conditions or in the control lines.

The effects of thapsigargin and ryanodine treatment on the calcium transient rate of decay were also preliminarily evaluated in hiPSC-CMs (Figure 5.12). Due to low n numbers across experimental culture conditions full analyses were not possible. In RYR2 hiPSC-CMs thapsigargin and ryanodine treatment had no effect on the calcium transient rate of decay (Figure 5.12A). In control 1 hiPSC-CMs cultured on a smooth surface with supplementary hormones, incubation with thapsigargin led to a significantly reduced rate of calcium decay compared to both baseline and following ryanodine treatment (Figure 5.12B). In cells cultured on a nanopatterned surface without additional hormones thapsigargin treatment caused a significantly reduced rate of decay; the subsequent ryanodine treatment led to a further deceleration of calcium decay (Figure 5.12B). Similarly, in control 2 hiPSC-CMs the calcium decay rate was also observed to reduce after ryanodine treatment (compared to baseline) in cells cultured on nanopatterned surface without hormone supplementation (Figure 5.12C).

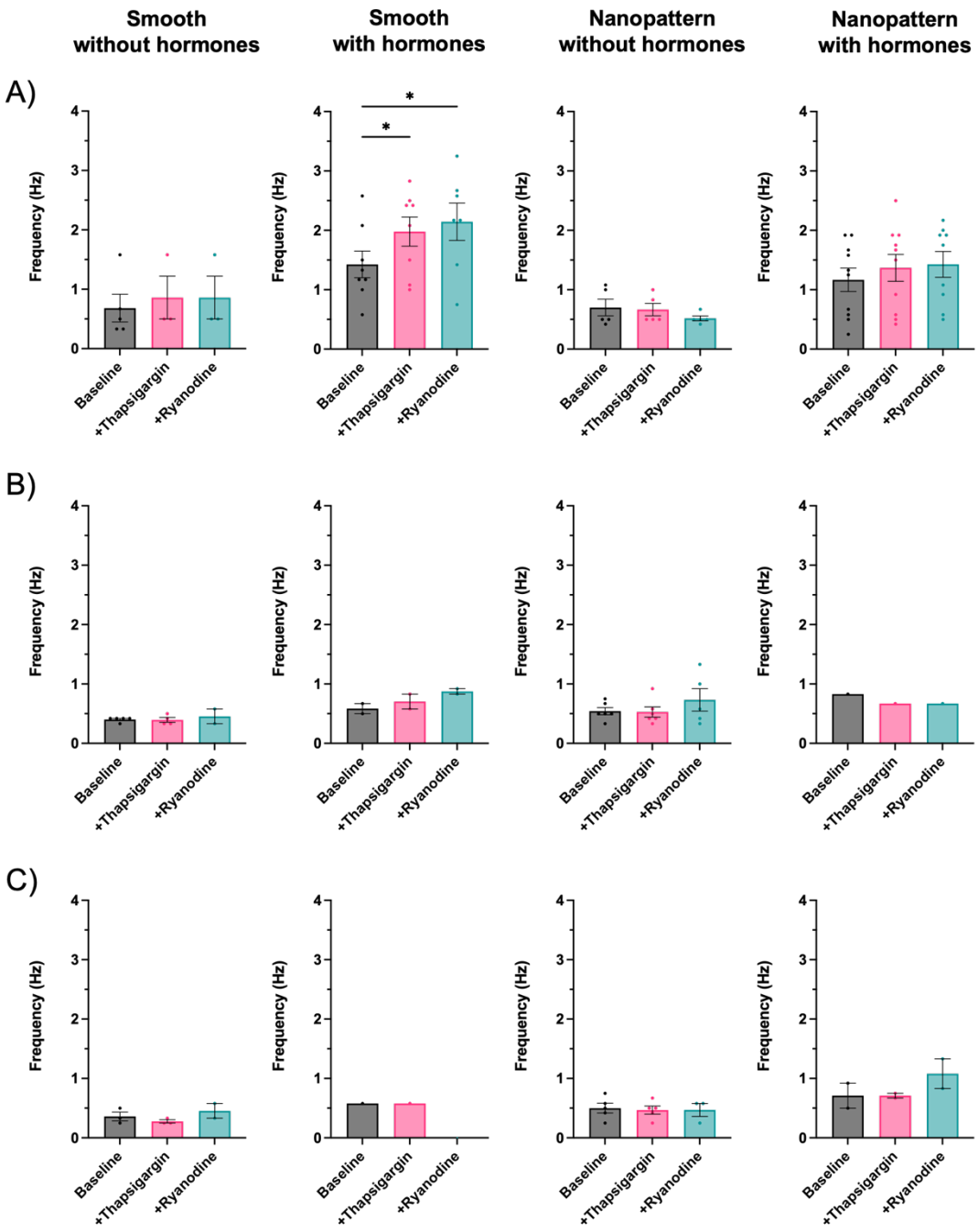

Figure 5.11: Effect of SR blockade on calcium transient frequency

Calcium transient frequency in hiPSC-CMs cultured on smooth and nanopatterned surfaces ±hormone supplementation (T3 and Dex) before (grey) and after SR blockade by sequential treatment with thapsigargin (10 μM, pink) and ryanodine (10 μM, turquoise). (A) RYR2 hiPSC-CMs, (B) control 1 hiPSC-CMs, (C) control 2 hiPSC-CMs. Values are mean ±SEM, n=1-10 dishes, 1-4 independent differentiations. One-way ANOVA was performed followed by Tukey's multiple comparisons test. *p<0.05

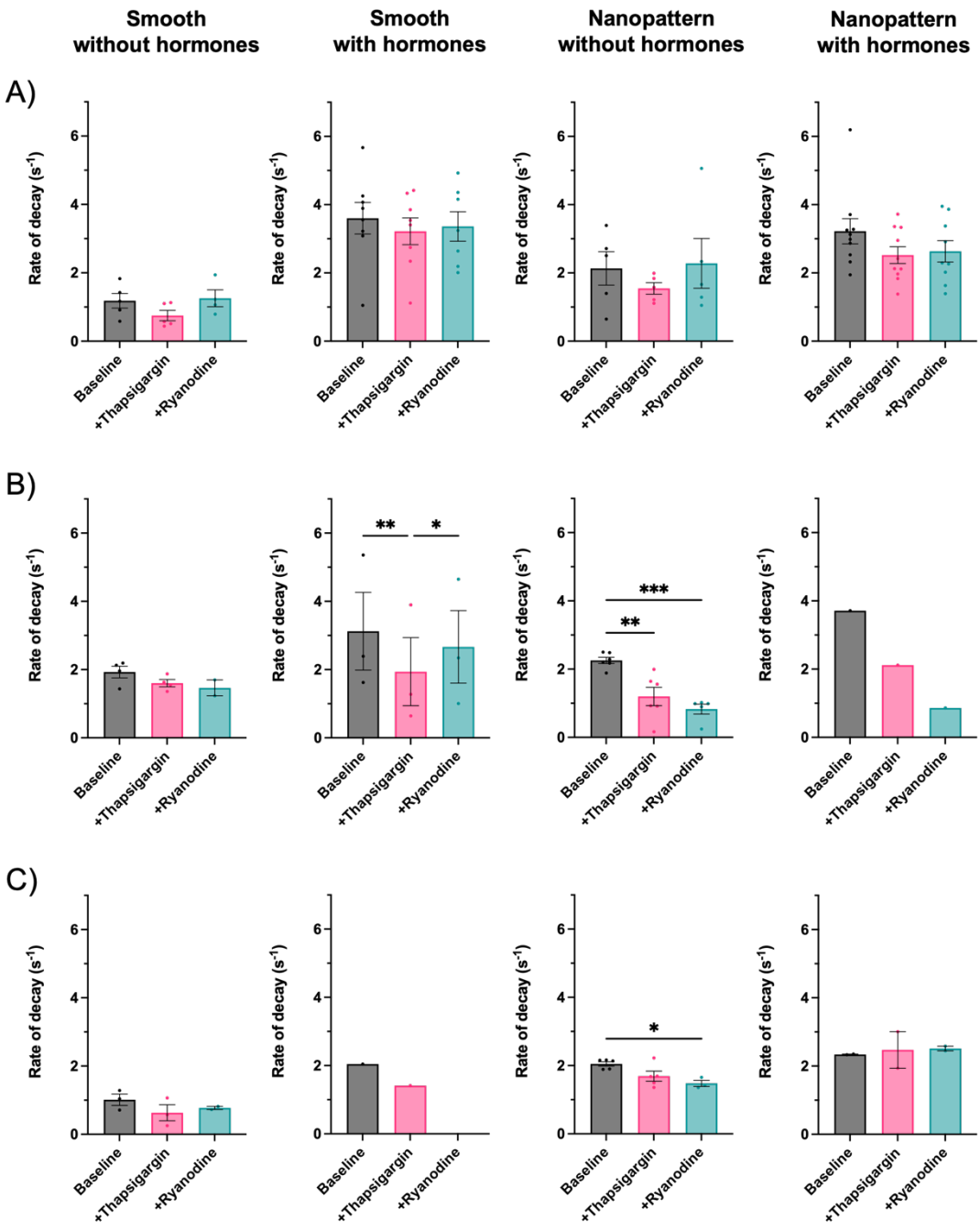

Figure 5.12: Effect of SR blockade on calcium transient rate of decay

Calcium transient rate of decay measured from fluo-4 loaded hiPSC-CMs cultured on smooth and nanopatterned surfaces ±hormone supplementation (T3 and Dex) before (grey) and after SR blockade by sequential treatment with thapsigargin (10 μM, pink) and ryanodine (10 μM, turquoise). (A) RYR2 hiPSC-CMs, (B) Control 1 hiPSC-CMs, (C) Control 2 hiPSC-CMs. Values are mean ±SEM, n=1-10 dishes, 1-4 independent differentiations. One-way ANOVA was performed followed by Tukey's multiple comparisons test. *p<0.05 **p<0.01 ***p<0.001

5.2.9 β-adrenergic receptor stimulation of RYR2 hiPSC-CMs

To test the maturity of the β-AR signalling pathway, RYR2 cardiomyocytes were incubated with accumulating concentrations of the non-selective β-AR agonist isoprenaline. Figure 5.13 shows the effects of isoprenaline on RYR2 hiPSC-CM calcium transient frequency and rate of decay for each culture condition. Only cardiomyocytes cultured on a nanopatterned topography with hormones responded to isoprenaline. With increasing isoprenaline concentration there was a decrease in transient frequency – although significance was only reported at 5 μM and 10 μM (compared to baseline, Figure 5.13A). Furthermore, there was a significant increase in the decay constant at 0.5 μM, 1 μM and 5 μM isoprenaline (Figure 5.13B) suggesting a positive lusitropic effect (faster myocardial relaxation).

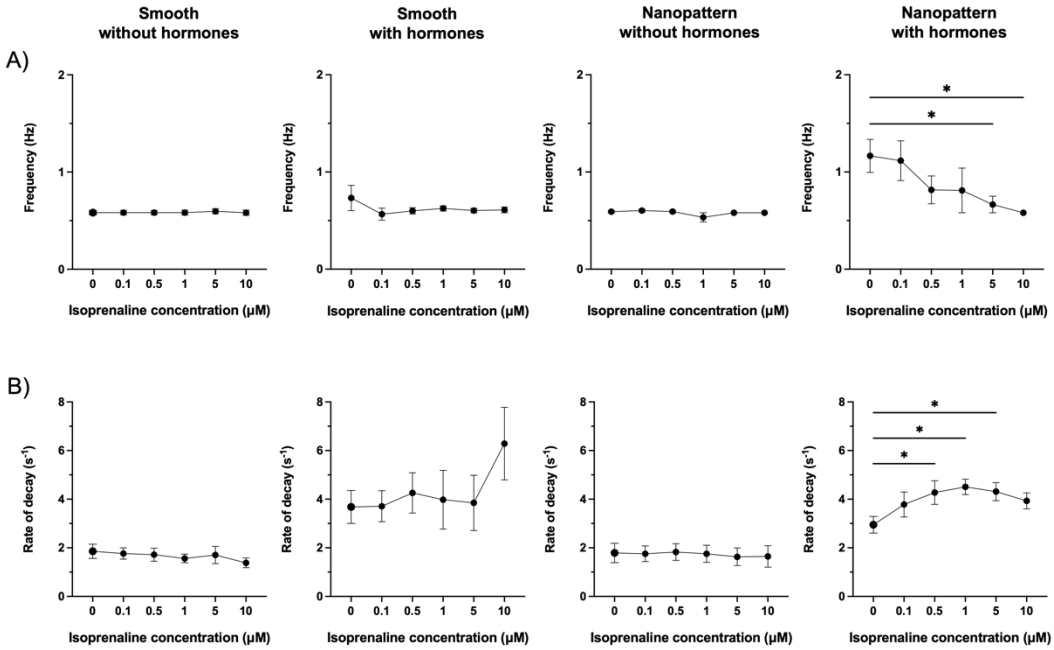

Figure 5.13: β-adrenergic stimulation results in a positive lusitropic response in RYR2 hiPSC-CM

Isoprenaline-induced changes to the frequency (A) and rate of decay (B) of intracellular calcium transients recorded from fluo-4 loaded RYR2 hiPSC-CMs cultured on smooth and nanopatterned surfaces ±hormone supplementation (T3 and Dex). Values are mean ±SEM, n=5-9 dishes, 2-3 independent differentiations. One-way ANOVA was performed followed by Dunnett's multiple comparisons test. *p<0.05

5.2.10 Expression of proteins fundamental to cardiac calcium handling

So far, the results presented in this chapter suggest the combined use of a nanopatterned culture surface with culture media hormone supplementation can

promote morphological and structural hiPSC-CM maturation, despite limited functional development. Subsequently the expression of key proteins crucial for diastolic calcium sequestration to the SR, or its' modulation, were assessed in order to further understand these observations. The limited number of control samples however is noteworthy when considering the data presented. SERCA2a is responsible for the majority of cytosolic calcium removal. There were no significant changes in the protein expression of SERCA2a in RYR2 or control hiPSC-CMs. However, despite statistical significance not being reached, both control hiPSC-CM lines demonstrated a trend towards increased expression with hormone supplementation - independent of culture surface topography (Figure 5.14A). SERCA2a translocation of calcium into the SR is regulated by PLN. In its' unphosphorylated state PLN inhibits SERCA2a activity by decreasing its' affinity for calcium. In its' phosphorylated form, PLN disinhibits SERCA2a – the inhibition is reversed, promoting calcium reuptake into the SR from the cytosol[39]. In RYR2 hiPSC-CMs, hormone treatment significantly reduced total PLN expression (Figure 5.14B). Yet interestingly, there was a non-significant trend towards increased phosPLN in hiPSC-CMs cultured on a nanopatterned surface (Figure 5.14C). There was no change in total PLN (Figure 5.14B) or phosPLN (Figure 5.14C) expression in either control line. See Appendix for representative full western blot images.

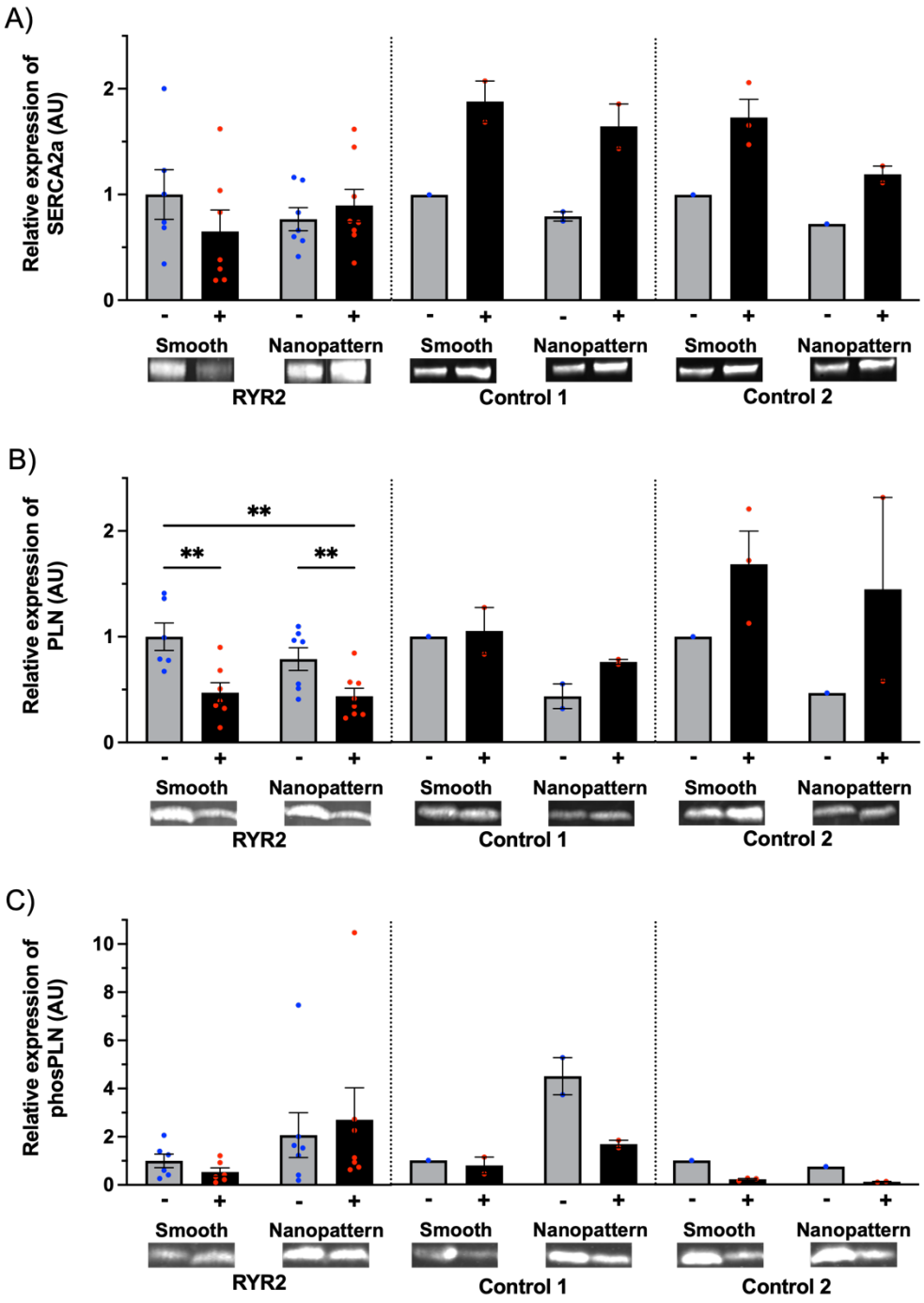

Figure 5.14: Expression of proteins involved in calcium sequestration to the SR

Quantified relative expression and representative western blots of SERCA2a (A), PLN (B), phosPLN (C) in RYR2 and control hiPSC-CMs cultured on smooth and nanopatterned culture surface ±hormone supplementation (T3 and Dex). Expression is shown relative to smooth surface without hormones in arbitrary units (AU). Values are mean ±SEM, n=1-8 biological samples performed in duplicate. Two-way ANOVA was performed followed by Tukey's multiple comparisons test. **p<0.01

To further understand how the expression of these proteins may be affecting calcium transient phases and properties, the expression ratio of SERCA2a and total PLN, and the proportion of total PLN phosphorylated was considered. In RYR2 hiPSC-CMs, the SERCA2a:PLN ratio non-significantly increased with hormone treatment. In combination with the nanopatterned surface however the expression ratio was significantly increased (compared to baseline culture conditions, Figure 5.15A). The phosPLN:PLN ratio also significantly increased but in contrast the effect was induced by the nanopatterned surface (Figure 5.15B). Both these observations infer increased SERCA2a activity in RYR2 hiPSC-CMs cultured under maturation factor conditions. No significant changes in either the SERCA:PLN or phosPLN:PLN ratios were observed in the control hiPSC-CMs. However, in line with the expression data displayed in Figure 5.14, there was a trend towards a significantly reduced proportion of phosPLN with hormone treatment in control 2 hiPSC-CMs (Figure 5.15B).

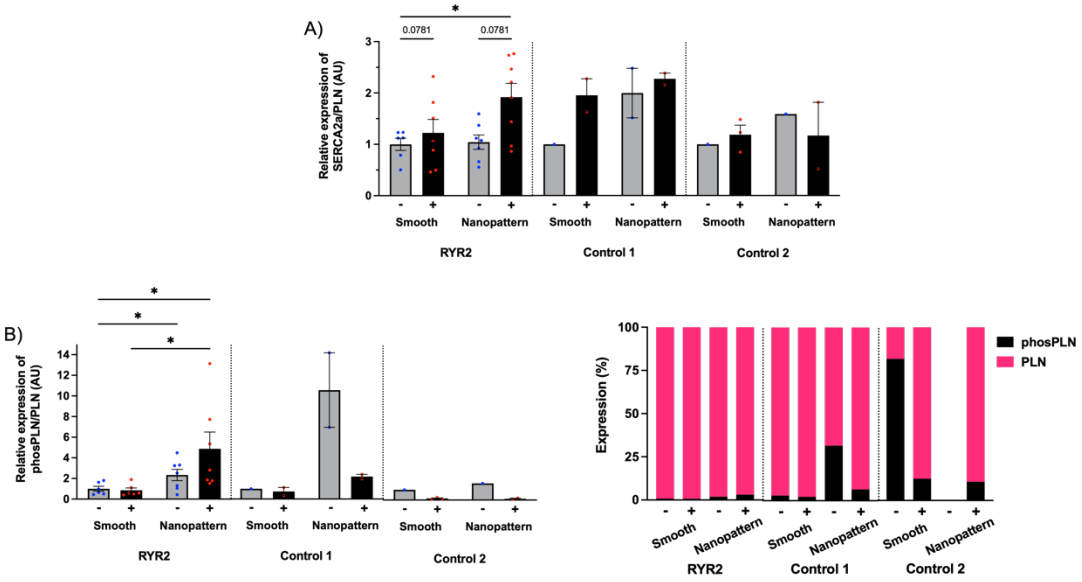

Figure 5.15: Modulation of SR calcium reuptake – key expression ratios

(A) Relative expression ratio of SERCA2a and total PLN. (B) The relative proportion of total PLN phosphorylated in RYR2 and control hiPSC-CMs cultured on smooth and nanopatterned surfaces ±hormone supplementation (T3 and Dex). Left: ratio is shown relative to smooth surface without hormones in arbitrary units (AU). Right: expression shown as a percentage. Values are means. ±SEM, n=1-8 biological samples performed in duplicate. Two-way ANOVA was performed followed by Tukey's multiple comparisons test. *p<0.05

NCX is also responsible for removal of intracellular calcium during the diastolic period when in forward mode. No expression changes were observed in RYR2 or control hiPSC-

CMs (Figure 5.16A). Stimulation of β_1-ARs promotes phosphorylation of calcium handling proteins, including PLN, to increase the rate and force of contractility. No statistically significant changes in ADRβ1 protein expression were detected either (Figure 5.16B). See Appendix for representative full western blot images.

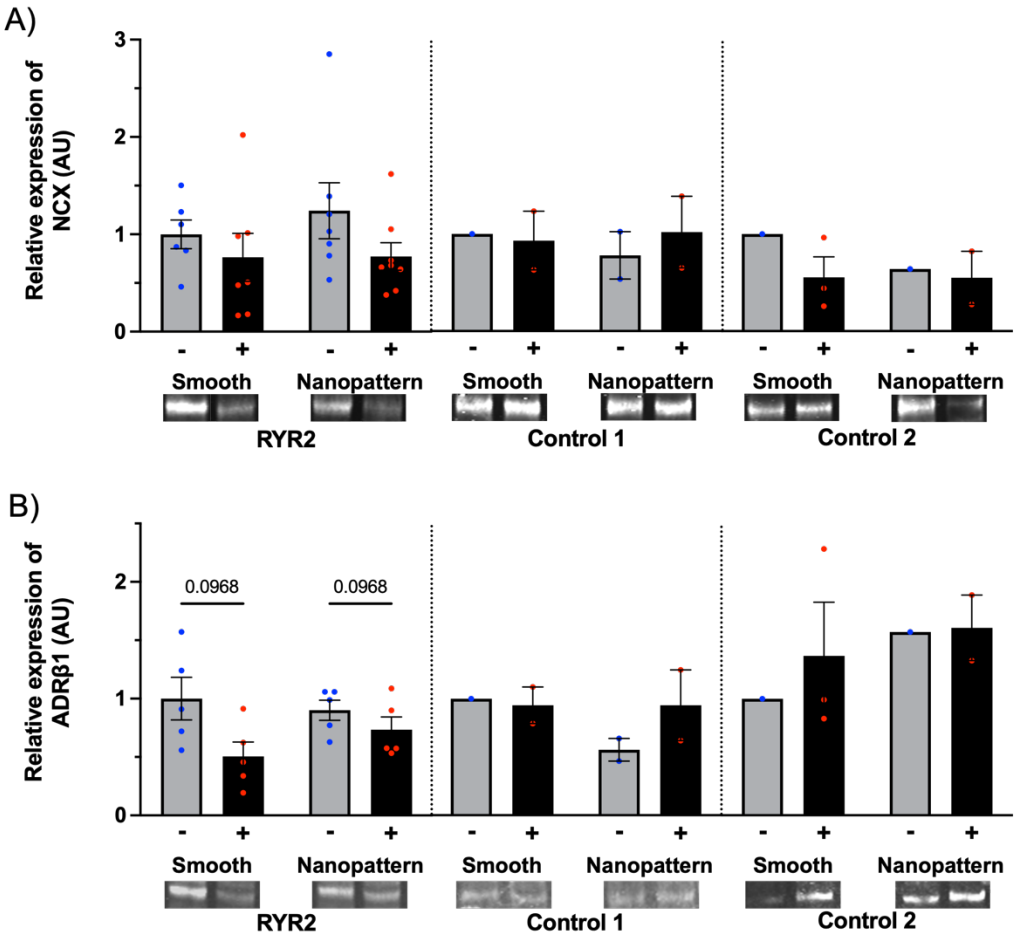

Figure 5.16: No change in NCX or ADRβ1 protein expression with maturation factors

Quantified protein expression and representative western blots of NCX (A) and ADRβ1 (B) in RYR2 and control hiPSC-CMs cultured on smooth and nanopatterned culture surface ±hormone supplementation (T3 and Dex). Expression is shown relative to smooth surface without hormones in arbitrary units (AU). Values are mean ±SEM, n=1-8 biological samples performed in duplicate. Two-way ANOVA was performed followed by Tukey's multiple comparisons test.

5.3 Discussion

To date research into developmental cardiology has focussed on the first two stages of mammalian heart development: specification and morphogenesis. The new era of

personalised, or precision, medicine has highlighted our lack of knowledge regarding the third stage, cardiomyocyte maturation. This stage encompasses physiological hypertrophy and cell- and tissue-level adaptations to gene expression, structure, function and metabolism that allow the progression of foetal cardiomyocytes to adult cardiomyocytes. Consequently, implementation of *in vitro* modelling for mechanistic and pharmacological purposes is limited by the incomplete maturation of cardiomyocytes.

The structural status of cardiomyocytes is heavily interlinked with the intricate electrophysiological and mechanical processes of coupling excitation to contraction. The localisation and spatial arrangement of the calcium release unit components aid CICR, ensuring the synchronous rise of calcium during systole. The close association of LTCCs of the surface membrane and RYR2 channels of the jSR is assisted by deep invaginations of the surface membrane known as the T-tubular network. In this chapter the effect of biochemical and topographical cues on the maturation of hiPSC-CM structure and calcium handling properties have been described. Following differentiation and culture purification, hiPSC-CMs were seeded onto smooth or nanopatterned culture dishes and maintained in culture medium with or without hormone supplementation. For each culture condition length and width measurements, and the aspect ratio of RYR2 hiPSC-CMs were presented. Furthermore, observed differences in shape and myofilament organisation (represented by alpha actinin staining) were illustrated. To understand the functional maturity of hiPSC-CM calcium handling, changes in calcium transient characteristics were assessed at baseline and following pharmacological studies in RYR2 and control line hiPSC-CMs.

The main findings were:

- Structure
    - Development of morphologically relevant RYR2 hiPSC-CMs
    - Qualitative indication of improved sarcomere organisation and alignment with cell orientation
- Function
    - Increased calcium transient frequency
    - Decreased calcium transient rate of rise and amplitude

- Increased calcium transient rate of decay

5.3.1 Morphological maturation induces sarcomeric organisation in RYR2 hiPSC-CMs

The nanopatterned culture surface was introduced in order to mimic the cardiac ECM - inducing cues for orientation, morphological elongation, and cellular organisation. Prior to implementation it was confirmed Matrigel-coating of the culture dishes did not alter the optimal parameters of the topographical pattern. The maintenance of RYR2 hiPSC-CMs on the nanopatterned surface provoked the desired effects – cells arranged in the direction of the nanopattern in a parallel array, and significant elongation was observed. The approximate doubling of cell length resulted in hiPSC-CMs of length equivalent to native adult cardiomyocytes (typically 100 -150 μm[189,190]). The unchanged width of the RYR2 hiPSC-CMs also corresponded to that of native adult cardiomyocytes (20-35 μm[189,190]). Consequently, the aspect ratio of RYR2 hiPSC-CMs significantly increased from ~2.5 to ~5 – comparable to smaller native adult cardiomyocytes (aspect ratio mean ~7[187,188]).

Despite increased heterogeneity of the morphological parameters, the overall changes induced by the nanopatterned surface (independent of hormone treatment) developed rod-shaped RYR2 hiPSC-CMs in contrast to the round/triangular/irregular hiPSC-CMs observed on the smooth surface. Additional quantitative analysis of the circularity index could have substantiated these observations.

In addition to improved hiPSC-CM morphology the nanopatterned culture surface, enhanced by hormone treatment, promoted sarcomere organisation and alignment with cell orientation. These observations correspond with reports that sarcomere alignment is regulated by cardiomyocyte shape. Insights into sarcomerogenesis indicate that sarcomeres emanate from the perinuclear region converging on angular boundaries of the cardiomyocyte, yet geometric cues from the cell periphery control their alignment[191,192]. This explains why rounded hiPSC-CMs display irregular or radial sarcomeric organisation, and those that appear triangular or irregular with internal angles can display patterns radiating from the nucleus towards the internal angles, or parallel with the cell periphery between internal angles. As the aspect ratio of rod-shaped cells increases, the arrangement of myofibrils switches from radial to

longitudinal oriented perpendicular to the long axis of the cardiomyocyte, and results in "parallel arrays of serially aligned and laterally registered sarcomeres"[191,192]. It has also been demonstrated that there is a direct correlation between healthy adult cardiomyocyte shape, and contractility and calcium handling - the aspect ratio and sarcomeric patterns of healthy cardiomyocytes are optimised for contractility and calcium handling[192].

Although the development of a T-tubular network was not directly assessed, fluorescent labelling of the cell membrane did not exhibit features indicating T-tubule formation; as has previously been demonstrated following hormone treatment in combination with the Matrigel mattress method[199,284]. The Matrigel mattress method uses undiluted growth factor-reduced Matrigel matrix (8-12 mg/ml) and is designed to provide a physiological load (5-7 kPa). In comparison the modulus of the polymer used to produce the nanopatterned dishes implemented in this study was 7 MPa. The polymer was coated with growth factor-reduced Matrigel diluted 1:200 prior to hiPSC-CM seeding. Changes in the mechanical properties of substrates can be used to modify physiological responses; for example, increasing substrate stiffness provides a greater resistance hence increases contractile demand[400]. Hence it is possible the decreased substrate stiffness of the diluted Matrigel used in this study, and thus physiological load (contraction stress), was responsible for the lack of development of a T-tubular network.

5.3.2 Calcium transient frequency

A crucial limitation of functional maturity in hiPSC-CMs is their spontaneous activity. In the adult heart the I_f current is responsible for the spontaneous activity of pacemaker cells[401] and the I_{K1} current is important for maintaining the resting membrane potential. Uncharacteristically of adult ventricular cardiomyocytes, hiPSC-CMs display a robust I_f current and minimal I_{K1} current[181,200,201]. Together they cause a less stable, depolarised resting membrane potential. Although it is suggested the density of the I_f current is insufficient on its own, combined with NCX activity and SR calcium leak it accounts for the spontaneous beating of hiPSC-CMs[185,200,402]. Hence it was hypothesised that hiPSC-CMs with matured electrophysiological properties would display slower spontaneous activity or even quiescent behaviour.

Batch to batch variability within and between cell lines resulted in a mix of quiescent and spontaneously beating cardiomyocytes. As demonstrated, spontaneously firing cells have variable firing rates which can affect the measured calcium transient parameters, and thus data interpretation. To control for potential differences caused by variable firing rates and not the MFs, electrical stimulation of the monolayers was favoured. In the absence of hormone treatment, the majority of RYR2 hiPSC-CMs were electrically stimulated at the pre-determined frequency of 0.5Hz. However, many of the cultures harboured high frequency spontaneous activity that could not be regulated by the slower electrical stimulation. RYR2 hiPSC-CMs cultured in the presence of additional hormones, and all cultures of both control hiPSC-CM lines spontaneously fired at variable frequencies. Consequently, it was important to present data according to calcium transient frequency.

Hormone-treated hiPSC-CMs exhibited significantly increased calcium transient frequencies. In control 1 hiPSC-CMs the nanopatterned surface also caused a significant increase in transient frequency. Instead of maturity these results are indicative of further immaturity and are in stark contrast to the results reported from the Knollmann laboratory group. They showed the spontaneous beating frequency of hormone-treated hiPSC-CMs cultured on the Matrigel mattress to significantly reduce[202]; despite T3 being a positive regulator of pacemaker-related genes[403]. Furthermore their voltage clamp results demonstrated increased repolarising (I_{Kr}, I_{Ks} and I_{K1}) current densities and a decreased I_f current density, consistent with changes in gene transcription levels[202].

The Knollmann group only supplemented the hiPSC-CM culture medium with hormones from day 16 to day 30 and seeded hiPSC-CMs on the Matrigel mattress from day 30 for 3-5 days before analysis[199,202]. The protocol used in this study involved culture on the nanopatterned surface from day 14 and hormone supplementation from day 16, until analysis at ~day 45. It is postulated that the extended period of hormone treatment in this study may have induced a state akin with hyperthyroidism. It is well-documented that hyperthyroidism can lead to increased heart rate[268]. Studies mimicking hyperthyroidism have reported increases in the amplitude of I_f in rabbit isolated SAN myocytes[404] and *HCN2* mRNA levels of rat ventricles[336,403]. Additionally, thyroid hormone negatively regulates NCX, and positively regulates ADRβ1 expression[268]

although neither of these effects were seen in this study. In the following sections, the calcium transient properties assessed will be discussed in more detail.

5.3.3 Rate of intracellular calcium rise

A faster rate of intracellular calcium rise, or reduced time to peak, would be expected with improved intracellular structure and organisation. However, the rate of calcium rise was significantly slower in hormone-treated RYR2 hiPSC-CMs cultured on the nanopatterned surface. Despite low sample numbers for the control hiPSC-CMs a slower rate of rise was identified in cells cultured on the nanopatterned surface. These findings oppose the expected outcome and contradict the previous report from the Knollmann group[199]. They observed a small but significant reduction in calcium transient time to peak, and synchronisation of calcium release. However, notably Parikh *et al*. also reported development of a T-tubular network. In this study no evidence of T-tubule development was observed following cell membrane labelling of RYR2 hiPSC-CMs. The T-tubular network is crucial for EC coupling and the spatial proximity of the calcium release unit components: LTCC and the RYR2 channels of the jSR. Taking into consideration the absence of a T-tubular network, it is unsurprising that the morphologically advanced hiPSC-CMs in this study display a slower rate of calcium rise – the greater cell size would increase the distance between LTCCs and the SR, and create a larger volume for calcium to distribute, thus reducing the effectiveness of CICR. It is further postulated that the slower rate of calcium rise could be associated with differences in the characteristics/gating kinetics of the LTCCs. This idea has been reported previously: LTCCs of hiPSC-CM populations had different inactivation kinetics[405]. In older cells with a greater cell size LTCCs appeared to inactivate more slowly. The authors suggested that the altered inactivation kinetics were determined by the surface to volume ratio and hence the effectiveness of released calcium to regulate calcium-dependent inactivation of the LTCCs.

5.3.4 Calcium transient amplitude

Similarly to rate of calcium rise, with hiPSC-CM maturation an increased amplitude would be anticipated due to greater I_{Ca} magnitude and SR contribution. Yet, calcium transient amplitude decreased in hormone-treated hiPSC-CMs of the RYR2 and control 1 lines, and in hiPSC-CMs cultured on the nanopatterned surface of both control lines.

In the Knollmann group study[199] no change in calcium transient amplitude was reported due to increased calcium-dependent inactivation of LTCCs – despite demonstrating an increased SR contribution. It would therefore seem that there are cell line specific responses to MFs.

In adult cardiomyocytes, an increased frequency of stimulation is associated with a gradual increase in peak intracellular calcium amplitude and slower channel inactivation. This is a process termed 'facilitation'[406,407]. However with increasing frequency incomplete relaxation occurs, reducing cytosolic calcium efflux and thus raising diastolic intracellular calcium levels. Consequently, there is a decrease in calcium current and CICR from the SR due to an accumulation of inactivated channels[40,406,408]. It is widely acknowledged that functionally immature hiPSC-CMs are 'depolarised' – meaning they have a less negative resting membrane potential compared to native adult cardiomyocytes[181,183,202,328,409–411]. Although this idea has been challenged[412]. It is considered that the combination of a less negative membrane potential (which facilitates spontaneous activity) and prolonged hormone-treatment augmented calcium release frequency to the point where the interval was too short for complete relaxation and consequently caused a decline in calcium transient amplitude. However, the data here was initially presented and analysed according to calcium transient frequency and no differences were reported. From the results of the experiments conducted, SR calcium contribution cannot be confirmed but it is assumed to be limited due to reports of poorly developed SR in hiPSC-CMs[184,219,413]. Similarly to rate of rise, a decreased surface to volume ratio could decrease the effectiveness of any CICR thus transient amplitude. Alternative hypotheses for the reduction in calcium transient amplitude are also postulated: 1) in cells displaying morphological maturation, the influx of calcium ions distributed over a greater volume so fluorescence intensity was lower within the set ROI dimensions of calcium transient recordings; 2) as previously considered, LTCC gating kinetics changed under maturation factor conditions reducing calcium influx; 3) the density hence buffering capacity of the myofilaments was enhanced by increased cell size and sarcomere organisation reducing cytosolic calcium during systole[414–416]; 4) the contribution of mitochondrial calcium release was altered[417].

5.3.5 Rate of intracellular calcium decay

The rate of calcium transient decay in the hiPSC-CM lines in this study demonstrated differing responses to the MFs. RYR2 hiPSC-CMs displayed a significantly increased rate of decay when cultured with additional hormones. This result corresponds with the decreased expression of total PLN, and the consequent increase in SERCA2a and phosPLN ratios - both would enhance SERCA2a sequestration of calcium from the cytosol to the SR. Analysis of control 1 hiPSC-CMs indicated no change in the rate of calcium decay or expression ratios of SERCA2a and phosPLN with total PLN. In contrast culture on a nanopatterned surface significantly increased the rate of decay of control 2 hiPSC-CMs. The low number of biological replicates means the protein expression data cannot clearly explain this observation: no change in the proportion of phosPLN:PLN is observed with the nanopattern surface; yet irrespective of culture surface, hormone treatment non-significantly reduces the expression of phosPLN and consequently the proportion of PLN phosphorylated. It is possible the MFs are having opposing effects on PLN phosphorylation, or an alternative factor such as myofilament buffering could be involved. Increased myofilament phosphorylation (decreased affinity for calcium) would reduce calcium buffering hence accelerate the rate of calcium decay; low myofilament phosphorylation would increase calcium buffering therefore slow the rate of calcium decay. It is important to bear in mind the low sample numbers in the expression data presented so interpretations are suggested cautiously – additional investigations are required.

To further assess the function of the SR in hiPSC-CM calcium handling, SERCA2a and RYR2 channels were pharmacologically inhibited. Improved SERCA2a activity of RYR2 hiPSC-CMS could not be confirmed following blockade of SERCA2a. This could be explained by aberrant diastolic calcium release of dysfunctional RYR2 channels caused by the mutation. Nevertheless no change was reported following incubation with ryanodine (RYR2 channel block). Control hiPSC-CMs cultured under maturation factor conditions responded to SR blockade, although interpretations are again restricted by low sample numbers in some culture conditions. In control 1 cells incubation with thapsigargin significantly reduced the rate of calcium decay, an observation not seen in hiPSC-CMs cultured without MFs. Block of the RYR2 channels with ryanodine further decelerated the rate of calcium decay in cells cultured on the nanopattern surface.

These results indicate improved SERCA2a activity. In control 2 hiPSC-CMs there were similar trends to control 1 hiPSC-CMs.

5.3.6 β-adrenergic response induced by RYR2 hiPSC-CM maturation

Nanomolar concentrations of isoprenaline have positive chronotropic, inotropic and lusitropic effects on adult cardiomyocytes. However studies indicate micromolar concentrations are required for similar responses to be observed in immature hiPSC-CMs[42,329,400,418]. In contrast to the expected dose-dependent positive chronotropic effect, there was no change in RYR2 hiPSC-CM calcium transient frequency under baseline culture conditions, or under culture conditions with only one of the MFs – probably due to the hiPSC-CMs being electrically stimulated at 0.5Hz. In hormone-treated RYR2 hiPSC-CMs cultured on the nanopatterned surface the transient frequency decreased to the pacing frequency with 5 μM isoprenaline.

A significant lusitropic effect was observed following an accumulated isoprenaline concentration of 1 μM. However, this finding was only seen in hormone-treated RYR2 hiPSC-CMs cultured on the nanopatterned surface indicating maturation of the signalling pathway under these conditions. Interestingly, no change in ADRβ1 expression was reported between the culture conditions. This does not correspond with the accepted positive regulation of thyroid hormones on cardiac ADRβ1 expression[268,336] or data shown here in Chapter 4 – hormone-treated RYR2 hiPSC-CMs displayed significantly upregulated ADRβ1 expression at both the genomic and protein level. The most logical explanation for this unexpected result is a batch effect.

5.4 Study limitations and further work

5.4.1 Morphology and intracellular structure

In this chapter, it is reported that hiPSC-CMs seeded on the nanopatterned surface evolve morphologically and are more comparable to native adult cardiomyocytes. In order to further support this claim, additional properties could have been measured e.g. perimeter, volume, circularity. Sarcomeric organisation was illustrated through fluorescent labelling of alpha actinin molecules. Quantification of the fluorescence could have provided additional information such as changes in sarcomere density and

therefore supported/disputed the suggested hypothesis regarding increased calcium buffering capacity in morphologically matured hiPSC-CMs. With enhanced intracellular organisation, improved localisation of LTCC and RYR2 channels was expected. Functional analyses of calcium handling were inconclusive. Fluorescent labelling and super-resolution microscopy of calcium handling components simultaneously could be considered to establish their spatial organisation. Alternatively, further evaluation of cellular organisation could be performed at higher resolutions using electron microscopy.

The T-tubular network plays a critical role in maintaining intracellular calcium homeostasis and handling. Although T-tubule formation was not directly assessed no evidence of development was observed. As previously discussed, the physiological load provided by the substrate could play a key role in hiPSC-CM contraction stress and T-tubule formation. Assessment, and optimisation of substrate (Matrigel) concentration on the nanopatterned culture surface, by performing further atomic force microscopy analyses, could have identified an elastic moduli/stiffness with increased physiological relevance for mimicking cardiac tissue. Electron microscopy, or staining hiPSC-CMs with a lipophilic membrane dye (such as WGA) and confocal microscopy with z-stack imaging could be used to assess T-tubule formation and create 3D reconstructions of the network.

5.4.2 Calcium handling

Due to the COVID-19 pandemic the delivery and installation of the custom-made calcium and voltage dual channel optical mapping system was delayed. Additionally, the standard service and training opportunities for the new system from the manufacturing company were not available. As a result data collection was performed in a limited time period whilst gaining expertise in the use, and optimisation of the new system.

For calcium imaging experiments, hiPSC-CMs were loaded with the intracellular calcium indicator fluo-4 and incubated with probenecid to prolong retention of the dye. Inhibition of organic anion transporters is toxic to cells. The signal in loaded cardiomyocytes appeared to be viable for under 30 minutes. Generation of cell lines harbouring genetically encoded calcium indicator reporters for calcium imaging

experiments would thus be beneficial to allow for long-term imaging and more accurate signals.

A crucial limitation of the data presented in this chapter was hiPSC-CM batch and cell line variability. RYR2 hiPSC-CMs exhibited a mixed population of quiescent hiPSC-CMs requiring electrical stimulation, and spontaneously beating hiPSC-CMs. Furthermore, due to the high firing rates of spontaneously beating hiPSC-CMs at 37°C, particularly in the control lines, calcium transient traces were not analysable. Consequently, the temperature at which the calcium imaging experiments were performed had to be reduced to room temperature. The required experimental design adaptations resulted in data collection differences within and between RYR2 and control hiPSC-CMs. Accordingly, RYR2 and control lines could not be directly compared, and it was determined data should be presented by frequency. Expressing data according to frequency meant the sample numbers for each condition were subdivided, leading to small numbers of biological replicates – insufficient for full statistical analysis in some conditions.

In this study monolayers of hiPSC-CMs were analysed as this provides a more physiologically relevant environment than isolated single cells. However, difficulties in distinguishing individual cells in the monolayers meant recordings and analysis of calcium transient properties were conducted by regions of interest of predetermined area as opposed to individual cells. As a result it is likely that there will have been variability in the number of cells contributing to the fluorescence changes between regions of interest.

The optical mapping system and surrounding infrastructure did not allow for washing out of pharmacological reagents. Together with limited replicates and time pressures, this meant pharmacological assessments had to be performed in an accumulating, sequential manner and could not be returned to baseline. Furthermore, it would have been good practice to perform preliminary experiments to identify the optimal concentrations and incubation times for reagent exposure considering the immature nature of the hiPSC-CMs.

5.5 Conclusion

This chapter has demonstrated that a nanopatterned culture surface has important benefits for generating hiPSC-CMs with morphological parameters and structural organisation comparable to native adult cardiomyocytes. However, for development of a T-tubular network the Matrigel substrate needs to be assessed and optimised to a more physiologically relevant stiffness that provides increased contraction stress. The chapter also highlights variability in cell line responses to MFs – hormone treatment was responsible for the majority of changes in RYR2 hiPSC-CMs, whilst the culture surface was the main effector in the control lines. Importantly a faster rate of decay, in response to increased SERCA2a activity, is reported despite a slower rate of calcium rise and smaller transient amplitude. The increased cell size and absence of a T-tubular network are postulated to be responsible. It is hypothesised that with a physiologically relevant substrate stiffness, development of a T-tubular network and calcium handling maturation would occur in the RYR2 and control hiPSC-CMs. Furthermore, a recent report has demonstrated that the differentiation medium composition can affect hiPSC-CM metabolic status. By creating a media with physiologically appropriate levels of glucose and oxidative substrates, metabolic maturation of hiPSC-CMs has been observed and in turn enhanced electrophysiological, structural and functional properties[214]. In the next chapter, the effect of the differentiation medium adapted to the metabolic requirements of cardiomyocytes will be evaluated in RYR2 and control hiPSC-CMs.

Chapter 6

The effect of a physiologically relevant maturation medium on hiPSC-CM function

6 The effect of a physiologically relevant maturation medium on hiPSC-CM function

6.1 Introduction

The metabolic status of the heart at any given age is dependent on the activity of energy pathways, which are influenced by the availability of circulating substrates. During prenatal development, the heart exists in a relatively hypoxic, high lactate, low fatty acid environment. Furthermore, during this stage the distribution and activity of glycolytic enzymes are high, whilst the mitochondrial mass is low[212]. Consequently, the foetal heart is predominantly reliant on anaerobic glycolytic metabolism of carbohydrates for energy[211]. The cardiac foetal to adult transition occurs rapidly, and partly in response to birth. The sudden inflation of the pulmonary alveoli and new circulation pattern initiates major haemodynamic changes in oxygen levels, pressure and volume[212]. The postnatal period is also characterised by a constant increase in the workload demanded of the heart. However with development the heart to body weight ratio decreases thus the efficiency of the heart is required to improve[212].

The increased energy demand and efficiency of the heart is achieved initially through mitochondrial maturation and energy metabolism. Although the mature adult heart is capable of producing energy by metabolism of carbohydrates, lipids, proteins and lactate[211,212,419], the enhanced energy demands can only be met by fatty acid oxidation and mitochondrial ATP production. In response mitochondrial biogenesis, and the expression of enzymes and transporters critical for fatty acid oxidation are upregulated[211,212]. The metabolic switch is also promoted by reversal of the lactate to fatty acid ratio in the blood, as the content of maternal milk is enriched with lipids[212]. The energy provided by mitochondrial oxidative metabolism increases from <15% in the foetal heart to >90% in the adult heart[211,419]. This metabolic maturation precedes and assists in achieving further cardiac efficiency through development and compartmentalisation of cardiomyocyte architecture and EC coupling[212].

In immature hPSC-CMs mitochondria appear long and slender, clustering next to the nucleus or in the cell periphery[196] instead of dispersing across cytoplasmic regions.

Prolonged culture of hPSC-CMs has been demonstrated to increase the abundance of mitochondria however their size does not significantly change. Furthermore, measurements of respiratory complex activity displayed no change (when normalised to total protein or mitochondrial mass) with prolonged culture. In comparison, complex activity significantly increases with foetal development when normalised to total protein but not mitochondrial mass; this indicates a mitochondrial growth greater than other cellular components in foetal cardiomyocytes that is not observed in hPSC-CMs[420].

During and after differentiation, hiPSC-CMs are customarily maintained in culture media such as RPMI B27. Despite the established status of RPMI B27 to efficiently support cardiac differentiation and growth, the components: RPMI 1640 basal culture medium and the B27 supplement, are not sufficient to promote hiPSC-CM maturation to adult-like cardiomyocytes[184,199,214,402,420]. One of the major limitations of RPMI B27 is its' glucose-rich, lipid-poor composition. Consequently, there is no induction of mitochondrial maturation and the innate transition from glycolysis to oxidative metabolism is inhibited. The role of metabolic maturation in the physiological developments of hiPSC-CMs is therefore restricted.

To address the shortcomings in the composition of cardiac differentiation media, a maturation medium containing physiologically appropriate levels of glucose and oxidative substrates was designed by Feyen *et al*.[214]. Culture in the metabolic maturation medium (MMM) was reported to enhance hiPSC-CM fatty acid uptake capacity, respiration rate and ATP production. The content and distribution of mitochondria was also improved. Interestingly, hiPSC-CM maturation was not confined to metabolic indices. Multiple genes involved in cardiac calcium handling, contraction and ion channel assembly as well as those related to mitochondrial metabolism were differentially expressed. Accordingly, improvements in electrophysiological behaviour and calcium cycling were also reported.

In the previous chapters prolonged culture, hormone supplementation and a nanopatterned culture surface have each been shown to influence aspects of hiPSC-CM maturity. Nevertheless advances in calcium handling maturity have been limited. In this chapter the MMM is adopted. Following cardiac differentiation and reseeding of

purified hiPSC-CMs on nanopatterned dishes, the differentiation medium was switched to the MMM (Figure 6.1). The hiPSC-CMs were cultured in the physiologically relevant medium for 25 days prior to analysis at ~day 45. The media was refreshed twice a week.

The aims of this chapter were:

- To assess the effect of the metabolic maturation medium on hiPSC-CM calcium handling
- To evaluate the influence of the metabolic maturation medium on protein expression

To address these aims the approaches were similar to the previous chapter. Live calcium imaging was conducted on RYR2 and control 1 hiPSC-CMs, at baseline and following pharmacological challenges; subsequently characteristics of the obtained calcium transient traces were analysed. Western blots were also carried out to assess the expression of proteins involved in calcium handling. Calcium transient properties and protein expression data were compared to the data collected from hiPSC-CMs cultured under baseline conditions (smooth surface without hormone treatment) and with MFs (nanopatterned surface with hormone treatment), previously presented in Chapter 5.

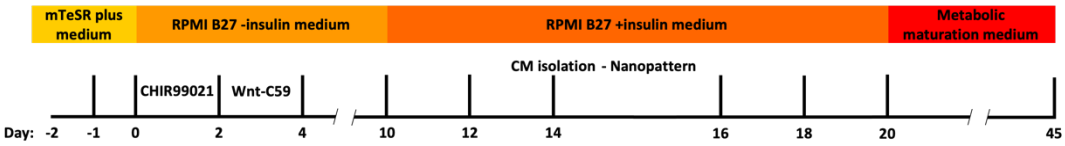

Figure 6.1: Cardiac differentiation protocol with metabolic maturation medium

On day 20 of differentiation, following cardiomyocyte (CM) isolation, the maintenance medium was switched from RPMI B27 +insulin to Feyen *et al*.[214] metabolic maturation medium. The medium was refreshed twice a week. Identical to Figure 2.4.

6.2 Results

To ascertain if a more metabolically relevant culture medium would promote the maturity of hiPSC-CM calcium handling, calcium transient frequency, rate of rise, amplitude, and rate of decay properties were analysed at baseline. Presented data is from cells with firing frequencies <1Hz. SR function was also evaluated following sequential application of thapsigargin and ryanodine (inhibitors of SERCA2a pumps and

RYR2 channels respectively). For reasons explained in the previous chapter (section 5.2.3) baseline data from hiPSC-CMs cultured in the MMM is from experiments conducted at 37°C for RYR2 hiPSC-CMs, and room temperature for control 1 hiPSC-CMs. All data from pharmacologically challenged hiPSC-CMs cultured in the MMM is from experiments conducted at room temperature.

6.2.1 Frequency of calcium transients in hiPSC-CMs

The spontaneous firing rate of hiPSC-CMs cultured in the MMM was variable, as expected. However the calcium transient frequency of RYR2 hiPSC-CMs cultured in the MMM was not significantly different to the rate recorded in RYR2 hiPSC-CMs cultured under baseline conditions or under MF conditions (Figure 6.2A). There was no difference in calcium transient frequency of control hiPSC-CMs cultured in the MMM compared to those cultured under baseline conditions, but frequency was significantly lower than in MF hiPSC-CMs (Figure 6.2B).

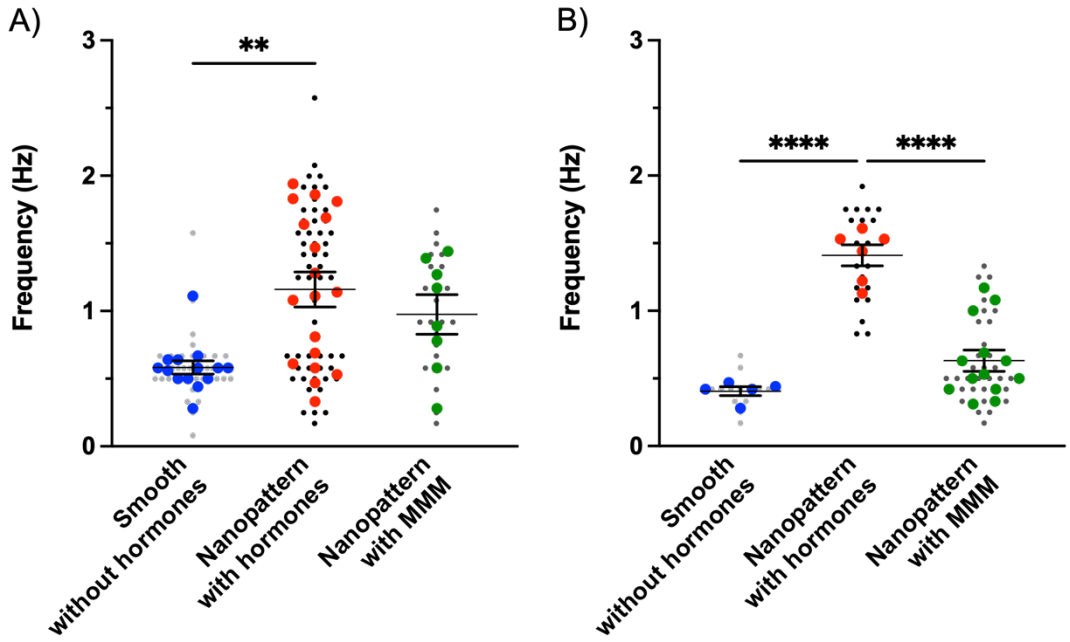

Figure 6.2: MMM protocol does not alter calcium transient frequency

Calcium transient frequency of hiPSC-CMs cultured in metabolic maturation medium (MMM) - shown in comparison to RPMI B27 control (smooth surface without hormone treatment) and maturation factors (nanopattern surface with hormones treatment, T3 & Dex) culture conditions. (A) RYR2 hiPSC-CMs at 37°C, (B) control 1 hiPSC-CMs at room temperature. The frequency was determined from 12s live calcium imaging recordings. Values are mean ±SEM, n=15-54 ROIs (grey/black), 5-18 dishes (blue/red/green), 2-5 independent differentiations. One-way ANOVA was performed followed by Tukey's multiple comparisons test. **p<0.01 ****p<0.0001

6.2.2 MMM protocol leads to a slower rate of calcium rise in hiPSC-CMs

Corresponding to culture under MF conditions, RYR2 hiPSC-CMs cultured in the MMM exhibited a significantly decelerated rate of intracellular calcium rise compared to culture under baseline conditions (Figure 6.3A). A significantly reduced rate of calcium rise was also observed in control 1 hiPSC-CMs when compared to baseline culture conditions (Figure 6.3B).

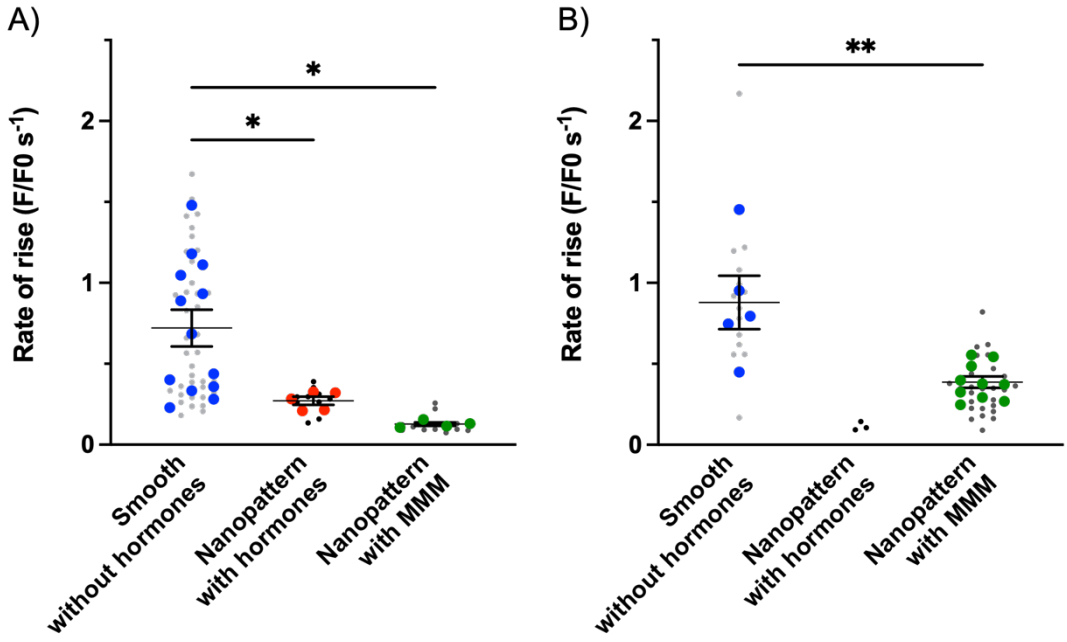

Figure 6.3: MMM protocol decelerates calcium rise in hiPSC-CMs

Rate of intracellular calcium rise measured from fluo-4 loaded hiPSC-CMs cultured in metabolic maturation medium (MMM) - shown in comparison to RPMI B27 control (smooth surface without hormone treatment) and maturation factors (nanopattern surface with hormones treatment, T3 & Dex) culture conditions. (A) RYR2 hiPSC-CMs at 37°C, (B) control 1 hiPSC-CMs at room temperature. Values are mean ±SEM, n=3-38 ROIs (grey/black), 4-13 dishes (blue/red/green), 2-5 independent differentiations. One-way ANOVA was performed followed by Tukey's multiple comparisons test or two-tailed, unpaired t-test. *p<0.05 **p<0.01

6.2.3 Reduced calcium transient amplitude in MMM protocol hiPSC-CMs

Also consistent with hiPSC-CMs cultured with MFs, both RYR2 and control hiPSC-CMs cultured with the MMM protocol displayed significantly reduced calcium transient amplitudes compared to under baseline culture conditions (Figure 6.4).

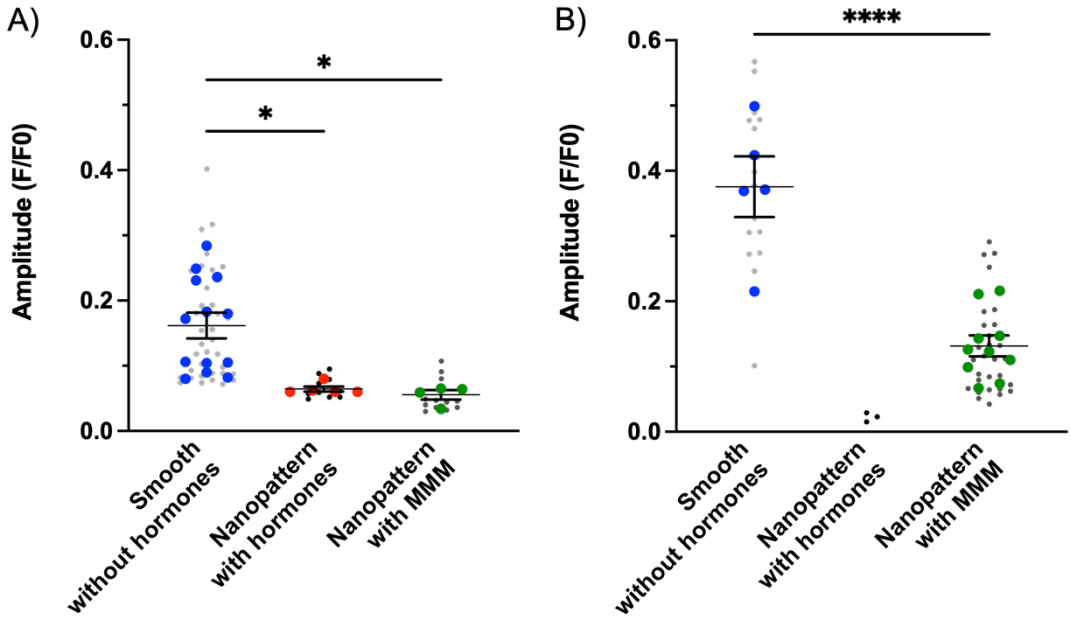

Figure 6.4: Reduced calcium transient amplitude in MMM protocol hiPSC-CMs

Calcium transient amplitude measured from fluo-4 loaded hiPSC-CMs cultured in metabolic maturation medium (MMM) - shown in comparison to RPMI B27 control (smooth surface without hormone treatment) and maturation factors (nanopattern surface with hormones treatment, T3 & Dex) culture conditions. (A) RYR2 hiPSC-CMs at 37°C, (B) control 1 hiPSC-CMs at room temperature. Values are mean ±SEM, n=3-38 ROIs (grey/black), 4-13 dishes (blue/red/green), 2-5 independent differentiations. One-way ANOVA was performed followed by Tukey's multiple comparisons test or two-tailed, unpaired t-test. *p<0.05 ****p<0.0001

6.2.4 MMM protocol has no effect on rate of intracellular calcium decay

In contrast with MF hiPSC-CMs, there was no change in the calcium transient rate of decay in either RYR2 or control 1 hiPSC-CMs cultured using the MMM protocol, when compared to baseline culture conditions (Figure 6.5).

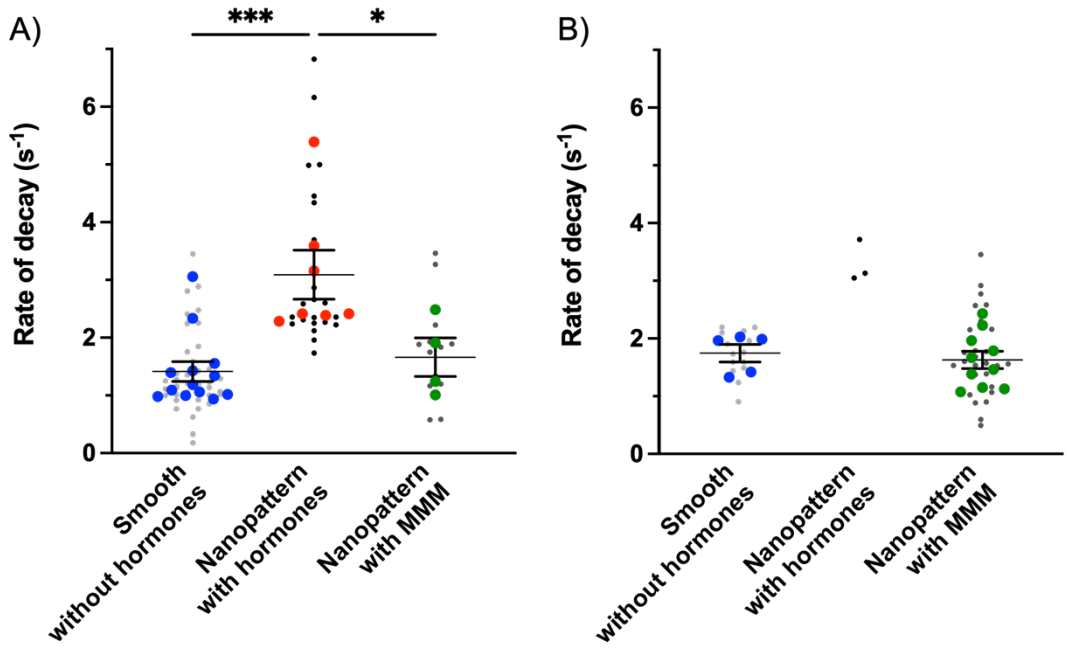

Figure 6.5: MMM protocol has no effect on rate of intracellular calcium decay

Rate of calcium decay measured from fluo-4 loaded hiPSC-CMs cultured in metabolic maturation medium (MMM) - shown in comparison to RPMI B27 control (smooth surface without hormone treatment) and maturation factors (nanopattern surface with hormones treatment, T3 & Dex) culture conditions. (A) RYR2 hiPSC-CMs at 37°C, (B) control 1 hiPSC-CMs at room temperature. Values are mean ±SEM, n=3-40 ROIs (grey/black), 4-13 dishes (blue/red/green), 2-5 independent differentiations. One-way ANOVA was performed followed by Tukey's multiple comparisons test or two-tailed, unpaired t-test. *p<0.05 ***p<0.001

6.2.5 Inhibition of SR function has no effect on hiPSC-CM calcium transient frequency

To assess SR function, hiPSC-CMs cultured using the MMM protocol were incubated with thapsigargin (SERCA2a pump inhibitor) and ryanodine (RYR2 channel inhibitor) sequentially. No change in calcium transient frequency was observed in either RYR2 or control 1 hiPSC-CMs following application of the inhibitors (Figure 6.6).

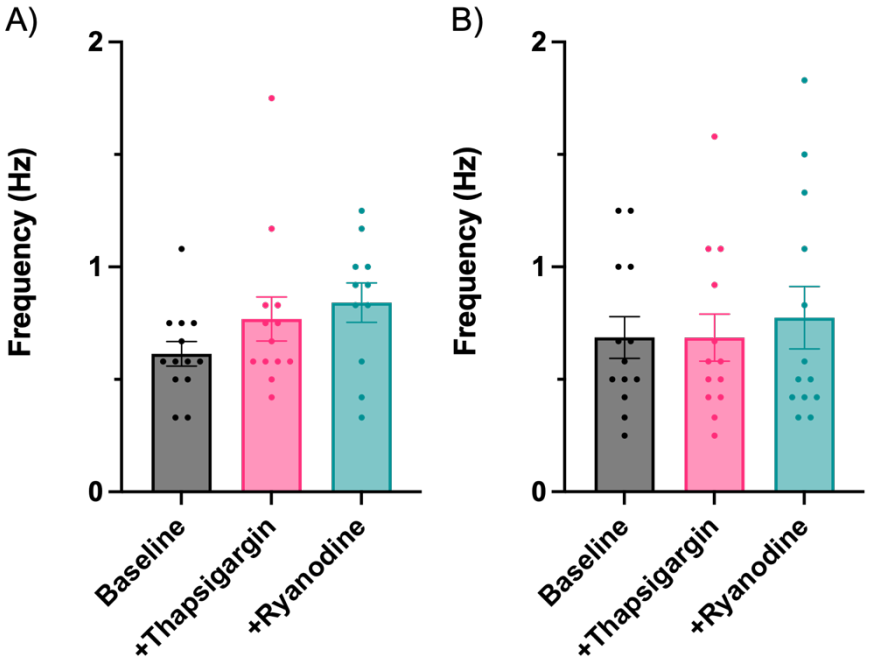

Figure 6.6: Inhibition of SR function has no effect on hiPSC-CM calcium transient frequency

Calcium transient frequency of hiPSC-CMs cultured in metabolic maturation medium (MMM) before (grey) and after SR blockade by sequential treatment with thapsigargin (10 μM, pink) and ryanodine (10 μM, turquoise). (A) RYR2 hiPSC-CMs, (B) control 1 hiPSC-CMs. All data collected at room temperature. Values are mean ±SEM, n=12-13 dishes, 5 independent differentiations. One-way ANOVA was performed followed by Tukey's multiple comparisons test.

6.2.6 SR block decelerates calcium transient rate of decay in MMM protocol hiPSC-CMs

The effects of thapsigargin and ryanodine treatment on calcium transient rate of decay were also evaluated. In RYR2 hiPSC-CMs, thapsigargin significantly reduced the rate of calcium decay. The addition of ryanodine had no effect (Figure 6.7A). This result contrasts the effect reported of RYR2 hiPSC-CMs cultured under MF conditions - no change was observed following SERCA2a or RYR2 channel blockade (refer to section 5.2.8). In control 1 hiPSC-CMs, there was a trend towards a slower rate of decay following incubation with thapsigargin. This further reduced after ryanodine treatment however neither reached statistical significance (Figure 6.7B). A similar trend was observed in control 1 hiPSC-CMs cultured under MF conditions (refer to section 5.2.8).

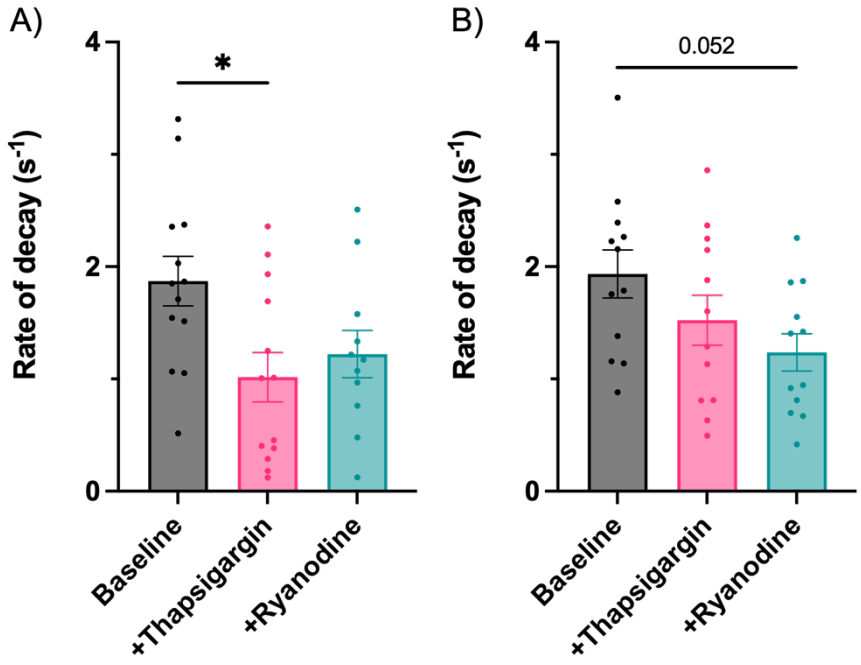

Figure 6.7: SR block decelerates calcium transient rate of decay in MMM protocol hiPSC-CMs

Calcium transient rate of decay measured from fluo-4 loaded hiPSC-CMs cultured in metabolic maturation medium (MMM) before (grey) and after SR blockade by sequential treatment with thapsigargin (10 μM, pink) and ryanodine (10 μM, turquoise). (A) RYR2 hiPSC-CMs, (B) control 1 hiPSC-CMs. All data collected at room temperature. Values are mean ±SEM, n=12-13 dishes, 5 independent differentiations. One-way ANOVA was performed followed by Tukey's multiple comparisons test. *p<0.05

6.2.7 Protein expression in hiPSC-CMs cultured using the MMM protocol

The expression of key calcium handling proteins was assessed in hiPSC-CMs cultured using the MMM protocol and compared to the respective expression levels of hiPSC-CMs cultured under baseline culture conditions and with MFs. It should be noted that the baseline and MF data are taken from Chapter 5 and were not analysed on the same western blot membranes as the MMM protocol samples.

In RYR2 hiPSC-CMs cultured using the MMM protocol, the expression of SERCA2a (Figure 6.8A) and total PLN (Figure 6.8B) was observed to be significantly lower than in both baseline and MF hiPSC-CMs. Conversely, the expression levels of phosPLN (Figure 6.8C), NCX (Figure 6.8D) and ADRβ1 (Figure 6.8E) were significantly upregulated in RYR2 hiPSC-CMs compared to baseline and MF culture conditions. Few conclusions can be drawn

from the control 1 hiPSC-CM expression data due to a low number of biological replicates. See Appendix for representative full western blot images.

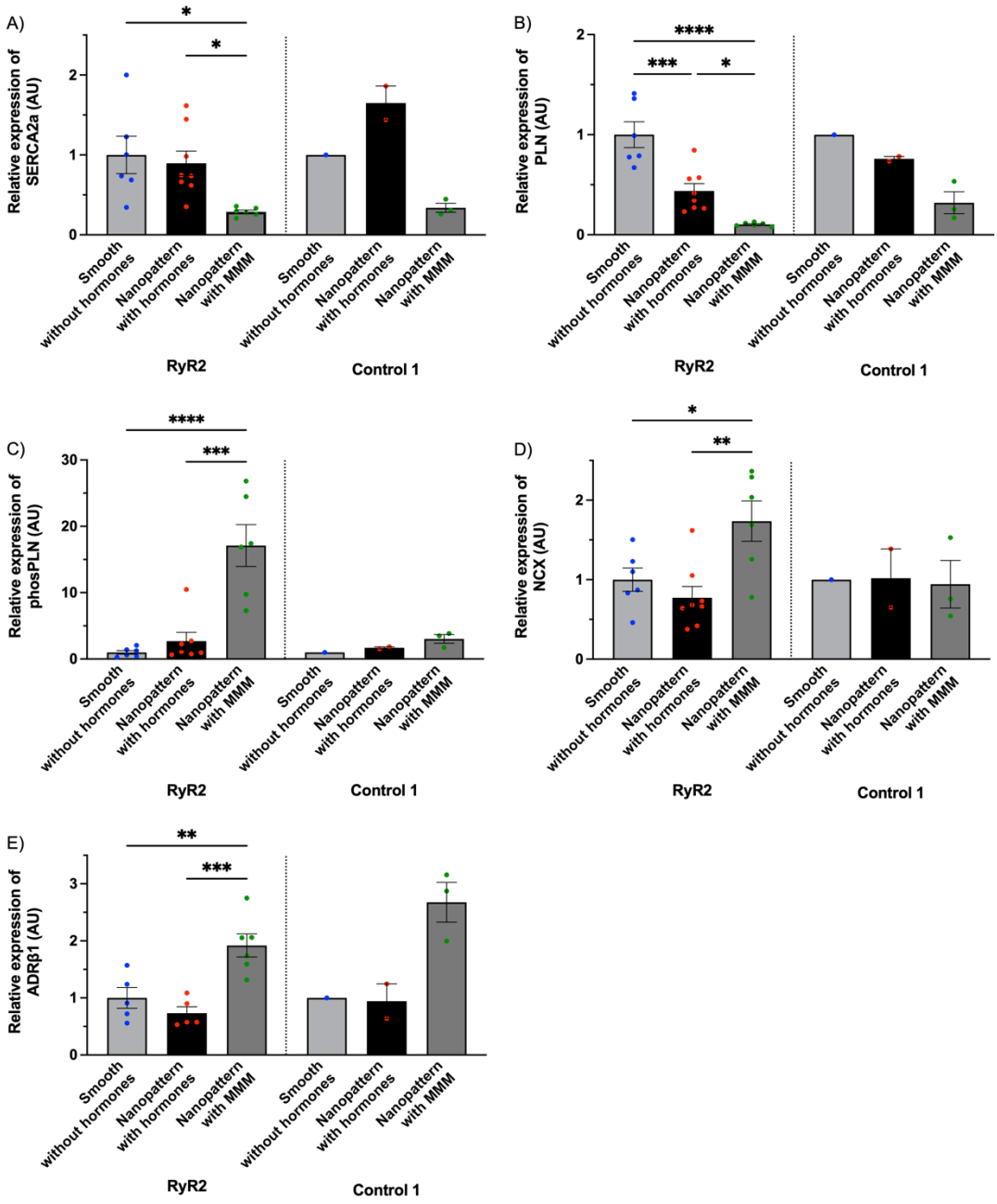

Figure 6.8: Protein expression in hiPSC-CMs cultured using the MMM protocol

Quantification of the expression of key proteins involved in cardiac calcium handling performed on RYR2 and control 1 hiPSC-CMs cultured in metabolic maturation medium (MMM) - shown in comparison to RPMI B27 control (smooth surface without hormone treatment) and maturation factors (nanopattern surface with hormones treatment, T3 & Dex) culture conditions. It is important to note that the MMM protocol samples were not analysed on the same western blot membranes as the control and maturation factor samples taken from Chapter 5. (A) SERCA2a, (B) PLN, (C) phosPLN, (D) NCX, (E) ADRβ1. Expression is shown relative to smooth surface without hormones in arbitrary units (AU). Values are mean ±SEM, n=1-8 biological samples performed in duplicate. One-way ANOVA was performed followed by Tukey's multiple comparisons test. *p<0.05 **p<0.01 ***p<0.001 ****p<0.0001

6.3 Discussion

The current most widely utilised hiPSC-CM culture/maintenance medium (RPMI B27) does not represent the physiological environment - in terms of both the formulation components and their respective concentrations. As a result, the metabolic maturation of native cardiomyocytes (ie. switch from glycolytic metabolism to oxidative phosphorylation) is not replicated in hiPSC-CMs. Furthermore, the maturation of electromechanical coupling and physiology are also limited[214]. By designing and implementing a medium that supports fatty acid oxidation, thus has a greater metabolic relevance, Feyen *et al*.[214] (Mercola group) observed metabolic and calcium handling maturation in hiPSC-CMs. Moreover, they reported reproducible and robust modelling of two genetic cardiac disorders.

In this chapter the effect of the MMM on RYR2 hiPSC-CMs calcium handling maturation has been described. Following differentiation and reseeding of purified hiPSC-CMs cultures on nanopatterned culture dishes, the culture medium was transitioned from the high glucose RPMI B27 to the oxidative substrate containing MMM. The differentiation timeline and hiPSC-CM maintenance closely resembled the protocol outlined by the Mercola group. The most notable difference was the use of culture dishes with a nanopatterned surface in this study. Calcium transient characteristics were analysed at baseline and following pharmacological studies to evaluate calcium handling competency. Protein expression studies were performed to gain an insight into the underlying molecular basis for the changes. In many ways the findings of this study were very similar to those observed in the previous chapter assessing the effects of hormone supplementation and a nanopatterned culture surface.

The main findings were:

- Decelerated rate of rise and lower amplitude of calcium transients
- Downregulated SERCA2a and PLN expression
- Upregulated phosPLN, NCX and ADRβ1 expression
- Improved SERCA2a pump efficiency

6.3.1 Calcium transient frequency

Calcium transient frequency was not reported to increase in MMM protocol hiPSC-CMs compared to baseline culture conditions. Although interestingly, when compared to MF hiPSC-CMs the frequency was significantly lower in the control cell line only, and not the RYR2 cell line. This observation could suggest that the MMM is having an effect that gives rise to phenotype manifestations of the RYR2 mutation in the patient-derived cell line; in this case calcium leak from the SR through the RYR2 channels. As it is assumed the immature cells have a depolarised resting membrane potential, the calcium leak (due to increase RYR2 channel open probability during diastole) would contribute to further depolarisation of the membrane potential and trigger premature action potentials, thus resulting in a greater calcium transient frequency.

The Mercola group reported a non-significant lower spontaneous beating frequency in their MMM hiPSC-CMs compared to RPMI B27 hiPSC-CMs, and used a pace rate of 1Hz for experiments[214]. Although there was no change in calcium transient frequency reported between MMM and control (RPMI B27) culture conditions in this study, the spontaneous activity likely indicates the continued presence of the depolarising I_f current and a minimal I_{K1} current - responsible for pacemaker activity and the resting membrane potential respectively.

6.3.2 Rate of intracellular calcium rise

Similar to the observed effects of MF culture conditions, the MMM protocol also caused a significantly slower rate of calcium rise compared to baseline culture conditions. The Mercola group reported a non-significant faster calcium rise time. These contrasting findings could be explained by a difference in cell size caused by the surface topography. Although no morphology metrics were performed on MMM protocol hiPSC-CMs, it was previously shown that a nanopatterned culture surface significantly increased RYR2 hiPSC-CM length (section 5.2.2). Assuming a T-tubular network did not develop (due to suboptimal physiological load as discussed in section 5.3.1) the MMM protocol hiPSC-CMs in this study are likely to have a smaller surface to volume ratio hence calcium entry would only occur at the cell periphery. As a result non-uniform calcium release would occur due to a delayed calcium rise at the cell centre. Furthermore the distribution of calcium would be greater, reducing the effectiveness of calcium-dependent inactivation

of LTCCs thus prolonging the overall rise time. T-tubules also promote dyad formation. Without T-tubules the spatial proximity of calcium release unit components is expected to be decreased reducing the efficiency of CICR. However, RYR2 hiPSC-CMs cultured on the nanopatterned surface without hormone treatment exhibited no change in the rate of calcium rise when compared to baseline culture conditions. This finding indicates an influential role of hormone treatment and the MMM.

6.3.3 Calcium transient amplitude

The significantly lower calcium transient amplitude of MMM protocol hiPSC-CMs, compared to baseline culture conditions, corresponded to the effect of the MF protocol. This finding was consistent with the Mercola group. They attributed the lower amplitude to a greater capability of the SR to regulate fluxes in calcium[214]. The upregulation of *KCNJ2*, and the consequent I_{K1} density comparable with adult human ventricular myocytes will also have assisted in reaching and maintaining a more negative resting membrane potential. This deduction cannot be confirmed by the data presented in this study. SR calcium release would need to be assessed following the application of caffeine. Thus the hypotheses provided in the previous chapter: a decreased surface to volume ratio (hence effectiveness of CICR); altered LTCC gating kinetics; increased myofilament calcium buffering capacity and modified mitochondrial calcium release could also be possible. Additionally, the observed lower expression levels of SERCA2a will contribute to a raised resting membrane potential due to reduced SR calcium reuptake which would in turn lead to increased calcium-dependent inactivation of LTCCs.

6.3.4 Calcium transient rate of decay

In contrast to MF hiPSC-CMs, the rate of decay of MMM protocol hiPSC-CMs did not change relative to baseline culture conditions. The Mercola group reported a significantly lower tau/faster relaxation rate consistent with significantly increased SERCA2a expression, and higher levels of phosPLN upon β-AR stimulation[214]. Despite significantly higher expression of phosPLN, NCX and ADRβ1 (and reduced total PLN) in the MMM protocol RYR2 hiPSC-CMs in this study (relative to baseline culture conditions), SERCA2a expression was significantly lower. As the SERCA2a pump is responsible for the majority of cytosolic calcium removal, with reduced expression a

decreased/slower diastolic calcium removal would be expected. The increased reliance on the upregulated NCX to remove calcium would also promote premature depolarisations due to sodium influx. This latter postulation corresponds with the small, non-significant rise in calcium transient frequency observed following SR block, particularly of the RYR2 hiPSC-CMs in which calcium leak will also play a role. An increased affinity for calcium of the myofilaments would further influence a slower rate of calcium decay.

Although the observations suggest limited SR/calcium handling maturity in MMM hiPSC-CMs at baseline, inhibition of SR function caused a significantly reduced rate of decay not seen in hiPSC-CMs cultured under baseline conditions of either line, or RYR2 hiPSC-CMs with MFs (independently or combined, section 5.2.8). This indicates that there is improved contribution/efficiency of the SERCA2a pump in MMM protocol hiPSC-CMs.

6.4 Study limitations and further work

In this study hiPSC-CMs were assessed in the MMM whilst cultured on a nanopatterned surface. A major limitation is that the protein expression data presented in this chapter is not derived from direct comparison of samples. The protein samples from MMM protocol hiPSC-CMs were not run and analysed on the same western blot membranes as the samples from baseline and MF hiPSC-CMs.

As demonstrated in Chapter 4, the nanopatterned culture surface influences hiPSC-CM maturity albeit mainly regarding morphology and structural organisation. It would have been beneficial to also evaluate the effects of the MMM on a smooth culture surface, and/or compared the data to the data from the hiPSC-CMs cultured on the nanopatterned surface without hormone supplementation (shown in Chapter 5) so the independent effects of MMM could be identified and compared to the additive/synergistic effects of the combined factors. It would have also been interesting to explore the effects of the MMM and nanopatterned culture surface in combination with hormone treatment.

The MMM was primarily developed to promote metabolic maturation. Yet here only calcium handling properties were analysed to evaluate the maturation effects of the MMM protocol. Additional studies investigating the glycolytic capacity and mitochondrial characteristics would have provided a more in-depth insight into the potential influences of MMM on hiPSC-CM maturation. Furthermore supplementary experiments are required to substantiate or explain the underlying molecular basis for the data presented. For example patch clamp and gene expression studies could be performed to confirm that the MMM protocol hiPSC-CMs harbour a depolarised resting membrane potential and low I_{K1} density leading to spontaneous beating; line scan calcium imaging could verify non-uniform calcium release; immunostaining would allow for evaluation of myofilament density and assessment of T-tubule development; and an isoprenaline dose-response curve could be generated to support the upregulation of ADRβ1 expression to demonstrate maturation of the signalling pathway and response of its' targets.

6.5 Conclusion

This chapter has illustrated that a culture medium with a formulation more relevant to native metabolic substrates can promote some functional maturation of hiPSC-CMs. The main finding was that hiPSC-CMs cultured in the MMM demonstrate improved SERCA2a pump efficiency. Consistent with the previous chapter, investigating the maturation effects of a nanopatterned surface alongside hormone supplementation, it is postulated that to dramatically improve hiPSC-CM calcium handling the development of a T-tubular network is required.

Chapter 7

General discussion

7 General discussion

The overall aim of this PhD study was to develop an established hiPSC cardiac differentiation protocol in order to generate hiPSC-CMs with improved maturity; thus providing an experimental model more phenotypically representative of native adult cardiomyocytes. The effects of four previously reported MFs were studied - predominantly in terms of cardiac calcium handling function. The main focus of this study was an hiPSC cell line generated from a patient harbouring a pathogenic *RYR2* nonsense variant, *RYR2*$^{(wt/R4790*)}$. Mutations in *RYR2* typically cause CPVT, a condition associated with adrenergically mediated arrhythmias. Two control hiPSC lines (derived from healthy volunteers) were also utilised. The results presented demonstrated limited maturity of calcium handling despite morphological and structural improvements.

Generated by dedifferentiating adult somatic cells, hiPSCs are capable of being re-differentiated into specialised cell types. Together with their ability to be cultured *in vitro* and propagated indefinitely, there is the opportunity for an unlimited supply of human cardiomyocytes. As hiPSCs retain the genetic background of the donor, they provide an unprecedented model for investigating human cardiac diseases, drug screening and personalised (or precision) medicine. However current established protocols generate hiPSC-CMs with foetal-like characteristics. The immature phenotype means the complex physiology underlying adult heart function does not fully develop, hence presents critical limitations to modelling diseases such as CPVT. With the race on to identify factors that will assist hiPSC-CM maturation, replicating the native environment and maturation signals as closely as possible seems the most logical plan. However the lack of understanding of native cardiomyocyte maturation has been exposed, hindering progress.

Following optimisation of the initial differentiation protocol, four factors with the potential to advance hiPSC-CM maturation were evaluated: 1) a prolonged culture period; 2) culture medium supplementation with thyroid and glucocorticoid hormones; 3) a nanopatterned culture surface topography; 4) and a metabolic maturation medium. Molecular studies showed that a prolonged culture period and hormone treatment of hiPSC-CMs significantly increased the abundance of ADRβ1 – a compelling result with

regards to modelling CPVT. Significant hiPSC-CM elongation and sarcomeric organisation were primarily attributed to the nanopatterned culture surface, although facilitation by hormone supplementation was observed. Calcium imaging demonstrated that the MMM enhanced SR SERCA2a pump activity and efficiency.

7.1 The optimal cardiac differentiation kinetics for RYR2 hiPSCs

Although a detailed characterisation of the RYR2 hiPSC cell line had been previously conducted[300], hiPSCs can spontaneously differentiate during the expansion process. Monitoring for signs of spontaneous differentiation in hiPSC cultures is important as it can impact their quality and directed differentiation, and cells cannot be re-differentiated into another cell type without reprogramming. Therefore it was best practice to ensure pluripotency had been retained in cryopreserved hiPSC cultures subsequent to thawing.

In addition to hiPSC culture quality, the differentiation kinetics can severely impact the success of cardiac differentiation. For efficient differentiation it is necessary to optimise variable factors for each cell line. The development of CDM3, a fully defined culture medium formulated with only the essential components for cardiac differentiation, was expected to improve reproducibility and elucidate the requirements of hiPSC-CMs - in comparison to RPMI B27 (-insulin) culture medium, which was originally designed for culture of hippocampal neurons and is incompletely defined[179]. Parallel RYR2 hiPSC differentiation revealed that cardiomyocyte generation was much more efficient in RPMI B27 (-insulin) than CDM3 culture medium. This finding was in contrast with that of the developers of CDM3 who reported the medium to produce cardiomyocytes at equivalent yields and efficiencies to RPMI B27 (-insulin)[179]. However the result appeared in line with the literature as the vast majority of published cardiac differentiation protocols utilise RPMI B27 (-insulin) culture medium during the initial phases[199,202,210,214,266,319]. It is unclear why RPMI B27 (-insulin) medium is superior but its' more complex nature, inclusive of inessential factors for cardiac differentiation, implies no one single component is responsible.

The optimal concentration of the GSK3β inhibitor CHIR99021, used to induce differentiation to mesoderm derivatives in RYR2 hiPSC cultures, was identified as 6-8

μM. It was beneficial to investigate the small molecule as the most favourable dose is dependent on the pluripotency and cell-cycle profile (affected by density and endogenous signalling) of cultures, thus varies from cell line to cell line[177,322].

7.2 Prolonged culture periods for hiPSC-CMs

Current literature indicates that a prolonged culture period promotes enhanced cardiomyocyte structure and function[210,220,263,265]. These findings are consistent with the notion that the complex physiology of native adult cardiomyocytes takes up to 10 years to fully develop[184]. In this study, cardiac-specific gene expression data from RYR2 hiPSC-CMs cultured for 30 days was compared to those cultured for 45 days. Only one significant change was observed with prolonged culture alone: increased *ADRβ1* expression. The lack of differential expression between the two time points was unexpected, despite a difference of only 15 days. It is consistent however with a previous study that compared gene expression at similar culture time points[220]. Studies that have assessed hiPSC-CM culture length and observed maturation have compared time points with greater increments over a period of up to one year[210,263,265]. The spontaneous beat rate of the hiPSC-CMs was the variable that limited the current study most – by 90 days of culture this is shown to significantly reduce[210,265]. Using current established protocols, it is suggested that a culture period of up to three months is required for meaningful maturation of hiPSC-CM structure and function based on the published literature[263,265]. However, these time frames for yielding hiPSC-CMs with improved maturity are unrealistic and not financially viable for their desired purposes, thus evoke questions regarding the potential for implementation of hiPSC-CMs as a biological tool.

7.3 Hormone-treatment of hiPSC-CM culture media

Biochemical cues in the form of culture medium thyroid (T3) and glucocorticoid (Dex) hormone supplementation have been reported to enhance hiPSC-CM maturation[199,202,270]. Both are essential during cardiac development[268,273,274]. The effect of hormone supplementation on RYR2 hiPSC-CM gene expression and calcium handling was assessed.

The only gene to be significantly upregulated with hormone treatment alone was *ADRβ1*. This result is consistent with the reported transcriptional effects, and changes to cardiac performance of thyroid hormone[268]. Interestingly, *PAK1* was significantly downregulated. The PAK1 protein is involved in a signalling pathway which maintains ventricular calcium homeostasis and electrophysiological stability by counteracting the positive regulatory effects of β-AR stimulation, and hence plays a protective role against arrhythmic activity[363]. *CASQ2*, *BIN1* and *SCN1A* were also significantly downregulated with hormone treatment. Reduced *CASQ2* expression may promote the CPVT phenotype of RYR2 hiPSC-CMs through a reduced capacity to buffer calcium ions. *BIN1* has been implicated in T-tubular biogenesis. Downregulation of its' expression is consistent with a lack of T-tubule development in this study. T-tubule formation has been previously reported in 2D cultures following hormone supplemented culture but only when used in combination with physiological ECM substrate stiffness provided by the Matrigel mattress[199]. A trend of decreased expression was observed for sodium channel subunits more commonly associated with the nervous system. This could be signifying the onset of a switch in dominance to the cardiac isoform, *SCN5A,* for which they might have been compensating.

Hormone supplementation of the culture medium caused significant changes to the calcium handling properties of RYR2 hiPSC-CMs. Few changes were seen in the control lines however. In hormone-treated RYR2 hiPSC-CMs PLN displayed significantly reduced expression levels. The decrease in PLN, with no change in SERCA2a and increased proportion of phosPLN, would allow for increased SERCA2a activity consistent with the observed faster rate of decay. Inhibition of SERCA2a activity would be expected to confirm the observation yet no change was reported. In RYR2 hiPSC-CMs calcium leak from the SR via mutant RYR2 channels could be masking enhanced SERCA2a activity and explain the findings. Applying ryanodine prior to thapsigargin would confirm the hypothesis. Contrary to expectations, the rate of rise and amplitude of calcium transients were decreased. The absence of T-tubules in cells of greater size is thought to be responsible. Alternatively, changes in the LTCC current characteristics such as slowed channel opening might explain the immature calcium transient properties.

Surprisingly few signs of maturity were observed considering the roles the hormones play in native cardiac development. During development there are stage-specific concentration increases of each hormone. Thyroid hormone levels increase within a few hours of birth[267] whereas glucocorticoid hormones are important during late gestation[272]. It is also recognised that both thyroid and glucocorticoid hormone levels fluctuate over time – they demonstrate circadian rhythms[421,422]. In this study, they were added simultaneously to the hiPSC-CMs. The interactive effects (glucocorticoids such as Dex are known to significantly decrease levels of thyroid stimulating hormone[423]) and/or timing of supplementation may be in part responsible for the lack of differential gene expression that would enhance the calcium transient profile. It is therefore possible the hormone combination has counterproductive as well as additive or synergistic effects. Furthermore, excess supplementation may cause receptor desensitisation or induce pathophysiological effects. In view of this, it would be interesting to consider the time course and doses of hormone supplementation to hiPSC-CM culture medium.

7.4 Nanopatterned culture surface for hiPSC-CMs

A patterned culture surface provides spatial cues that promote maturation of cardiomyocyte morphology and intracellular structure[191,397]. Published reports utilising a patterned topography during hiPSC-CMs culture have often been of microscale dimensions[283,424,425]. Yet dimensions in the upper nanometre range have been shown to be optimal for hiPSC-CM culture[286], and is consistent with the knowledge that cardiomyocytes are influenced by ECM fibres with nanoscale features[285]. In this study, cultures dishes with a nanopatterned surface were implemented. The effects on RYR2 hiPSC-CM morphology, structural organisation, and functional calcium handling properties were evaluated.

Images from immunostained RYR2 hiPSC-CM monolayers on the nanopatterned surface illustrated organisation and alignment of cells in a single orientation. Qualitative judgement of nanopattern-induced cardiomyocyte elongation was confirmed by measurement of morphology parameters. It is considered that the elongation resulting in rod-shaped cells promoted the observed sarcomeric organisation[191,192]. These observations are consistent with previous reports utilising patterned surfaces for hiPSC-

CM culture[286,425]. It was hypothesised that this maturation of cardiomyocyte structure, albeit still lacking a T-tubular network, would improve calcium handling properties.

Independently the nanopatterned culture surface had no effect on calcium handling properties of RYR2 hiPSC-CMs although it was responsible for significant changes in the control cell lines. Both rate of rise and amplitude significantly decreased. Morphology parameters of control hiPSC-CMs were not analysed but it is postulated that the nanopatterned surface led to a greater cell size and hence further reduced the spatial proximity of LTCCs to RYR2 channels and therefore the temporal effect of calcium influx. Furthermore, the induced maturation of the sarcomeres could have augmented sarcomere density and consequently the calcium buffering capacity of myofilaments. Lastly, any changes to LTCC activation and/or inactivation properties might have altered the calcium current.

7.5 Combined effects of maturation factors

The concurrent implementation of two MFs: prolonged culture with hormone supplementation, and hormone supplementation with a nanopatterned culture surface also had interactive (additive, synergistic or antagonistic) effects. 1) Prolonged culture and hormone supplementation had antagonistic effects on *CASQ2* expression: prolonged culture in the absence of hormones increased *CASQ2* expression ($p=0.070$), yet in the presence of hormones expression was significantly reduced at 45 days. 2) Prolonged culture potentiated the positive regulation of hormone treatment on *ADRβ1* expression. This finding was translated to the protein level. 3) Regarding morphology and structure, hormone supplementation enhanced the aspect ratio and sarcomeric organisation (inferred from qualitative assessment) effects of the nanopatterned surface. 4) There was a concentration-dependent lusitropic effect of β-AR stimulation in hiPSC-CMs cultured in the presence of hormones and on a nanopatterned surface not seen in hiPSC-CMs cultured under baseline conditions or with only one MF. Overall introducing multiple MFs into the differentiation protocol had beneficial outcomes. However due to their interactive effects and specific temporal roles in development establishing the optimal conditions is important for achieving hiPSC-CM maturation.

7.6 Transition to a metabolic maturation medium

Transitioning from a glucose-rich culture medium to one designed for mature metabolism has previously been demonstrated to enhance hiPSC-CM calcium handling in addition to mitochondrial maturation[214]. In this study, calcium transient properties of hiPSC-CMs cultured with the MMM (on a nanopatterned surface) were compared to those cultured in RPMI B27 under baseline conditions (smooth culture surface without hormones) and with MFs (nanopattern culture surface with hormones).

In comparison with the calcium transients from baseline culture conditions, MMM hiPSC-CMs displayed similar trends to those of MF hiPSC-CMs for both RYR2 and control 1 lines: the rate of rise was significantly decelerated, and the amplitude was significantly smaller. Although immunostaining and morphology parameters were not assessed it is assumed cell size was greater (induced by the nanopatterned surface) than under baseline culture conditions hence the slower rate of rise and smaller amplitude can be explained by the same reasons discussed for MF hiPSC-CMs. The rate of decay of MMM hiPSC-CMs however did not increase as under MF conditions and was much more similar to baseline culture conditions. Despite a slower rate of calcium extrusion and reduced SERCA2a expression (compared to MF RYR2 hiPSC-CMs), inhibition of SERCA2a and RYR2 channels demonstrated an SR contribution to the calcium transient previously not seen in RYR2 hiPSC-CMs cultured under baseline or MF conditions. This finding indicated SR maturation. The slower decay is inconsistent with the previous report from Feyen *et al*.[214] on which the MMM was based, despite comparable differentiation and culture maintenance protocols – this can be attributed to the contrasting effects of the MMM on SERCA2a and PLN expression between the two studies. The effects of the nanopatterned culture surface used in this study may also play a role. The improved contribution of the SR was consistent however.

7.7 Differential responses of cell lines

Hormone supplementation of the culture medium caused significant changes to the calcium handling properties of RYR2 hiPSC-CMs. Few changes were seen in the control lines. On the other hand, the nanopatterned culture surface had no effect on calcium handling properties of RYR2 hiPSC-CMs yet was responsible for significant changes in the control cell lines. This observation indicates line specific responses to MFs and could

be explained by differential expression of key proteins between cell lines, particularly in those affected by disease causing variants. In contrast, MMM protocol RYR2 and control 1 hiPSC-CMs demonstrated similar trends in calcium transient characteristics when compared to respective baseline and MF hiPSC-CMs. This suggests the calcium handling maturation effects of the MMM are relevant for control and patient-derived cell lines.

7.8 Study limitations

Experiments performed in this study were performed on hiPSC-CM cultures generated from single clones of the cell lines. It would have been beneficial to perform all experiments on multiple clones to confirm and validate the findings reported, as hiPSCs can experience genetic instability when cultured and expanded *in vitro* for long periods of time. To minimise this risk cultures underwent no more than 10 passages.

The control lines used were commercially available and unrelated to the patient-derived cell line. In order to be confident the nonsense variant in the RYR2 hiPSC-CMs was responsible for the contrasting phenotypes observed (compared to control hiPSC-CMs) an isogenic control line is required. An isogenic control line provides enhanced certainty the variant of interest is accountable for the observed phenotype, as the genetic background of the line is identical aside from the variant being studied. This limitation is highlighted in this study by the different rates of spontaneous beating identified between cell lines. Consequently different experimental designs were used - RYR2 hiPSC-CMs were studied at 37°C whilst control line hiPSC-CMs were studied at room temperature; hence the calcium transient properties of the different cell lines could not be directly compared.

Current established cardiac differentiation protocols, including the small molecule based protocol used in this study, generate heterogenous populations of cardiomyocyte subtypes (atrial, nodal and ventricular). The differing physiology and contribution of each subtype might obscure the overall phenotypes reported. The development of subtype specific differentiation protocols is crucial for derivation of homogenous subtype populations for disease modelling and drug screening. In recent years such protocols have been successfully designed[325,426]. The absence of electrical activity

investigations in this study is a further limitation. Consideration and analysis of action potential shape/characteristics could have allowed for subtype categorisation, as well as indicating any electrical maturation of the hiPSC-CMs. Detection and imaging of the action potential can be performed by voltage-sensitive fluorescent indicators such as Fluovolt.

7.9 Further work

In the present study hiPSC-CMs were cultured for a maximum of 45 days and promising foetal to adult isoform transitions appeared to be initiating. Based on data from previous studies, further prolonging the culture period would have enhanced maturation. It would be interesting to establish if culture for an extended period results in a greater number of significant changes that reflect a gene expression profile more representative of native adult cardiomyocytes. Additionally, a more comprehensive study of cardiac gene expression would be desirable. This could be performed by RNA sequencing technologies.

Hormone supplementation of the culture medium had effects on both gene expression and calcium handling of RYR2 hiPSC-CMs. However the temporal dynamics and concentration of hormone supplementation were not investigated. Further studies to determine the most appropriate conditions to achieve optimal hiPSC-CM maturation are required.

The nanopatterned culture surface promoted substantial maturation of hiPSC-CM morphology and intracellular structure. Further analysis of morphology (e.g. circularity index, volume, myofilament density), and assessment of the spatial organisation of key calcium handling proteins by additional fluorescent imaging studies would have strengthened this finding. Crucially the development of T-tubular structures was not formally investigated. Reports indicate a physiological substrate stiffness/elastic modulus is required[199]. Introducing a culture surface that more closely resembles and mimics the physical interactions of the native environment, by combining the optimal pattern and substrate stiffness, could be critical to obtaining hiPSC-CMs with a functional T-tubular network and intracellular organisation.

Maturation of SR function, specifically SERCA2a activity, was attributed to the MMM. It would be interesting to understand if this functional maturation was independent of the nanopatterned culture surface or an additive/synergistic effect. Supplementing the MMM with hormones may have promoted further beneficial maturation of hiPSC-CM function through their influence on gene transcription. No experiments were performed to assess changes in energy substrate metabolism, or mitochondrial morphology and physiology. As the MMM was designed to support mature cardiomyocyte energetics it would be important to demonstrate maturation of these phenotype characteristics.

Abnormalities in calcium handling can cause changes to the currents underlying the action potential shape (and lead to arrhythmic activity such as in CPVT), and also the contractility of the heart. Conducting studies to investigate the effect of the induced changes to structure and calcium handling on the action potential and contractility of the hiPSC-CMs would provide further insight into the maturation capacity of the factors, and the recapitulation of the CPVT disease phenotype. Action potentials could be visualised through loading hiPSC-CMs with Fluovolt, a fluorescent membrane potential indicator. Contractility could be assessed through changes in cell or sarcomere length (fractional shortening), or alternatively by measurement of force production using traction force microscopy.

In order to assess the calcium transients, hiPSC-CMs were loaded with the fluorescent calcium indicator, fluo-4. Such indicators are thought to be toxic to cells due to their mode of action – inhibition of organic anion transporters. Consequently the viability of cells is affected and their potential influence on the variable being measured should be considered. The use of biological indicator technology could resolve this issue and allow for extended collection of paired serial measurement data sets. It should be noted however that integration of biological indicators often involves transduction of viral vectors, thus variable adverse effects may be detected.

7.10 Conclusion

The optimised cardiac differentiation protocol for RYR2 hiPSCs improved the efficiency, and reduced the variability, of cardiomyocyte generation. The RYR2 hiPSC-CMs exhibited significantly increased ADRβ1 expression with prolonged culture and hormone treatment of the culture medium – this was a compelling finding with respect to modelling CPVT. The cells displayed significant elongation following culture on a nanopatterned surface. This resulted in rod-shaped cells characteristic of cardiomyocytes, and organisation of the sarcomeres. Both observations were enhanced by hormone supplementation. Functional analysis of hiPSC-CMs by calcium imaging demonstrated cell line specific responses to MFs. Enhanced contribution of the SR to the calcium transient was attributed to the MMM. For further development of calcium handling the generation of a T-tubular network is required and the implementation of a substrate with physiological stiffness is indicated. As a disease model, hiPSC-CMs require further development to fully recapitulate cardiac channelopathies such as CPVT and become an established model for drug screening. It would be interesting to incorporate each of the MFs assessed here with the addition of a more physiologically relevant substrate stiffness into a single protocol (under optimal conditions) and assess the hiPSC-CM phenotype produced.

References

1. Zipes D, Wellens H. Sudden Cardiac Death. *Circulation*. 1998;98:2334–2351.
2. Hayashi M, Shimizu W, Albert CM. The spectrum of epidemiology underlying sudden cardiac death. *Circ Res*. 2015;116:1887–1906.
3. Fishman GI, Chugh SS, Dimarco JP, Albert CM, Anderson ME, Bonow RO, Buxton AE, Chen PS, Estes M, Jouven X, Kwong R, Lathrop DA, Mascette AM, Nerbonne JM, O'Rourke B, Page RL, Roden DM, Rosenbaum DS, Sotoodehnia N, Trayanova NA, Zheng ZJ. Sudden cardiac death prediction and prevention: Report from a national heart, lung, and blood institute and heart rhythm society workshop. *Circulation*. 2010;122:2335–2348.
4. Garcia-Elias A, Benito B. Ion channel disorders and sudden cardiac death. *Int J Mol Sci*. 2018;19:1–30.
5. Mellor G, Raju H, De Noronha S V., Papadakis M, Sharma S, Behr ER, Sheppard MN. Clinical characteristics and circumstances of death in the sudden arrhythmic death syndrome. *Circ Arrhythmia Electrophysiol*. 2014;7:1078–1083.
6. Van Der Werf C, Van Langen IM, Wilde AAM. Sudden death in the young: What do we know about it and how to prevent? *Circ Arrhythmia Electrophysiol*. 2010;3:96–104.
7. van Weerd JH, Christoffels VM. The formation and function of the cardiac conduction system. *Dev*. 2016;143:197–210.
8. Grant AO. Cardiac ion channels. *Circ Arrhythmia Electrophysiol.* 2009;2:185–194.
9. Skinner JR, Winbo A, Abrams D, Vohra J, Wilde AA. Channelopathies That Lead to Sudden Cardiac Death: Clinical and Genetic Aspects. *Heart Lung Circ*. 2019;28:22–30.
10. Han D, Tan H, Sun C, Li G. Dysfunctional Nav1.5 channels due to SCN5A mutations. *Exp Biol Med*. 2018;243:852–863.
11. Chiamvimonvat N, Chen-Izu Y, Clancy CE, Deschenes I, Dobrev D, Heijman J, Izu L, Qu Z, Ripplinger CM, Vandenberg JI, Weiss JN, Koren G, Banyasz T, Grandi E, Sanguinetti MC, Bers DM, Nerbonne JM. Potassium currents in the heart: functional roles in repolarization, arrhythmia and therapeutics. *J Physiol*. 2017;595:2229–2252.
12. Landstrom AP, Dobrev D, Wehrens XHT. Calcium Signaling and Cardiac

Arrhythmias. *Circ Res*. 2017;120:1969–1993.

13. Antzelevitch C, Burashnikov A. Overview of Basic Mechanisms of Cardiac Arrhythmia. *Card Electrophysiol Clin*. 2011;3:23–45.
14. Barrio-Lopez T, Almendral J. Mechanisms of Cardiac Arrhythmias. *Antiarrhythmic Drugs*. 2020:1–29.
15. Xu L, Ding X, Wang T, Mou S, Sun H, Hou T. Voltage-gated sodium channels: structures, functions, and molecular modeling. *Drug Discov Today*. 2019;24:1389–1397.
16. Song W, Shou W. Cardiac sodium channel Nav1.5 mutations and cardiac arrhythmia. *Pediatr Cardiol*. 2012;33:943–949.
17. Maier SKG, Westenbroek RE, McCormick KA, Curtis R, Scheuer T, Catterall WA. Distinct Subcellular Localization of Different Sodium Channel α and β Subunits in Single Ventricular Myocytes from Mouse Heart. *Circulation*. 2004;109:1421–1427.
18. Grandi E, Sanguinetti MC, Bartos DC, Bers DM, Chen-Izu Y, Chiamvimonvat N, Colecraft HM, Delisle BP, Heijman J, Navedo MF, Noskov S, Proenza C, Vandenberg JI, Yarov-Yarovoy V. Potassium channels in the heart: structure, function and regulation. *J Physiol*. 2017;595:2209–2228.
19. Schwartz PJ, Stramba-Badiale M, Crotti L, Pedrazzini M, Besana A, Bosi G, Gabbarini F, Goulene K, Insolia R, Mannarino S, Mosca F, Nespoli L, Rimini A, Rosati E, Salice P, Spazzolini C. Prevalence of the congenital long-qt syndrome. *Circulation*. 2009;120:1761–1767.
20. Itzhaki I, Maizels L, Huber I, Zwi-Dantsis L, Caspi O, Winterstern A, Feldman O, Gepstein A, Arbel G, Hammerman H, Boulos M, Gepstein L. Modelling the long QT syndrome with induced pluripotent stem cells. *Nature*. 2011;471:225–230.
21. Adler A, Novelli V, Amin AS, Abiusi E, Care M, Nannenberg EA, Feilotter H, Amenta S, Mazza D, Bikker H, Sturm AC, Garcia J, Ackerman MJ, Hershberger RE, Perez M V., Zareba W, Ware JS, Wilde AAM, Gollob MH. An International, Multicentered, Evidence-Based Reappraisal of Genes Reported to Cause Congenital Long QT Syndrome. *Circulation*. 2020;141:418–428.
22. Schwartz PJ, Ackerman MJ, George AL, Wilde AAM. Impact of Genetics on the Clinical Management of Channelopathies. *J Am Coll Cardiol*. 2013;62:169–180.
23. Liu GX, Choi BR, Ziv O, Li W, de Lange E, Qu Z, Koren G. Differential conditions for

early after-depolarizations and triggered activity in cardiomyocytes derived from transgenic LQT1 and LQT2 rabbits. *J Physiol*. 2012;590:1171–1180.

24. Banyasz T, Jian Z, Horvath B, Khabbaz S, Izu LT, Chen-Izu Y. Beta-adrenergic stimulation reverses the I Kr–I Ks dominant pattern during cardiac action potential. *Pflugers Arch Eur J Physiol*. 2014;466:2067–2076.
25. Kang C, Badiceanu A, Brennan JA, Gloschat C, Qiao Y, Trayanova NA, Efimov IR. β-adrenergic stimulation augments transmural dispersion of repolarization via modulation of delayed rectifier currents IKs and IKr in the human ventricle. *Sci Rep*. 2017;7.
26. Tristani-Firouzi M, Jensen JL, Donaldson MR, Sansone V, Meola G, Hahn A, Bendahhou S, Kwiecinski H, Fidzianska A, Plaster N, Fu YH, Ptacek LJ, Tawil R. Functional and clinical characterization of KCNJ2 mutations associated with LQT7 (Andersen syndrome). *J Clin Invest*. 2002;110:381–388.
27. Pérez-Riera AR, Barbosa-Barros R, Daminello Raimundo R, da Costa de Rezende Barbosa MP, Esposito Sorpreso IC, de Abreu LC. The congenital long QT syndrome Type 3: An update. *Indian Pacing Electrophysiol J*. 2018;18:25–35.
28. Weiss JN, Garfinkel A, Karagueuzian HS, Chen PS, Qu Z. Early afterdepolarizations and cardiac arrhythmias. *Heart Rhythm*. 2010;7:1891–1899.
29. Tse G. Mechanisms of cardiac arrhythmias. *J Arrhythmia*. 2016;32:75–81.
30. Berne P, Brugada J. Brugada syndrome 2012. *Circ J*. 2012;76:1563–1571.
31. Watanabe H, Minamino T. Genetics of Brugada syndrome. *J Hum Genet*. 2016;61:57–60.
32. Le Scouarnec S, Karakachoff M, Gourraud JB, Lindenbaum P, Bonnaud S, Portero V, Duboscq-Bidot L, Daumy X, Simonet F, Teusan R, Baron E, Violleau J, Persyn E, Bellanger L, Barc J, Chatel S, Martins R, Mabo P, Sacher F, Haïssaguerre M, Kyndt F, Schmitt S, Bézieau S, Le Marec H, Dina C, Schott JJ, Probst V, Redon R. Testing the burden of rare variation in arrhythmia-susceptibility genes provides new insights into molecular diagnosis for brugada syndrome. *Hum Mol Genet*. 2015;24:2757–2763.
33. Hosseini SM, Kim R, Udupa S, Costain G, Jobling R, Liston E, Jamal SM, Szybowska M, Morel CF, Bowdin S, Garcia J, Care M, Sturm AC, Novelli V, Ackerman MJ, Ware JS, Hershberger RE, Wilde AAM, Gollob MH. Reappraisal of reported genes for sudden arrhythmic death: Evidence-based evaluation of gene validity for brugada

syndrome. *Circulation*. 2018;138:1195–1205.

34. Tse G, Liu T, Li KHC, Laxton V, Yin YW, Keung W, Li RA, Yan BP. Electrophysiological mechanisms of Brugada syndrome: Insights from pre-clinical and clinical studies. *Front Physiol*. 2016;7.
35. Wilde AAM, Postema PG, Di Diego JM, Viskin S, Morita H, Fish JM, Antzelevitch C. The pathophysiological mechanism underlying Brugada syndrome. Depolarization versus repolarization. *J Mol Cell Cardiol*. 2010;49:543–553.
36. Priori SG, Napolitano C, Memmi M, Colombi B, Drago F, Gasparini M, DeSimone L, Coltorti F, Bloise R, Keegan R, Cruz Filho FES, Vignati G, Benatar A, DeLogu A. Clinical and molecular characterization of patients with catecholaminergic polymorphic ventricular tachycardia. *Circulation*. 2002;106:69–74.
37. Medeiros-Domingo A, Bhuiyan ZA, Tester DJ, Hofman N, Bikker H, Tintelen JP van, Mannens MMAM, Wilde AAM, Ackerman MJ. The RYR2-Encoded Ryanodine Receptor/Calcium Release Channel in Patients Diagnosed Previously With Either Catecholaminergic Polymorphic Ventricualr Tachycardia or Genotype Negative, Exercise-Induced Long QT Syndrome. *J Am Coll Cardiol*. 2009;54:2065–2074.
38. Meissner G. The structural basis of ryanodine receptor ion channel function. *J Gen Physiol*. 2017;149:1065–1089.
39. Bers DM. Cardiac excitation-contraction coupling. *Nature*. 2002;415:198–205.
40. Eisner DA, Caldwell JL, Kistamás K, Trafford AW. Calcium and Excitation-Contraction Coupling in the Heart. *Circ Res*. 2017;121:181–195.
41. Terentyev D, Viatchenko-Karpinski S, Valdivia HH, Escobar AL, Györke S. Luminal Ca2+ controls termination and refractory behavior of Ca2+-induced Ca2+ release in cardiac myocytes. *Circ Res*. 2002;91:414–420.
42. Hopton C, Tijsen AJ, Maizels L, Arbel G, Gepstein A, Bates N, Brown B, Huber I, Kimber SJ, Newman WG, Venetucci L, Gepstein L. Characterization of the mechanism by which a nonsense variant in RYR2 leads to disordered calcium handling. *Physiol Rep*. 2022;10:15265.
43. George CH, Jundi H, Thomas NL, Fry DL, Lai FA. Ryanodine receptors and ventricular arrhythmias: Emerging trends in mutations, mechanisms and therapies. *J Mol Cell Cardiol*. 2007;42:34–50.
44. Liu Y, Wang R, Sun B, Mi T, Zhang J, Mu Y, Chen J, Bround MJ, Johnson JD, Gillis AM, Wayne Chen SR. Generation and characterization of a mouse model

harboring the exon-3 deletion in the cardiac ryanodine receptor. *PLoS One*. 2014;9.

45. Priori SG, Chen SRW. Inherited dysfunction of sarcoplasmic reticulum Ca2+ handling and arrhythmogenesis. *Circ Res*. 2011;108:871–883.
46. Bhuiyan ZA, Van Den Berg MP, Van Tintelen JP, Bink-Boelkens MTE, Wiesfeld ACP, Alders M, Postma A V., Van Langen I, Mannens MMAM, Wilde AAM. Expanding spectrum of human RYR2-related disease: New electrocardiographic, structural, and genetic features. *Circulation*. 2007;116:1569–1576.
47. Gyorke I, Gyorke S. Regulation of the cardiac ryanodine receptor channel by luminal Ca 2+ involves luminal Ca 2+ sensing sites. *Biophys J*. 1998;75:2801–2810.
48. Fabiato A, Fabiato F. Contractions induced by a calcium-triggered release of calcium from the sarcoplasmic reticulum of single skinned cardiac cells. *J Physiol*. 1975;249:469–495.
49. Jiang D, Xiao B, Yang D, Wang R, Choi P, Zhang L, Cheng H, Chen SRW. RyR2 mutations linked to ventricular tachycardia and sudden death reduce the threshold for store-overload-induced Ca2+ release (SOICR). *Proc Natl Acad Sci*. 2004;101:13062–13067.
50. Mitchell RD, Simmerman HKB, Jones LR. Ca2+ binding effects on protein conformation and protein interactions of canine cardiac calsequestrin. *J Biol Chem*. 1988;263:1376–1381.
51. Park HJ, Park Y Il, Kim EJ, Youn B, Fields K, Dunker AK, Kang CH. Comparing skeletal and cardiac calsequestrin structures and their calcium binding: A proposed mechanism for coupled calcium binding and protein polymerization. *J Biol Chem*. 2004;279:18026–18033.
52. Zhang L, Kelley J, Schmeisser G, Kobayashi YM, Jones LR. Complex Formation between Junctin, Triadin, Calsequestrin, and the Ryanodine Receptor. *J Biol Chem*. 1997;272:23389–23397.
53. Beard NA, Sakowska MM, Dulhunty AF, Laver DR. Calsequestrin is an inhibitor of skeletal muscle ryanodine receptor calcium release channels. *Biophys J*. 2002;82:310–320.
54. Beard NA, Laver DR, Dulhunty AF. Calsequestrin and the calcium release channel of skeletal and cardiac muscle. *Prog Biophys Mol Biol*. 2004;85:33–69.
55. Györke I, Hester N, Jones LR, Györke S. The Role of Calsequestrin, Triadin, and

Junctin Conferring Cardiac Ryanodine Receptor Responsiveness to Luminal Calcium. *Biophys J*. 2004;86:2121–2128.

56. Moniotte S, Kobzik L, Feron O, Trochu J, Gauthier C, Balligand J. Upregulation of β3-Adrenoceptors and Altered Response to Inotropic Amines in Human Failing Myocardium. *Circulation*. 2001;103:1649–1655.
57. Myagmar BE, Flynn JM, Cowley PM, Swigart PM, Montgomery MD, Thai K, Nair D, Gupta R, Deng DX, Hosoda C, Melov S, Baker AJ, Simpson PC. Adrenergic receptors in individual ventricular myocytes: the beta-1 and alpha-1B are in all cells, the alpha-1A is in a subpopulation, and the beta-2 and beta-3 are mostly absent. *Circ Res*. 2017;120:1103–1115.
58. de Lucia C, Eguchi A, Koch WJ. New insights in cardiac β-Adrenergic signaling during heart failure and aging. *Front Pharmacol*. 2018;9:1–14.
59. Grimm M, Brown JH. β-Adrenergic receptor signaling in the heart: Role of CaMKII. *J Mol Cell Cardiol*. 2010;48:322–330.
60. Fearnley CJ, Llewelyn Roderick H, Bootman MD. Calcium signaling in cardiac myocytes. *Cold Spring Harb Perspect Biol*. 2011;3:1–20.
61. Beckendorf J, van den Hoogenhof MMG, Backs J. Physiological and unappreciated roles of CaMKII in the heart. *Basic Res Cardiol*. 2018;113:1–12.
62. Jiang D, Wang R, Xiao B, Kong H, Hunt DJ, Choi P, Zhang L, Chen SRW. Enhanced store overload-induced Ca2+ release and channel sensitivity to luminal Ca2+ activation are common defects of RyR2 mutations linked to ventricular tachycardia and sudden death. *Circ Res*. 2005;97:1173–1181.
63. Venetucci LA, Trafford AW, Eisner DA. Increasing ryanodine receptor open probability alone does not produce arrhythmogenic calcium waves: Threshold sarcoplasmic reticulum calcium content is required. *Circ Res*. 2007;100:105–111.
64. Brunello L, Slabaugh JL, Radwanski PB, Ho H-T, Belevych AE, Lou Q, Chen H, Napolitano C, Lodola F, Priori SG, Fedorov V V., Volpe P, Fill M, Janssen PML, Gyorke S. Decreased RyR2 refractoriness determines myocardial synchronization of aberrant Ca2+ release in a genetic model of arrhythmia. *Proc Natl Acad Sci*. 2013;110:10312–10317.
65. Itzhaki I, Maizels L, Huber I, Gepstein A, Arbel G, Caspi O, Miller L, Belhassen B, Nof E, Glikson M, Gepstein L. Modeling of catecholaminergic polymorphic ventricular tachycardia with patient-specific human-induced pluripotent stem

cells. *J Am Coll Cardiol*. 2012;60:990–1000.

66. Reid DS, Tynan M, Braidwood L, Fitzgerald GR. Bidirectional tachycardia in a child. A study using His bundle electrography. *Br Heart J*. 1975;37:339–44.
67. van der Werf C, Wilde AAM. Catecholaminergic polymorphic ventricular tachycardia: from bench to bedside. *Heart*. 2013;99:497 LP – 504.
68. Postma A V., Denjoy I, Kamblock J, Alders M, Lupoglazoff JM, Vaksmann G, Dubosq-Bidot L, Sebillon P, Mannens MMAM, Guicheney P, Wilde AAM. Catecholaminergic polymorphic ventricular tachycardia: RYR2 mutations, bradycardia, and follow up of the patients. *J Med Genet*. 2005;42:863–870.
69. Ackerman MJ, Priori SG, Willems S, Berul C, Brugada R, Calkins H, Camm AJ, Ellinor PT, Gollob M, Hamilton R, Hershberger RE, Judge DP, Le Marec H, McKenna WJ, Schulze-Bahr E, Semsarian C, Towbin JA, Watkins H, Wilde A, Wolpert C, Zipes DP. HRS/EHRA expert consensus statement on the state of genetic testing for the channelopathies and cardiomyopathies: This document was developed as a partnership between the Heart Rhythm Society (HRS) and the European Heart Rhythm Association (EHRA). *Heart Rhythm*. 2011;8:1308–1339.
70. Ackerman MJ. Genetic purgatory and the cardiac channelopathies: Exposing the variants of uncertain/unknown significance issue. *Heart Rhythm*. 2015;12:2325–2331.
71. Silvia G. Priori, MD P, Carlo Napolitano, MD P, Natascia Tiso P, Mirella Memmi P, Gabriele Vignati M, Raffaella Bloise M, Vincenzo Sorrentino, MD; Gian Antonio Danieli Bs. Mutations in the Cardiac Ryanodine Receptor Gene (hRyR2) Underlie Catecholaminergic Polymorphic Ventricular Tachycardia. *Circulation*. 2001;103:196–200.
72. Lahat H, Eldar M, Levy-Nissenbaum E, Bahan T, Friedman E, Khoury A, Lorber A, Kastner DL, Goldman B, Pras E. Autosomal recessive catecholamine- or exercise-induced polymorphic ventricular tachycardia: Clinical features and assignment of the disease gene to chromosome 1p13-21. *Circulation*. 2001;103:2822–2827.
73. Lahat H, Pras E, Olender T, Avidan N, Ben-Asher E, Man O, Levy-Nissenbaum E, Khoury A, Lorber A, Goldman B, Lancet D, Eldar M. A missense mutation in a highly conserved region of CASQ2 is associated with autosomal recessive catecholamine-induced polymorphic ventricular tachycardia in Bedouin families from Israel. *Am J Hum Genet*. 2001;69:1378–1384.

74. Devalla HD, Gélinas R, Aburawi EH, Beqqali A, Goyette P, Freund C, Chaix M, Tadros R, Jiang H, Le Béchec A, Monshouwer-Kloots JJ, Zwetsloot T, Kosmidis G, Latour F, Alikashani A, Hoekstra M, Schlaepfer J, Mummery CL, Stevenson B, Kutalik Z, Vries AA, Rivard L, Wilde AA, Talajic M, Verkerk AO, Al-Gazali L, Rioux JD, Bhuiyan ZA, Passier R. TECRL, a new life-threatening inherited arrhythmia gene associated with overlapping clinical features of both LQTS and CPVT. *EMBO Mol Med*. 2016;8:1390–1408.

75. Nyegaard M, Overgaard MT, Sondergaard MT, Vranas M, Behr ER, Hildebrandt LL, Lund J, Hedley PL, Camm AJ, Wettrell G, Fosdal I, Christiansen M, Borglum AD. Mutations in calmodulin cause ventricular tachycardia and sudden cardiac death. *Am J Hum Genet*. 2012;91:703–712.

76. Jensen HH, Brohus M, Nyegaard M, Overgaard MT. Human Calmodulin Mutations. *Front Mol Neurosci*. 2018;11.

77. Roux-Buisson N, Cacheux M, Fourest-lieuvin A, Fauconnier J, Brocard J, Denjoy I, Durand P, Guicheney P, Kyndt F, Leenhardt A, Le marec H, Lucet V, Mabo P, Probst V, Monnier N, Ray PF, Santoni E, Trémeaux P, Lacampagne A, Fauré J, Lunardi J, Marty I. Absence of triadin, a protein of the calcium release complex, is responsible for cardiac arrhythmia with sudden death in human. *Hum Mol Genet*. 2012;21:2759–2767.

78. Swan H, Piippo K, Viitasalo M, Heikkilä P, Paavonen T, Kainulainen K, Kere J, Keto P, Kontula K, Toivonen L. Arrhythmic disorder mapped to chromosome 1q42-q43 causes malignant polymorphic ventricular tachycardia in structurally normal hearts. *J Am Coll Cardiol*. 1999;34:2035–2042.

79. Priori SG, Wilde AA, Horie M, Cho Y, Behr ER, Berul C, Blom N, Brugada J, Chiang CE, Huikuri H, Kannankeril P, Krahn A, Leenhardt A, Moss A, Schwartz PJ, Shimizu W, Tomaselli G, Tracy C. HRS/EHRA/APHRS Expert Consensus Statement on the Diagnosis and Management of Patients with Inherited Primary Arrhythmia Syndromes: Document endorsed by HRS, EHRA, and APHRS in May 2013 and by ACCF, AHA, PACES, and AEPC in June 2013. *Heart Rhythm*. 2013;10:1932–1963.

80. Priori SG, Blomstrom-Lundqvist C, Mazzanti A, Bloma N, Borggrefe M, Camm J, Elliott PM, Fitzsimons D, Hatala R, Hindricks G, Kirchhof P, Kjeldsen K, Kuck KH, Hernandez-Madrid A, Nikolaou N, Norekval TM, Spaulding C, Van Veldhuisen DJ, Kolh P, Lip GYH, Agewall S, Barón-Esquivias G, Boriani G, Budts W, Bueno H,

Capodanno D, Carerj S, Crespo-Leiro MG, Czerny M, Deaton C, Dobrev D, Erol Ç, Galderisi M, Gorenek B, Kriebel T, Lambiase P, Lancellotti P, Lane DA, Lang I, Manolis AJ, Morais J, Moreno J, Piepoli MF, Rutten FH, Sredniawa B, Zamorano JL, Zannad F, Aboyans V, Achenbach S, Badimon L, Baumgartner H, Bax JJ, Dean V, Fitzsimons D, Gaemperli O, Nihoyannopoulos P, Ponikowski P, Roffi M, Torbicki A, Vaz Carneiro A, Windecker S, Piruzyan A, Roithinger FX, Mairesse GH, Goronja B, Shalganov T, Puljević D, Antoniades L, Kautzner J, Larsen JM, Aboulmaaty M, Kampus P, Hedman A, Kamcevska-Dobrkovic L, Piot O, Etsadashvili K, Eckardt L, Deftereos S, Gellér L, Gizurarson S, Keane D, Haim M, Della Bella P, Abdrakhmanov A, Mirrakhimov A, Kalejs O, Ben Lamin H, Marinskis G, Groben L, Sammut M, Raducan A, Chaib A, Tande PM, Lenarczyk R, Morgado FB, Vatasescu R, Mikhaylov EN, Hlivak P, et al. 2015 ESC Guidelines for the management of patients with ventricular arrhythmias and the prevention of sudden cardiac death the Task Force for the Management of Patients with Ventricular Arrhythmias and the Prevention of Sudden Cardiac Death of the Europea. *Eur Heart J*. 2015;36:2793–2867.

81. Hayashi M, Denjoy I, Extramiana F, Maltret A, Buisson NR, Lupoglazoff JM, Klug D, Hayashi M, Takatsuki S, Villain E, Kamblock J, Messali A, Guicheney P, Lunardi J, Leenhardt A. Incidence and risk factors of arrhythmic events in catecholaminergic polymorphic ventricular tachycardia. *Circulation*. 2009;119:2426–2434.

82. Leren IS, Saberniak J, Majid E, Haland TF, Edvardsen T, Haugaa KH. Nadolol decreases the incidence and severity of ventricular arrhythmias during exercise stress testing compared with β1-selective β-blockers in patients with catecholaminergic polymorphic ventricular tachycardia. *Heart Rhythm*. 2016;13:433–440.

83. Zhou Q, Xiao J, Jiang D, Wang R, Vembaiyan K, Wang A, Smith CD, Xie C, Chen W, Zhang J, Tian X, Jones PP, Zhong X, Guo A, Chen H, Zhang L, Zhu W, Yang D, Li X, Chen J, Gillis AM, Duff HJ, Cheng H, Feldman AM, Song LS, Fill M, Back TG, Chen SRW. Carvedilol and its new analogs suppress arrhythmogenic store overload-induced Ca 2+ release. *Nat Med*. 2011;17:1003–1009.

84. Zhang J, Zhou Q, Smith CD, Chen H, Tan Z, Chen B, Nani A, Wu G, Song LS, Fill M, Back TG, Chen SRW. Non-β-blocking R-carvedilol enantiomer suppresses Ca2+ waves and stress-induced ventricular tachyarrhythmia without lowering heart

rate or blood pressure. *Biochem J*. 2015;470:233–242.

85. Roston TM, Vinocur JM, Maginot KR, Mohammed S, Salerno JC, Etheridge SP, Cohen M, Hamilton RM, Pflaumer A, Kanter RJ, Potts JE, LaPage MJ, Collins KK, Gebauer RA, Temple JD, Batra AS, Erickson C, Miszczak-Knecht M, Kubuš P, Bar-Cohen Y, Kantoch M, Thomas VC, Hessling G, Anderson C, Young ML, Ortega MC, Lau YR, Johnsrude CL, Fournier A, Kannankeril PJ, Sanatani S. Catecholaminergic polymorphic ventricular tachycardia in children: analysis of therapeutic strategies and outcomes from an international multicenter registry. *Circ Arrhythmia Electrophysiol*. 2015;8:633–642.
86. Steinfurt J, Dechant MJ, Böckelmann D, Zumhagen S, Stiller B, Schulze-Bahr E, Bode C, Odening KE. High-dose flecainide with low-dose β-blocker therapy in catecholaminergic polymorphic ventricular tachycardia: A case report and review of the literature. *J Cardiol Cases*. 2015;11:10–13.
87. O'Donovan CE, Waddell-Smith KE, Skinner JR, Broadbent E. Predictors of β-blocker adherence in cardiac inherited disease. *Open Heart*. 2018;5:1–7.
88. Salvage SC, Chandrasekharan KH, Jeevaratnam K, Dulhunty AF, Thompson AJ, Jackson AP, Huang CLH. Multiple targets for flecainide action: implications for cardiac arrhythmogenesis. *Br J Pharmacol*. 2018;175:1260–1278.
89. Watanabe H, Chopra N, Laver D, Hwang HS, Davies SS, Roach DE, Duff HJ, Roden DM, Wilde AAM, Knollmann BC. Flecainide prevents catecholaminergic polymorphic ventricular tachycardia in mice and humans. *Nat Med*. 2009;15:380–383.
90. Van Der Werf C, Kannankeril PJ, Sacher F, Krahn AD, Viskin S, Leenhardt A, Shimizu W, Sumitomo N, Fish FA, Bhuiyan ZA, Willems AR, Van Der Veen MJ, Watanabe H, Laborderie J, Hassaguerre M, Knollmann BC, Wilde AAM. Flecainide therapy reduces exercise-induced ventricular arrhythmias in patients with catecholaminergic polymorphic ventricular tachycardia. *J Am Coll Cardiol*. 2011;57:2244–2254.
91. Padfield GJ, Alahmari L, Lieve KVV, Alahmari T, Roston TM, Wilde AA, Krahn AD, Sanatani S. Flecainide monotherapy is an option for selected patients with catecholaminergic polymorphic ventricular tachycardia intolerant of β-blockade. *Heart Rhythm*. 2016;13:609–613.
92. Kannankeril PJ, Moore JP, Cerrone M, Priori SG, Kertesz NJ, Ro PS, Batra AS,

Kaufman ES, Fairbrother DL, Saarel E V., Etheridge SP, Kanter RJ, Carboni MP, Dzurik M V., Fountain D, Chen H, Ely EW, Roden DM, Knollmann BC. Efficacy of flecainide in the treatment of catecholaminergic polymorphic ventricular tachycardia a randomized clinical trial. *JAMA Cardiol*. 2017;2:759–766.

93. Swan H, Laitinen P, Kontula K, Toivonen L. Calcium channel antagonism reduces exercise-induced ventricular arrhythmias in catecholaminergic polymorphic ventricular tachycardia patients with RyR2 mutations. *J Cardiovasc Electrophysiol*. 2005;16:162–166.
94. Valdivia HH, Valdivia C, Ma J, Coronado R. Direct binding of verapamil to the ryanodine receptor channel of sarcoplasmic reticulum. *Biophys J*. 1990;58:471–481.
95. Rosso R, Kalman JM, Rogowski O, Diamant S, Birger A, Biner S, Belhassen B, Viskin S. Calcium channel blockers and beta-blockers versus beta-blockers alone for preventing exercise-induced arrhythmias in catecholaminergic polymorphic ventricular tachycardia. *Heart Rhythm*. 2007;4:1149–1154.
96. Roses-Noguer F, Jarman JWE, Clague JR, Till J. Outcomes of defibrillator therapy in catecholaminergic polymorphic ventricular tachycardia. *Heart Rhythm*. 2014;11:58–66.
97. Miyake CY, Webster G, Czosek RJ, Kantoch MJ, Dubin AM, Avasarala K, Atallah J. Efficacy of implantable cardioverter defibrillators in young patients with catecholaminergic polymorphic ventricular tachycardia: Success depends on substrate. *Circ Arrhythmia Electrophysiol*. 2013;6:579–587.
98. Nattel S, Andrade J, Macle L, Rivard L, Dyrda K, Mondesert B, Khairy P. New directions in cardiac arrhythmia management: Present challenges and future solutions. *Can J Cardiol*. 2014;30:S420–S430.
99. Linder J, Hidayatallah N, Stolerman M, McDonald T V, Marion R, Walsh C, Dolan S. Perceptions of an implantable cardioverter-defibrillator: A qualitative study of families with a history of sudden life-threatening cardiac events and recommendations to improve care. *Einstein J Biol Med*. 2013;29:3–14.
100. Schwartz PJ. The Rationale and the Role of Left Stellectomy for the Prevention of Malignant Arrhythmias. *Ann N Y Acad Sci*. 1984;427:199–221.
101. Schwartz PJ, Stone HL. Effects of unilateral stellectomy upon cardiac performance during exercise in dogs. *Circ Res*. 1979;44:637–645.

102. Randall WC, Rohse WG. The augmentor action of the sympathetic cardiac nerves. *Circ Res*. 1956;4:470–475.
103. Dusi V, De Ferrari GM, Pugliese L, Schwartz PJ. Cardiac Sympathetic Denervation in Channelopathies. *Front Cardiovasc Med*. 2019;6.
104. Wilde AAM, Bhuiyan ZA, Crotti L, Facchini M, De Ferrari GM, Paul T, Ferrandi C, Koolbergen DR, Odero A, Schwartz PJ. Left cardiac sympathetic denervation for catecholaminergic polymorphic ventricular tachycardia. *N Engl J Med*. 2008;358:2024–2029.
105. De Ferrari GM, Dusi V, Spazzolini C, Bos JM, Abrams DJ, Berul CI, Crotti L, Davis AM, Eldar M, Kharlap M, Khoury A, Krahn AD, Leenhardt A, Moir CR, Odero A, Nordkamp LO, Paul T, Rosés I Noguer F, Shkolnikova M, Till J, Wilde AAM, Ackerman MJ, Schwartz PJ. Clinical management of catecholaminergic polymorphic ventricular tachycardia the role of left cardiac sympathetic denervation. *Circulation*. 2015;131:2185–2193.
106. Milani-Nejad N, Janssen PML. Small and large animal models in cardiac contraction research: Advantages and disadvantages. *Pharmacol Ther*. 2014;141:235–249.
107. Nerbonne JM. Studying cardiac arrhythmias in the mouse - A reasonable model for probing mechanisms? *Trends Cardiovasc Med*. 2004;14:83–93.
108. Kaese S, Verheule S. Cardiac electrophysiology in mice: A matter of size. *Front Physiol*. 2012;3 SEP:1–19.
109. Odening KE, Ziupa D. Transgenic Animal Models of Cardiac Channelopathies: Benefits and Limitations. *Cardiac and Vascular Biology*. 2018;379–420.
110. Salama G, London B. Mouse models of long QT syndrome. *J Physiol*. 2007;578:43–53.
111. Barry DM, Xu H, Schuessler RB, Nerbonne JM. Functional knockout of the transient outward current, long-QT syndrome, and cardiac remodeling in mice expressing a dominant-negative Kv4 α subunit. *Circ Res*. 1998;83:560–567.
112. Demolombe S, Lande G, Charpentier F, Van Roon MA, Van Den Hoff MJB, Toumaniantz G, Baro I, Guihard G, Le Berre N, Corbier A, De Bakker J, Opthof T, Wilde A, Moorman AFM, Escande D. Transgenic mice overexpressing human KvLQT1 dominant-negative isoform. Part I: Phenotypic characterisation. *Cardiovasc Res*. 2001;50:314–327.

113. Brunner M, Guo W, Mitchell GF, Buckett PD, Nerbonne JM, Koren G. Characterization of mice with a combined suppression of Ito and Ik,slow. *Am J Physiol - Heart Circ Physiol*. 2001;281.

114. McLerie M, Lopatin A. Dominant-negative suppression of IK1 in the mouse heart leads to altered cardiac excitability. *J Mol Cell Cardiol*. 2003;35:367–378.

115. Li H, Guo W, Yamada KA, Nerbonne JM. Selective elimination of IK,slow1 in mouse ventricular myocytes expressing a dominant negative Kv1.5α subunit. *Am J Physiol - Heart Circ Physiol* . 2004;286:319–328.

116. London B, Jeron A, Zhou J, Buckett P, Han X, Mitchell GF, Koren G. Long QT and ventricular arrhythmias in transgenic mice expressing the N terminus and first transmembrane segment of a voltage-gated potassium channel. *Proc Natl Acad Sci USA*. 1998;95:2926–2931.

117. Salama G, Baker L, Wolk R, Barhanin J, London B. Arrhythmia phenotype in mouse models of human long QT. *J Interv Card Electrophysiol*. 2009;24:77–87.

118. Zhou J, Kodirov S, Murata M, Buckett PD, Nerbonne JM, Koren G. Regional upregulation of kv2.1-encoded current, IKslow2, in Kv1DN mice is abolished by crossbreeding with Kv2DN mice. *Am J Physiol - Heart Circ Physiol*. 2003;284.

119. Guo W, Jung WE, Marionneau C, Aimond F, Xu H, Yamada KA, Schwarz TL, Demolombe S, Nerbonne JM. Targeted deletion of Kv4.2 eliminates Ito,f and results in electrical and molecular remodeling, with no evidence of ventricular hypertrophy or myocardial dysfunction. *Circ Res*. 2005;97:1342–1350.

120. Nuyens D, Stengl M, Dugarmaa S, Rossenbacker T, Compernolle V, Rudy Y, Smits JF, Flameng W, Clancy CE, Moons L, Vos MA, Dewerchin M, Benndorf K, Collen D, Carmeliet E, Carmeliet P. Abrupt rate accelerations or premature beats cause life-threatening arrhythmias in mice with long-QT3 syndrome. *Nat Med*. 2001;7:1021–1027.

121. Tian XL, Yong SL, Wan X, Wu L, Chung MK, Tchou PJ, Rosenbaum DS, Van Wagoner DR, Kirsch GE, Wang Q. Mechanisms by which SCN5A mutation N1325S causes cardiac arrhythmias and sudden death in vivo. *Cardiovasc Res*. 2004;61:256–267.

122. Head CE, Balasubramaniam R, Thomas G, Goddard CA, Lei M, Colledge WH, Grace AA, Huang CLH. Paced electrogram fractionation analysis of arrhythmogenic tendency in ΔKPQ Scn5a mice. *J Cardiovasc Electrophysiol*. 2005;16:1329–1340.

123. Wan E, Abrams J, Weinberg RL, Katchman AN, Bayne J, Zakharov SI, Yang L,

Morrow JP, Garan H, Marx SO. Aberrant sodium influx causes cardiomyopathy and atrial fibrillation in mice. *J Clin Invest*. 2016;126:112–122.

124. Fabritz L, Damke D, Emmerich M, Kaufmann SG, Theis K, Blana A, Fortmüller L, Laakmann S, Hermann S, Aleynichenko E, Steinfurt J, Volkery D, Riemann B, Kirchhefer U, Franz MR, Breithardt G, Carmeliet E, Schäfers M, Maier SKG, Carmeliet P, Kirchhof P. Autonomic modulation and antiarrhythmic therapy in a model of long QT syndrome type 3. *Cardiovasc Res*. 2010;87:60–72.
125. Calvillo L, Spazzolini C, Vullo E, Insolia R, Crotti L, Schwartz PJ. Propranolol prevents life-threatening arrhythmias in LQT3 transgenic mice: Implications for the clinical management of LQT3 patients. *Heart Rhythm*. 2014;11:126.
126. Antzelevitch C, Brugada P, Borggrefe M, Brugada J, Brugada R, Corrado D, Gussak I, LeMarec H, Nademanee K, Perez Riera AR, Shimizu W, Schulze-Bahr E, Tan H, Wilde A. Brugada Syndrome: Report of the second consensus conference. Circulation. 2005;659–670.
127. Li Y, Lang S, Akin I, Zhou X, El-Battrawy I. Brugada Syndrome: Different Experimental Models and the Role of Human Cardiomyocytes From Induced Pluripotent Stem Cells. *J Am Heart Assoc*. 2022;11.
128. Papadatos GA, Wallerstein PMR, Head CEG, Ratcliff R, Brady PA, Benndorf K, Saumarez RC, Trezise AEO, Huang CLH, Vandenberg JI, Colledge WH, Grace AA. Slowed conduction and ventricular tachycardia after targeted disruption of the cardiac sodium channel gene Scn5a. *Proc Natl Acad Sci USA*. 2002;99:6210–6215.
129. Remme CA, Verkerk AO, Nuyens D, Van Ginneken ACG, Van Brunschot S, Belterman CN, Wilders R, Van Roon MA, Tan HL, Wilde AA, Carmeliet P, De Bakker JMT, Veldkamp MW, Bezzina CR. Overlap syndrome of cardiac sodium channel disease in mice carrying the equivalent mutation of human SCN5A-1795insD. *Circulation*. 2006;114:2584–2594.
130. Shy D, Gillet L, Ogrodnik J, Albesa M, Verkerk AO, Wolswinkel R, Rougier JS, Barc J, Essers MC, Syam N, Marsman RF, Van Mil AM, Rotman S, Redon R, Bezzina CR, Remme CA, Abriel H. PDZ domain-binding motif regulates cardiomyocyte compartment-specific nav1.5 channel expression and function. *Circulation*. 2014;130:147–160.
131. Martin CA, Guzadhur L, Grace AA, Lei M, Huang CLH. Mapping of reentrant spontaneous polymorphic ventricular tachycardia in a Scn5a+/- mouse model. *Am*

J Physiol - Heart Circ Physiol. 2011;300:1853–1862.

132. Li Y, Lang S, Akin I, Zhou X, El-Battrawy I. Brugada Syndrome: Different Experimental Models and the Role of Human Cardiomyocytes From Induced Pluripotent Stem Cells. *J Am Heart Assoc*. 2022;11:24410.
133. Cerrone M, Colombi B, Santoro M, Raffaele di Barletta M, Scelsci M, Villani L, Napolitano C, Priori S. Bidirectional ventricular tachycardia and fibrillation elicited in a knock-in mouse model carrier of a mutation in the cardiac ryanodine receptor. *Circ Res*. 2005;96:e77–e82.
134. Kannankeril PJ, Mitchell BM, Goonasekera SA, Chelu MG, Zhang W, Sood S, Kearney DL, Danila CI, De Biasi M, Wehrens XHT, Pautler RG, Roden DM, Taffet GE, Dirksen RT, Anderson ME, Hamilton SL. Mice with the R176Q cardiac ryanodine receptor mutation exhibit catecholamine-induced ventricular tachycardia and cardiomyopathy. *Proc Natl Acad Sci USA*. 2006;103:12179–12184.
135. Cerrone M, Noujaim SF, Tolkacheva EG, Talkachou A, O'Connell R, Berenfeld O, Anumonwo J, Pandit S V., Vikstrom K, Napolitano C, Priori SG, Jalife J. Arrhythmogenic mechanisms in a mouse model of catecholaminergic polymorphic ventricular tachycardia. *Circ Res*]. 2007;101:1039–1048.
136. Kashimura T, Briston SJ, Trafford AW, Napolitano C, Priori SG, Eisner DA, Venetucci LA. In the RyR2R4496C mouse model of CPVT, β-adrenergic stimulation induces ca waves by increasing SR Ca content and not by decreasing the threshold for Ca Waves. *Circ Res*. 2010;107:1483–1489.
137. Kobayashi S, Yano M, Uchinoumi H, Suetomi T, Susa T, Ono M, Xu X, Tateishi H, Oda T, Okuda S, Doi M, Yamamoto T, Matsuzaki M. Dantrolene, a therapeutic agent for malignant hyperthermia, inhibits catecholaminergic polymorphic ventricular tachycardia in a RyR2R2474S/+ knock-in mouse model. *Circ J*. 2010;74:2579–2584.
138. Loaiza R, Benkusky NA, Powers PP, Hacker T, Noujaim S, Ackerman MJ, Jalife J, Valdivia HH. Heterogeneity of ryanodine receptor dysfunction in a mouse model of catecholaminergic polymorphic ventricular tachycardia. *Circ Res*. 2013;112:298–308.
139. Zhao YT, Valdivia CR, Gurrola GB, Powers PP, Willis BC, Moss RL, Jalife J, Valdivia HH. Arrhythmogenesis in a catecholaminergic polymorphic ventricular

tachycardia mutation that depresses ryanodine receptor function. *Proc Natl Acad Sci USA*. 2015;112:E1669–E1677.

140. Knollmann BC, Chopra N, Hlaing T, Akin B, Yang T, Ettensohn K, Knollmann BEC, Horton KD, Weissman NJ, Holinstat I, Zhang W, Roden DM, Jones LR, Franzini-Armstrong C, Pfeifer K. Casq2 deletion causes sarcoplasmic reticulum volume increase, premature Ca2+ release, and catecholaminergic polymorphic ventricular tachycardia. *J Clin Invest*. 2006;116:2510–2520.
141. Song L, Alcalai R, Arad M, Wolf CM, Toka O, Conner DA, Berul CI, Eldar M, Seidman CE, Seidman JG. Calsequestrin 2 (CASQ2) mutations increase expression of calreticulin and ryanodine receptors, causing catecholaminergic polymorphic ventricular tachycardia. *J Clin Invest*. 2007;117:1814–1823.
142. Katz G, Khoury A, Kurtzwald E, Hochhauser E, Porat E, Shainberg A, Seidman JG, Seidman CE, Lorber A, Eldar M, Arad M. Optimizing catecholaminergic polymorphic ventricular tachycardia therapy in calsequestrin-mutant mice. *Heart Rhythm*. 2010;7:1676–1682.
143. Hwang HS, Hasdemir C, Laver D, Mehra D, Turhan K, Faggioni M, Yin H, Knollmann BC. Inhibition of cardiac Ca2+ release channels (RyR2) determines efficacy of class i antiarrhythmic drugs in catecholaminergic polymorphic ventricular tachycardia. *Circ Arrhythmia Electrophysiol*. 2011;4:128–135.
144. Knollmann BC. Power and pitfalls of using transgenic mice to optimize therapy for CPVT: A need for prospective placebo-controlled clinical trials in genetic arrhythmia disorders. *Heart Rhythm*. 2010;7:1683–1685.
145. Baczkó I, Jost N, Virág L, Bősze Z, Varró A. Rabbit models as tools for preclinical cardiac electrophysiological safety testing: Importance of repolarization reserve. *Prog Biophys Mol Biol*. 2016;121:157–168.
146. Baczkó I, Hornyik T, Brunner M, Koren G, Odening KE. Transgenic Rabbit Models in Proarrhythmia Research. *Front Pharmacol*. 2020;11.
147. Hornyik T, Rieder M, Castiglione A, Major P, Baczko I, Brunner M, Koren G, Odening KE. Transgenic rabbit models for cardiac disease research. *Br J Pharmacol*. 2022;179:938–957.
148. Brunner M, Peng X, Gong XL, Ren XQ, Ziv O, Choi BR, Mathur R, Hajjiri M, Odening KE, Steinberg E, Folco EJ, Pringa E, Centracchio J, Macharzina RR, Donahay T, Schofield L, Rana N, Kirk M, Mitchell GF, Poppas A, Zehender M, Koren G.

Mechanisms of cardiac arrhythmias and sudden death in transgenic rabbits with long QT syndrome. *J Clin Invest*. 2008;118:2246–2259.

149. Ziupa D, Beck J, Franke G, Feliz SP, Hartmann M, Koren G, Zehender M, Bode C, Brunner M, Odening KE. Pronounced effects of HERG-blockers E-4031 and erythromycin on APD, spatial APD dispersion and triangulation in transgenic long-QT type 1 rabbits. *PLoS One*. 2014;9.
150. Lau E, Kossidas K, Kim TY, Kunitomo Y, Ziv O, Zhen S, Taylor C, Schofield L, Yammine J, Liu G, Peng X, Qu Z, Koren G, Choi BR. Spatially discordant alternans and arrhythmias in tachypacing-induced cardiac myopathy in transgenic LQT1 rabbits: The importance of IKsand Ca2+ cycling. *PLoS One*. 2015;10.
151. Morita H, Wu J, Zipes DP. The QT syndromes: long and short. *Lancet*. 2008;372:750–763.
152. Wakula P, Bisping E, Kockskämper J, Post H, Brauer S, Deuter M, Oehlmann R, Besenfelder U, Lai FA, Brem G, Pieske B. CMV promoter is inadequate for expression of mutant human RyR2 in transgenic rabbits. *J Pharmacol Toxicol Methods*. 2011;63:180–185.
153. Matsuhisa F, Kitajima S, Nishijima K, Akiyoshi T, Morimoto M, Fan J. Transgenic rabbit models: Now and the future. *Appl Sci*. 2020;10:1–15.
154. Fan J, Wang Y, Chen YE. Genetically Modified Rabbits for Cardiovascular Research. *Front Genet*. 2021;12:614379.
155. O'Hara T, Rudy Y. Quantitative comparison of cardiac ventricular myocyte electrophysiology and response to drugs in human and nonhuman species. *Am J Physiol - Heart Circ Physiol*. 2012;302.
156. Jost N, Virág L, Comtois P, Ördög B, Szuts V, Seprényi G, Bitay M, Kohajda Z, Koncz I, Nagy N, Szél T, Magyar J, Kovács M, Puskás LG, Lengyel C, Wettwer E, Ravens U, Nánási PP, Papp JG, Varró A, Nattel S. Ionic mechanisms limiting cardiac repolarization reserve in humans compared to dogs. *J Physiol*. 2013;591:4189–4206.
157. Li GR, Du XL, Siow YL, Karmin O, Tse HF, Lau CP. Calcium-activated transient outward chloride current and phase 1 repolarization of swine ventricular action potential. *Cardiovasc Res*. 2003;58:89–98.
158. Odening KE, Gomez AM, Dobrev D, Fabritz L, Heinzel FR, Mangoni ME, Molina CE, Sacconi L, Smith G, Stengl M, Thomas D, Zaza A, Remme CA, Heijman J. ESC

working group on cardiac cellular electrophysiology position paper: Relevance, opportunities, and limitations of experimental models for cardiac electrophysiology research. *Europace*. 2021;23:1795–1814.

159. Park DS, Cerrone M, Morley G, Vasquez C, Fowler S, Liu N, Bernstein SA, Liu FY, Zhang J, Rogers CS, Priori SG, Chinitz LA, Fishman GI. Genetically engineered SCN5A mutant pig hearts exhibit conduction defects and arrhythmias. *J Clin Invest*. 2015;125:403–412.
160. Shimizu W, Antzelevitch C. Sodium channel block with mexiletine is effective in reducing dispersion of repolarization and preventing torsade de pointes in LQT2 and LQT3 models of the long-QT syndrome. *Circulation*. 1997;96:2038-2047.
161. Szél T, Antzelevitch C. Abnormal repolarization as the basis for late potentials and fractionated electrograms recorded from epicardium in experimental models of brugada syndrome. *J Am Coll Cardiol*. 2014;63:2037–2045.
162. Patocskai B, Yoon N, Antzelevitch C. Mechanisms Underlying Epicardial Radiofrequency Ablation to Suppress Arrhythmogenesis in Experimental Models of Brugada Syndrome. *JACC Clin Electrophysiol*. 2017;3:353–363.
163. Takahashi K, Yamanaka S. Induction of Pluripotent Stem Cells from Mouse Embryonic and Adult Fibroblast Cultures by Defined Factors. *Cell*. 2006;126:663–676.
164. Takahashi K, Tanabe K, Ohnuki M, Narita M, Ichisaka T, Tomoda K, Yamanaka S. Induction of pluripotent stem cells from adult human fibroblasts by defined factors. *Cell*. 2007;131:861–872.
165. Parrotta EI, Lucchino V, Scaramuzzino L, Scalise S, Cuda G. Modeling cardiac disease mechanisms using induced pluripotent stem cell-derived cardiomyocytes: Progress, promises and challenges. *Int J Mol Sci*. 2020;21:1–30.
166. Loh YH, Agarwal S, Park IH, Urbach A, Huo H, Heffner GC, Kim K, Miller JD, Ng K, Daley GQ. Generation of induced pluripotent stem cells from human blood. *Blood*. 2009;113:5476–5479.
167. Romito A, Cobellis G. Pluripotent stem cells: Current understanding and future directions. *Stem Cells Int*. 2016;2016.
168. Regev D, Baskin P, Dolgopyat I, Davidor M, Kermani F, Ullrich ND, Binah O. Induced pluripotent stem cell-derived cardiomyocytes: generation and enrichment protocols, immature and mature structure and function. In: Recent

Advances in iPSC-Derived Cell Types. *Academic Press*; 2021:191–226.

169. Laflamme MA, Chen KY, Naumova A V., Muskheli V, Fugate JA, Dupras SK, Reinecke H, Xu C, Hassanipour M, Police S, O'Sullivan C, Collins L, Chen Y, Minami E, Gill EA, Ueno S, Yuan C, Gold J, Murry CE. Cardiomyocytes derived from human embryonic stem cells in pro-survival factors enhance function of infarcted rat hearts. *Nat Biotechnol*. 2007;25:1015–1024.
170. Paige SL, Osugi T, Afanasiev OK, Pabon L, Reinecke H, Murry CE. Endogenous wnt/β-Catenin signaling is required for cardiac differentiation in human embryonic stem cells. *PLoS One*. 2010;5.
171. Gessert S, Kühl M. The multiple phases and faces of Wnt signaling during cardiac differentiation and development. *Circ Res*. 2010;107:186–199.
172. Gordon MD, Nusse R. Wnt signaling: Multiple pathways, multiple receptors, and multiple transcription factors. *J Biol Chem*. 2006;281:22429–22433.
173. Ueno S, Weidinger G, Osugi T, Kohn AD, Golob JL, Pabon L, Reinecke H, Moon RT, Murry CE. Biphasic role for Wnt/β-catenin signaling in cardiac specification in zebrafish and embryonic stem cells. *Proc Natl Acad Sci USA*. 2007;104:9685–9690.
174. Lian X, Hsiao C, Wilson G, Zhu K, Hazeltine LB, Azarin SM, Raval KK, Zhang J, Kamp TJ, Palecek SP. Robust cardiomyocyte differentiation from human pluripotent stem cells via temporal modulation of canonical Wnt signaling. *Proc Natl Acad Sci USA*. 2012;109:E1848–E1857.
175. Kattman SJ, Witty AD, Gagliardi M, Dubois NC, Niapour M, Hotta A, Ellis J, Keller G. Stage-specific optimization of activin/nodal and BMP signaling promotes cardiac differentiation of mouse and human pluripotent stem cell lines. *Cell Stem Cell*. 2011;8:228–240.
176. Burridge PW, Holmström A, Wu JC. Chemically Defined Culture and Cardiomyocyte Differentiation of Human Pluripotent Stem Cells. *Curr Protoc Hum Genet*. 2015;87:21.3.1.
177. Laco F, Woo TL, Zhong Q, Szmyd R, Ting S, Khan FJ, Chai CLL, Reuveny S, Chen A, Oh S. Unraveling the Inconsistencies of Cardiac Differentiation Efficiency Induced by the GSK3β Inhibitor CHIR99021 in Human Pluripotent Stem Cells. *Stem Cell Reports*. 2018;10:1851–1866.
178. Lian X, Zhang J, Azarin SM, Zhu K, Hazeltine LB, Bao X, Hsiao C, Kamp TJ, Palecek SP. Directed cardiomyocyte differentiation from human pluripotent stem cells by

modulating Wnt/β-catenin signaling under fully defined conditions. *Nat Protoc*. 2013;8:162–175.

179. Burridge PW, Matsa E, Shukla P, Lin ZC, Churko JM, Ebert AD, Lan F, Diecke S, Huber B, Mordwinkin NM, Plews JR, Abilez OJ, Cui B, Gold JD, Wu JC. Chemically defined generation of human cardiomyocytes. *Nat Methods*. 2014;11:855–860.
180. Zhang J, Wilson GF, Soerens AG, Koonce CH, Yu J, Palecek SP, Thomson JA, Kamp TJ. Functional cardiomyocytes derived from human induced pluripotent stem cells. *Circ Res*. 2009;104.
181. Ma J, Guo L, Fiene SJ, Anson BD, Thomson JA, Kamp TJ, Kolaja KL, Swanson BJ, January CT. High purity human-induced pluripotent stem cell-derived cardiomyocytes: Electrophysiological properties of action potentials and ionic currents. *Am J Physiol - Heart Circ Physiol*. 2011;301:H2006.
182. Mummery CL, Zhang J, Ng ES, Elliott DA, Elefanty AG, Kamp TJ. Differentiation of Human ES and iPS Cells to Cardiomyocytes: A Methods Overview. *Circ Res*. 2012;111:344.
183. Hoekstra M, Mummery CL, Wilde AAM, Bezzina CR, Verkerk AO. Induced pluripotent stem cell derived cardiomyocytes as models for cardiac arrhythmias. *Front Physiol*. 2012;3:1–14.
184. Ahmed RE, Anzai T, Chanthra N, Uosaki H. A Brief Review of Current Maturation Methods for Human Induced Pluripotent Stem Cells-Derived Cardiomyocytes. *Front Cell Dev Biol*. 2020;8.
185. Zhang X hua, Morad M. Ca2+ signaling of human pluripotent stem cells-derived cardiomyocytes as compared to adult mammalian cardiomyocytes. *Cell Calcium*. 2020;90:102244.
186. Kane C, Couch L, Terracciano CMN. Excitation–contraction coupling of human induced pluripotent stem cell-derived cardiomyocytes. *Front Cell Dev Biol*. 2015;3:1–8.
187. Gerdes AM, Kellerman SE, Moore JA, Muffly KE, Clark LC, Reaves PY, Malec KB, McKeown PP, Schocken DD. Structural remodeling of cardiac myocytes in patients with ischemic cardiomyopathy. *Circulation*. 1992;86:426–430.
188. Gerdes AM, Capasso JM. Structural remodeling and mechanical dysfunction of cardiac myocytes in heart failure. *J Mol Cell Cardiol*. 1995;27:849–856.
189. Severs NJ. The cardiac muscle cell. *BioEssays*. 2000;22:188–199.

190. Ohler A, Weisser-Thomas J, Piacentino V, Houser SR, Tomaselli GF, O'Rourke B. Two-Photon Laser Scanning Microscopy of the Transverse-Axial Tubule System in Ventricular Cardiomyocytes from Failing and Non-Failing Human Hearts. *Cardiol Res Pract*. 2009;2009.
191. Bray MA, Sheehy SP, Parker KK. Sarcomere alignment is regulated by myocyte shape. *Cell Motil Cytoskeleton*. 2008;65:641–651.
192. Kuo PL, Lee H, Bray MA, Geisse NA, Huang YT, Adams WJ, Sheehy SP, Parker KK. Myocyte shape regulates lateral registry of sarcomeres and contractility. *Am J Pathol*. 2012;181:2030–2037.
193. Brette F, Orchard C. T-tubule function in mammalian cardiac myocytes. *Circ Res*. 2003;92:1182–1192.
194. Orchard C, Brette F. t-tubules and sarcoplasmic reticulum function in cardiac ventricular myocytes. *Cardiovasc Res*. 2008;77:237–244.
195. Barth E, Stämmler G, Speiser B, Schaper J. Ultrastructural quantitation of mitochondria and myofilaments in cardiac muscle from 10 different animal species including man. *J Mol Cell Cardiol*. 1992;24:669–681.
196. Gherghiceanu M, Barad L, Novak A, Reiter I, Itskovitz-Eldor J, Binah O, Popescu LM. Cardiomyocytes derived from human embryonic and induced pluripotent stem cells: Comparative ultrastructure. *J Cell Mol Med*. 2011;15:2539–2551.
197. Hwang HS, Kryshtal DO, Feaster TK, Sánchez-Freire V, Zhang J, Kamp TJ, Hong CC, Wu JC, Knollmann BC. Comparable calcium handling of human iPSC-derived cardiomyocytes generated by multiple laboratories. *J Mol Cell Cardiol*. 2015;85:79–88.
198. Parker KK, Tan J, Chen CS, Tung L. Myofibrillar architecture in engineered cardiac myocytes. *Circ Res*. 2008;103:340–342.
199. Parikh S s, Blackwell DJ, Gomez-Hurtado N, Frisk M, Wang L, Kim K, Dahl CP, Fiane AE, Tønnessen T, Kryshtal DO, Louch WE, Knollmann BC. Thyroid and glucocorticoid hormones promote functional t-tubule development in human-induced pluripotent stem cell derived cardiomyocytes. *Circ Res*. 2017;121:1323–1330.
200. Kim JJ, Yang L, Lin B, Zhu X, Sun B, Kaplan AD, Bett GCL, Rasmusson RL, London B, Salama G. Mechanism of automaticity in cardiomyocytes derived from human induced pluripotent stem cells. *J Mol Cell Cardiol*. 2015;81:81–93.

201. Lemoine MD, Krause T, Koivumäki JT, Prondzynski M, Schulze ML, Girdauskas E, Willems S, Hansen A, Eschenhagen T, Christ T. Human Induced Pluripotent Stem Cell-Derived Engineered Heart Tissue as a Sensitive Test System for QT Prolongation and Arrhythmic Triggers. *Circ Arrhythmia Electrophysiol*. 2018;11.

202. Wang L, Wada Y, Ballan N, Schmeckpeper J, Huang J, Rau CD, Wang Y, Gepstein L, Knollmann BC. Triiodothyronine and dexamethasone alter potassium channel expression and promote electrophysiological maturation of human-induced pluripotent stem cell-derived cardiomyocytes. *J Mol Cell Cardiol*. 2021;161:130–138.

203. Casini S, Verkerk AO, Remme CA. Human iPSC-Derived Cardiomyocytes for Investigation of Disease Mechanisms and Therapeutic Strategies in Inherited Arrhythmia Syndromes: Strengths and Limitations. *Cardiovasc Drugs Ther*. 2017;31:325–344.

204. Moretti A, Bellin M, Welling A, Jung C, Lam J, Bott-Flugel L, Dorn T, Goedel A, Hohnke C, Hofmann F, Seyfarth M, Sinnecker D, Schomig A, Laugwitz K. Patient-specific induced pluripotent stem-cell models for long-QT syndrome. *N Engl J Med*. 2010;363:1397–1409.

205. Zeng H, Wang J, Clouse H, Lagrutta A, Sannajust F. Human-induced pluripotent stem cell-derived cardiomyocytes have limited I Ks for repolarization reserve as revealed by specific KCNQ1/KCNE1 blocker. *JRSM Cardiovasc Dis*. 2019;8:204800401985491.

206. Karbassi E, Fenix A, Marchiano S, Muraoka N, Nakamura K, Yang X, Murry CE. Cardiomyocyte maturation: advances in knowledge and implications for regenerative medicine. *Nat Rev Cardiol*. 2020;17:341–359.

207. Novak A, Barad L, Zeevi-Levin N, Shick R, Shtrichman R, Lorber A, Itskovitz-Eldor J, Binah O. Cardiomyocytes generated from CPVT D307H patients are arrhythmogenic in response to β-adrenergic stimulation. *J Cell Mol Med*. 2012;16:468–482.

208. Nikolaev VO, Bünemann M, Schmitteckert E, Lohse MJ, Engelhardt S. Cyclic AMP imaging in adult cardiac myocytes reveals far-reaching β1-adrenergic but locally confined β2-adrenergic receptor-mediated signaling. *Circ Res*. 2006;99:1084–1091.

209. Nikolaev VO, Moshkov A, Lyon AR, Miragoli M, Novak P, Paur H, Lohse MJ,

Korchev YE, Harding SE, Gorelik J. β2-adrenergic receptor redistribution in heart failure changes cAMP compartmentation. *Science*. 2010;327:1653–1657.

210. Jung G, Fajardo G, Ribeiro AJS, Kooiker KB, Coronado M, Zhao M, Hu DQ, Reddy S, Kodo K, Sriram K, Insel PA, Wu JC, Pruitt BL, Bernstein D. Time-dependent evolution of functional vs. remodeling signaling in induced pluripotent stem cell-derived cardiomyocytes and induced maturation with biomechanical stimulation. *FASEB J*. 2016;30:1464–1479.
211. Lopaschuk GD, Jaswal JS. Energy metabolic phenotype of the cardiomyocyte during development, differentiation, and postnatal maturation. *J Cardiovasc Pharmacol*. 2010;56:130–140.
212. Piquereau J, Ventura-Clapier R. Maturation of cardiac energy metabolism during perinatal development. *Front Physiol*. 2018;9:959.
213. Zhang H, Badur MG, Spiering S, Divakaruni A, Meurs NE, Yu MS, Colas AR, Murphy AN, Mercola M, Metallo CM. Lipid availability influences the metabolic maturation of human pluripotent stem cell-derived cardiomyocytes. *bioRxiv*. 2020;2020.03.14.991927.
214. Feyen DAM, McKeithan WL, Bruyneel AAN, Spiering S, Hörmann L, Ulmer B, Zhang H, Briganti F, Schweizer M, Hegyi B, Liao Z, Pölönen RP, Ginsburg KS, Lam CK, Serrano R, Wahlquist C, Kreymerman A, Vu M, Amatya PL, Behrens CS, Ranjbarvaziri S, Maas RGC, Greenhaw M, Bernstein D, Wu JC, Bers DM, Eschenhagen T, Metallo CM, Mercola M. Metabolic Maturation Media Improve Physiological Function of Human iPSC-Derived Cardiomyocytes. *Cell Rep*. 2020;32:107925.
215. Katrukha IA. Human cardiac troponin complex. structure and functions. *Biochem*. 2013;78:1447–1465.
216. Bedada FB, Chan SS-K, Metzger SK, Zhang L, Zhang J, Garry DJ, Kamp TJ, Kyba M, Metzger JM. Acquisition of a quantitative, stoichiometrically conserved ratiometric marker of maturation status in stem cell-derived cardiac myocytes. *Stem Cell Reports*. 2014;3:594–605.
217. Reiser PJ, Portman MA, Ning XH, Moravec CS. Human cardiac myosin heavy chain isoforms in fetal and failing adult atria and ventricles. *Am J Physiol - Heart Circ Physiol*. 2001;280.
218. Lahmers S, Wu Y, Call DR, Labeit S, Granzier H. Developmental Control of Titin

Isoform Expression and Passive Stiffness in Fetal and Neonatal Myocardium. *Circ Res*. 2004;94:505–513.

219. Denning C, Borgdorff V, Crutchley J, Firth KSA, George V, Kalra S, Kondrashov A, Hoang MD, Mosqueira D, Patel A, Prodanov L, Rajamohan D, Skarnes WC, Smith JGW, Young LE. Cardiomyocytes from human pluripotent stem cells: From laboratory curiosity to industrial biomedical platform. *Biochim Biophys Acta - Mol Cell Res*. 2016;1863:1728–1748.
220. Lewandowski J, Rozwadowska N, Kolanowski TJ, Malcher A, Zimna A, Rugowska A, Fiedorowicz K, Łabędź W, Kubaszewski Ł, Chojnacka K, Bednarek-Rajewska K, Majewski P, Kurpisz M. The impact of in vitro cell culture duration on the maturation of human cardiomyocytes derived from induced pluripotent stem cells of myogenic origin. *Cell Transplant*. 2018;27:1047–1067.
221. Egashira T, Yuasa S, Suzuki T, Aizawa Y, Yamakawa H, Matsuhashi T, Ohno Y, Tohyama S, Okata S, Seki T, Kuroda Y, Yae K, Hashimoto H, Tanaka T, Hattori F, Sato T, Miyoshi S, Takatsuki S, Murata M, Kurokawa J, Furukawa T, Makita N, Aiba T, Shimizu W, Horie M, Kamiya K, Kodama I, Ogawa S, Fukuda K. Disease characterization using LQTS-specific induced pluripotent stem cells. *Cardiovasc Res*. 2012;95:419–429.
222. Zhang M, D'Aniello C, Verkerk AO, Wrobel E, Frank S, Ward-Van Oostwaard D, Piccini I, Freund C, Rao J, Seebohm G, Atsma DE, Schulze-Bahr E, Mummery CL, Greber B, Bellin M. Recessive cardiac phenotypes in induced pluripotent stem cell models of Jervell and Lange-Nielsen syndrome: Disease mechanisms and pharmacological rescue. *Proc Natl Acad Sci USA*. 2014;111:E5383–E5392.
223. Ma D, Wei H, Lu J, Huang D, Liu Z, Loh LJ, Islam O, Liew R, Shim W, Cook SA. Characterization of a novel KCNQ1 mutation for type 1 long QT syndrome and assessment of the therapeutic potential of a novel IKs activator using patient-specific induced pluripotent stem cell-derived cardiomyocytes. *Stem Cell Res Ther*. 2015;6.
224. Kiviaho AL, Ahola A, Larsson K, Penttinen K, Swan H, Pekkanen-Mattila M, Venäläinen H, Paavola K, Hyttinen J, Aalto-Setälä K. Distinct electrophysiological and mechanical beating phenotypes of long QT syndrome type 1-specific cardiomyocytes carrying different mutations. *IJC Heart Vasc*. 2015;8:19–31.
225. Kuusela J, Larsson K, Shah D, Prajapati C, Aalto-Setala K. Low extracellular

potassium prolongs repolarization and evokes early after depolarization in human induced pluripotent stem cell-derived cardiomyocytes. *Biol Open*. 2017;6:777–784.

226. Wuriyanghai Y, Makiyama T, Sasaki K, Kamakura T, Yamamoto Y, Hayano M, Harita T, Nishiuchi S, Chen J, Kohjitani H, Hirose S, Yokoi F, Gao J, Chonabayashi K, Watanabe K, Ohno S, Yoshida Y, Kimura T, Horie M. Complex aberrant splicing in the induced pluripotent stem cell–derived cardiomyocytes from a patient with long QT syndrome carrying KCNQ1-A344Aspl mutation. *Heart Rhythm*. 2018;15:1566–1574.
227. Matsa E, Rajamohan D, Dick E, Young L, Mellor I, Staniforth A, Denning C. Drug evaluation in cardiomyocytes derived from human induced pluripotent stem cells carrying a long QT syndrome type 2 mutation. *Eur Heart J*. 2011;32:952–962.
228. Lahti AL, Kujala VJ, Chapman H, Koivisto A-P, Pekkanen-Mattila M, Kerkela E, Hyttinen J, Kontula K, Swan H, Conklin BR, Yamanaka S, Silvennoinen O, Aalto-Setala K. Model for long QT syndrome type 2 using human iPS cells demonstrates arrhythmogenic characteristics in cell culture. *Dis Model Mech*. 2012;5:220–230.
229. Bellin M, Casini S, Davis RP, D'Aniello C, Haas J, Ward-Van Oostwaard D, Tertoolen LGJ, Jung CB, Elliott DA, Welling A, Laugwitz KL, Moretti A, Mummery CL. Isogenic human pluripotent stem cell pairs reveal the role of a KCNH2 mutation in long-QT syndrome. *EMBO J*. 2013;32:3161–3175.
230. Matsa E, Dixon JE, Medway C, Georgiou O, Patel MJ, Morgan K, Kemp PJ, Staniforth A, Mellor I, Denning C. Allele-specific RNA interference rescues the long-QT syndrome phenotype in human-induced pluripotency stem cell cardiomyocytes. *Eur Heart J*. 2014;35:1078–1087.
231. Mehta A, Sequiera GL, Ramachandra CJ, Sudibyo Y, Chung Y, Sheng J, Wong KY, Tan TH, Wong P, Liew R, Shim W. Re-trafficking of hERG reverses long QT syndrome 2 phenotype in human iPS-derived cardiomyocytes. *Cardiovasc Res*. 2014;102:497–506.
232. Spencer CI, Baba S, Nakamura K, Hua EA, Sears MAF, Fu CC, Zhang J, Balijepalli S, Tomoda K, Hayashi Y, Lizarraga P, Wojciak J, Scheinman MM, Aalto-Setälä K, Makielski JC, January CT, Healy KE, Kamp TJ, Yamanaka S, Conklin BR. Calcium transients closely reflect prolonged action potentials in iPSC models of inherited cardiac arrhythmia. *Stem Cell Reports*. 2014;3:269–281.

233. Mehta A, Ramachandra CJA, Singh P, Chitre A, Lua CH, Mura M, Crotti L, Wong P, Schwartz PJ, Gnecchi M, Shim W. Identification of a targeted and testable antiarrhythmic therapy for long-QT syndrome type 2 using a patient-specific cellular model. *Eur Heart J*. 2018;39:1446–1455.

234. Shah D, Prajapati C, Penttinen K, Cherian RM, Koivumäki JT, Alexanova A, Hyttinen J, Aalto-Setälä K. hiPSC-Derived Cardiomyocyte Model of LQT2 Syndrome Derived from Asymptomatic and Symptomatic Mutation Carriers Reproduces Clinical Differences in Aggregates but Not in Single Cells. *Cells*. 2020;9.

235. Malan D, Friedrichs S, Fleischmann BK, Sasse P. Cardiomyocytes obtained from induced pluripotent stem cells with Long-QT syndrome 3 recapitulate typical disease-specific features in vitro. *Circ Res*. 2011;109:841–847.

236. Ma D, Wei H, Zhao Y, Lu J, Li G, Sahib NBE, Tan TH, Wong KY, Shim W, Wong P, Cook SA, Liew R. Modeling type 3 long QT syndrome with cardiomyocytes derived from patient-specific induced pluripotent stem cells. *Int J Cardiol*. 2013;168:5277–5286.

237. Fatima A, Kaifeng S, Dittmann S, Xu G, Gupta MK, Linke M, Zechner U, Nguemo F, Milting H, Farr M, Hescheler J, Šarić T. The disease-specific phenotype in cardiomyocytes derived from induced pluripotent stem cells of two long qt syndrome type 3 patients. *PLoS One*. 2013;8:83005.

238. Terrenoire C, Wang K, Chan Tung KW, Chung WK, Pass RH, Lu JT, Jean JC, Omari A, Sampson KJ, Kotton DN, Keller G, Kass RS. Induced pluripotent stem cells used to reveal drug actions in a long QT syndrome family with complex genetics. *J Gen Physiol*. 2013;141:61–72.

239. Malan D, Zhang M, Stallmeyer B, Müller J, Fleischmann BK, Schulze-Bahr E, Sasse P, Greber B. Human iPS cell model of type 3 long QT syndrome recapitulates drug-based phenotype correction. *Basic Res Cardiol*. 2016;111:1–11.

240. Portero V, Casini S, Hoekstra M, Verkerk AO, Mengarelli I, Belardinelli L, Rajamani S, Wilde AA, Bezzina CR, Veldkamp MW, Remme CA. Anti-arrhythmic potential of the late sodium current inhibitor GS-458967 in murine Scn5a-1798insD+/- and human SCN5A-1795insD+/- iPSC-derived cardiomyocytes. *Cardiovasc Res*. 2017;113:829–838.

241. Liang P, Sallam K, Wu H, Li Y, Itzhaki I, Garg P, Zhang Y, Vermglinchan V, Lan F, Gu M, Gong T, Zhuge Y, He C, Ebert AD, Sanchez-Freire V, Churko J, Hu S, Sharma A,

Lam CK, Scheinman MM, Bers DM, Wu JC. Patient-Specific and Genome-Edited Induced Pluripotent Stem Cell–Derived Cardiomyocytes Elucidate Single-Cell Phenotype of Brugada Syndrome. *J Am Coll Cardiol*. 2016;68:2086–2096.

242. Kosmidis G, Veerman CC, Casini S, Verkerk AO, Van De Pas S, Bellin M, Wilde AAM, Mummery CL, Bezzina CR. Readthrough-promoting drugs gentamicin and PTC124 Fail to Rescue Na v 1.5 function of human-induced pluripotent stem cell-derived cardiomyocytes carrying nonsense mutations in the sodium channel gene SCN5A. *Circ Arrhythmia Electrophysiol*. 2016;9.
243. Ma D, Liu Z, Loh LJ, Zhao Y, Li G, Liew R, Islam O, Wu J, Chung YY, Teo WS, Ching CK, Tan BY, Chong D, Ho KL, Lim P, Yong RYY, Panama BK, Kaplan AD, Bett GCL, Ware J, Bezzina CR, Verkerk AO, Cook SA, Rasmusson RL, Wei H. Identification of an I Na-dependent and I to-mediated proarrhythmic mechanism in cardiomyocytes derived from pluripotent stem cells of a Brugada syndrome patient. *Sci Rep*. 2018;8:11246.
244. Selga E, Sendfeld F, Martinez-Moreno R, Medine CN, Tura-Ceide O, Wilmut SI, Pérez GJ, Scornik FS, Brugada R, Mills NL. Sodium channel current loss of function in induced pluripotent stem cell-derived cardiomyocytes from a Brugada syndrome patient. *J Mol Cell Cardiol*. 2018;114:10–19.
245. de la Roche J, Angsutararux P, Kempf H, Janan M, Bolesani E, Thiemann S, Wojciechowski D, Coffee M, Franke A, Schwanke K, Leffler A, Luanpitpong S, Issaragrisil S, Fischer M, Zweigerdt R. Comparing human iPSC-cardiomyocytes versus HEK293T cells unveils disease-causing effects of Brugada mutation A735V of NaV1.5 sodium channels. *Sci Rep*. 2019;9:11173.
246. Li W, Stauske M, Luo X, Wagner S, Vollrath M, Mehnert CS, Schubert M, Cyganek L, Chen S, Hasheminasab SM, Wulf G, El-Armouche A, Maier LS, Hasenfuss G, Guan K. Disease Phenotypes and Mechanisms of iPSC-Derived Cardiomyocytes From Brugada Syndrome Patients With a Loss-of-Function SCN5A Mutation. *Front Cell Dev Biol*. 2020;8.
247. Miller DC, Harmer SC, Poliandri A, Nobles M, Edwards EC, Ware JS, Sharp T V., McKay TR, Dunkel L, Lambiase PD, Tinker A. Ajmaline blocks INa and IKr without eliciting differences between Brugada syndrome patient and control human pluripotent stem cell-derived cardiac clusters. *Stem Cell Res*. 2017;25:233–244.
248. Fatima A, Xu G, Shao K, Papadopoulos S, Lehmann M, Arnáiz-Cot JJ, Rosa AO,

Nguemo F, Matzkies M, Dittmann S, Stone SL, Linke M, Zechner U, Beyer V, Hennies HC, Rosenkranz S, Klauke B, Parwani AS, Haverkamp W, Pfitzer G, Farr M, Cleemann L, Morad M, Milting H, Hescheler J, Šaric T. In vitro Modeling of Ryanodine Receptor 2 Dysfunction Using Human Induced Pluripotent Stem Cells. *Cell Physiol Biochem*. 2011;28:579.

249. Park SJ, Zhang D, Qi Y, Li Y, Lee KY, Bezzerides VJ, Yang P, Xia S, Kim SL, Liu X, Lu F, Pasqualini FS, Campbell PH, Geva J, Roberts AE, Kleber AG, Abrams DJ, Pu WT, Parker KK. Insights into the Pathogenesis of Catecholaminergic Polymorphic Ventricular Tachycardia from Engineered Human Heart Tissue. *Circulation*. 2019;140:390–404.
250. Kujala K, Paavola J, Lahti A, Larsson K, Pekkanen-Mattila M, Viitasalo M, Lahtinen AM, Toivonen L, Kontula K, Swan H, Laine M, Silvennoinen O, Aalto-Setälä K. Cell Model of Catecholaminergic Polymorphic Ventricular Tachycardia Reveals Early and Delayed Afterdepolarizations. *PLoS One*. 2012;7.
251. Jung CB, Moretti A, Mederos y Schnitzler M, Iop L, Storch U, Bellin M, Dorn T, Ruppenthal S, Pfeiffer S, Goedel A, Dirschinger RJ, Seyfarth M, Lam JT, Sinnecker D, Gudermann T, Lipp P, Laugwitz KL. Dantrolene rescues arrhythmogenic RYR2 defect in a patient-specific stem cell model of catecholaminergic polymorphic ventricular tachycardia. *EMBO Mol Med*. 2012;4:180–191.
252. Di Pasquale E, Lodola F, Miragoli M, Denegri M, Avelino-Cruz JE, Buonocore M, Nakahama H, Portararo P, Bloise R, Napolitano C, Condorelli G, Priori SG. CaMKII inhibition rectifies arrhythmic phenotype in a patient-specific model of catecholaminergic polymorphic ventricular tachycardia. *Cell Death Dis*. 2013;4:843.
253. Zhang XH, Haviland S, Wei H, Šarić T, Fatima A, Hescheler J, Cleemann L, Morad M. Ca2+ signaling in human induced pluripotent stem cell-derived cardiomyocytes (iPS-CM) from normal and catecholaminergic polymorphic ventricular tachycardia (CPVT)-afflicted subjects. *Cell Calcium*. 2013;54:57–70.
254. Penttinen K, Swan H, Vanninen S, Paavola J, Lahtinen AM, Kontula K, Aalto-Setälä K. Antiarrhythmic effects of dantrolene in patients with catecholaminergic polymorphic ventricular tachycardia and replication of the responses using iPSC models. *PLoS One*. 2015;10:125366.
255. Paavola J, Väänänen H, Larsson K, Penttinen K, Toivonen L, Kontula K, Laine M,

Aalto-Setälä K, Swan H, Viitasalo M. Slowed depolarization and irregular repolarization in catecholaminergic polymorphic ventricular tachycardia: A study from cellular Ca2+ transients and action potentials to clinical monophasic action potentials and electrocardiography. *Europace*. 2016;18:1599–1607.

256. Preininger MK, Jha R, Maxwell JT, Wu Q, Singh M, Wang B, Dalal A, Mceachin ZT, Rossoll W, Hales CM, Fischbach PS, Wagner MB, Xu C. A human pluripotent stem cell model of catecholaminergic polymorphic ventricular tachycardia recapitulates patient-specific drug responses. *Dis Model Mech*. 2016;9:927–939.
257. Pölönen RP, Swan H, Aalto-Setälä K. Mutation-specific differences in arrhythmias and drug responses in CPVT patients: simultaneous patch clamp and video imaging of iPSC derived cardiomyocytes. *Mol Biol Rep*. 2020;47:1067–1077.
258. Bohnen MS, Peng G, Robey SH, Terrenoire C, Iyer V, Sampson KJ, Kass RS. Molecular pathophysiology of congenital long QT syndrome. *Physiol Rev*. 2017;97:89–134.
259. Mannhardt I, Breckwoldt K, Letuffe-Brenière D, Schaaf S, Schulz H, Neuber C, Benzin A, Werner T, Eder A, Schulze T, Klampe B, Christ T, Hirt MN, Huebner N, Moretti A, Eschenhagen T, Hansen A. Human Engineered Heart Tissue: Analysis of Contractile Force. *Stem Cell Reports*. 2016;7:29–42.
260. Peters NS, Severs NJ, Rothery SM, Lincoln C, Yacoub MH, Green CR. Spatiotemporal relation between gap junctions and fascia adherens junctions during postnatal development of human ventricular myocardium. *Circulation*. 1994;90:713–725.
261. Bergmann O, Bhardwaj RD, Bernard S, Zdunek S, Barnabé-Heider F, Walsh S, Zupicich J, Alkass K, Buchholz BA, Druid H, Jovinge S, Frisén J. Evidence for cardiomyocyte renewal in humans. *Science*. 2009;324:98–102.
262. Vreeker A, Van Stuijvenberg L, Hund TJ, Mohler PJ, Nikkels PGJ, Van Veen TAB. Assembly of the cardiac intercalated disk during pre and postnatal development of the human heart. *PLoS One*. 2014;9.
263. Kamakura T, Makiyama T, Sasaki K, Yoshida Y, Wuriyanghai Y, Chen J, Hattori T, Ohno S, Kita T, Horie M, Yamanaka S, Kimura T. Ultrastructural maturation of human-induced pluripotent stem cell-derived cardiomyocytes in a long-term culture. *Circ J*. 2013;77:1307–1314.
264. Wu H, Lee J, Vincent LG, Wang Q, Gu M, Lan F, Churko JM, Sallam KI, Matsa E,

Sharma A, Gold JD, Engler AJ, Xiang YK, Bers DM, Wu JC. Epigenetic Regulation of Phosphodiesterases 2A and 3A Underlies Compromised β-adrenergic Signaling in an iPSC Model of Dilated Cardiomyopathy. *Cell Stem Cell*. 2015;17:89–100.

265. Lundy SD, Zhu W-Z, Regnier M, Laflamme MA. Structural and Functional Maturation of Cardiomyocytes Derived from Human Pluripotent Stem Cells. *Stem Cells Dev*. 2013;22:1991–2002.
266. Hasan A, Mohammadi N, Nawaz A, Kodagoda T, Diakonov I, Harding SE, Gorelik J. Age-Dependent Maturation of iPSC-CMs Leads to the Enhanced Compartmentation of β2AR-cAMP Signalling. *Cells*. 2020;9.
267. Li M, Iismaa SE, Naqvi N, Nicks A, Husain A, Graham RM. Thyroid hormone action in postnatal heart development. *Stem Cell Res*. 2014;13:582–591.
268. Klein I, Ojamaa K. Thyroid Hormone and the Cardiovascular System. *N Engl J Med*. 2001;344.
269. Ivashchenko CY, Pipes GC, Lozinskaya IM, Lin Z, Xiaoping X, Needle S, Grygielko ET, Hu E, Toomey JR, Lepore JJ, Willette RN. Human-induced pluripotent stem cell-derived cardiomyocytes exhibit temporal changes in phenotype. *Am J Physiol - Heart Circ Physiol*. 2013;305:913–922.
270. Yang X, Rodriguez M, Pabon L, Fischer KA, Reinecke H, Regnier M, Sniadecki NJ, Ruohola-Baker H, Murry CE. Tri-iodo-l-thyronine promotes the maturation of human cardiomyocytes-derived from induced pluripotent stem cells. *J Mol Cell Cardiol*. 2014;72:296–304.
271. Birket MJ, Ribeiro MC, Kosmidis G, Ward D, Leitoguinho AR, van de Pol V, Dambrot C, Devalla HD, Davis RP, Mastroberardino PG, Atsma DE, Passier R, Mummery CL. Contractile Defect Caused by Mutation in MYBPC3 Revealed under Conditions Optimized for Human PSC-Cardiomyocyte Function. *Cell Rep*. 2015;13:733–745.
272. Fowden AL, Li J, Forhead AJ. Glucocorticoids and the preparation for life after birth: are there long-term consequences of the life insurance? *Proc Nutr Soc*. 1998;57:113–122.
273. Rog-Zielinska EA, Thomson A, Kenyon CJ, Brownstein DG, Moran CM, Szumska D, Michailidou Z, Richardson J, Owen E, Watt A, Morrison H, Forrester LM, Bhattacharya S, Holmes MC, Chapman KE. Glucocorticoid receptor is required for foetal heart maturation. *Hum Mol Genet*. 2013;22:3269–3282.
274. Rog-Zielinska EA, Craig MA, Manning JR, Richardson R V., Gowans GJ, Dunbar DR,

Gharbi K, Kenyon CJ, Holmes MC, Hardie DG, Smith GL, Chapman KE. Glucocorticoids promote structural and functional maturation of foetal cardiomyocytes: A role for PGC-1α. *Cell Death Differ*. 2015;22:1106–1116.

275. Kosmidis G, Bellin M, Ribeiro MC, Van Meer B, Ward-Van Oostwaard D, Passier R, Tertoolen LGJ, Mummery CL, Casini S. Altered calcium handling and increased contraction force in human embryonic stem cell derived cardiomyocytes following short term dexamethasone exposure. *Biochem Biophys Res Commun*. 2015;467:998–1005.
276. Yang X, Rodriguez ML, Leonard A, Sun L, Fischer KA, Wang Y, Ritterhoff J, Zhao L, Kolwicz SC, Pabon L, Reinecke H, Sniadecki NJ, Tian R, Ruohola-Baker H, Xu H, Murry CE. Fatty Acids Enhance the Maturation of Cardiomyocytes Derived from Human Pluripotent Stem Cells. *Stem Cell Reports*. 2019;13:657–668.
277. Bergmann O, Zdunek S, Felker A, Salehpour M, Alkass K, Bernard S, Sjostrom SL, Szewczykowska M, Jackowska T, Dos Remedios C, Malm T, Andrä M, Jashari R, Nyengaard JR, Possnert G, Jovinge S, Druid H, Frisén J. Dynamics of Cell Generation and Turnover in the Human Heart. *Cell*. 2015;161:1566–1575.
278. Zhou P, Pu WT. Recounting cardiac cellular composition. *Circ Res.* 2016;118:368–370.
279. Xuan Y, Chen C, Wen Z, Wang DW. The Roles of Cardiac Fibroblasts and Endothelial Cells in Myocarditis. *Front Cardiovasc Med*. 2022;9:882027.
280. Yoshida S, Miyagawa S, Fukushima S, Kawamura T, Kashiyama N, Ohashi F, Toyofuku T, Toda K, Sawa Y. Maturation of Human Induced Pluripotent Stem Cell-Derived Cardiomyocytes by Soluble Factors from Human Mesenchymal Stem Cells. *Mol Ther*. 2018;26:2681–2695.
281. Abecasis B, Gomes-Alves P, Rosa S, Gouveia PJ, Ferreira L, Serra M, Alves PM. Unveiling the molecular crosstalk in a human induced pluripotent stem cell-derived cardiac model. *Biotechnol Bioeng*. 2019;116:1245–1252.
282. Giacomelli E, Meraviglia V, Campostrini G, Cochrane A, Cao X, van Helden RWJ, Krotenberg Garcia A, Mircea M, Kostidis S, Davis RP, van Meer BJ, Jost CR, Koster AJ, Mei H, Míguez DG, Mulder AA, Ledesma-Terrón M, Pompilio G, Sala L, Salvatori DCF, Slieker RC, Sommariva E, de Vries AAF, Giera M, Semrau S, Tertoolen LGJ, Orlova V V., Bellin M, Mummery CL. Human-iPSC-Derived Cardiac Stromal Cells Enhance Maturation in 3D Cardiac Microtissues and Reveal Non-cardiomyocyte

Contributions to Heart Disease. *Cell Stem Cell*. 2020;26:862-879.e11.

283. Ribeiro AJS, Ang Y-S, Fu J-D, Rivas RN, Mohamed TMA, Higgs GC, Srivastava D, Pruitt BL. Contractility of single cardiomyocytes differentiated from pluripotent stem cells depends on physiological shape and substrate stiffness. *Proc Natl Acad Sci*. 2015;112:12705–12710.

284. Feaster TK, Cadar AG, Wang L, Williams CH, Chun YW, Hempel J, Bloodworth N, Merryman WD, Lim CC, Wu JC, Knollmann BC, Hong CC. Matrigel mattress: A method for the generation of single contracting human-induced pluripotent stem cell-derived cardiomyocytes. *Circ Res*. 2015;

285. Kim DH, Lipke EA, Kim P, Cheong R, Thompson S, Delannoy M, Suh KY, Tung L, Levchenko A. Nanoscale cues regulate the structure and function of macroscopic cardiac tissue constructs. *Proc Natl Acad Sci*. 2010;107:565–570.

286. Carson D, Hnilova M, Yang X, Nemeth CL, Tsui JH, Smith AST, Jiao A, Regnier M, Murry CE, Tamerler C, Kim DH. Nanotopography-Induced Structural Anisotropy and Sarcomere Development in Human Cardiomyocytes Derived from Induced Pluripotent Stem Cells. *ACS Appl Mater Interfaces*. 2016;8:21923–21932.

287. Eder A, Vollert I, Hansen A, Eschenhagen T. Human engineered heart tissue as a model system for drug testing. *Adv Drug Deliv Rev*. 2016;96:214–224.

288. Tulloch NL, Muskheli V, Razumova M V, Korte FS, Regnier M, Hauch KD, Pabon L, Reinecke H, Murry CE. Growth of engineered human myocardium with mechanical loading and vascular coculture. *Circ Res*. 2011;109:47–59.

289. Uzun AU, Mannhardt I, Breckwoldt K, Horváth A, Johannsen SS, Hansen A, Eschenhagen T, Christ T. Ca2+-currents in human induced pluripotent stem cell-derived cardiomyocytes effects of two different culture conditions. *Front Pharmacol*. 2016;7:300.

290. Lemoine MD, Mannhardt I, Breckwoldt K, Prondzynski M, Flenner F, Ulmer B, Hirt MN, Neuber C, Horváth A, Kloth B, Reichenspurner H, Willems S, Hansen A, Eschenhagen T, Christ T. Human iPSC-derived cardiomyocytes cultured in 3D engineered heart tissue show physiological upstroke velocity and sodium current density. *Sci Rep*. 2017;7.

291. Correia C, Koshkin A, Duarte P, Hu D, Carido M, Sebastião MJ, Gomes-Alves P, Elliott DA, Domian IJ, Teixeira AP, Alves PM, Serra M. 3D aggregate culture improves metabolic maturation of human pluripotent stem cell derived

cardiomyocytes. *Biotechnol Bioeng*. 2018;115:630–644.

292. Ulmer BM, Stoehr A, Schulze ML, Patel S, Gucek M, Mannhardt I, Funcke S, Murphy E, Eschenhagen T, Hansen A. Contractile Work Contributes to Maturation of Energy Metabolism in hiPSC-Derived Cardiomyocytes. *Stem Cell Reports*. 2018;10:834–847.
293. Nunes SS, Miklas JW, Liu J, Aschar-Sobbi R, Xiao Y, Zhang B, Jiang J, Massé S, Gagliardi M, Hsieh A, Thavandiran N, Laflamme MA, Nanthakumar K, Gross GJ, Backx PH, Keller G, Radisic M. Biowire: A platform for maturation of human pluripotent stem cell-derived cardiomyocytes. *Nat Methods*. 2013;10:781–787.
294. Ronaldson-Bouchard K, Ma SP, Yeager K, Chen T, Song LJ, Sirabella D, Morikawa K, Teles D, Yazawa M, Vunjak-Novakovic G. Advanced maturation of human cardiac tissue grown from pluripotent stem cells. *Nature*. 2018;556:239–243.
295. Lu K, Seidel T, Cao-Ehlker X, Dorn T, Batcha AMN, Schneider CM, Semmler M, Volk T, Moretti A, Dendorfer A, Tomasi R. Progressive stretch enhances growth and maturation of 3D stem-cell-derived myocardium. *Theranostics*. 2021;11:6138–6153.
296. Tohyama S, Hattori F, Sano M, Hishiki T, Nagahata Y, Matsuura T, Hashimoto H, Suzuki T, Yamashita H, Satoh Y, Egashira T, Seki T, Muraoka N, Yamakawa H, Ohgino Y, Tanaka T, Yoichi M, Yuasa S, Murata M, Suematsu M, Fukuda K. Distinct Metabolic Flow Enables Large-Scale Purification of Mouse and Human Pluripotent Stem Cell-Derived Cardiomyocytes. *Cell Stem Cell*. 2013;12:127–137.
297. Ruijter JM, Ramakers C, Hoogaars WMH, Karlen Y, Bakker O, van den hoff MJB, Moorman AFM. Amplification efficiency: linking baseline and bias in the analysis of quantitative PCR data. *Nucleic Acids Res*. 2009;37:e45.
298. Ramos K, Acosta D. Prevention by L(-) ascorbic acid of isoproterenol-induced cardiotoxicity in primary cultures of rat myocytes. 1983.
299. Greensmith DJ. Ca analysis: An excel based program for the analysis of intracellular calcium transients including multiple, simultaneous regression analysis. *Comput Methods Programs Biomed*. 2014;113:241–250.
300. Hopton C. Using human induced pluripotent stem cells to characterise a novel nonsense variant in RYR2. PhD thesis. University of Manchester. 2019.
301. Smith A. Design principles of pluripotency. *EMBO Mol Med*. 2009;1:251.
302. Schleich JM, Abdulla T, Summers R, Houyel L. An overview of cardiac

morphogenesis. *Arch Cardiovasc Dis*. 2013;106:612–623.

303. Naito AT, Shiojima I, Akazawa H, Hidaka K, Morisaki T, Kikuchi A, Komuro I. Developmental stage-specific biphasic roles of Wnt/β-catenin signaling in cardiomyogenesis and hematopoiesis. *Proc Natl Acad Sci USA*. 2006;103:19812–19817.
304. Huang TS, Li L, Moalim-Nour L, Jia D, Bai J, Yao Z, Bennett SAL, Figeys D, Wang L. A regulatory network involving β-catenin, e-Cadherin, PI3k/Akt, and slug balances self-renewal and differentiation of human pluripotent stem cells in response to wnt signaling. *Stem Cells*. 2015;33:1419–1433.
305. Rao J, Pfeiffer MJ, Frank S, Adachi K, Piccini I, Quaranta R, Araúzo-Bravo M, Schwarz J, Schade D, Leidel S, Schöler HR, Seebohm G, Greber B. Stepwise Clearance of Repressive Roadblocks Drives Cardiac Induction in Human ESCs. *Cell Stem Cell*. 2016;18:341–353.
306. Freund C, Ward-van Oostwaard D, Monshouwer-Kloots J, van den Brink S, van Rooijen M, Xu X, Zweigerdt R, Mummery C, Passier R. Insulin redirects differentiation from cardiogenic mesoderm and endoderm to neuroectoderm in differentiating human embryonic stem cells. *Stem Cells*. 2008;26:724–733.
307. Brewer GJ, Cotman CW. Survival and growth of hippocampal neurons in defined medium at low density: advantages of a sandwich culture technique or low oxygen. *Brain Res*. 1989;494:65–74.
308. Hellemans J, Mortier G, De Paepe A, Speleman F, Vandesompele J. qBase relative quantification framework and software for management and automated analysis of real-time quantitative PCR data. *Genome Biol*. 2007;8:R19.
309. Inamura M, Kawabata K, Takayama K, Tashiro K, Sakurai F, Katayama K, Toyoda M, Akutsu H, Miyagawa Y, Okita H, Kiyokawa N, Umezawa A, Hayakawa T, Furue MK, Mizuguchi H. Efficient Generation of Hepatoblasts From Human ES Cells and iPS Cells by Transient Overexpression of Homeobox Gene HEX. *Mol Ther*. 2011;19:400.
310. Patsch C, Challet-Meylan L, Thoma EC, Urich E, Heckel T, O'Sullivan JF, Grainger SJ, Kapp FG, Sun L, Christensen K, Xia Y, Florido MHC, He W, Pan W, Prummer M, Warren CR, Jakob-Roetne R, Certa U, Jagasia R, Freskgard PO, Adatto I, Kling D, Huang P, Zon LI, Chaikof EL, Gerszten RE, Graf M, Iacone R, Cowan CA. Generation of vascular endothelial and smooth muscle cells from human pluripotent stem

cells. *Nat Cell Biol*. 2015;17:994–1003.

311. Fernandopulle MS, Prestil R, Grunseich C, Wang C, Gan L, Ward ME. Transcription Factor–Mediated Differentiation of Human iPSCs into Neurons. *Curr Protoc Cell Biol*. 2018;79.
312. Zujur D, Kanke K, Onodera S, Tani S, Lai J, Azuma T, Xin X, Lichtler AC, Rowe DW, Saito T, Tanaka S, Masaki H, Nakauchi H, Chung U il, Hojo H, Ohba S. Stepwise strategy for generating osteoblasts from human pluripotent stem cells under fully defined xeno-free conditions with small-molecule inducers. *Regen Ther*. 2020;14:19–31.
313. Iriguchi S, Yasui Y, Kawai Y, Arima S, Kunitomo M, Sato T, Ueda T, Minagawa A, Mishima Y, Yanagawa N, Baba Y, Miyake Y, Nakayama K, Takiguchi M, Shinohara T, Nakatsura T, Yasukawa M, Kassai Y, Hayashi A, Kaneko S. A clinically applicable and scalable method to regenerate T-cells from iPSCs for off-the-shelf T-cell immunotherapy. *Nat Commun*. 2021;12.
314. Gupta P, Hourigan K, Jadhav S, Bellare J, Verma P. Effect of lactate and pH on mouse pluripotent stem cells: Importance of media analysis. *Biochem Eng J*. 2017;118:25–33.
315. Holmgren G, Ghosheh N, Zeng X, Bogestål Y, Sartipy P, Synnergren J. Identification of stable reference genes in differentiating human pluripotent stem cells. *Physiol Genomics*. 2015;47:232–239.
316. Vandesompele J, De Preter K, Pattyn F, Poppe B, Van Roy N, De Paepe A, Speleman F. Accurate normalization of real-time quantitative RT-PCR data by geometric averaging of multiple internal control genes. *Genome Biol*. 2002;3.
317. Passier R, Oostwaard DW, Snapper J, Kloots J, Hassink RJ, Kuijk E, Roelen B, Riviere AB de la, Mummery C. Increased Cardiomyocyte Differentiation from Human Embryonic Stem Cells in Serum-Free Cultures. *Stem Cells*. 2005;23:772–780.
318. Zhao X, Chen H, Xiao D, Yang H, Itzhaki I, Qin X, Chour T, Aguirre A, Lehmann K, Kim Y, Shukla P, Holmström A, Zhang JZ, Zhuge Y, Ndoye BC, Zhao M, Neofytou E, Zimmermann WH, Jain M, Wu JC. Comparison of Non-human Primate versus Human Induced Pluripotent Stem Cell-Derived Cardiomyocytes for Treatment of Myocardial Infarction. *Stem Cell Reports*. 2018;10:422–435.
319. Zhang JZ, Termglinchan V, Shao NY, Itzhaki I, Liu C, Ma N, Tian L, Wang VY, Chang ACY, Guo H, Kitani T, Wu H, Lam CK, Kodo K, Sayed N, Blau HM, Wu JC. A human

iPSC double reporter system enables purification of cardiac lineage subpopulations with distinct function and drug response profiles. *Cell Stem Cell*. 2019;24:802.

320. Kitani T, Ong SG, Lam CK, Rhee JW, Zhang JZ, Oikonomopoulos A, Ma N, Tian L, Lee J, Telli ML, Witteles RM, Sharma A, Sayed N, Wu JC. Human-Induced Pluripotent Stem Cell Model of Trastuzumab-Induced Cardiac Dysfunction in Patients with Breast Cancer. *Circulation*. 2019;139:2451–2465.
321. Yang H, Shao N, Holmström A, Zhao X, Chour T, Chen H, Itzhaki I, Wu H, Ameen M, Cunningham NJ, Tu C, Zhao MT, Tarantal AF, Abilez OJ, Wu JC. Transcriptome analysis of non human primate-induced pluripotent stem cell-derived cardiomyocytes in 2D monolayer culture vs. 3D engineered heart tissue. *Cardiovasc Res*. 2021;117:2125–2136.
322. Jacobs K, Zambelli F, Mertzanidou A, Smolders I, Geens M, Nguyen HT, Barbé L, Sermon K, Spits C. Higher-Density Culture in Human Embryonic Stem Cells Results in DNA Damage and Genome Instability. *Stem Cell Reports*. 2016;6:330–341.
323. Devalla HD, Schwach V, Ford JW, Milnes JT, El-Haou S, Jackson C, Gkatzis K, Elliott DA, Chuva de Sousa Lopes SM, Mummery CL, Verkerk AO, Passier R. Atrial-like cardiomyocytes from human pluripotent stem cells are a robust preclinical model for assessing atrial-selective pharmacology. *EMBO Mol Med*. 2015;7:394–410.
324. Ren J, Han P, Ma X, Farah EN, Bloomekatz J, Zeng XXI, Zhang R, Swim MM, Witty AD, Knight HG, Deshpande R, Xu W, Yelon D, Chen S, Chi NC. Canonical Wnt5b signaling directs outlying Nkx2.5+ mesoderm into pacemaker cardiomyocytes. *Dev Cell*. 2019;50:729.
325. Kleinsorge M, Cyganek L. Subtype-Directed Differentiation of Human iPSCs into Atrial and Ventricular Cardiomyocytes. *STAR Protoc*. 2020;1:100026.
326. Ulmer BM, Eschenhagen T. Human pluripotent stem cell-derived cardiomyocytes for studying energy metabolism. *Biochim Biophys Acta Mol Cell Res*. 2020;1867.
327. Wleklinski MJ, Kannankeril PJ, Knollmann BC. Molecular and tissue mechanisms of catecholaminergic polymorphic ventricular tachycardia. *Journal of Physiology*. 2020:2817–2834.
328. Liang P, Lan F, Lee AS, Gong T, Sanchez-Freire V, Wang Y, Diecke S, Sallam K, Knowles JW, Wang PJ, Nguyen PK, Bers DM, Robbins RC, Wu JC. Drug screening using a library of human induced pluripotent stem cell-derived cardiomyocytes

reveals disease-specific patterns of cardiotoxicity. *Circulation*. 2013;127:1677–1691.

329. Zhao Z, Lan H, El-Battrawy I, Li X, Buljubasic F, Sattler K, Yücel G, Lang S, Tiburcy M, Zimmermann WH, Cyganek L, Utikal J, Wieland T, Borggrefe M, Zhou XB, Akin I. Ion Channel Expression and Characterization in Human Induced Pluripotent Stem Cell-Derived Cardiomyocytes. *Stem Cells Int*. 2018;2018.
330. Kodama M, Furutani K, Kimura R, Ando T, Sakamoto K, Nagamori S, Ashihara T, Kurachi Y, Sekino Y, Furukawa T, Kanda Y, Kurokawa J. Systematic expression analysis of genes related to generation of action potentials in human iPS cell-derived cardiomyocytes. *J Pharmacol Sci*. 2019;140:325–330.
331. Goversen B, van der Heyden MAG, van Veen TAB, de Boer TP. The immature electrophysiological phenotype of iPSC-CMs still hampers in vitro drug screening: Special focus on IK1. *Pharmacol Ther*. 2018;183:127–136.
332. Germanguz I, Sedan O, Zeevi-Levin N, Shtrichman R, Barak E, Ziskind A, Eliyahu S, Meiry G, Amit M, Itskovitz-Eldor J, Binah O. Molecular characterization and functional properties of cardiomyocytes derived from human inducible pluripotent stem cells. *J Cell Mol Med*. 2011;15:38–51.
333. Sasaki K, Makiyama T, Yoshida Y, Wuriyanghai Y, Kamakura T, Nishiuchi S, Hayano M, Harita T, Yamamoto Y, Kohjitani H, Hirose S, Chen J, Kawamura M, Ohno S, Itoh H, Takeuchi A, Matsuoka S, Miura M, Sumitomo N, Horie M, Yamanaka S, Kimura T. Patient-specific human induced pluripotent stem cell model assessed with electrical pacing validates S107 as a potential therapeutic agent for catecholaminergic polymorphic ventricular tachycardia. *PLoS One*. 2016;11.
334. Klein I, Danzi S. Thyroid Disease and the Heart. *Curr Probl Cardiol*. 2016;41:65–92.
335. Brent GA. The Molecular Basis of Thyroid Hormone Action. *N Engl J Med*. 1994;331:847–853.
336. Klein I, Danzi S. Thyroid disease and the heart . *Circulation*. 2007;116:1725–1735.
337. Davis PJ, Davis FB. Nongenomic Actions of Thyroid Hormone on the Heart. *Thyroid*. 2002;12.
338. Hofhuis J, Bersch K, Büssenschütt R, Drzymalski M, Liebetanz D, Nikolaev VO, Wagner S, Maier LS, Gärtner J, Klinge L, Thoms S. Dysferlin mediates membrane tubulation and links T-tubule biogenesis to muscular dystrophy. *J Cell Sci*. 2017;130:841–852.

339. Hofhuis J, Bersch K, Wagner S, Molina C, Fakuade FE, Iyer LM, Streckfuss-Bömeke K, Toischer K, Zelarayán LC, Voigt N, Nikolaev VO, Maier LS, Klinge L, Thoms S. Dysferlin links excitation-contraction coupling to structure and maintenance of the cardiac transverse-axial tubule system. *Europace*. 2020;22:1119–1131.

340. Caldwell JL, Smith CER, Taylor RF, Kitmitto A, Eisner DA, Dibb KM, Trafford AW. Dependence of cardiac transverse tubules on the BAR domain protein amphiphysin II (BIN-1). *Circ Res*. 2014;115:986–996.

341. De La Mata A, Tajada S, O'Dwyer S, Matsumoto C, Dixon RE, Hariharan N, Moreno CM, Santana LF. BIN1 Induces the Formation of T-Tubules and Adult-Like Ca 2+ Release Units in Developing Cardiomyocytes. *Stem Cells*. 2019;37:54–64.

342. Reynolds JO, Chiang DY, Wang W, Beavers DL, Dixit SS, Skapura DG, Landstrom AP, Song LS, Ackerman MJ, Wehrens XHT. Junctophilin-2 is necessary for T-tubule maturation during mouse heart development. *Cardiovasc Res*. 2013;100:44–53.

343. Chen B, Guo A, Zhang C, Chen R, Zhu Y, Hong J, Kutschke W, Zimmerman K, Weiss RM, Zingman L, Anderson ME, Wehrens XHT, Song LS. Critical roles of junctophilin-2 in T-tubule and excitation-contraction coupling maturation during postnatal development. *Cardiovasc Res*. 2013;100:54–62.

344. Poulet C, Sanchez-Alonso J, Swiatlowska P, Mouy F, Lucarelli C, Alvarez-Laviada A, Gross P, Terracciano C, Houser S, Gorelik J. Junctophilin-2 tethers T-tubules and recruits functional L-type calcium channels to lipid rafts in adult cardiomyocytes. *Cardiovasc Res*. 2021;117:149–161.

345. Bilezikian JP, Loeb JN. The Influence of Hyperthyroidism and Hypothyroidism on α and β-Adrenergic Receptor Systems and Adrenergic Responsiveness. *Endocr Rev*. 1983;4:378–388.

346. Hoit BD, Khoury SF, Shao Y, Gabel M, Liggett SB, Walsh RA. Effects of thyroid hormone on cardiac β-adrenergic responsiveness in conscious baboons. *Circulation*. 1997;96:592–598.

347. Liggett SB, Shah SD, Cryer PE. Increased fat and skeletal muscle β-adrenergic receptors but unaltered metabolic and hemodynamic sensitivitiy to epinephrine in vivo in experimental human thyrotoxicosis. *J Clin Invest*. 1989;83:803–809.

348. Revelli JP, Pescini R, Muzzin P, Seydoux J, Fitzgerald MG, Fraser CM, Giacobino JP. Changes in β1-and β2-adrenergic receptor mRNA levels in brown adipose tissue and heart of hypothyroid rats. *Biochem J*. 1991;277:625–629.

349. Kawano F, Tanihata J, Sato S, Nomura S, Shiraishi A, Tachiyashiki K, Imaizumi K. Effects of dexamethasone on the expression of β1-, β2- and β3-adrenoceptor mRNAs in skeletal and left ventricle muscles in rats. *J Physiol Sci*. 2009;59:383–390.

350. Mysliveček J, Říčný J, Kolář F, Tuček S. The effects of hydrocortisone on rat heart muscarinic and adrenergic α1, β1 and β2 receptors, propranolol-resistant binding sites and on some subsequent steps in intracellular signalling. *Naunyn Schmiedebergs Arch Pharmacol*. 2003;368:366–376.

351. Dangel V, Giray J, Ratge D, Wisser H. Regulation of β-adrenoceptor density and mRNA levels in the rat heart cell-line H9c2. *Biochem J*. 1996;317:925–931.

352. Bristow MR, Ginsburg R, Umans V, Fowler M, Minobe W, Rasmussen R, Zera P, Menlove R, Shah P, Jamieson S. β1- and β2-adrenergic-receptor subpopulations in nonfailing and failing human ventricular myocardium: Coupling of both receptor subtypes to muscle contraction and selective β1-receptor down-regulation in heart failure. *Circ Res*. 1986;59:297–309.

353. Steinfath M, Lavicky J, Schmitz W, Scholz H, Döring V, Kalmár P. Regional distribution of β1- and β2-adrenoceptors in the failing and nonfailing human heart. *Eur J Clin Pharmacol*. 1992;42:607–611.

354. Yiu A, Woo H, Xiao R-P. β-Adrenergic receptor subtype signaling in heart: From bench to bedside. *Acta Pharmacol Sin*. 2012;33:335–341.

355. Sassone-Corsi P. The Cyclic AMP pathway. *Cold Spring Harb Perspect Biol*. 2012;4.

356. Boularan C, Gales C. Cardiac cAMP: Production, hydrolysis, modulation and detection. *Front Pharmacol*. 2015;6.

357. Hutchings D, Anderson S, Caldwell J, Trafford A. Phosphodiesterase-5 inhibitors and the heart: compound cardioprotection? *Heart*. 2018;104:1244–1250.

358. Ojamaa K, Klein I, Sabet A, Steinburg SF. Changes in adenylyl cyclase isoforms as a mechanism for thyroid hormone modulation of cardiac β-adrenergic receptor responsiveness. *Metab - Clin Exp*. 2000;49:275/279.

359. Carvalho-Bianco SD, Kim BW, Zhang JX, Harney JW, Ribeiro RS, Gereben B, Bianco AC, Mende U, Larsen PR. Chronic cardiac-specific thyrotoxicosis increases myocardial β-adrenergic responsiveness. *Mol Endocrinol*. 2004;18:1840–1849.

360. DuBell WH, Lederer WJ, Rogers TB. Dynamic modulation of excitation-contraction coupling by protein phosphatases in rat ventricular myocytes. *J Physiol*.

1996;493:793–800.

361. Ke Y, Wang L, Pyle WG, De Tombe PP, Solaro RJ. Intracellular Localization and Functional Effects of P 21-Activated Kinase-1 (Pak1) in Cardiac Myocytes. *Circ Res*. 2004;94:194–200.

362. Ke Y, Sheehan KA, Egom EEA, Lei M, Solaro RJ. Novel bradykinin signaling in adult rat cardiac myocytes through activation of p21-activated kinase. *Am J Physiol - Heart Circ Physiol*. 2010;298:H1283.

363. Wang Y, Tsui H, Ke Y, Shi Y, Li Y, Davies L, Cartwright EJ, Venetucci L, Zhang H, Terrar DA, Huang CLH, Solaro RJ, Wang X, Lei M. Pak1 is required to maintain ventricular Ca2+ homeostasis and electrophysiological stability through SERCA2a regulation in mice. *Circ Arrhythmia Electrophysiol*. 2014;7:938–948.

364. Kim SO, Irwin P, Katz S, Pelech SL. Expression of Mitogen-Activated Protein Kinase Pathways During Postnatal Development of Rat Heart. *J Cell Biochem*. 1998;71:286-301.

365. Dolnikov K, Shilkrut M, Zeevi-Levin N, Gerecht-Nir S, Amit M, Danon A, Itskovitz-Eldor J, Binah O. Functional Properties of Human Embryonic Stem Cell–Derived Cardiomyocytes: Intracellular Ca2+ Handling and the Role of Sarcoplasmic Reticulum in the Contraction. *Stem Cells*. 2006;24:236–245.

366. Liu J, Dong Fu J, Wah Siu C, Li RA, Dong JF. Functional Sarcoplasmic Reticulum for Calcium Handling of Human Embryonic Stem Cell-Derived Cardiomyocytes: Insights for Driven Maturation. *Stem Cells*. 2007;25:3038–3044.

367. Itzhaki I, Rapoport S, Huber I, Mizrahi I, Zwi-Dantsis L, Arbel G, Schiller J, Gepstein L. Calcium handling in human induced pluripotent stem cell derived cardiomyocytes. *PLoS One*. 2011;6.

368. Jiang D, Xiao B, Yang D, Wang R, Choi P, Zhang L, Cheng H, Chen SRW. RyR2 mutations linked to ventricular tachycardia and sudden death reduce the threshold for store-overload-induced Ca2+ release (SOICR). *Proc Natl Acad Sci USA*. 2004;101:13062–13067.

369. Qu Y, Boutjdir M. Gene expression of SERCA2a and L- and T-type Ca channels during human heart development. *Pediatr Res*. 2001;50:569–574.

370. Arai M, Otsu K, MacLennan DH, Alpert NR, Periasamy M. Effect of thyroid hormone on the expression of mRNA encoding sarcoplasmic reticulum proteins. *Circ Res*. 1991;69:266–276.

371. Kiss E, Jakab G, Kranias EG, Edes I. Thyroid hormone-induced alterations in phospholamban protein expression: Regulatory effects on sarcoplasmic reticulum Ca2+ transport and myocardial relaxation. *Circ Res*. 1994;75:245–251.
372. Rao MK, Xu A, Narayanan N. Glucocorticoid modulation of protein phosphorylation and sarcoplasmic reticulum function in rat myocardium. *Am J Physiol - Heart Circ Physiol*. 2001;281.
373. Wacker C, Dams N, Schauer A, Ritzer A, Volk T, Wagner M. Region-specific mechanisms of corticosteroid-mediated inotropy in rat cardiomyocytes. *Sci Rep*. 2020;10.
374. Hong TT, Shaw RM. Cardiac t-tubule microanatomy and function. *Physiol Rev*. 2017;97:227–252.
375. Seki S, Nagashima M, Yamada Y, Tsutsuura M, Kobayashi T, Namiki A, Tohse N. Fetal and postnatal development of Ca2+ transients and Ca2+ sparks in rat cardiomyocytes. *Cardiovasc Res*. 2003;58:535–548.
376. Marston SB, Redwood CS. Modulation of Thin Filament Activation by Breakdown or Isoform Switching of Thin Filament Proteins: Physiological and Pathological Implications. *Circ Res*. 2003;93:1170–1178.
377. England J, Loughna S. Heavy and light roles: Myosin in the morphogenesis of the heart. *Cell Mol Life Sci*. 2013;70:1221–1239.
378. Edwards JG, Bahl JJ, Flink IL, Cheng SY, Morkin E. Thyroid Hormone Influences Beta Myosin Heavy Chain (βMHC) Expression. *Biochem Biophys Res Commun*. 1994;199:1482–1488.
379. Haddad F, Jiang W, Bodell PW, Qin AX, Baldwin KM. Cardiac myosin heavy chain gene regulation by thyroid hormone involves altered histone modifications. *Am J Physiol - Heart Circ Physiol*. 2010;299:H1968.
380. Morkin E. Stimulation of cardiac myosin adenosine triphosphatase in thyrotoxicosis. *Circ Res*. 1979;44:1–7.
381. Lompre AM, Mercadier JJ, Wisnewsky C, Bouveret P, Pantaloni C, D'Albis A, Schwartz K. Species- and age-dependent changes in the relative amounts of cardiac myosin isoenzymes in mammals. *Dev Biol*. 1981;84:286–290.
382. Ottolia M, Torres N, Bridge JHB, Philipson KD, Goldhaber JI. Na/Ca exchange and contraction of the heart. *J Mol Cell Cardiol*. 2013;61:28–33.
383. Qu Y, Ghatpande A, El-Sherif N, Boutjdir M. Gene expression of Na+/Ca2+

exchanger during development in human heart. *Cardiovasc Res*. 2000;45:866–873.

384. Kruger LC, Isom LL. Voltage-gated Na+ channels: Not just for conduction. *Cold Spring Harb Perspect Biol*. 2016;8.

385. Maier LS, Sossalla S, Schulze-Bahr E. SCN10A-Dependent Late I Na Current: Never Too Late for Cardiac Conduction?. *Circ Genomic Precis Med*. 2018;11:e002167.

386. Veerman CC, Mengarelli I, Lodder EM, Kosmidis G, Bellin M, Zhang M, Dittmann S, Guan K, Wilde AAM, Schulze-Bahr E, Greber B, Bezzina CR, Verkerk AO. Switch from fetal to adult SCN5A isoform in human induced pluripotent stem cell-derived cardiomyocytes unmasks the cellular phenotype of a conduction disease-causing mutation. *J Am Heart Assoc*. 2017;6.

387. Krause U, Alflen C, Steinmetz M, Müller MJ, Quentin T, Paul T. Characterization of maturation of neuronal voltage-gated sodium channels SCN1A and SCN8A in rat myocardium. *Mol Cell Pediatr*. 2015;2.

388. Veerman CC, Mengarelli I, Guan K, Stauske M, Barc J, Tan HL, Wilde AAM, Verkerk AO, Bezzina CR. HiPSC-derived cardiomyocytes from Brugada Syndrome patients without identified mutations do not exhibit clear cellular electrophysiological abnormalities. *Sci Rep*. 2016;6:1–10.

389. Sendfeld F, Selga E, Scornik FS, Pérez GJ, Mills NL, Brugada R. Experimental models of brugada syndrome. *Int J Mol Sci*. 2019;20.

390. Ceelen L, De Spiegelaere W, David M, De Craene J, Vinken M, Vanhaecke T, Rogiers V. Critical selection of reliable reference genes for gene expression study in the HepaRG cell line. *Biochem Pharmacol*. 2011;81:1255–1261.

391. Kanzaki Y, Terasaki F, Okabe M, Fujita S, Katashima T, Otsuka K, Ishizaka N. Three-dimensional architecture of cardiomyocytes and connective tissue in human heart revealed by scanning electron microscopy. *Circulation*. 2010;122:1973–1974.

392. Mathur A, Ma Z, Loskill P, Jeeawoody S, Healy KE. In vitro cardiac tissue models: Current status and future prospects. *Adv Drug Deliv Rev*. 2016;96:203–213.

393. Thavandiran N, Nunes SS, Xiao Y, Radisic M. Topological and electrical control of cardiac differentiation and assembly. *Stem Cell Res Ther*. 2013;4:1–9.

394. Zeiger AS, Hinton B, Van Vliet KJ. Why the dish makes a difference: Quantitative comparison of polystyrene culture surfaces. *Acta Biomater*. 2013;9:7354–7361.

395. Simpson DG, Terracio L, Terracio M, Price RL, Turner DC, Borg TK. Modulation of cardiac myocyte phenotype in vitro by the composition and orientation of the extracellular matrix. *J Cell Physiol*. 1994;161:89–105.

396. Bursac N, Parker KK, Iravanian S, Tung L. Cardiomyocyte cultures with controlled macroscopic anisotropy: a model for functional electrophysiological studies of cardiac muscle. *Circ Res*. 2002;91.

397. McDevitt TC, Angello JC, Whitney ML, Reinecke H, Hauschka SD, Murry CE, Stayton PS. In vitro generation of differentiated cardiac myofibers on micropatterned laminin surfaces. *J Biomed Mater Res*. 2002;60:472–479.

398. Chen A, Lieu DK, Freschauf L, Lew V, Sharma H, Wang J, Nguyen D, Karakikes I, Hajjar RJ, Gopinathan A, Botvinick E, Fowlkes CC, Li RA, Khine M. Shrink-film configurable multiscale wrinkles for functional alignment of human embryonic stem cells and their cardiac derivatives. *Adv Mater*. 2011;23:5785–5791.

399. Ribeiro MC, Tertoolen LG, Guadix JA, Bellin M, Kosmidis G, D'Aniello C, Monshouwer-Kloots J, Goumans MJ, Wang Y li, Feinberg AW, Mummery CL, Passier R. Functional maturation of human pluripotent stem cell derived cardiomyocytes in vitro - correlation between contraction force and electrophysiology. *Biomaterials*. 2015;51:138–150.

400. Hazeltine LB, Simmons CS, Salick MR, Lian X, Badur MG, Han W, Delgado SM, Wakatsuki T, Crone WC, Pruitt BL, Palecek SP. Effects of substrate mechanics on contractility of cardiomyocytes generated from human pluripotent stem cells. *Int J Cell Biol*. 2012;2012.

401. Baruscotti M, Barbuti A, Bucchi A. The cardiac pacemaker current. *J Mol Cell Cardiol*. 2010;48:55–64.

402. Koivumäki JT, Naumenko N, Tuomainen T, Takalo J, Oksanen M, Puttonen KA, Lehtonen Š, Kuusisto J, Laakso M, Koistinaho J, Tavi P. Structural immaturity of human iPSC-derived cardiomyocytes: In silico investigation of effects on function and disease modeling. *Front Physiol*. 2018;9:1–17.

403. Pachucki J, Burmeister LA, Larsen PR. Thyroid hormone regulates hyperpolarization-activated cyclic nucleotide- gated channel (HCN2) mRNA in the rat heart. *Circ Res*. 1999;85:498–503.

404. Renaudon B, Lenfant J, Decressac S, Bois P. Thyroid hormone increases the conductance density of f-channels in rabbit sino-atrial node cells. *Receptors*

Channels. 2000;7:1–8.

405. Fernández-Morales JC, Hua W, Yao Y, Morad M. Regulation of Ca 2+ signaling by acute hypoxia and acidosis in cardiomyocytes derived from human induced pluripotent stem cells. *Cell Calcium*. 2019;78:1–14.
406. Richard S, Perrier E, Fauconnier J, Perrier R, Pereira L, Gõmez AM, Bénitah JP. 'Ca2+-induced Ca2+ entry' or how the L-type Ca2+ channel remodels its own signalling pathway in cardiac cells. *Prog Biophys Mol Biol*. 2006;90:118–135.
407. Sejersted OM. Calcium controls cardiac function – by all means! *J Physiol*. 2011;589:2919.
408. Antoons G, Mubagwa K, Nevelsteen I, Sipido KR. Mechanisms underlying the frequency dependence of contraction and [Ca2+]i transients in mouse ventricular myocytes. *J Physiol*. 2002;543:889.
409. Doss MX, Di Diego JM, Goodrow RJ, Wu Y, Cordeiro JM, Nesterenko V V., Barajas-Martínez H, Hu D, Urrutia J, Desai M, Treat JA, Sachinidis A, Antzelevitch C. Maximum Diastolic Potential of Human Induced Pluripotent Stem Cell-Derived Cardiomyocytes Depends Critically on IKr. *PLoS One*. 2012;7:40288.
410. Karakikes I, Stillitano F, Nonnenmacher M, Tzimas C, Sanoudou D, Termglinchan V, Kong CW, Rushing S, Hansen J, Ceholski D, Kolokathis F, Kremastinos D, Katoulis A, Ren L, Cohen N, Gho JMIH, Tsiapras D, Vink A, Wu JC, Asselbergs FW, Li RA, Hulot JS, Kranias EG, Hajjar RJ. Correction of human phospholamban R14del mutation associated with cardiomyopathy using targeted nucleases and combination therapy. *Nat Commun*. 2015;6.
411. Vaidyanathan R, Markandeya YS, Kamp TJ, Makielski JC, January CT, Eckhardt LL. Arrhythmias, Electrophysiology, and Optical Mapping: IK1-enhanced human-induced pluripotent stem cell-derived cardiomyocytes: an improved cardiomyocyte model to investigate inherited arrhythmia syndromes. *Am J Physiol - Heart Circ Physiol*. 2016;310:H1611.
412. Horváth A, Lemoine MD, Löser A, Mannhardt I, Flenner F, Uzun AU, Neuber C, Breckwoldt K, Hansen A, Girdauskas E, Reichenspurner H, Willems S, Jost N, Wettwer E, Eschenhagen T, Christ T. Low Resting Membrane Potential and Low Inward Rectifier Potassium Currents Are Not Inherent Features of hiPSC-Derived Cardiomyocytes. *Stem Cell Reports*. 2018;10:822.
413. Yang X, Pabon L, Murry CE. Engineering adolescence: Maturation of human

pluripotent stem cell-derived cardiomyocytes. *Circ Res*. 2014;114:511–523.

414. Schober T, Huke S, Venkataraman R, Gryshchenko O, Kryshtal D, Hwang HS, Baudenbacher FJ, Knollmann BC. Myofilament Ca sensitization increases cytosolic Ca binding affinity, alters intracellular Ca homeostasis, and causes pause-dependent Ca-triggered arrhythmia. *Circ Res*. 2012;111:170–179.
415. Wang L, Kryshtal DO, Kim K, Parikh S, Cadar AG, Bersell KR, He H, Pinto JR, Knollmann BC. Myofilament Calcium-Buffering Dependent Action Potential Triangulation in Human-Induced Pluripotent Stem Cell Model of Hypertrophic Cardiomyopathy. *J Am Coll Cardiol*. 2017;70:2600–2602.
416. Jung P, Seibertz F, Fakuade FE, Ignatyeva N, Sampathkumar S, Ritter M, Li H, Mason FE, Ebert A, Voigt N. Increased cytosolic calcium buffering contributes to a cellular arrhythmogenic substrate in iPSC-cardiomyocytes from patients with dilated cardiomyopathy. *Basic Res Cardiol*. 2022;117:5.
417. Ernst P, Chen K, Tang Y, Kim S, Guan J, He J, Xie M, Zhang JJ, Liu XM, Zhou L. Investigation into the difference in mitochondrial-cytosolic calcium coupling between adult cardiomyocyte and hiPSC-CM using a novel multifunctional genetic probe. *Pflugers Arch Eur J Physiol*. 2021;473:447–459.
418. Maizels L, Huber I, Arbel G, Tijsen AJ, Gepstein A, Khoury A, Gepstein L. Patient-Specific Drug Screening Using a Human Induced Pluripotent Stem Cell Model of Catecholaminergic Polymorphic Ventricular Tachycardia Type 2. *Circ Arrhythmia Electrophysiol*. 2017;10.
419. Gaspar JA, Doss MX, Hengstler JG, Cadenas C, Hescheler J, Sachinidis A. Unique metabolic features of stem cells, cardiomyocytes, and their progenitors. *Circ Res.* 2014;114:1346–1360.
420. Dai DF, Danoviz ME, Wiczer B, Laflamme MA, Tian R. Mitochondrial maturation in human pluripotent stem cell derived cardiomyocytes. *Stem Cells Int*. 2017;2017.
421. Oster H, Challet E, Ott V, Arvat E, de Kloet ER, Dijk DJ, Lightman S, Vgontzas A, Van Cauter E. The functional and clinical significance of the 24-hour rhythm of circulating glucocorticoids. *Endocr Rev*. 2017;38:3–45.
422. Russell W, Harrison RF, Smith N, Darzy K, Shalet S, Weetman AP, Ross RJM. Free triiodothyronine has a distinct circadian rhythm that is delayed but parallels thyrotropin levels. *J Clin Endocrinol Metab*. 2008;93:2300–2306.
423. Jahagirdar V, McNay EC. Thyroid hormone's role in regulating brain glucose

metabolism and potentially modulating hippocampal cognitive processes. Metab. *Brain Dis*. 2012;27:101–111.

424. Rao C, Prodromakis T, Kolker L, Chaudhry UAR, Trantidou T, Sridhar A, Weekes C, Camelliti P, Harding SE, Darzi A, Yacoub MH, Athanasiou T, Terracciano CM. The effect of microgrooved culture substrates on calcium cycling of cardiac myocytes derived from human induced pluripotent stem cells. *Biomaterials*. 2013;34:2399–2411.
425. Skorska A, Johann L, Chabanovska O, Vasudevan P, Kussauer S, Hillemanns M, Wolfien M, Jonitz-Heincke A, Wolkenhauer O, Bader R, Lang H, David R, Lemcke H. Monitoring the maturation of the sarcomere network: a super-resolution microscopy-based approach. *Cell Mol Life Sci*. 2022;79:149.
426. Cyganek L, Tiburcy M, Sekeres K, Gerstenberg K, Bohnenberger H, Lenz C, Henze S, Stauske M, Salinas G, Zimmermann WH, Hasenfuss G, Guan K. Deep phenotyping of human induced pluripotent stem cell-derived atrial and ventricular cardiomyocytes. *JCI insight*. 2018;3.

Appendix

Representative raw western blot images

Chapter 4

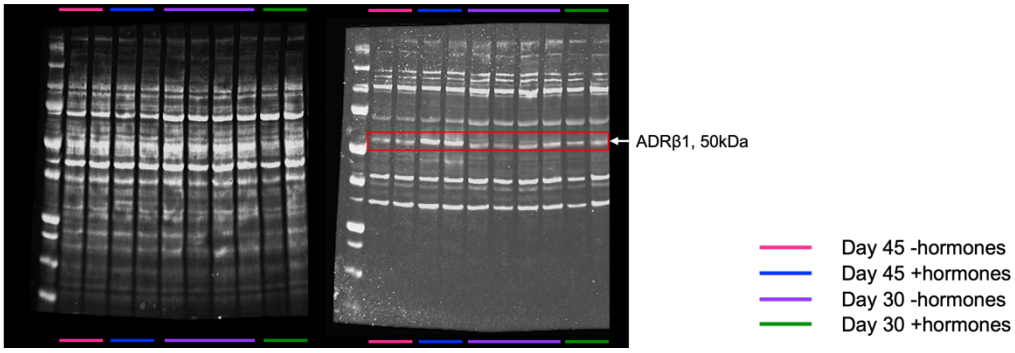

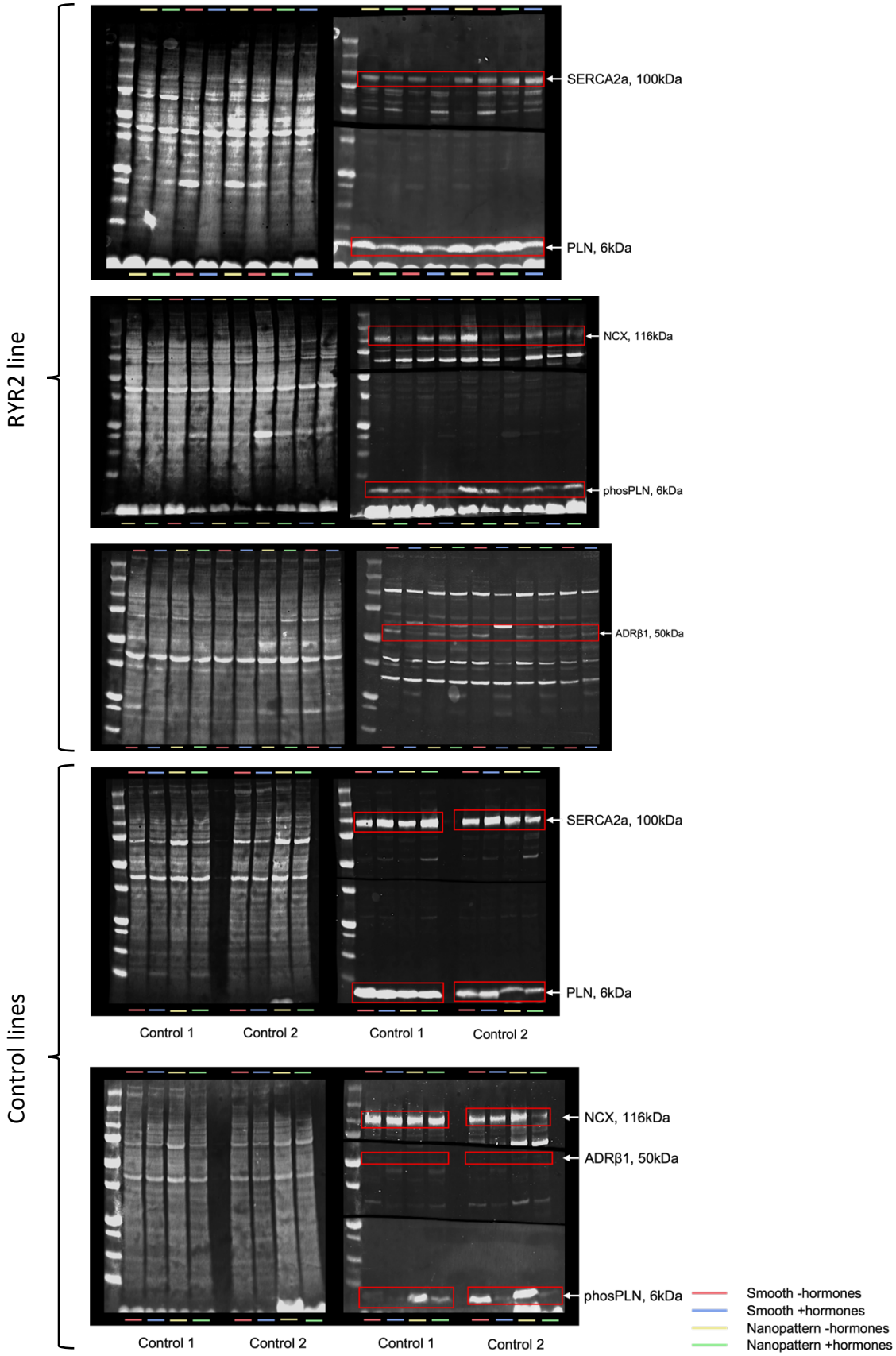
RYR2 line
SERCA2a, 100kDa
PLN, 6kDa
NCX, 116kDa
phosPLN, 6kDa
ADRβ1, 50kDa
Control lines
SERCA2a, 100kDa
PLN, 6kDa
Control 1
Control 2
Control 1
Control 2
NCX, 116kDa
ADRβ1, 50kDa
phosPLN, 6kDa
Control 1
Control 2
Control 1
Control 2
Smooth -hormones
Smooth +hormones
Nanopattern -hormones
Nanopattern +hormones

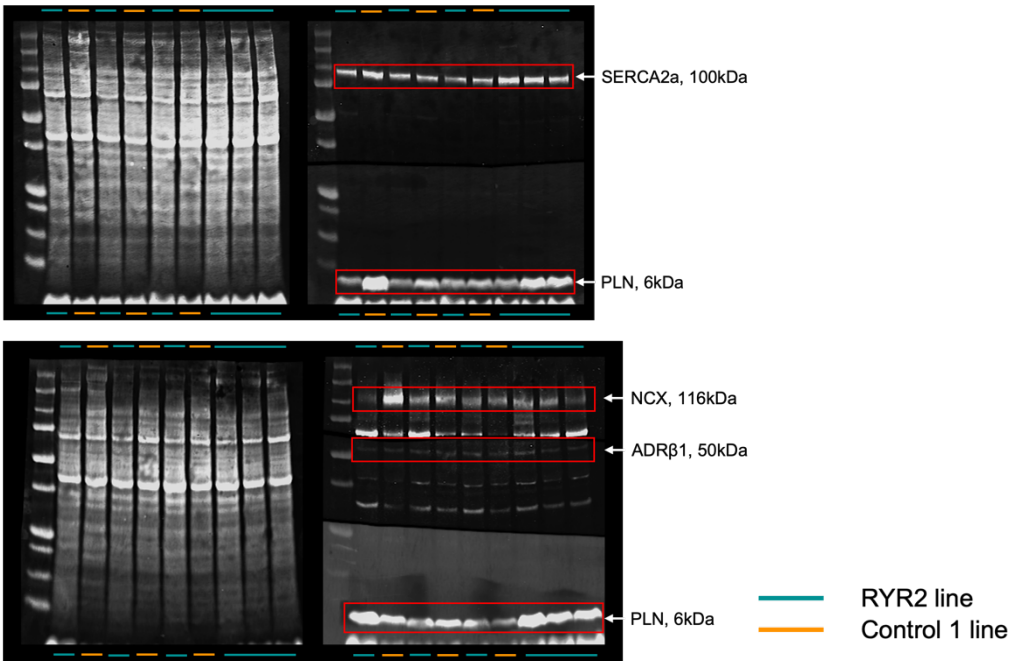
SERCA2a, 100kDa
PLN, 6kDa
NCX, 116kDa
ADRβ1, 50kDa
PLN, 6kDa
RYR2 line
Control 1 line